Fonctionnalisation de nanopore unique par des polymères : conformation, transport et applications

Tianji Ma

THÈSE POUR OBTENIR LE GRADE DE DOCTEUR DE L'UNIVERSITÉ DE MONTPELLIER

En Chimie et Physicochimie des matériaux

École doctorale SCIENCE CHIMIQUES BALARD (SCB)-ED 459

Unité de recherche Institut Européen des Membranes (UMR 5635, CNRS, UM, ENSCM)

FONCTIONNALISATION DE NANOPORE UNIQUE PAR DES POLYMERES: CONFORMATION, TRANSPORT ET APPLICATIONS

Présentée par Tianji MA

Le 14 Novembre 2019

Sous la direction de Sebastien BALME du Directeur de thèse

Devant le jury composé de

M. Bernard TINLAND, Directeur de Recherche, CNRS, CINaM	Rapporteur
M. Laurent BACRI, Maître de conférences, Université d'Évry	Rapporteur
M. Juan PELTA, Professeur, Université d'Évry	Examinateur
Mme Sophie TINGRY, Directrice de Recherche, CNRS, IEM	Examinateur
Mme Mathilde P. LEPOITEVIN, Maître de conférences, ENS Paris	Examinateur
M. Sébastien BALME, Maître de conférences, Université de Montpellier	Directeur de thèse

UNIVERSITÉ DE MONTPELLIER

Table of contents

General introduction

Biological channels takes on the task to keep ion equilibrium and molecule transport through cell membranes. These protein channels can respond to multiple stimuli like light, pH, ion strength and trans-membrane potential to regulate their permeability and selectivity. Since a long time, the multipore membranes used in industry for filtration or as catalyst are inspired by these “smart” channels to improve their properties. Since more than two decades, it appeared nanopore technology that essentially talks about single nanopore. These artificial nanopores based on solid-state or polymer materials are small holes with diameter at nanometer scale on thin membranes. When the pores down scale on single level, changing in quantity leads to changing in quality. A single pore allows us to characterize the real transport behaviors of ions or molecules. This permits a quantitative control of ion flux and single molecule detection that open the door to delicately design nanopores/membranes for numerous applications as DNA/protein sensing, (bio)molecule detection, stimuli-responsive membrane and osmotic energy harvesting.

The road from artificial nanopore to the real applications is still tough. One big question is how to design the nanopore to have required properties? For a targeted application, nanopore requires two aspects: the choice of materials according to their own properties and the functionalization to give them additional properties. For DNA sequencing, a pore diameter at around 1 to 2 nanometer and a minimum membrane thickness is desired; for (bio)molecule detection, specific interactions with target molecules are required; for stimuli-responsive membranes, stimuli-responsive functions are needed and for osmotic energy harvesting, high surface charge and small membrane thickness can bring high energy. Other than these, biosensors need also high accuracy, reusability and membranes for industry should have high mechanical and chemical stabilities and so on. So functionalization is the crucial tool to ensure these desired properties.

Polyelectrolytes and specific molecules modified polyelectrolytes can be good candidates for nanopore functionalization as they have stimuli responsiveness, variable and suitable size as well as numerous possibilities to be immobilized in nanopores. They can be industrial products with low cost or can be natural substances like nucleic acids, peptides and proteins etc.

This thesis focus on the functionalization of track-etched polymer nanopore by (bio)polyelectrolytes for stimuli-responsive ion channels, biosensors and membranes for

osmotic energy harvesting. Track-etched polymer nanopore is a good platform. Indeed, it has advantages such as possibility to fabricate both single pore and multipore membrane under the same condition, low cost, various and controllable shapes as well as simplicity for chemical modifications. So the objectives of the thesis work are: (1) using various polyelectrolytes immobilization methods including layer-by-layer self-assembly and chemical grafting to introduce functions inside the pore; (2) give nanopore abilities to regulate ion transport by surface charge and molecule conformation change to respond to external stimuli like pH, ionic strength and light; (3) give nanopore ability of specific interaction with target molecules to build biosensors or to study interactions between molecules; (4) give nanopore ability to generate osmotic currents under salinity gradient with a maximum of the output energy.

Following by these objectives, the manuscript is organized on four chapters. In the first chapter, the fundamentals of polyelectrolytes and stimuli-responsive polyelectrolyte membranes; cell membrane channels and biomimetic nanopores; transport properties of nanopore and applications of polymer and polyelectrolytes functionalized track-etched nanopore are introduced and discussed.

The second chapter presents the design of stimuli-responsive ion channel with polyelectrolytes that can change their permeability and selectivity in responding to pH, ion concentrations and UV/visible light changes. The conformation and charge changes when these environmental parameters change are discussed.

The third chapter is contributed to build ion selective membranes to take the used osmotic power from salinity gradient. Two strategies are considered including surface modifications by multiple polyelectrolyte layers and *in situ* synthesis of highly charged hydrogel frameworks inside the pore. The experiments from single nanopore to multipore membrane until to stacked membranes are achieved.

The last chapter talks about specific interaction studies. Nanopores functionalized by poly-L-lysine are designed to detect over-sulfated chondroitin sulfate in heparin. Nanopores functionalized with hyaluronidases are utilized to study enzymatic reaction products and enzyme-substrate interactions at single molecule level.

Chapter 1:

Bibliography study

1 Polyelectrolytes and stimuli-responsive polyelectrolyte membranes

1.1 Polyelectrolytes

Polyelectrolytes are molecules of high molecular weight that contain a large number of charges when dissolved in a polar solvent[1]. The charges come from chemical moieties that covalently linked to periodic units. If only one type of charge (positive or negative) exists along the polymer chain, it is called homogeneous polyelectrolyte; otherwise if a polymer has both two kinds of charged groups, it is called polyampholyte. Polyelectrolytes can be strong ones if all the ion groups are dissociated and they can be weak ones if ion groups dissociate partially. As the weakly charged groups can have different states according to external conditions, they can have responsive properties on pH which are interesting for stimuli-responsive applications.

1.1.1 Electric double layer

For all the processes of the charge formation, chemical potential and entropy are the driving forces to minimize the Gibbs free energy when the system reaches to equilibrium with outer ions in solution. At the same time, an electric double layer forms around the polymer. Due to electric attractions between opposite charged groups, ions will be closely adsorbed to polyelectrolytes to get a minimized potential. These absorbed ions are called Stern layer or condensed ions layer specifically in polyelectrolyte science. They can induce a screening effect of the polymer charges. Then outer of this counterion layer, the diffusive layer is formed by relatively free ions to neutralize the Stern layer. This electric double layer as shown in figure 1 becomes the essential model to study ion concentrations and charge distributions around the charged substance in polyelectrolytes science.

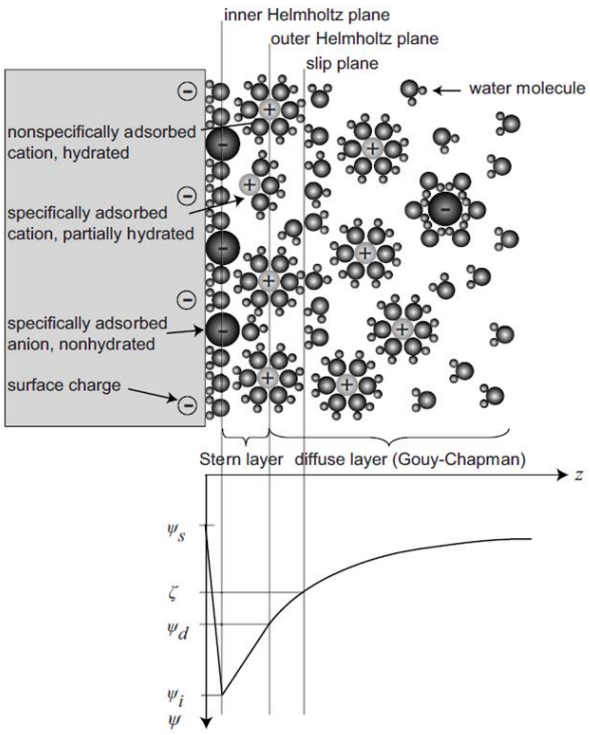

Fig. 1 Schematic representation of electrical double layer and the corresponding potential profile[2].

The ionic concentration and the distribution of charge density in electrolyte solutions can be described by Poisson-Boltzmann Equation (PBE) which is obtained by mean field approximation of the potential of mean force. Poisson equation in electrolyte solution system reads:

$$\nabla^2 \emptyset(\mathbf{r}) = -\frac{4\pi}{\epsilon} \sum_i z_i q c_i(r) \qquad (1)$$

where $\emptyset$ is the electric potential, ϵ is the dielectric constant, z_i is the electric charge of the ion i, c_i is the concentration of ion i at *r*.

In the Gouy-Chapman model of electric double layer theory, the ions close to the surface follow Boltzmann distribution:

$$c_i(r) = c_i^0 e^{-\beta \omega_i(r)} \qquad (2)$$

where $\omega_i(r)$ is the potential of mean force of ion i, c_i^0 is the counterion concentration at the point of zero potential, $\beta = {}^{1}/_{k_B T}$ where k_B is Boltzmann constant.

In mean field approximation, if we neglect interactions between ions and make potential of mean force approximately equal to its electric potential:

$$\omega_i(r) \cong z_i q \emptyset(r) \quad (3)$$

we get the Poisson-Boltzmann equation:

$$\nabla^2 \emptyset(\boldsymbol{r}) = -\frac{4\pi}{\epsilon} \sum_i c_i^0 z_i q e^{-\beta z_i q \emptyset(r)} \quad (4)$$

If we define that the Stern layer radius is *a*, the diffusive layer radius is *R*. At the boundary of Stern layer the surface charge density at *r* = *a* is given by $v/2\pi a$, (v is the linear charge density of polyelectrolyte molecule) which gives a first boundary condition:

$$\frac{\beta \partial \omega_i(r)}{\partial r}|_{r=a} = \frac{e^2 v}{2\pi\epsilon k T a} \quad (5)$$

while at the boundary of diffusive layer, the electric field should vanish, then we get the second boundary condition:

$$\frac{\beta \partial \omega_i(r)}{\partial r}|_{r=R} = 0. \quad (6)$$

1.1.2 Polyelectrolyte conformation

1.1.2.1 Polyelectrolytes in solutions

In pure water, homogenous polyelectrolytes adopt a rod-like linear conformation due to the extension of chains (Figure 2). This extension comes from the electrostatic repulsion of the charged groups along the polymer. The electrostatic repulsion ensures that a minimum distance between two polyelectrolyte molecules is kept. When electrolytes are added, the hydrodynamic volume of the polyelectrolyte will be reduced. Indeed, the counter-ions are absorbed to the charged moieties reducing the electrostatic repulsion. In this case, the polyelectrolyte adopts a coil-like conformation. This process is called polyelectrolyte effect[3]. At very high salt concentrations, it could be assumed that the electrostatic repulsions between charged groups of polyelectrolytes are totally screened by the counter-ions.

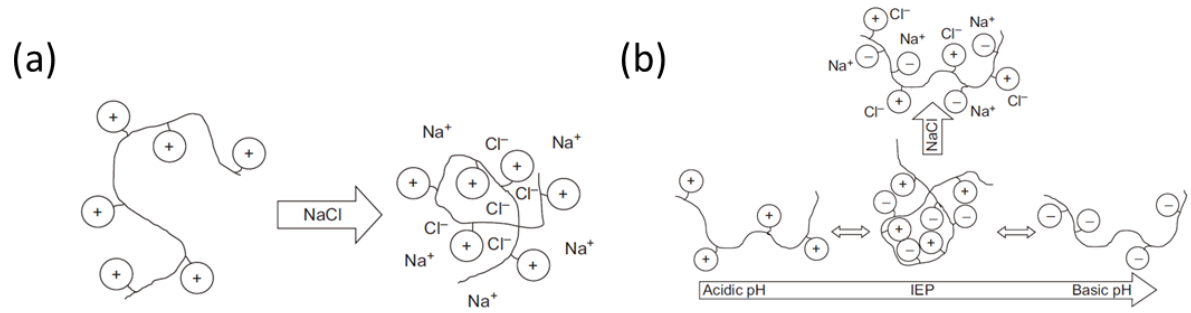

Figure 2 Schematic representation of (a) salt ions influence on polyelectrolytes and (b) salt ions and pH influences on polyampholytes[4].

The behavior of polyampholytes is opposite than that of homogeneous polyelectrolytes. As polyampholytes have both positive and negative charges, when dissolved in pure water, electrostatic attraction occurs instead of repulsion so that they become coiled. When ions are added, the charges of the chain are shielded by counter-ions around or in other words, charges are screened by ions. Therefore the chains will be extended. If all charged groups on the zwitterionic polymers are weak, the chain charges can turn to be one type (positive or negative) due to protonation/ deprotonation by changing pH. As a consequence, the chain will be also extended. This phenomenon is called anti-polyelectrolyte effect.

1.1.2.2 Grafted brushes

When the polymer is grafted onto the surface, the situation is different because it can swell only in one direction. In addition, the density of polymer chain is a key factor that governs their conformation as “mushroom” or “brush”. At low density, the polymer chains adopt the conformation of separate coils that is also dependent of the solvent. Here, the distance between grafting sites should be larger than coil radius which is expressed by Flory radius (Fig. 3) in good solvent[5]:

$$R_F = N^{3/5}a \qquad (7)$$

where *a* is the size of monomer, *N* is the number of monomers.

In the case of ideal solvent and bad solvent, the Flory radius can be calculated as:

$$R_I = N^{1/2}a \qquad (8)$$

$$R_B = N^{1/3}a. \qquad (9)$$

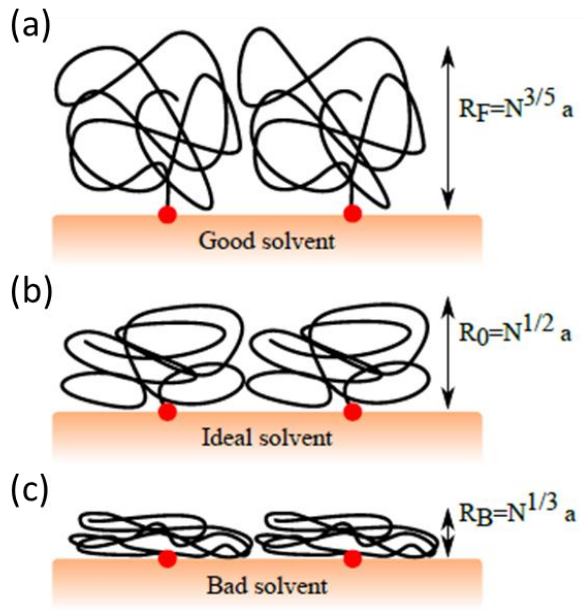

Fig. 3 Mushroom polymer conformation in (a) good solvent, (b) ideal solvent and (c) bad solvent[6].

When the grafted sites are closer to the Flory radius, the polymer chains will be extended until to adopt a brush conformation corresponding to stretched chains regime[7]. In this case, the polymer layer thickness *L* can be expressed approximately as:

$$L \cong Na\sigma^{1/3} \qquad (10)$$

where σ is the fraction of grafted sites.

Under this conformation, the layer thickness is proportional to the number of monomers per chain. For the polyelectrolytes, the grafted layer thickness can be influenced by ionic strength and pH[8,9].

1.1.3 Stimuli responsiveness of polyelectrolytes

Conformational and charge changes of polyelectrolytes resulting from external stimulus are used to design "smart" materials[10,11]. Among the stimuli, the pH is the most studied because it is an important parameter of solution in biomedical[12,13] and membrane industry[14].

Figure 4 illustrates examples of several weak polyelectrolytes. Typically, weak polyelectrolytes can adopt different conformations according to pH because the protonation and deprotonation induce overall charge state changes. This effect can strongly influence weak cation and anion groups. In solutions with a pH lower than pKa of polyelectrolytes,

polyelectrolytes can protonate for a positively charged tendency and in solutions with a pH higher than pKa of polyelectrolytes, they can deprotonate which is favorable for appearance of negative charges. Thus pH changes induce charge variance that influence the adsorption and desorption.

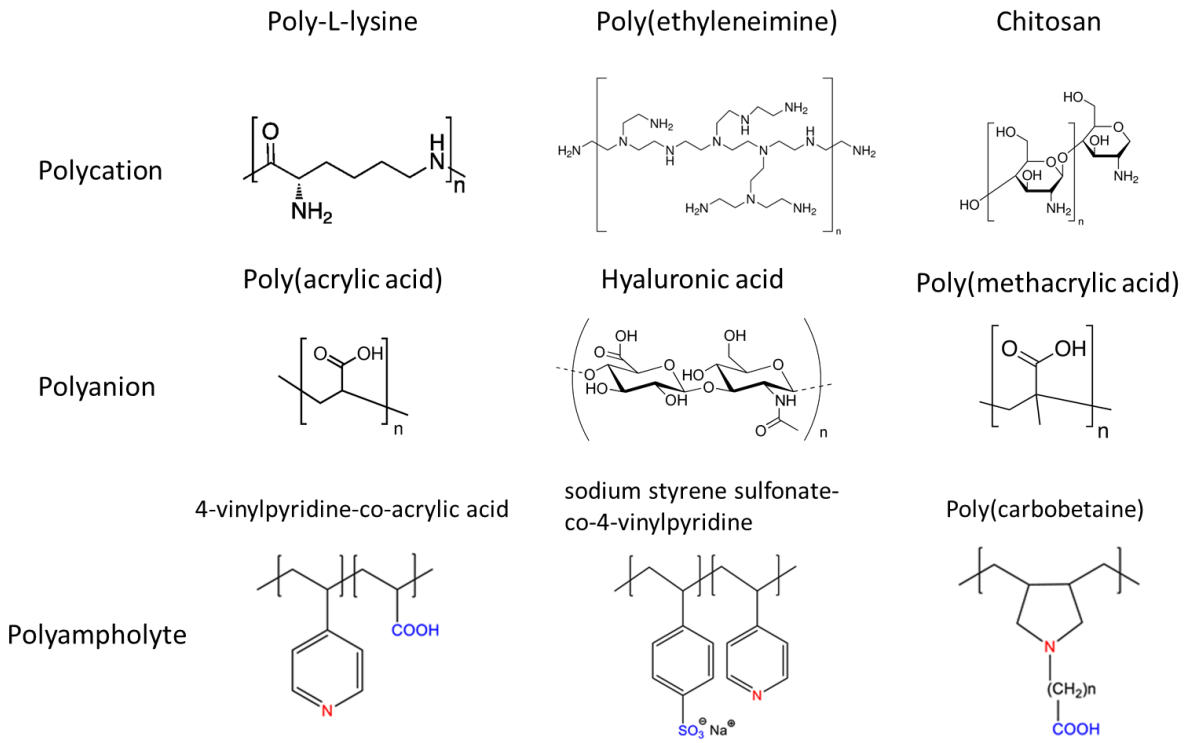

Fig. 4: Examples of polycations, polyanions and polyampholytes.

Salt concentration is also a very common stimulus. The conformation changes under different ionic strength depend on the polymer nature (polyelectrolytes or anti-polyelectrolyte as discussed in section 1.1.2). Swelling and deswelling are major resulting phenomenon due to ionic strength that makes polyelectrolytes playing an important role in controllable drug delivery[15,16] and membrane gating[17,18].

Temperature responsiveness has been achieved with polyelectrolytes or polyampholytes[11,19]. Similarly than the pH, temperature can also involve conformational changes when the polymers is upper or lower critical solution temperature[20,21] (UCST or LCST). It results a phase transition leading to a change in polymer density and conformation. The most studied and used thermal-responsive polymer is poly(N-isopropylacrylamide) (PNIPAAM)[22,23], it can undergo from a swollen hydrated state to a shrunken dehydrated state at 32℃.

Polymer materials can also respond to electric potential[24], light (UV-vis)[11,19], and solvent[25]. Electric potential can cause changes of charge to conducting polymers such as polyaniline[26,27] (PANI) and poly(3,4-ethylenedioxothiophene)[28] (PEDOT). At certain potential values, these polymers can be oxidized or reduced to get charges. Light responsiveness can be introduced in polymers by using photoswitchable groups such as azobenzene[29–31] or spiropyran[32]. Typically, the azobenzene molecules switch between *cis* and *trans* conformation, while the spyropyran switch between charged state and non-charged state by changing irradiation wavelength. The introduction of these small molecules and their small changes in polymers matrix can involve macroscopic conformational changes[19].

1.2 Stimuli-responsive membrane using polyelectrolytes modification

A membrane is a selective barrier which separates two reservoirs with different composition and only several species can pass through. It has been used widely in industries[33] during a long history essentially in filtration[34], desalination[35,36] and energy generation[37–41] where pressure and chemical potential are two major driving forces. The membrane process is simple and does not require additives like adsorbent or solvent which can be expensive and difficult to recycle. In addition, the equipment is relatively simple which occupies small spaces[41]. Permeability and selectivity are two parameters to define the membrane performances. The permeability presents the trans-membrane flux which characterizes the production rate. The selectivity is the ratio of specific substances permeation over rejection. These two parameters have usually opposite effects. Once the membrane pores are large, the permeation will be increased but the selectivity will often decrease at the same time. To develop membranes with both high permeability and selectivity is always of interest. Despite the large amount of membranes being widely used, traditional membranes cannot respond to environmental changes like cell membranes because of their structures and physical/chemical surface properties are unchangeable[10].

The stimuli-responsive polyelectrolytes can help membrane to get such stimuli-responsible properties. They allow to modulate their permeation and selectivity properties in response to environmental changes such as pH[18], pressure[42], ionic strength[43], electrical potential[44], light[45,46], temperature[47], magnetic field[48,49], specific molecule[50], specific ions[51] etc. Thanks to

the charges and specific functional groups on polyelectrolytes, they can change their structures or charge states under different conditions.

Two strategies were used to design membranes by polyelectrolytes. The first one is to synthesize materials using stimuli-responsive polymers and process them into membranes directly[52]. In this way, stimuli-responsive polymers can be the main networks or can be additives. A bunch of membrane processing methods are developed such as radiation curing[53], solvent casting[54], interpenetrating polymer networks[55] and phase inversion[56].

The second one is to decorate membrane surface by such stimuli-responsive polymers[52]. This method refers to surface modification by direct surface initiated polymerization known as "grafting from" methods or by immobilization of pre-prepared polymers known as "grafting to" methods[52].

1.2.1 Surface modification by polyelectrolytes

Introduction of new properties into the existing membranes by surface modification is a method relatively simple. It can involve polymers which cannot be used to fabricate the entire membranes limited by mechanical stabilities etc. Such modification allows giving new stimuli-responsive properties to the membrane. Two methods are employed for surface functionalization by stimuli-responsive polymers: "grafting from"[57] and "grafting to"[58]. "Grafting from" is an *in situ* polymerization from a surface and "grafting to" involves to anchor the already prepared polymer to the membrane surface. One or the other method should be chosen according to the base membrane physical and chemical properties, polymerization conditions and so on. There is a common difference between "grafting to" and "grafting from". For the "grafting to" methods, the grafted point density depends on the polymer molecular weight: larger the molecule size is, lower the covering rate will be. While for the "grafting from" methods these two factors are less dependent.

1.2.1.1 "Grafting from" methods

The "Grafting from" methods for polymer decorations of surface refer to series of surface initiated polymerization. In the three past decades, the polymerization techniques have undergone a period of active development especially in controllable polymerization such as atom transfer radical polymerization (ATRP)[59–61] and reversible addition fragmentation chain transfer polymerization (RAFT)[62–64]. Since their found, their applications in surface

initiated[65–6768,69] domain have been investigated. Surface initiated polymerization[70,71] requires firstly the immobilization of reactive monomers on the surface. Then, the propagation of chains obeys the same process of the polymerization than in bulk conditions.

Atom transfer radical polymerization (ATRP) utilizes transition metal complexes (Cu, Fe, Ru, Ni) as catalysts and initiators of alkyl halides (R-X). Among them, Cu complexes are the most used ones. The ATRP reaction begins with the activation of dormant species (R-X) by the transition metal which creates alkyl radicals and oxidization of the metal atom. Then, the activated alkyl moieties keep growing with monomers. In addition, the reaction equilibrium is shifted toward the formation of halogen stopped species with low radical concentrations. Because each chain has the same probability to grow or to form dormant species, the polymers will have similar molecular weights and narrow molecular weight distribution. During the polymerization, as initiators, catalysts and monomers interact together to form different intermediate states, the reaction process depends on many factors such as catalyst concentration, initiator concentration, type of ligands and solvent.

Reversible addition fragmentation chain transfer polymerization (RAFT) is also one of the most popular techniques for surface initiated polymer brushes preparation. It requires an initiator which can decompose as free radical and a RAFT agent which has a form of thiocarbonyl moieties to control the reaction. The reaction begins from the fragmentation of initiator for radical release. Then monomers undergo a radical polymerization with initiators. The controllable step comes from the participation of RAFT agent to the chain growth. The polymer reacts with RAFT agent to transfer the radical to the alkyl chain in the agent under a reversible process. The new formed radical species will continue to polymerize. From certain size, they will establish the equilibrium with RAFT agent connecting another pre-formed polymer. This procedure is known as the main RAFT equilibrium. Thus by controlling both temperature and chemical factors, desired polymer size can be obtained with a narrow size distribution.

Beside ATRP and RAFT, many other surface initiated polymerizations have also been developed including nitroxide-mediated polymerization[72–75], anionic polymerization[76–78], photoiniferter-mediated polymerization[79–82], ring-opening metathesis polymerization[83,84] and living ring-opening polymerization[85,86]. All of them have been successfully investigated in

surface initiated polymerization and each of them has corresponding advantages and disadvantages that should be well chosen according to needs.

1.2.1.2 “Grafting to” methods

Pre-prepared responsive polymers can be attached onto a membrane surface by adsorption, covalent grafting and coordination grafting to form self-assembled monolayers (SAMs).

Adsorption is a kind of bottom-up fabrication method which takes advantages of self-assembling processes. Electrostatic attraction and inter-molecular interactions as well as hydrogen bonds, Van der Waal’s forces and specific biological interactions can be driving forces. Layer-by-layer deposition technique[87–91] (Fig. 5) is a good example for fabrication or functionalization of membranes by sequential physical adsorption of complementary macromolecules. This method has the merit to be simple and low cost. As the energy level of physical interaction is relatively low compared to chemical bonds, the physical adsorbed layers can be desorbed by changing pH, ionic strength, solvent or other conditions. This soft and flexible structure thanks to the weak interactions makes it more suitable to design stimuli-responsive membranes. While, it is also a disadvantage for the possible undesirable desorption when environment changes.

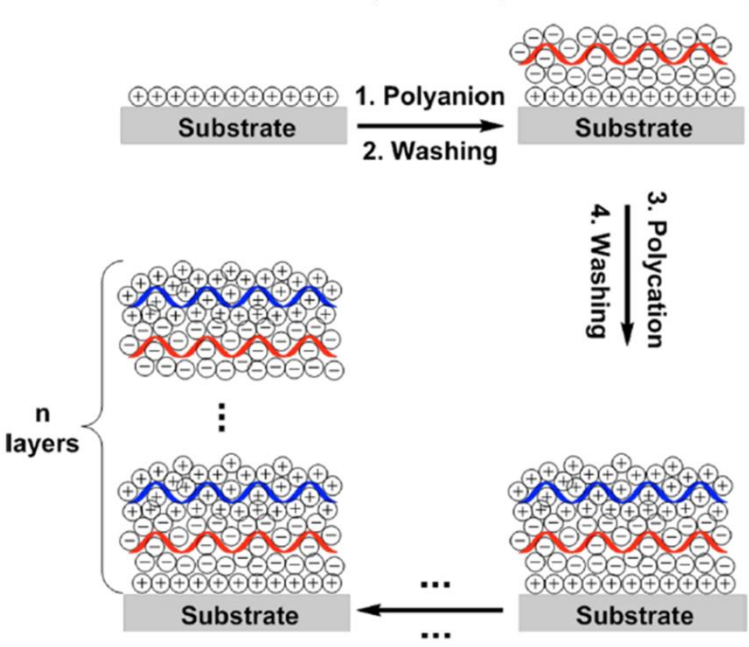

Fig. 5 Schematic presentation of layer-by-layer polyelectrolytes adsorption[92].

Covalent grafting aims to form chemical bonds between surface and pre-prepared polymers which can form the most stable covers. For organic membranes, amide moieties are usually preferred because the reaction between an amine and carboxyl moieties catalyzed by 1-Éthyl-3-(3-dimethylaminopropyl)carbodiimide (EDC)[93] and N-Hydroxysuccinimide (NHS)[94] is simple and fast. The mechanism is depicted in Fig. 6 (a), (b). Carboxylic acid moieties are activated by EDC to form an o-acrylisourea active ester intermediate; then amine moieties replace EDC to form amides. The EDC is a zero-length crosslinking agent[95] which means that no additional chemical structure is introduced during the reaction. Besides of amide bond, it can also catalyze phosphate groups to form phosphoramidate bond with amines[96]. NHS molecules can form easily a NHS-ester derivative which can then react with a carboxylic for amide bond formation. Pre-prepared polymers can be mixed with EDC to activate carboxylic groups and also can be mixed with EDC/NHS to activate both carboxylic and amine groups. The reactions can be either one-step or two-step. One step reaction has a higher conversion rate but the reaction conditions may destroy reactive especially some biomolecules. Two-step reaction has less conversion rate while reactive are added after the activation step in rough conditions.

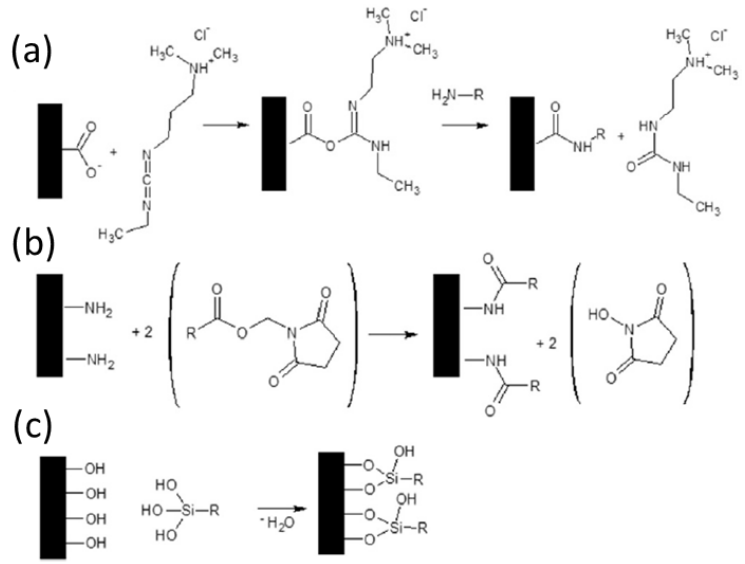

Fig. 6 Schematic representation of carboxamide formations by (a) EDC, (b) NHS and (c) Silicon oxide bond formation[97].

The inorganic membranes based on Si or metal oxides can be also functionalized by silanisation thanks to their hydroxyl moieties (Fig. 6). The surface oxidation by treatment by piranha (H_2SO_4:H_2O_2 = 3:1), plasma O_2 or ozonolyse of Si, SiN and SiO_2 surfaces generate

hydroxyl groups and make the membrane more hydrophilic. Then the abundant hydroxyl groups can have condensations with organosilanes to graft functional organic molecules.

Another kind of grafting widely used is self-assembled monolayers (SAMs) using thiol-Au coordination bond (Fig. 7). It consists to immobilize thiol or disulfide terminated molecules onto gold substrate[98–100]. The chemisorption of thiol moieties on gold can form stable Au-S bonds. We mentioned above that "grafting to" methods suffer from low grafting density because of the steric effect of macromolecules. However, the SAMs can offer a very dense layer thanks to inter-molecule forces. Although it takes usually a long time for obtaining SAMs because of the multi-steps of the process includes physical adsorption, lying formation phase, standing nucleation phase and completion phase. It draws still great interest for researchers for its simplicity and broad application range. This last convenience comes from the possibility of a pre-step of covering surfaces with gold using electroless deposition, sputtering or vapor deposition on various substrate including polymer membranes[101] and SiN nanopores[102].

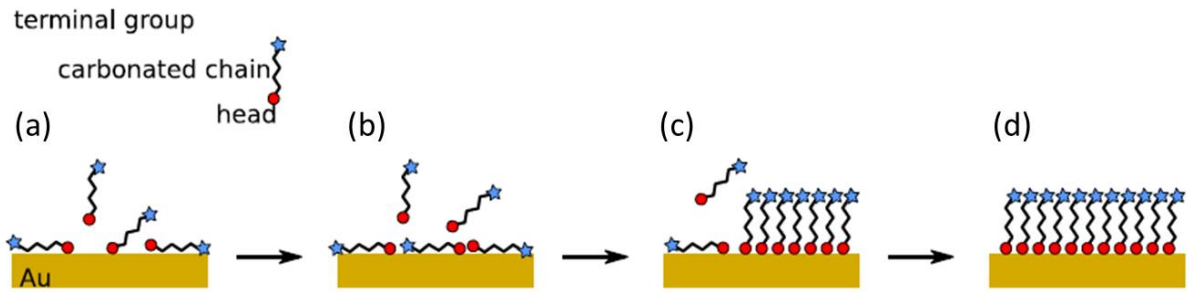

Fig. 7 Schematic representation of thiol SAMs formation at step (a) physisorption, step (b) lying formation phase, step (c) standing nucleation phase step and (d) completion phase. [97]

2 From cell membrane channels to biomimetic nanopores

2.1 Trans-membrane transport in cell

Cell membrane forms the barrier which differentiates cells from their external environment[103]. It has two functions. It protects the cell and keeps the cell constituents as a barrier. At the same time, it has a transporter role allowing absorbing nutrients and expelling the wastes out of cell. Composed of phospholipid molecules, the membrane has a lipid bilayer structure. The trans-membrane proteins are incorporated in the lipid bilayer working as membrane transporters (Fig. 8). Briefly, two kinds of transports are identified according to transport direction along the concentration gradient or against. Permeation rate as the diffusion velocity across membrane of different substances varies in a wide range according to different transport modes.

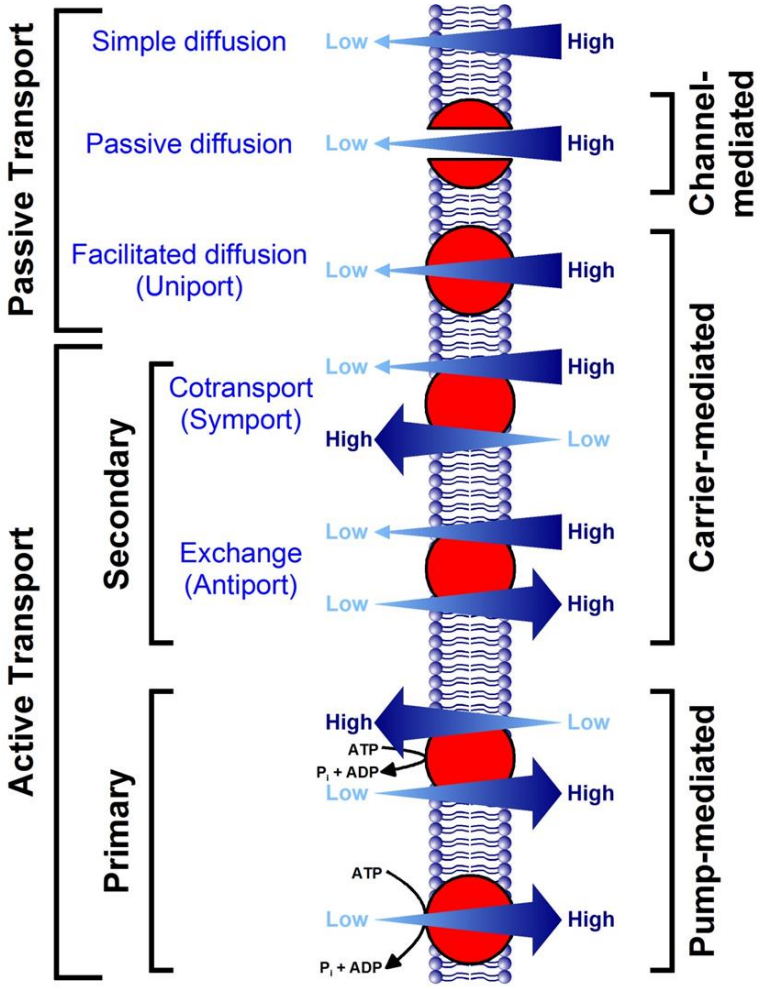

Fig. 8 membrane transport processes. Physiologyweb www.physiologyweb.com

The diffusion along concentration gradient is driven by high free energy of the concentrated part. The permeation rate is relatively high. Two trans-membrane proteins exist for that, one is membrane channel[104,105] which is constructed as a hole. Some channels are always open but most of them are gated by chemical[106], mechanical[107] or electrical potential actions[108]. Some large channels are permeable to different ions with the same charge, anions or cations. Specific narrow structures of other channels allow the passage of only one type ion: such as potassium, sodium or chlorine. The electrical potential gating channels play important roles to transform physiological signals into electrical signals which are the basis of many nerve-nerve or nerve-muscle interactions. This selectivity and responsiveness inspires researcher to mimic such biological properties on artificial membrane. Besides ions, some other small molecules and water can also pass through membrane channels. The transporter[109,110] is another type of trans-membrane proteins that facilitate diffusion of larger molecule. Sugar or amino acid molecules are chemically bounded onto the specific transporters, and then the protein brings it to the other side and releases it.

The transport of substances against their concentration gradient requires another source of energy. According to energy origin, two kinds of active transports exist. The primary active transport[111] utilizes directly the energy of cell metabolism (ATP). The secondary active transport[112,113] take advantage of energy released from a spontaneous along-concentration-gradient diffusion. Ion pumps are good examples as primary active transports which transport various ions like sodium, potassium or calcium from low concentration side to high concentration side.

Even still a lot of transport mechanisms across membrane are not totally understood, in the domain already well exploited researchers have learned from abundant precise, smart biological process and structures. They developed over last decade biomimetic solid-state channels for biosensing, energy and responsive ion channels.

2.2 Biomimetic solid-state channel

The first DNA sensing with a single nanopore was achieved using an α-hemolysin pore[114]. The latter biological channel is a toxin which self-assembles onto lipid bilayer and cause cell lysis such as aerolysin[115], gramicidin A[116], anthrax toxin[117], lysenin[118] etc. The other types of channels used for DNA sequencing are outer-membrane channel including OmpG[119] and

MspA[120–122]. Even many applications have been achieved by biological nanopores for nucleic acid analyses[123–126], peptide/protein characterization[127] and the numerous development of new biological pores like FraC[128], ClyA[129] and FhuA[130], there are always two limiting factors : their fixed size and limiting stability[131].

A reliable solution for these weaknesses is artificial solid-state and polymer nanopores[131]. These nanopores have generally excellent mechanical properties, physical and chemical stabilities, surface tunable which makes it developing rapidly in the last two decades. At the end of last century, with the development of nuclear industry and particle accelerators, track etching techniques burned for fabrication of track-etched membranes[132,133] and single nanopores using polymer films[134,135]. At the same period, carbon nanotubes[136,137] were found by S. Lijima and developed for numerous applications from electronics to physics being followed by other nanotubes including boron nitride[138,139], halide[140], aluminosilicate[141,142]. Soon after that, single nanopores are achieved in thin SiN membrane by ion bean sculpting at Harvard[143] and then are fabricated in Si, SiN, SiO_2 by silicon technology and transmission electron microscopy at Delft[144,145]. More recently, 2D nanopores of graphene[146–148] and MoS_2[149] turned into reality and showed specific advantages for energy generation[150] and polymer sequencing[151,152]. A novel plasmonic nanopore[153–155] was created by combining a plasmonic nanoantenna, Raman spectroscopy and optical tweezers with solid-state nanopore for high performance molecule detection. The use of artificial nanopores becomes now a promised technology as manipulation controlled technique for applications from single molecule detection[156], DNA/RNA/peptide sequencing[157] to responsive channel construction[97] and energy harvesting[158].

2.2.1 Silicon based nanopore (SiN and SiO_2)

For most time, solid state nanopores refer specifically nanopores fabricated in silicon based-materials including Si, SiO_2, SiN. The nanometer-scale controlled pore fabrication became true thanks to the development of microelectronics and nanofabrication techniques. The first method for nanopore drilling in SiN and SiO_2 materials was achieved by ion beam sculpting. Li *et al*. sputtered the SiN thin film on a substrate with a cavity, and then a focused ion beam irradiated SiN to drill a single nanopore[143]. The procedure was stopped when ions were detected on the back side which is a feedback-controlled system. After that, a more common method was proposed by C. Dekker's group using a TEM technique[144,145]. A focused

electron beam of TEM was utilized on sputter SiO_2 deposited on Si membrane in order to shrink pores of large size. Conveniently, the whole procedure can be observed lively by TEM. The shrinking velocity of SiO_2 to Si is reported to be about 0.3 nm min^{-1}, which is slow enough for a precise control of nanopore size. Then, the main deviation comes from the surface roughness of the silicon oxide. The advantages of these techniques of high accuracy and high controllability are also limiting conditions that with these techniques, the fabrication need expensive instruments such as FIB and TEM. Actually such nanopores are costly and can produce only one pore at a time. About 10 years after, a new low cost technique as reported using controlled dielectric breakdown (CDB) technique[159,160]. A strong electric field was applied to a SiNx membrane on silicon chip in aqueous solution. Through trap-assisted tunneling mechanism, leakage of current appeared and then after charge traps accumulation, the membrane was finally perforated. When these solid-state nanopores are fabricated, the main work to make sure the applications becomes nanopore wetting, stability enhancing and noise reduction[161].

Different noise sources such as flicker noise, thermal noise, dielectric noise, and amplifier noise are identified. A series of efforts were tried including surface modification, using other substrate materials than Si and developing high performance amplifier. With the achievement in progress of noise reduction, spatial resolution and surface functionalization, nanopores based on Si derives become a powerful tool for detections of nucleic acids and proteins[161].

2.2.2 Nanotubes

Carbon nanotubes (CNTs) are channel-like form in rolled-up 2D graphene. They have a diameter of a couple of angstroms to several nanometers while the length can reach some millimeters[162]. They can be synthesized by catalytic particles coupled with chemical vapor deposition, carbon-arc discharge and laser[163]. Its ultrahigh aspect ratio makes it a good tool to study interfacial transport phenomenon[162]. The highly hydrophobic surface and sub-nanometer size give to CNT special properties for water transport. When water molecules pass through a sub-nanometer CNT, water can form a hydrogen bonded wire and with the decrease of hydrogen bonds, the nanoconfined water become different from bulk one in terms of Helmholtz free energy. The friction free water transport of CNTs can reach a speed of 4 - 6 molecules per nanosecond which is comparative to aquaporins as water transporters

in cell membrane[164]. This is due to de high slip length as the flow velocity at the surface keeps still a high value[165,166].

Boron nitride nanotubes (BNNTs) have very similar structures with CNTs but have different chemical compositions[138,139]. Thanks to different electronegativity of boron and nitrogen from carbon, water molecules dissociate that a hydrogen atom bound to a nitrogen atom. Thus hydroxyl groups are widely distributed on BNNTs surface which bring a high charge density[167,168]. This unexpected, interesting chemical property gives BNNTs a high performance on osmotic energy harvesting[158].

2.2.3 2D Nanopore

From nucleic acid to peptides, biomolecule sequencing accuracy is limited by signal-to-noise ratio, translocation speed and spatial resolution. The latter limitation can be solved by a nanopore with a thickness in the same order than the distances between two nucleotides or two amino-acids. Thus, 2D nanopores become an ideal solution thank to their thickness less than 1 nm. The graphene nanopore was the most investigated due to its finest thickness of carbon monolayer about 0.335 nm that allowing to identify each nucleotide or amine acid with high accuracy[146,169]. However, pristine graphene nanopores exhibit strong hydrophobic interactions with DNA, which limits their long-term use because of clogging[152]. The effort are now also focus on boron nitride[170] and molybdenum disulfide[152,171]. The fabrication of these 2D nanopores is generally performed by ablation via focused electron-beam irradiation in a TEM[172]. Monolayer sheets are suspended on a SiNx frame punctured containing micropores. Then assisted by TEM, the sheets are drilled by a focused ion beam which can be done at single atom level.

Another application of 2D nanopore is the osmotic energy harvesting. In that case the ions diffuse across ion selective membranes along salinity gradient. This process directly generates electric current and transmembrane potential. The ionic selectivity is one essential factor influencing the performance. It can be increased by minimizing the membrane thickness. The molybdenum disulfide 2D nanopore was used for that purpose resulting in a breaking single pore performance[150].

2.2.4 Nanopipette

One of the solid-state nanopores with low cost and quick fabrication is nanopipette[173]. Beyond that, advantages such as low-noise performance, chemical stability, easier handling help them to be a good candidate for applications in biomolecule detection[174]. Made from quartz or borosilicate glass, nanopipettes are generally formed by laser-assisted pulling. A glass capillary is fixed and undergoes cycles of heating and pulling until it breaks into two identical tiny conical nanopores. The diameter of the tip side can be obtained to some tens of nanometers. Various methods are applied to decrease the diameter that such as atomic layer deposition[175], electron irradiation[176] and wet-chemical silanization[173]. The shrink of the pore size down to sub 10 nm give it a higher signal-to-noise ratio for detection of smaller molecules[174].

2.3 Track-etched polymer nanopore

Tracked etched membranes made of polymer foils were first fabricated as multipore membranes. The process follows two steps: irradiation and chemical etching. There are two methods for producing tracks on polymer films including polyethylene terephthalate (PET)[134], polycarbonate (PC)[133], polyimide (PI)[177], polypropylene (PP)[178] and polyvinylidene fluoride (PVDF)[179]: One is using fragments of nuclear fission[180] and the other one is based on high energy ion beams of accelerators[181]. The first one has low cost and stable particle flux but disadvantages like radioactive contamination, limited energy range and fragments complexity reduce the use of this method. Despite the high cost and lower particle flux stability, accelerator-based irradiation become more and more common with its controllability in energy, impact angle especially for single track fabrication.

The first step (call “track”) is the irradiation to perform a latent track. When a heavy swift ions bombard on polymer films, electronic energy losses by numerous particle material interactions. The energy lost can be expressed by:

$$\frac{dE}{dx} = \frac{4\pi e^4 Z_{eff}^2 Z_t N}{m_e v^2}\left[\ln\left(\frac{2m_e v^2}{I}\right) - \beta^2 - \delta - U\right], \qquad (11)$$

where e is elementary charge, Z_{eff} is effective charge of the projectile, Z_t is aomic number, N is number of target atoms per unit volume, m_e is electron mass, v is ion velocity, I is ionization energy, β is relative correction and U is inner electrons screening correction.

Thus, the effective penetrating range of an ion with initial kinetic energy E_0 can be calculated by integration:

$$\mathrm{R} = \int_0^{E_0} \left(\frac{dE}{dx}\right)^{-1} dE. \qquad (12)$$

Heavy swift ions break chemical bonds of polymers, the resulted latent tracks are then activated by Ultra Violet light (UV). The UV irradiation increase the chemical activity of the tracks and the duration time of this procedure can enhance the etching velocity along the track.

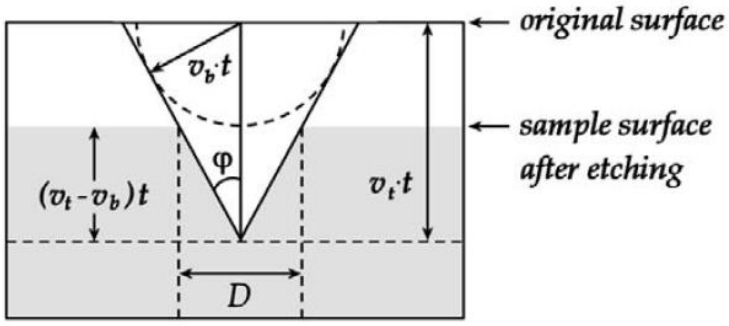

Fig. 9 Schematic representation of chemical etching process on an across section. Thesis Birgitta Schiedt,2007

The second step is chemical etching which will open the pores and determine its geometry and size. Etching solutions attack both track zone and polymer bulk with two different velocities V_t and V_b. The ratio of these two rates can determine pore geometries. They are influenced by etchant composition, temperature and the use of additive such as surfactant. Generally for a high concentration etchant at room temperature, V_t is higher than V_b but in the same range. Such conditions are suitable to obtain conical shape pore under dissymmetrical condition. At higher temperature and lower etchant concentration, $V_t >> V_b$ which will result in a cylindrical geometry. By combining symmetric etching (etching from both sides), asymmetric etching (etching from one side) and under condition where $V_t \approx V_b$, or $V_t >> V_b$, various shapes can be obtained including hourglass, funnel, dumbbell.

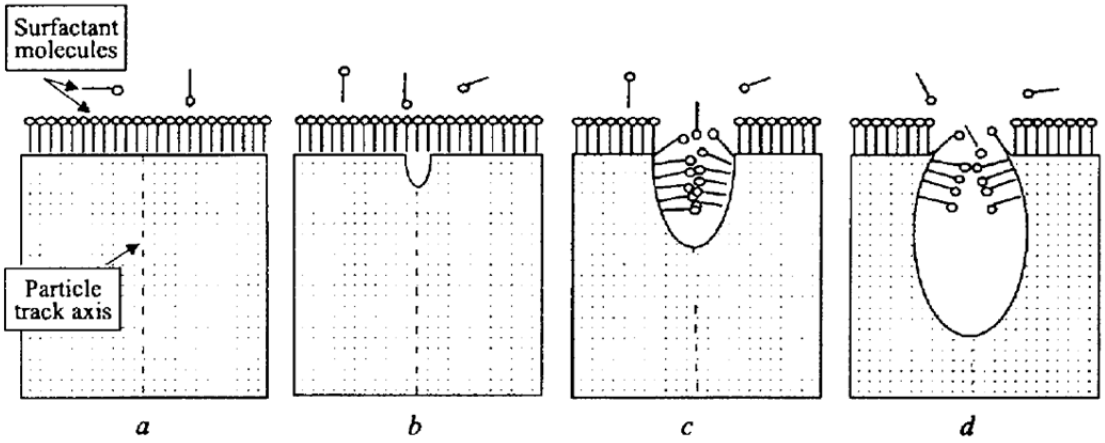

Fig. 10 Schematic representation of a chemical etching process with participation of surfactant molecules[132].

The use of surfactant allows to form cigar-like and bullet-like shapes[132] (Fig. 10). Surfactant molecules are adsorbed to entrance surface and protect it as shown in Fig. 10. The opening size depends on the surfactant molecules length. The length of protected zone depends on the molecule diffusing distance in the pore. It should be noted that it exists a minimum pore diameter of track etched nanopore because of the track size and the etching properties. A minimum of 2 nanometers was achieved for conical pore, while for cylindrical pore, the limit is upper than 20 nm.

For single nanopore, PET films are the most used. After chemical etching, the PET pore surface has carboxylate groups which are ideal for chemical functionalization by forming amide, ester bonds as well as for polyelectrolyte adsorption by electrostatic interactions. Thus, with controllable geometries and facile surface functionalization, track-etched nanopore has a wide range of applications in biosensing, stimuli-responsive channel and energy generation.

3 Transport properties through nanopore

3.1 Electrostatics near interface

The Poisson-Boltzmann equation is given to describe the potential distribution in electrical double layer (EDL) formed near the surface of polyelectrolytes. As shown in Fig. 1, a Stern layer composed of immobilized ions and a diffuse layer containing a number of mobile counter-ions coexist at the surface which leads a potential distribution as a function of the distance from the surface *z*.

The EDL becomes extremely important in transport properties close to the surface[2]. In nanopore the surface/volume ratio is high. Thus, when the nanopore diameter is close to EDL length, the ionic transport is governed by surface phenomenon. Let us rewrite the Poisson-Boltzmann equation:

$$\nabla^2\psi = \frac{d^2\psi}{dz^2} = -\frac{e}{\epsilon}\sum_i n_i^{\infty} z_i exp[-z_i e\psi(z)/k_B T], \quad (13)$$

where n_i^{∞} is the ion concentration. To solve this equation, approximations are required. If we assume that the surface potential is homogenous and small (25 < mV) in the whole EDL and use $e^{-\alpha} = 1 - \alpha$ for α, then we get Debye-Hückel approximation:

$$\nabla^2\psi = \frac{d^2\psi}{dz^2} = k^2\psi(z), \quad (14)$$

where

$$\mathrm{k} = \left(\frac{e^2\sum_i n_i^{\infty} z_i^2}{\epsilon k_B T}\right)^{1/2} \quad (15)$$

which is called Debye-Hückel parameter. For small surface potential, analytical solution can be obtained as:

$$\psi(z) = \psi_0 \exp(-z/\lambda_D), \quad (16)$$

where $\lambda_D = k^{-1}$ is the Debye length characterizing the thickness of the EDL, thus the Debye length is inversely proportional to ion concentrations of solution. For a high surface potential, Gouy-Chapman model is taken into account:

$$\tan h\left(\frac{e\psi(z)}{4k_B T}\right) = \tan h\left(\frac{e\psi_0}{4k_B T}\right) exp(-z/\lambda_D), \quad (17)$$

where the condition of equal valence of co-ion and counter-ion is applied for this result.

As Debye length depends only on ion concentration of solution, it can be simply expressed as a function of ion concentration n_i in the case of symmetrical electrolyte ($z_i = z_i$) at 25°C:

$$\lambda_D = \frac{2.15\times10^{-10}}{\sqrt{\frac{1}{2}\sum_i n_i z_i^2}}. \quad (18)$$

For a KCl concentration of 10^{-5} M, the Debye length is as long as 96.3 nm which create a zone big enough for various electrokinetic phenomenons close to interface.

3.2 Hydrodynamics and Electrokinetics near interface

3.2.1 Liquid slippage

Before discussing the movement of electrically charged ions and molecules inside a potential field (EDL), it should be introduced a more common phenomenon named slippage[182,183] that occurrs at liquid/solid interface under frictionless flux. In the case of nanopore, it can play important role on pressure drop, electrical and diffusive transport. The characteristic of slippage which has the opposite direction of Debye length is the slip length[184]. It is an extrapolated distance relative to the nanopore wall where the tangential velocity component vanishes as shown in figure 11. Various factors can influence the slip length including weak wall fluid attraction, surface roughness, high shear rates and nucleation of nanobubbles at hydrophobic surfaces. As it is an interfacial hydrodynamic phenomenon, to find the slip length *b*, we should begin with the liquid-solid friction. The friction force is linear to slip velocity under the form of:

$$F_f = -\mathcal{A}\lambda v_t, \quad (19)$$

where λ is the friction coefficient and $\mathcal{A}$ is the lateral area.

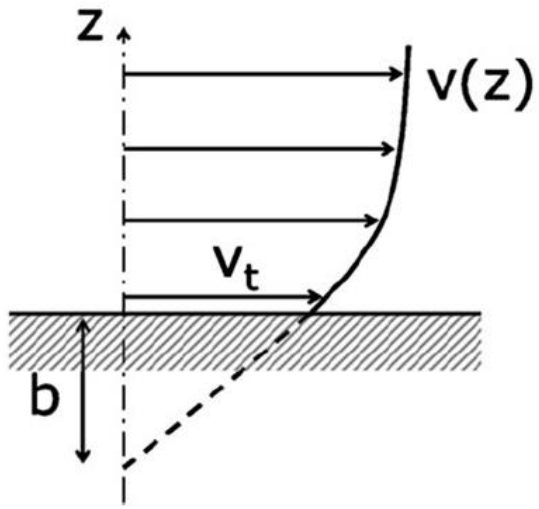

Fig. 11 Schematic representation of liquid velocity profile close to surface and the slip length b[184].

The slip length is defined as $b = \eta/\lambda$, where η is the bulk viscosity. According to this relation, the slip length should be large for a smooth surface especially a hydrophobic surface; this is why a high water transport velocity was reported in carbon nanotubes[165]and hydrophobic nanopore[185,186].

3.2.2 Electro-osmosis, electrophoresis and streaming potential

The liquid slippage can occur on charged or non-charged surface. If we re-focus to a charged surface with an EDL, the flow of liquid containing ions in EDL can involve interesting electrodynamic phenomenon. If the flow is driven by electric field, both electro-osmosis[187] and electrophoresis[188] will happen. If the flow is driven by hydrostatic pressure, a streaming potential will be obtained.

When an electrical field is applied parallel to the interface, from the slip plane, the liquid velocity increase from zero to a maximum value v described by Smoluchowski formula[189]:

$$v = -\frac{\varepsilon\zeta}{\eta}E_e, \qquad (20)$$

where ε is the dielectric constant, ζ is the zeta potential and η is the viscosity. Here we can find a linear relation between the liquid velocity and the applied electric field. This plug-like flow will be changed when the ionic strength is ultra-low with a large Debye length. Using Stokes and Poisson equations we can develop the $v_{(z)}$ as:

$$v_{(z)} = -\frac{\varepsilon\zeta}{\eta}E_e\left(1-\frac{\psi(z)}{\zeta}\right), \quad (21)$$

where the potential distribution appears as a variable of the velocity.

As an interfacial flow, the electro-osmotic transport will be influenced by slippage which can decrease the friction in EDL. Then as shown in Fig. 11, the hydrodynamic velocity gradient can contain $b+\lambda_D$. Thus if we apply ζ:

$$\zeta = v_0 \times \left(1+\frac{b}{\lambda_D}\right), \quad (22)$$

into Eq. (21), the velocity at surface $v_{(0)}$ becomes:

$$v_{(0)} = \frac{\varepsilon}{\eta}E_e\frac{b}{\lambda_D}, \quad (23)$$

$v_{(0)}$ is proportional to the slip length. It shows that surface properties can highly influence electric induced transport and can be optimized for osmotic energy harvesting.

Now, if an electric field is applied parallel to the interface the charged particles will move to form electrophoresis flow. The electrophoresis mobility can be different according to EDL thickness. For thin EDL thickness compared to the particle radius, the electrophoretic mobility can be expressed by Helmholtz-Smoluchowski limit:

$$\mu_{ep} = \frac{\varepsilon\zeta}{\eta}, \quad (24)$$

While for thick EDL, the electrophoretic mobility can be given by Hückel-Onsager limit:

$$\mu_{ep} = \frac{2\varepsilon\zeta}{3\eta}. \quad (25)$$

Beside electric field, the driving force for generating flows can be hydrostatic pressure which leads to the formation of streaming potential across a channel[190]. The mobile ions in the EDL move under pressure as a flow of ions is called streaming current. The accumulation of ions creates an electric field causing an opposite current as conductance one. The difference of electrical potential along the channel is called streaming potential. It can be very useful to experimentally determine surface charge density.

3.3 Transport in nanofluidics

3.3.1 Donnan and membrane potentials

Until this section, we discussed about the interfacial transport phenomenon with or without a charged surface. When the nanopore radius is of the same order than Debye length, the overlap of EDL will happen. Thus, the whole space in the nanochannel will be influenced by the surface charge. Under this condition, a nanochannel with charged surface (positive or negative) in an electrolyte solution will be selective to counter-ions. To reach the electrochemical equilibrium between outside and inside of the channel with different ion species concentrations, an electrical potential can be found so-called Donnan potential (Fig.12):

$$\Phi_D = \frac{RT}{z_i F} \ln\left(\frac{c_i^I}{c_i^{II}}\right), \tag{26}$$

where c_i^I and c_i^{II} are ion concentrations outside and inside the channel.

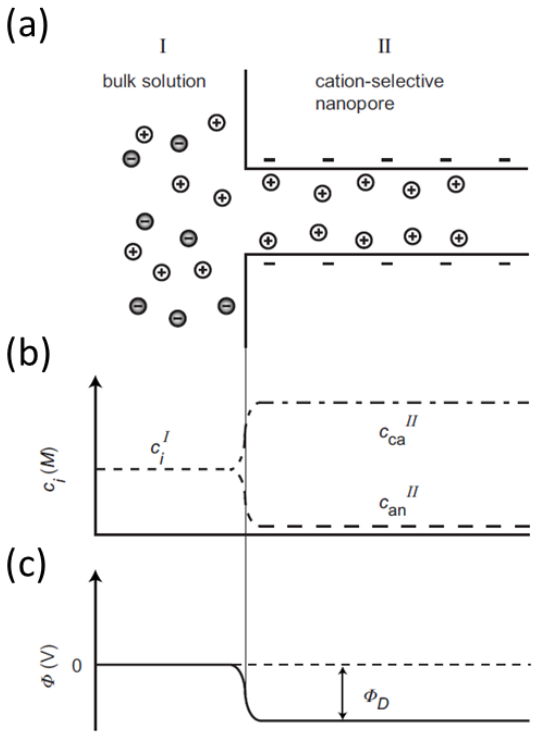

Fig. 12 Donnan equilibrium at the entrance of the nanochannel. (a) A different concentrations of ions in bulk solution I and in cation-selective nanochannel, (b) concentration profile and Donnan ratio appeared between I and II, (c) potential profile and Donnan potential.

If the channel connects two reservoirs with different salt concentrations which is a common case for membrane utilizations during desalination and reversed electro-dialysis energy harvesting, the membrane potential can be calculated by combining two Donnan potentials Φ_{D1}, Φ_{D2} of the two membranes sides and the diffusion potential Φ_{diff} (Fig. 13):

$$\Phi_m = \Phi_{D1} + \Phi_{D2} + \Phi_{diff}, \tag{27}$$

where Φ_{diff} is calculated as:

$$\Phi_{diff} = -\frac{t_{ca}^{II}}{z_{ca}}\frac{RT}{F}\ln\frac{c_{2ca}^{I}}{c_{1ca}^{I}} + \frac{t_{an}^{II}}{z_{an}}\frac{RT}{F}\ln\frac{c_{2an}^{I}}{c_{1an}^{I}}, \tag{28}$$

where t_{ca}^{II} and t_{an}^{II} are the transference numbers of cations and anions. Thus from Eq. (27) and Eq. (28) we obtain:

$$\Phi_m = \frac{RT}{F}\left(\ln\frac{c_1^{II}c_2^{I}}{c_1^{I}c_2^{II}} - \frac{t_{ca}^{II}}{z_{ca}}\ln\frac{c_{2ca}^{I}}{c_{1ca}^{I}} + \frac{t_{an}^{II}}{z_{an}}\ln\frac{c_{2an}^{I}}{c_{1an}^{I}}\right). \tag{29}$$

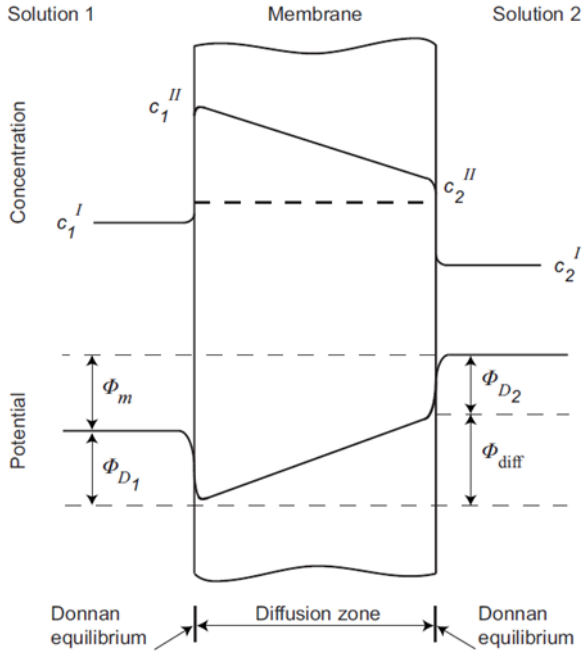

Fig. 13 Concentration profiles and potential profiles along membrane length separating two solutions with different concentrations (c_1>c_2)[2].

3.3.2 Perm-selectivity and pre-concentration

As the counter-ions of the charged surface are majority in the EDL, when Debye length is large (typically at low salt concentration), an enrichment of counter-ions occurs in the channel and a corresponding exclusion of co-ions will also occurs. This exclusion-enrichment effect generates perm-selectivity of membranes for diffusive ion transport. The effective diffusion coefficient is defined as:

$$J_{\pm} = -D_{eff}\frac{\Delta\rho}{L}, \quad (30)$$

where $J_{\pm}$ is the ion flux, $\Delta\rho$ is the concentration drop along nanochannel and L is the nanochannel length.

Other than asymmetrical concentration, an electric field applied across a nanochannel in an electrolyte solution can generate ion movement. As the surface charge promotes the presence of the counter-ion, the latter can be transported to the other side, thus an ion enrichment and ion depletion will occur at the both sides of the channel.

3.3.3 Nanochannel conductance

Ion enrichment and ion depletion are a consequence of ion flows. Other than that an electric potential applied to a nanochannel immersed in electrolyte solution generates an electric current. Thus, the channel can be considered as a resistance and inversely the conductance can be defined to a channel as the ratio of electric current to electric potential drop. The ionic conductance has two contributions from the bulk solution and the electro-osmosis in EDL[192] (Fig. 14). It can be expressed for a negatively charged nanochannel in a monovalent electrolyte solution as:

$$G = (\mu_+ + \mu_-)eC\frac{S}{L} + 2\mu_+\sigma_s\frac{w}{L}, \quad (31)$$

where μ is the mobility, C is the ion concentration, S is the cross section of channel, w is the channel width, L is the channel length and σ_s is the surface charge density.

Recently, Balme et *al*. developed a hybrid approach considering Debye length, advection, good co-ion exclusion and electro-osmosis[185]:

$$G_{hyb} = \frac{\pi R^2 \kappa_{hyb}}{L} \quad (32)$$

$$\kappa_{hyb} = e^2 c_s(\mu_+ + \mu_-)\sqrt{1 + \left(\frac{\sigma}{eRc_s}\right)^2} + \frac{e|\sigma|}{R}(\mu_+ - \mu_-) + \frac{\sigma^2}{2\eta} f(\sigma^*) \quad (33)$$

where c_s is the bulk concentration, R the pore radius, σ the surface charge density and $f(\sigma^*)$ a monotonous decline function which describes the correction for the large surface charge for the advective part of "Good Co-ion Exclusion" approximation:

$$\sigma^* = \pi l_B R \frac{\sigma}{e} \quad (34)$$

where l_B is the Bjerrum length.

It's also possible to consider the slip length as:

$$\kappa_{slip} = \kappa_{hyb} + \delta\kappa_{slip} = \kappa_{hyb} + \frac{2\sigma^2 b}{\eta R} \quad (35)$$

where *b* is the slip length.

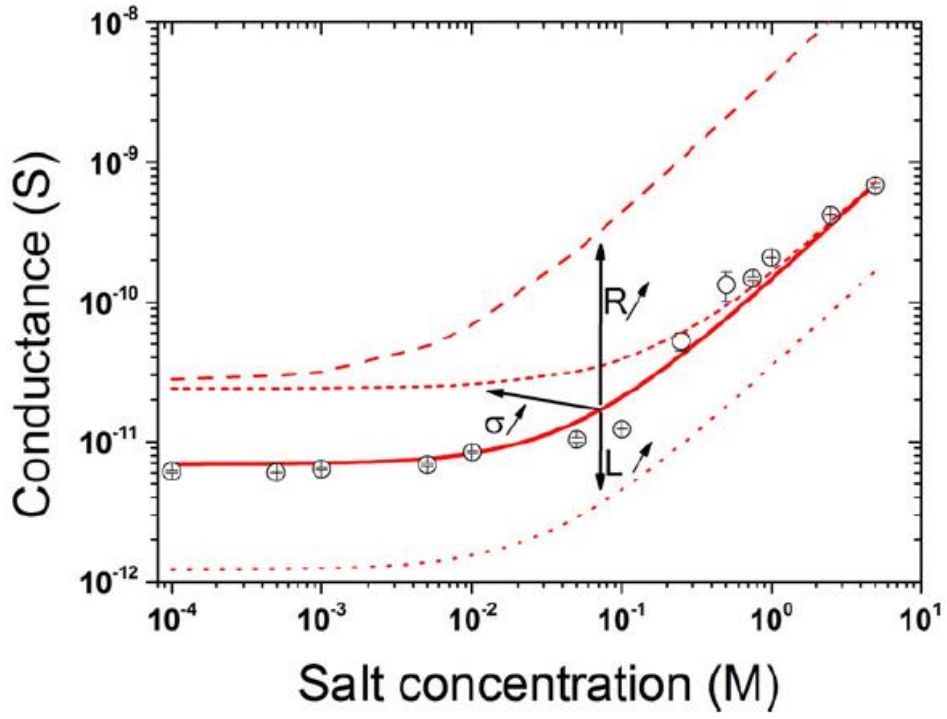

Fig. 14 Schematic behavior of a nanopore conductance as a function of the electrolyte concentration 1:1 (NaCl or KCl type). In full line is repported the fit using Eq. (31) and in dash lines are reported the impact of an increase of the surface charge density σ, the radius R or the length L of the nanopore on its conductance[97].

At high electrolyte concentrations, the conductance is contributed by ions in bulk solution inside the channel; while at low electrolyte concentrations, counter-ions in diffuse layer of EDL contribute essentially. When the two terms equal, a concentration C_t can be found as $0.5C_e$, where C_e is the concentration of excess mobile counter-ions.

3.3.4 Ion current rectification

Until now, all the nanochannels considered have a symmetric geometry and a homogeneous charge distribution. It means that under a positive or negative voltage (opposite direction), ionic current remains the same. While if we break the symmetry by considering nanochannel with dissymmetrical shape or heterogeneous distributed surface charge, the direction change of electric bias will cause a current change known as ion current rectification[193].

When a nanochannel has an asymmetrical shape such as conical, bullet-like, funnel geometries, the consequence is that the different cross sections of the two sides cause different conductances. For a conical channel, if the voltage drives counter-ions from the large side (base) to the small side (tip) (Fig. 15 a), the quantity of counter-ions entering in channel is larger than that getting out because of the different cross section area[194]. Thus an accumulation of counter-ions appears inside the channel close to the tip. To ensure the electroneutrality, co-ions will also accumulate in the same region. So both counter-ions and co-ions concentrations increase at tip which leads a global augmentation of channel conductance standing called open state. If the voltage is inversed (Fig. 15 b), with the same principle, ion depletion will take place in channel inducing a lower conductance called a closed state.

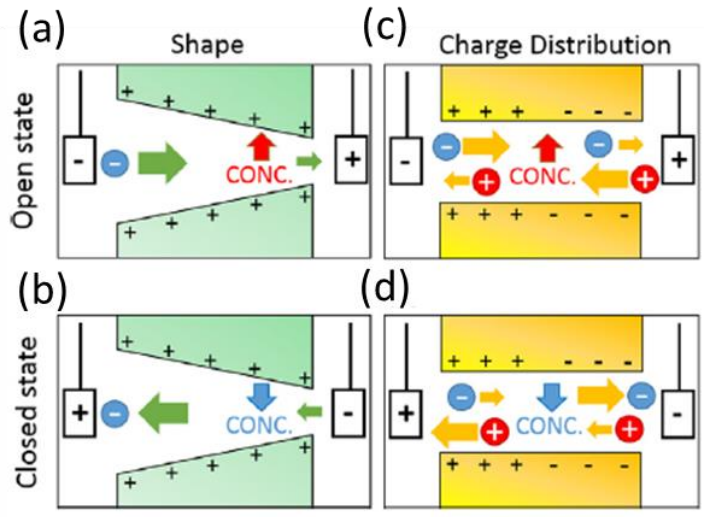

Fig. 15 Ion current rectification behavior due to asymmetry from (a) and (b) shape and (c) and (d) charge distribution. For (a) and (c), ions are accumulated in channel corresponding to an open state and for (b) and (d), ions are depleted in channel corresponding to a closed state[195].

In the case of asymmetrical surface charge distribution, the channel will also be opened or closed due to ion accumulation and ion depletion[195]. An example is shown in Fig. 15 c and d, a cylindrical channel has positive charges on the left and negative charge on the right. When the positive potential is applied on the side of negative charges (Fig. 15 c), both cations and anions can enter in the channel[195].However they have difficulties to get out because of the opposite charges compared to their entrance. An accumulation of anion and cation occurs, and thus, the pore will have an open state. Conversely, when the applied voltage is opposite, both cations and anions have difficulties to enter facing a large electric repulsion. The ion depletion that occurs in channel leads to a closed state.

The asymmetrical conditions of shapes and/or charge distributions are at the origin of ion current rectification. The amplitude of the phenomena is influenced by channel properties and electrolyte solution conditions. The ratio between pore diameters of two sides and surface charge density are two straightforward parameters. Additionally, the ion valence[196], and the ion adsorption on inner wall[9] are also reported experimentally and theoretically that can change the rectification behavior. As the rectification can be easily measured using an amplifier and can be influenced by a variety of parameters, it is thus a useful signal output for characterizing of ion-sensing, molecule-sensing, stimuli-responsiveness etc. in a channel.

4 Applications of polymer and PEs functionalized track-etched nanopore

As described in part 1, precise and systematic operations happened on cell membranes play a crucial role in life activities. Channel and pump proteins allow ions or molecules to pass through the membrane along or against concentration gradient, by direct diffusion or assisted transport respectively. Their opening or enclosure can be controlled by electric signals[108], the bind of a cargo[197] or other stimulus like pH[198], light[199] and temperature[200]. Bio-inspired functionalized solid-state and polymer nanopores can mimic these biological membrane proteins. With recent progresses, track etched nanopores become an important

platform for these applications thanks to their various pore geometries, simplicity to functionalization, the possibility to upscale from a single to multipore membrane and relatively low cost. In section 2, we discussed the properties of macromolecules especially stimuli-responsive polyelectrolytes and biomolecules that can change their conformation in response to external environmental changes. They are good candidates for track etched nanopores functionalization to mimic biological channels such ion pumps for energy uses and to involve specific interactions for biosensing.

4.1 Stimuli-responsive ion channel

Polyelectrolytes immobilized inside track-etched nanopores can change their charge density, effective thickness and/or structural conformations in responds to external stimuli such as pH, electrical potential, UV-Vis light and temperature. They were considered to achieve smart controllable artificial ion channels

4.1.1 pH responsive channels

The pH responsive ion channels are the most investigated for polyelectrolytes functionalized track-etched nanopores because of the general pH sensibilities of polyelectrolytes with weak cationic or anionic groups or both. The pH responsive ion gates based on steric effect of polymer brushes by changing polymer charges have been widely reported. Xia *et al*. grafted DNA brushes inside of PET conical nanopores by EDC/NHS chemistry[201]. When solution pH is at 4.5, DNA molecules take a dense packed rigid i-modif structure which has a larger effective size. While at pH 8.5, the DNA brushes get more charges and turn into a loosely packed single strand. This transition reduces the effective size of DNA molecules that enhances the pore diameter which is confirmed by a higher ionic conduction.

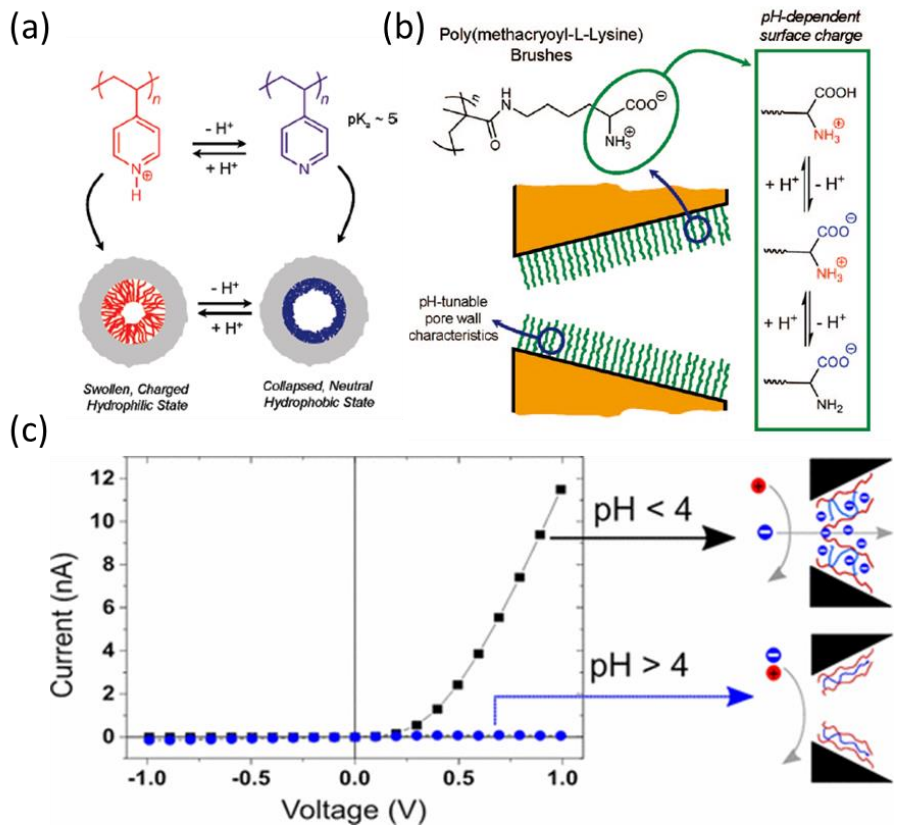

Fig. 16 pH-responsive nanochannels. (a) P4VP functionalized nanochannel[202], (b) PMALys functionalized nanochannel[203], (c) PEI/ChS layer-by-layer functionalized nanochannel[9].

Yameen, *et al*. used hydrophilic/hydrophobic effect of weak cationic polymer brushes (poly (4-vinyl pyridine) (P4VP))[204] (Fig. 16 a) and zwitteronic effect of polyampholytes brushes[205] (poly(methacrloyl-L-Lysine) (PMALys)) (Fig. 16 b) to construct different ion channels. The P4VP brushes were grafted in a cylindrical PET nanopore. At pH 2, the nitrogen atom of pyridine gets a proton to be positively charged. With the electro-repulsion, hydrophilic polymer chains take extended configuration to reduce the pore diameter. When pH is greater than 5.0, pyridine is deprotonated to be hydrophobic that makes polymer chains fold on the pore surface to open the pore spatially. PI nanopores functionalized by PMALys tune ionic transport by different surface charges in different pH. As PMALys has both carboxylic groups (-COOH) and amine groups (-NH_3), at different proton concentrations, the polymer charge can be positive, negative or zwitterionic. The different charged states modulate the selectivity of the channel. The same principles by using polyampholytes to design pH responsive ion channels are widely applied by several groups in PC conical nanopores[202,206]. The amphipol containing carboxylic acids and tertiary amines were immobilized on the tip

side of conical nanopore which is firstly coated by a gold layer[206]. Positive charges of amine in acidic condition give the pore selectivity to anions while negative charges of carboxylic acid in basic allow it selective to cations. The same polyampholites functionalization was also confirmed by direct polymerization of poly(3-aminephenylboronic acid) inside the pore[202]. More interestingly, because of negative charges due to the binding between boronic acids and cis-diols, this channel can be modulated by fructose which makes the pore more selective to cations with higher monosaccharide concentrations.

Recently another method to design pH responsive ion channels by using layer-by-layer deposition of polyelectrolytes in single nanopore[9] is studied by our group as shown in Fig. 16 c. The layer-by-layer embedded polyelectrolytes introduce both charges and swelling/deswelling properties into the pore. By alternating deposition of polyethylenimine (PEI) and chondroidine sulfate (ChS), a pH and ion strength double controlled channel was obtained. At low salt concentrations, the channel is closed at pH > 4 because of the charge compensation at pH < 4 the nanopore is open and selective to anions because of the global positive charge. At high salt concentrations, the swelling of the polyelectrolytes makes the pore not responsive to pH anymore.

4.1.2 Potential responsive channel

As ion channels play an essential role in regulating cell membrane potential, biomimetic potential responsive nanopore draw interests of researchers. Buchsbaum *et al.* reported a DNA-modified conical nanopore as pH- and voltage-responsive ion gate[207]. The DNA molecules have uniform negative charges at pH 5.5 while they became zwitterionic electrostatic mesh at pH 8. As shown in Fig. 17 a, negatively charged DNA functionalized conical nanopore does not obey the usual behavior. Indeed according to the surface charge, the current should be lower at positive voltages than at negative voltages because of the ion selectivity. This phenomenon was explained as at positive voltage, negatively charged DNA strands are deflected to the base side which opens the pore. While at negative voltages, the inverse movement of DNA molecules blocks the pore. This movement of the long charged polymer chain provides a possibility of potential direction sensing. This is similar to another potential responsive channel using DNA as functions in conical nanopore by Nguyen et *al*.[203] In this research, at negative electrical bias, two states have been observed. At moderate voltage around 2 V, ionic concentrations become higher which reduces DNA's extension;

while at high voltage around 3 to 4 V, DNA molecules become extended by high electric field leading to a small current.

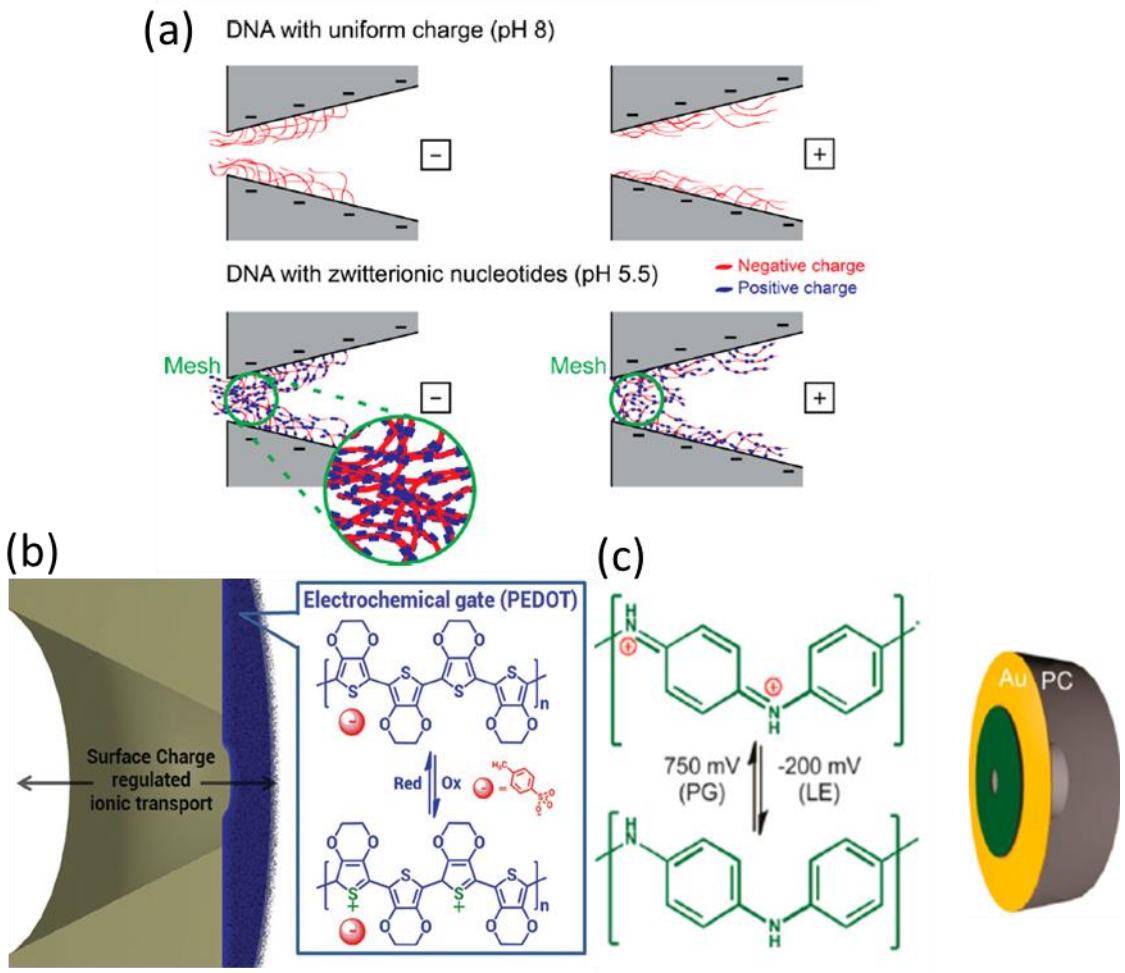

Fig. 17 Potential responsive nanochannels functionalized by (a) DNA[207], (b) PEDOT[208] and (c) PANI[209].

Perez-Mitta, et *al*. developed series of potential field effect ionic diodes by using conducting polymer. Two strategies were used, one by electrochemical polymerization of polyaniline (PANI)[209] and the other by coating a poly(3,4-ethylenedioxothiophene) (PEDOT)[208] layer (Fig. 17 b and c). Both of them use the electric conducting properties of polymers with conjugated double bonds in oxidation state. For PANI under original form, low proton binding degree equals to a low charge density. When 0.2 V is applied, the PEDOT pass to oxidized form with a high positive charge density. This transition makes the pore surface more hydrophilic that a higher conductance was observed. PEDOT has the same behavior while two oxidations are found to occur with an external potential of 0.2 V and 1.6 V by

cyclic voltammetry. The oxidation creates an electron vacancy as a default (p-type) in semi-conductors which contribute to the electron conducting known as anion-doping. Conversely, a reduction form under -0.5 V makes the polymer as n-doping or cation-doping. These oxydo-reduction changes were characterized by I-V dependence.

4.1.3 Light UV-Vis responsive channel

The transformation of visible light into electrical nerve signal makes Mammalia animals able to perceive the world by eyes. Rod and cone cells in retina play the job with the help of numerous photon sensitive ion channels controlled by retinol/retinal known as vision cycle. Many studies based on nanopores were design to mimic such light-responsive channel based on photo-switchable molecules like cumarine[210], azobenzene[211], spiropyran[212,213], etc. The combination of these photo-switchable molecules with polymers was also investigated in track-etched nanopore.

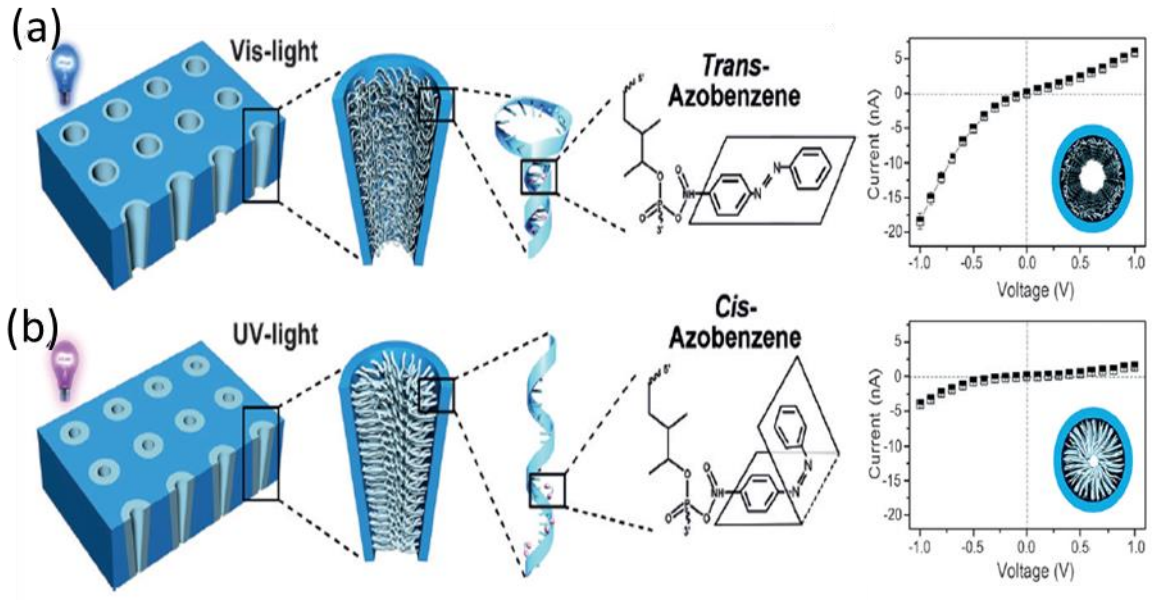

Fig. 18 UV-Vis light-responsive nanochannel functionalized by azobenzene-DNA in (a) Vis light and in (b) UV light[214].

Li, et *al*. combined azobenzene with DNA molecules as nanopore functions[214]. As shown in Fig. 18, chemically modified DNA chains by azobenzene are immobilized on surface of conical pore by Au-thiol chemistry. Under visible light, azobenzene molecules adopt a *trans* conformation which makes DNA chains collapse into hairpin structure. Thus the effective pore diameter is enlarged as characterized by a high ionic conductance. While under UV light,

the *cis*-azobenzene helps DNA to recover the relaxed, extended form. This leads to a closing state of the channel. Therefore by changing irradiation wavelength between visible light and UV light, the pore can open and close to modulate the transport. This photo switchable molecule-polymer cooperative control can amplify the difference between closure and opening state. This signal difference between two states is much higher compared to only photo switchable molecule functionalized channels where they are gated by photo induced surface wetting/dewetting[213] or surface hydrophobicity/hydrophilicity[215].

4.1.4 Temperature responsive channel

Temperature sensibility is one of the life being's ability. Biomimetic thermal controllable ion channels based on track-etched nanopore functionalized with polymer were designed according to two strategies. The first one involves temperature sensitive polyelectrolytes functions and the second one thermal controlled host guest interaction.

As described before, certain polyelectrolytes can react to temperature change by showing conformation variations. The most studied is poly(N-isopropylacrylamide) (PNIPAAM) that has a phase transition from a swollen hydrated state to a shrunken dehydrated state at lower critical solution temperature (LCST) about 32°C. This transition can be used to modulate ion transport in nanopore. Nasir *et al*. immobilized covalently PNIPAAM chains in a cylindrical and a conical nanopore membrane[216]. The two polymer states were characterized by ionic transport velocity of ionic molecules containing methylviologen (MV^{2+}) and 1, 5-naphthalenedisulfonate (NDS^{2-}). After PNIPAAM modification a clear increase of both ionic molecules transport rate was observed for both two nanopore geometries while it is more accented for conical pores. At low temperature, PNIPAAM chains behave like extended brushes which decrease the pore size; at high temperature, a pore opening happens as PNAPAAM becomes more hydrophobic and collapse to the surface. A very good reversibility was also tested by changing alternately the temperature between 39°C and 23°C. Then with the same thermal control principle, Liu et *al*. used azo-PNIPAAM and azo-poly-L-lysine (azo-PLL) to decorate a 3-amino-3-deoxy-α-cyclodextrin (α-CD) modified cylindrical nanopore by azo/α-CD host guest interactions[217] (Fig. 19 a). The latter is ultra-stable for a pH range from 4 to 10 and for a temperature range from 25°C to 40°C. Because of the bi-function of PLL and PNAPAAM, the ion transport can be modulated by both pH and temperature changes. Polystyrene block-poly(N,N-dimethylaminoethylmethacrylate) (PS14000-b-PDMAEMA3600)

is another thermo sensitive polymer. It was used to functionalize track-etched membrane by Zhang *et al.*[218]. As shown in Fig. 19 b, by measuring I-V curves, a LCST was found between 45°C to 50°C for the membrane undergoing swelling in ethanol and drying.

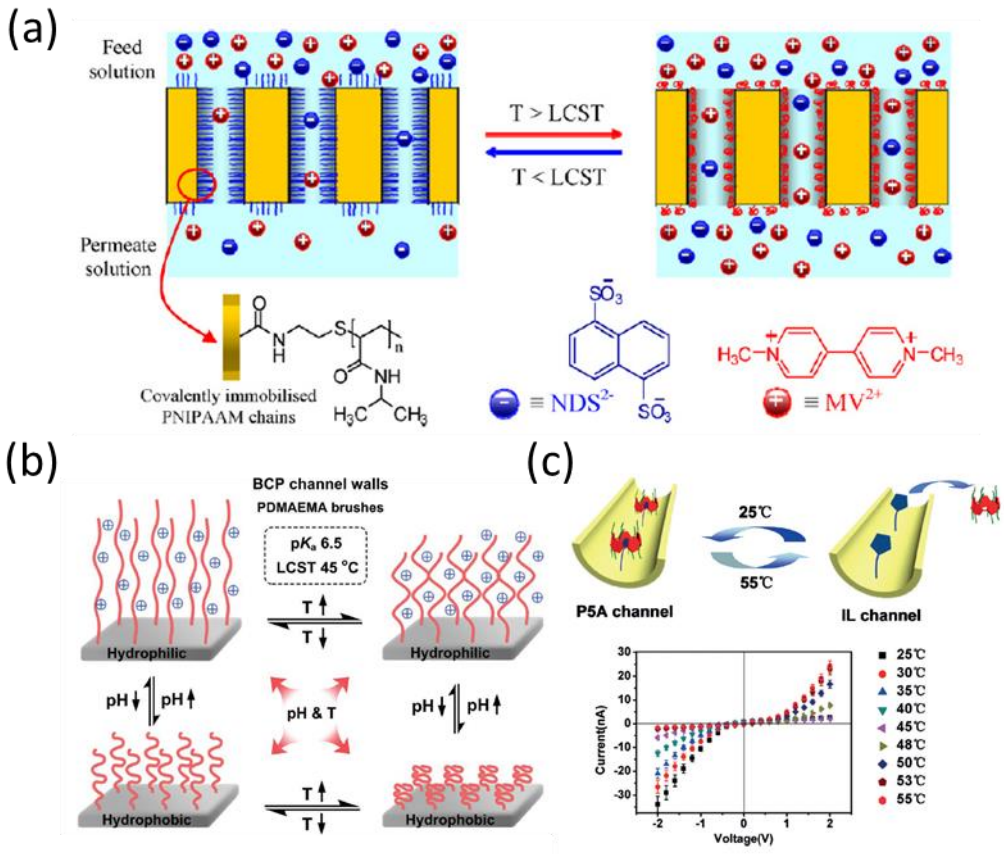

Fig. 19 Thermal-responsive nanochannel functionalized by (a) PNIPAAM brushes in solution of MV^{2+}/NDS^{2-},[216] (b) PDMAEMA brushes[218] and (c) P5A/IL host-guest[219].

Beside thermal sensible polyelectrolytes, another strategy was proposed by Wang *et al*. using host guest interactions to construct temperature-sensitive artificial channels[219]. The inner wall of nanopore was modified by ionic liquid molecules (IL). As shown in Fig. 19 c, an inversion of current rectification appears when a pillar[5]arebe (P5A) molecules self-assemble at 25°C onto the IL molecules by changing the surface charge from negative to positive. When the temperature rises to 55°C, the departure of the guest P5A molecule happens as shown in Fig. 19 c that the anionic transport channel returns to a cationic transport channel. This thermal energy controls host guest self-assembly interactions.

4.2 Ion gate

On cell membranes, ion channels are extremely selective for transporting corresponding ions. These ion-channels inspired people to develop ion sensing channels which can modulate their ion transport behaviors with presence of specific ions. The principle is that ions should bind to the channel surface specifically. To achieve this purpose, three strategies were investigated in track-etched membrane. The first one is ion binding by crown ether. The second one is ion binding by DNA, peptide or polyelectrolyte chains and the last one is by ion involved construction/destruction of a macrostructures inside the pore.

4.2.1 Crown ether cage approaches

Ethylene glycol crown ether containing several repeat units of -(O-CH2-CH2)- can form a cavity cage which has a comparative diameter with alkali metal ions (Fig. 20). The electron-rich oxygen atom on the circle permits the binding of positive ions. With these two properties crown ethers become one of the best molecules to bind alkali metal ions. More excitingly, 4'amninobenzo-18-crown-6 (4-AB18C6), 4'amninobenzo-15-crown- (4-AB15C5) and 4'amninobenzo-12-crown-4 (4-AB12C4) have the corresponding size for K^+, Na^+ and Li^+.

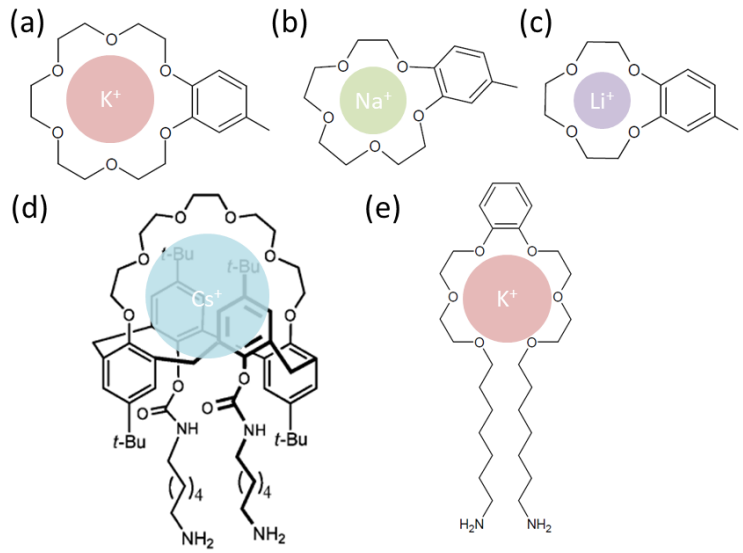

Fig. 20 Crown ether cage molecules (a) B18C6, (b) B15C5, (c) B12C4, (d) t-BuC[4]C, (e) bis-pod and and their corresponding alkali metal ions.

All of them were grafted inside track-etched nanopore. For K^+ sensing by 4-AB18C6 was achieved in three pore geometries. Perez-Mitta *et al*. grafted 4-AB18C6 by EDC/NHS chemistry in a bullet-like nanopore[220]. The I-V curves measured in 0.1 M KCl and NaCl

solutions showed a K^+ driven rectified anions transport which means a stronger binding effect for K^+ than Na^+. The same crown ether was studied by Wu *et al*. in a funnel-like nanopore[221]. The same behavior was reported. K^+ binds to 4-AB18C6 at voltage below 3 while at 3 V, the departure of K^+ outside of crown ether occurs. This K^+ binding/voltage cleaning was confirmed with a good reversibility. The conical nanopore functionalized with the same group with 4-AB18C6 and 4-AB15C5 was considered for K^+ and Na^+ sensing[222]. K^+ and Na^+ are specifically bind to 4-AB18C6 and 4-AB15C5 with a minimum sensitivity about 1 nM. The reversibility of this experiment was achieved by using [2.2.2]-crypt and which has a higher binding energy with cations than the crown ether of 4-AB18C6. For smaller alkali ions, the Li^+, Ali *et al*. achieved its detection using in a conical pore functionalized with 4-AB12C4[223]. The 4-AB12C4 bind much better of Li^+ than others monovalent cation including K^+, Na^+, Rb^+ and Cs^+ because of its cavity size. beside crown ethers, other molecules with similar structures were also reported like bis-podand for K^+[224] and p-tert-butylcalix[4]arene-crown (t-BuC[4]C) for Cs^+[225].

4.2.2 Polymer approaches DNA/Peptide

DNA strands peptides and polyelectrolyte with specific binding sites can also capture specific cations. Hou *et al*. investigated a G-quadruplex DNA binding of K^+ in track-etched nanopore[226]. As shown in Fig. 21, the G-rich DNA chains chemically immobilized in conical pore can combine K^+ ions to form a cuboid confined space. This K^+-induced structure formation is confirmed by an unusual low current level at 2 V for a concentration from 500 μM to 750 μM compare to Li^+. At this range of K^+ concentration, the as described G structure makes DNA brushes denser that decreases the pore size. The same group also investigated nanochannel functionalized with peptide and single-stranded DNA. The binding ability comes from the specific sites along polymer chains. The peptide chains contain Cys_2His_2 residues that can capture Zn^{2+}[227] while the DNA chains that contain an ion-specific thymine-thymine (T-T) base can form stable T-Hg^{2+}-T complexes[228]. The later complex can be broken by cysteine.

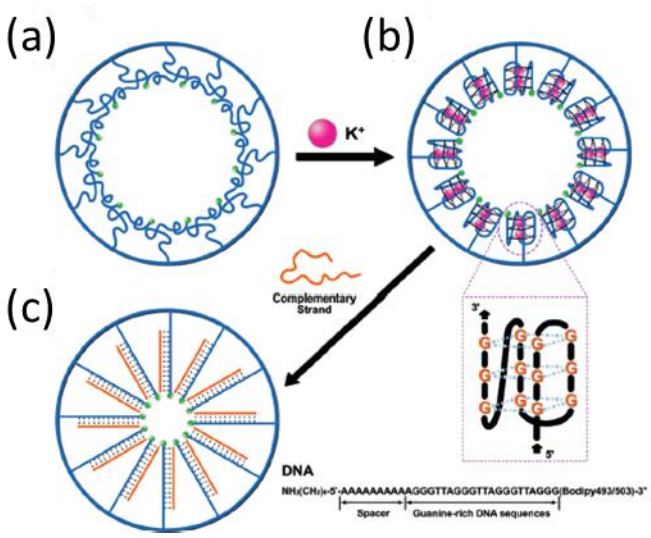

Fig. 21 G4 DNA functionalized K^+ sensor. (a) Loosely packed single-stranded DNA without K^+. (b) Densely packed rigid quadruplex structures with K^+. (c) K^+ departure with participation of complementary strand[226].

4.2.3 Reversible self-assembly of macro structure

Another strategy to detect ions is the reversible self-assembly of a macro structure inside nanopore thank to the presence of ion. This macro structure controlled by ions can be considered as a signal amplifier. Zhang *et al.* proposed a Pb^{2+} sensible ion channel based on DNAzyme[229] (Fig. 22 a). Briefly, DNAzyme molecules containing DNA chain and RNA chimera where an adenine nucleoside (rA) is the cleavage site were immobilized from the base side of conical pore by Au-thiol chemistry. The long chain DNA molecules decrease the effective pore size which corresponds to a closed state. When Pb^{2+} ions come into the system, DNA chains are cleaved into two short fragments at the rA site. This degradation effect of Pb^{2+} on DNA long chain will destroy the channel gate that leads the pore to an open state.

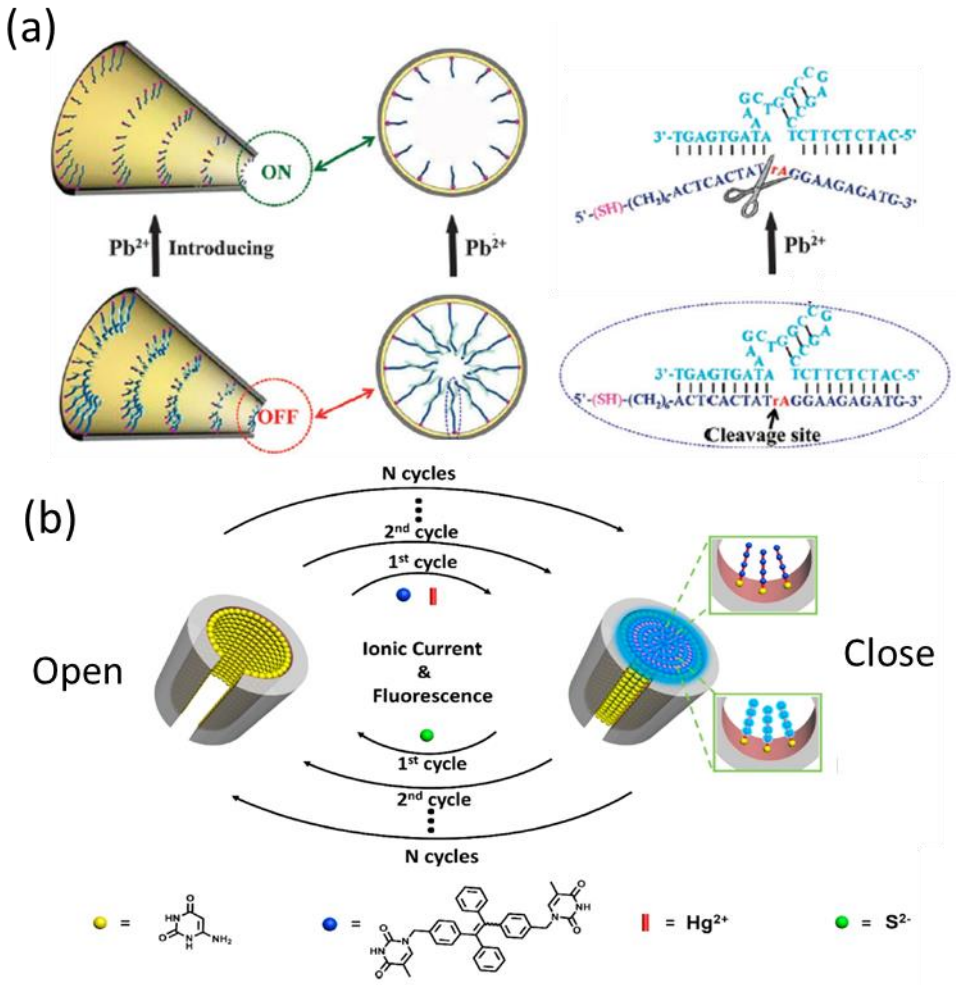

Fig. 22 Ions sensing by macro structure construction/destruction. (a) DNAzyme functionalized nanochannel between on and off state with Pb^{2+} due to its cleavage effect[229]. (b) TPE-2D/$Hg2^{+}$ formed macro structure and its destruction by S2- as Hg^{2+}/S^{2-} sensor[230].

The similar principle was investigated by Lou *et al.*[230]. In a cylindrical pore, a layer of 6-amino-uracil molecules was firstly grafted on the nanopore inner wall. Based on the specific molecule-ion bindings, they used (1,1′-(((1,2-diphenylethene-1,2-diyl)bis(4,1-phenylene))bis(5-methylpyrimidine-2,4(1H,3H)dione))) (TPE-2D) and Hg^{2+} as "bricks" to build a 3D macro structure inside the pore (Fig. 22 b). The pore size is extremely shrunken, thus a closed state was achieved in the presence of Hg^{2+}. An opposite effect was obtained by S^{2-} that destroy the macro complexes because of the extreme high binding force between Hg^{2+} and S^{2-} due to low solubility of H_gS (K_{sp} = 1.6 x 10^{-52}). The whole procedure was proved by both current and fluorescence measurements.

4.3 Molecule sensing

4.3.1 Steady state sensing

Steady state sensing is based on surface state changes in nanopore due to the target molecules. The surface state changes are mainly achieved by the charge or effective pore size. It modulates the ion transport characterized by current rectification and/or the pore conductance. To do so, specific functional groups are required inside nanopore to provide specific interactions with the target molecules. These interactions can be various including bioconjugated binding, nucleic-acid hybridation, enzyme-substrate reaction, or small molecule trigging. With polyelectrolytes as functional groups, all of the above principles of sensing were considered in track-etched nanopores. With the simplicity of surface functionalization and the various pore geometries the track-etched nanopores make a robust platform for stead sate sensing.

4.3.1.1 Sensing by small molecule trigging

As macromolecules can form molecule cage to trigger ions, the same principle can be also performed for small molecules. Li *et al*. have investigates immobilized sequence-specific aptamers (SSA) as probes inside a conical nanopore to detect adenosine[231]. Due to the binding effect of the specific nucleotide sequence to adenosine, SSA can form a stable complex that adenosine molecules are wrapped by nucleotide chains. The chain folding leads to a pore opening that induces a higher current under $\pm$2V than extended DNA probes. The cocaine was detected by Wang *et al*. using a capture bullet-like nanopore functionalized with an aptamer[232] (Fig. 23 a). In this work, a bodipy493/503-modified target DNA aptamer was added with cocaine. The latter is inserted into the partially hybrid structure. This sandwich complex of probe-cocaine-aptamer modulates the ion transport with a high current change ratio measured at +2V. This is enough to identify cocaine from other molecules with similar structures such as tropinone, atropine and glucose.

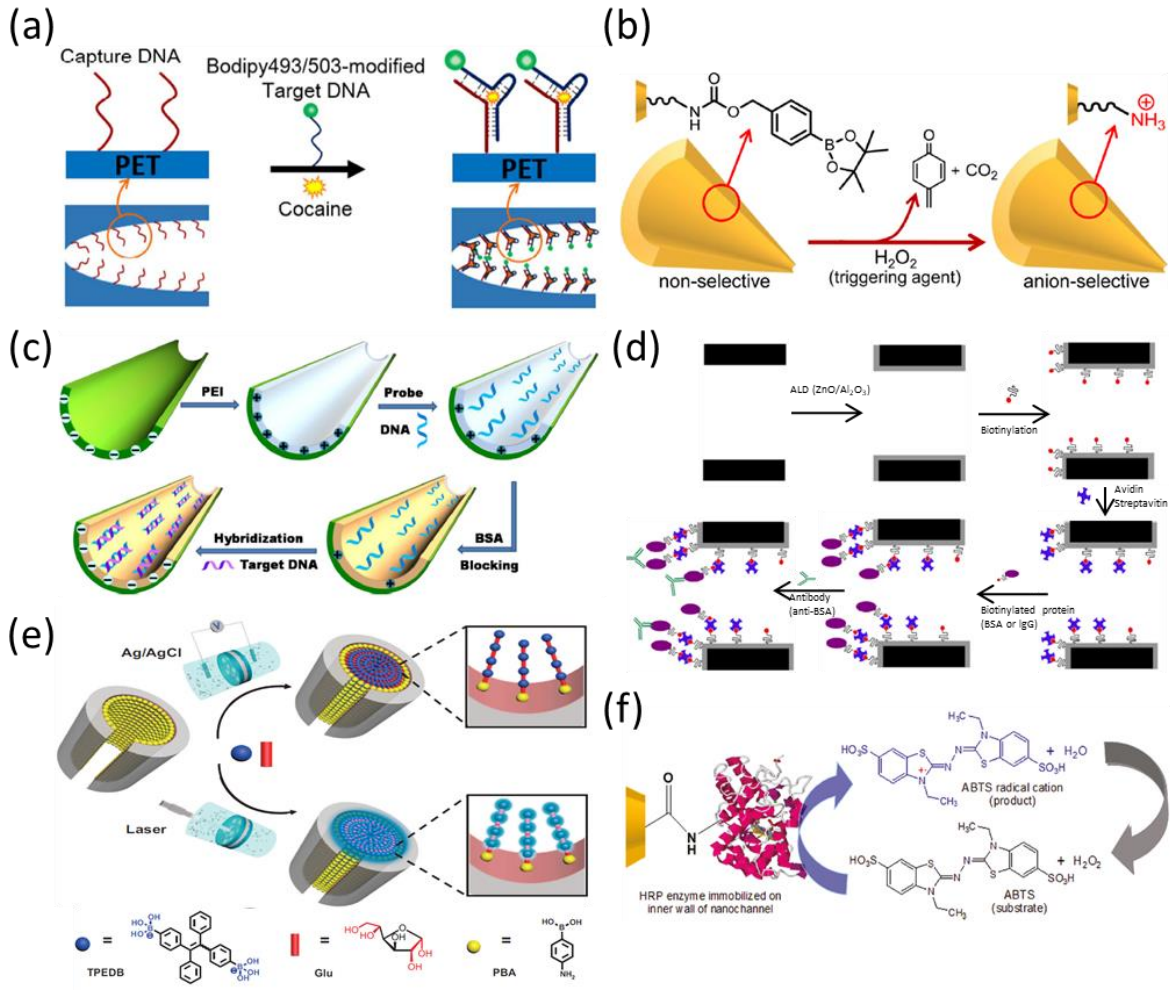

Fig. 23 Molecule sensing by (a) small molecule trigging: cocaine molecules triggered in DNA probe[232], (b) molecule-functional group reactions: H_2O_2 oxidation of BEC[233], (c) nucleic acid hybridations: DNA probe and target DNA hybridation[234], (d) bio-molecular recognitions: recognition of biotin/avidin and protein/antibody[235], (e) macro structure constructions/destructions: TPEDB and Glu for 3D constructions[236], (f) enzyme-substrate reactions: HRP enzyme with ABTS[237].

4.3.1.2 Sensing by molecule-functional group reaction

The molecule sensing can be based on chemical reactions between functional groups and target molecules. Oxidation can be a good example to illustrate that. Ali *et al*. have grafted boronic ester carbamate (BEC), a reductive molecule, inside a conical nanopore to detect hydrogen peroxides (H_2O_2)[233] (Fig. 22 b). Due to the strong oxidation ability of H_2O_2, it can break carbamate bonds to expose the amine moieties. The nanopore surface changes from relatively hydrophobic to hydrophilic and positively charged. Another interesting research

based on peptides functionalized conical nanopore was done by Xiao, et *al*. [238]. In this paper, the peptide contains CGGC sequences, in which thiol groups can be oxidized to form a disulfide bond. The peptide chain was then forced to fold because of the S-S bond. Therefor an O_2 sensor was achieved sensitive to a concentration at least 0.91 mg/L.

4.3.1.3 Sensing by nucleic acid hybridization

Hydrogen bond is the inter-molecular interaction responsive to the nucleic acid structure. It is the key for DNA/RNA hybridation. Ali et *al*.[239] and Sun et *al*.[234,240] have developed a method to detect the DNA/RNA mismatch based on nucleic acid hybridization using conical pore. Briefly, single strand probes such as phosphodiamidate morpholino-oligos (PMO), peptide nucleic acid (PNA) and DNA were firstly grafted onto the channel inner surface. Then BSA was used to cover the rest of pore surface to prevent the non-specific adsorption. Finally, all complementary DNA or RNA strands without as well as with one or two base mismatchs were added to the nanopore sensor. As shown in Fig. 23 c, as the complementary strands form more hydrogen bonds, more probes will be hybridized compared to the ones with mismatch. Due to the high charge density of the back bones of target chains, an enhanced selectivity to cation transport (ion current rectification (ICR) change) will be measured as consequence. It is also confirmed that the number of base mismatches on target has a quantitative relationship with ICR changes.

4.3.1.4 Sensing by bio-molecular recognition

In biology systems, specific bio-molecular recognition plays an important role in such as immune-response, ligand mediated cell activation, cell communication and embryogenesis. Biosensors inspired by ligand-gated ion channel have been largely developed using track-etched nanochannels. The general ideal is that one a probe is immobilized on the pore surface and then a target biomolecules with specific recognitions can be bounded. The specific binding of target molecules can be shown by the behavior change of ionic transport. Ali's group has reported numerous of system based on that concept. A streptavidin sensor was prepared by grafting biotin-PEO3-Amine in a conical pore[241]. The strong and specific biotin-avidin interaction ensures the accurate detection of streptavidin was characterized by a change of I-V curves that did not happen for lysozyme and BSA. A sensor of Concanavalin A (Con A) based on sugar-lectin interactions was achieved by grafting horseradish peroxidase

(HRP) in nanochannels of two geometries[242]. Blocking effect in cylindrical pore was observed by a decrease of pore conductance. In addition a change of current rectification was shown in conical pore because of the modification of surface state due to the specific binding. Another sensor to detect Con A was also achieved using lectin-carbohydrate interaction in bullet-like pores by grafting p-aminophenil α-D-mannopyranoside (APMP)[243]. The sensor was confirmed by its specificity to bind Con A compared to lysozyme and BSA. By using mannose, the sensor can be used re-used. Our group has proposed a reversible PLL-PEG biotin functionalized nanopore. It shows a reliable ability to detect streptavidin with a very quick functionalization procedure[244]. To go further from that, another system of "multi-step biosensing" was also demonstrated by our group on combining biotin-avidin and protein-antibody interactions by successively grafting PEG-biotin, avidin, biotinylated protein and antibody[245] (Fig. 23 d). This complex building shows possibility to design multiple steps, multiple targets sensing process using bio-molecular recognitions.

4.3.1.5 Sensing by macro structure construction/destruction

Similar to principles reported in section 4.2.3, sensing by macro structure reversible self-assembly can be also applied for molecules. A macro structure can sterically block the pore to reduce ionic conductance confirming the presence of target molecules. F. Xia, *et al*. used DNA molecules as bricks to build long DNA chains using DNA linker and one signal probe for ATP sensing[246]. The probe DNA was firstly immobilized in pore. Then, the signal probes with aptamer sequence and DNA linkers were added to the system. The signal probes and DNA hybrid linkers together to form a long chain which can block the channel by steric effect. When target molecule was added, a strong binding interaction between aptamers and ATPs make the long chain breakup leading to the pore opening. A dense macro structures were designed by Lou et *al*. using ((1, 2-diphenylethene-1, 2-diyl) bis (1, 4-phenylene)-1, 1'-diboronic acid (TPEDB)) and glucose in a capture probes (4-aminophenylboronic acid (PBA)) modified cylindrical nanopore for glucose sensing[236] (Fig. 23 e). In this PBA functionalized nanopore, if the solution contains glucose, it can be combined with TPEDB under laser to form a 3D structure. Another 3D DNA keepers using Y-DNA, ATP aptamer as probe and linker DNA for ATP and DNase I were proposed by Guo, et *al*.[247]. Both of them used target molecules as building blocks for constructing signal amplifiers.

4.3.1.6 Sensing by enzyme-substrate reaction

A specific biochemical reaction as enzymatic reaction with corresponding substrate was as well investigated for biosensing in track-etched nanopore. Ali and co-workers successfully immobilized horseradish peroxidase (HRP) in a conical pore[237] (Fig. 23 f).If there is H_2O_2 in the solution, the immobilized HRP enzyme can be activated by H_2O_2 turning to be an oxidative form. The oxidative HRP enzyme can then oxidize substrates of 2, 2'-azino-bis (3-ethylbenzothiazoline-6-sulphonic acid) (ABTS). Finally, the resulted ABTS radical cations can decrease the current under +2V because of its positive charges. The sensibility can reach 10 nM of H_2O_2. Moreover, a urea sensing was achieved by Pérez-Mitta et *al*. using physical adsorbed PAH-Urease in bullet-like nanopores[248].

4.4 Energy conversion

Biomimetic ion channels can be a good candidate to improve the membrane for osmotic energy harvesting. The osmotic energy are harvested using two methods: the pressure retarded osmosis (PRO)[249,250] and the reversed electro-dialysis (RED)[38]. Even some facilities based on PRO technique are in working[250]; it still remains a lot of improvement. The RED utilizes ion selective membranes (IEMs). When ions diffuse selectively through IEMs driven by salinity gradient, the movements of the ion can generate electron flux by coupling redox electrodes. To get this electric current and transmembrane potential, high ion selectivity is requested to make sure that positive ions go for one direction while negative ions go oppositely. Thus a high charge density and a high charge asymmetry inside pores are required to modulate ion transport properties for high ion selectivity. The progresses on RED were done at the lab scale. High performance single pore were obtained by single boron nitride nanotube[158] with a single pore power of 20 pW and molybdenum disulfide 2D nanopore[150] of 500 pW. At multipore scale, dissymetrical membranes are also investigated recently[251]. The ion selectivity and membrane resistance are always two limiting factors for this technique. Researches based on track-etched nanopore/membrane functionalized by polyelectrolytes can be a good candidate because of the low cost, the good chemical, mechanical properties and the high ion selectivity involved by the high charge density of polyelectrolytes.

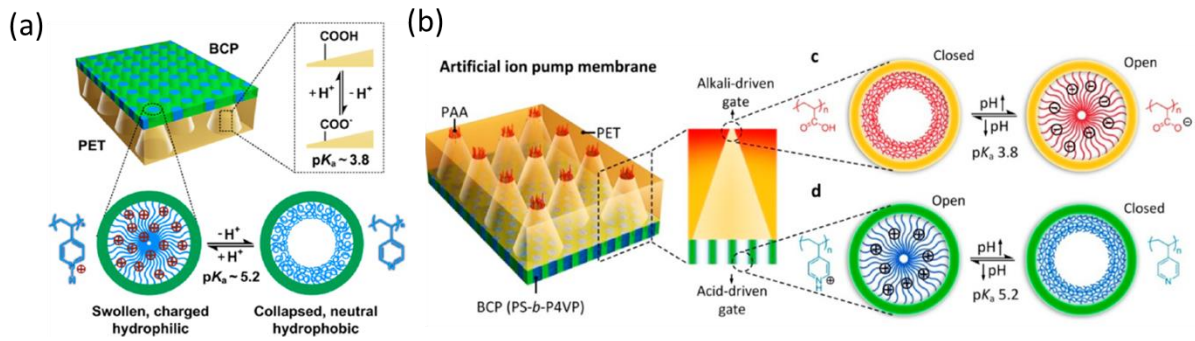

Fig. 24 pH controlled high ion selective nanochannels functionalized by (a) PS_{48400}-b-$P4VP_{21300}$ coating[252] and (b) PS-b-P4VP/PAA coating[253].

Wen, et *al*. developed series of heterogeneous membrane to perform as ion pumps[252]. A highly positively charged block copolymer (BCP) as polystyrene-b-poly(4-vinylpyridine) (PS_{48400}-b-$P4VP_{21300}$) is coated on the tip side of conical membrane as shown in Fig. 24 a. The success of this coating and the introduction of related high charge density are confirmed by an increase of pore conductance at low electrolytes concentration. As the track etched nanopore wall is covered by carboxylic acid groups which has negative charges at pH 7. The positively charged BCP layer and negatively charged track-etched pore wall form an ionic diode with ion rectification ratio as high as 1075 highly controlled by pH. A maximum power density of 0.35 W m^{-2} was reached using 0.5 and 0.01 M NaCl solutions. Then the same group designed a double gated hybrid membrane by coating a layer of BCP (PS-b-P4VP) on the base side of conical nanopore and grafting PAA at the tip side[253] (Fig. 24 b). Thus a pH gated ion pump is ready. By changing pH of two reservoirs separately, the pump shows different behaviors as alternating gates ion pump, pump-channel or fail-safe ion pump. The pore is highly selective to anions that can pump them unidirectionally. Well it can be good candidate for osmotic energy harvesting or desalination.

References

(1) Manning, G. S. Polyelectrolytes. Annu. Rev. Phys. Chem. 1972, 23 (1), 117–140. https://doi.org/10.1146/annurev.pc.23.100172.001001.

(2) Schoch, R. B.; Han, J.; Renaud, P. Transport Phenomena in Nanofluidics. Rev. Mod. Phys. 2008, 80 (3), 839–883. https://doi.org/10.1103/RevModPhys.80.839.

(3) McCormick, C. L. Stimuli-Responsive Water Soluble and Amphiphilic Polymers; American Chemical Society, 2000; Vol. 780. https://doi.org/doi:10.1021/bk-2001-0780.

(4) Bernards, M. T. 2 - Environmentally Responsive Polyelectrolytes and Zwitterionic Polymers; Zhang, Z. B. T.-S. and R. S. and M. for B. A., Ed.; Woodhead Publishing: Oxford, 2015; pp 45–64. https://doi.org/https://doi.org/10.1016/B978-0-85709-713-2.00002-X.

(5) Roman, J.; Français, O.; Jarroux, N.; Patriarche, G.; Bacri, L.; Pioufle, B. Le; Roman, J.; Français, O.; Jarroux, N.; Patriarche, G.; et al. Solid-State Nanopore Easy Chip Integration in a Cheap and Reusable Microfluidic Device for Ion Transport and Polymer Conformation Sensing To Cite This Version : HAL Id : Hal-01891773 Solid-State Nanopore Easy Chip Integration in a Cheap and Reusable Micro. 2018.

(6) Roman, J.; Français, O.; Jarroux, N.; Patriarche, G.; Pelta, J.; Bacri, L.; Le Pioufle, B. Solid-State Nanopore Easy Chip Integration in a Cheap and Reusable Microfluidic Device for Ion Transport and Polymer Conformation Sensing. ACS Sensors 2018, 3 (10), 2129–2137. https://doi.org/10.1021/acssensors.8b00700.

(7) de Gennes, P. G. Conformations of Polymers Attached to an Interface. Macromolecules 1980, 13 (5), 1069–1075. https://doi.org/10.1021/ma60077a009.

(8) Ma, T.; Gaigalas, P.; Lepoitevin, M.; Plikusiene, I.; Bechelany, M.; Janot, J. M.; Balanzat, E.; Balme, S. Impact of Polyelectrolyte Multilayers on the Ionic Current Rectification of Conical Nanopores. Langmuir 2018, 34 (11), 3405–3412. https://doi.org/10.1021/acs.langmuir.8b00222.

(9) Zhao, Y.; Janot, J. M.; Balanzat, E.; Balme, S. Mimicking PH-Gated Ionic Channels by Polyelectrolyte Complex Confinement Inside a Single Nanopore. Langmuir 2017, 33 (14), 3484–3490. https://doi.org/10.1021/acs.langmuir.7b00377.

(10) Xie, R.; Chu, L. Stimuli-Responsive Smart Gating Membranes. Chem. Soc. Rev. 2016, 45 (3), 460–475. https://doi.org/10.1039/C5CS00692A.

(11) Jochum, F. D.; Theato, P. Temperature- and Light-Responsive Smart Polymer Materials. Chem. Soc. Rev. 2013, 42 (17), 7468–7483. https://doi.org/10.1039/C2CS35191A.

(12) Bernards, M. T.; Cheng, G.; Zhang, Z.; Chen, S.; Jiang, S. Nonfouling Polymer Brushes via Surface-Initiated, Two-Component Atom Transfer Radical Polymerization. Macromolecules 2008, 41 (12), 4216–4219. https://doi.org/10.1021/ma800185y.

(13) Cao, B.; Li, L.; Tang, Q.; Cheng, G. The Impact of Structure on Elasticity, Switchability, Stability and Functionality of an All-in-One Carboxybetaine Elastomer. Biomaterials 2013, 34 (31), 7592–7600. https://doi.org/https://doi.org/10.1016/j.biomaterials.2013.06.063.

(14) Zhao, C.; Nie, S.; Tang, M.; Sun, S. Progress in Polymer Science Polymeric PH-Sensitive Membranes — A Review. 2011, 36, 1499–1520. https://doi.org/10.1016/j.progpolymsci.2011.05.004.

(15) Bulmus, V.; Woodward, M.; Lin, L.; Murthy, N.; Stayton, P.; Hoffman, A. A New PH-Responsive and Glutathione-Reactive, Endosomal Membrane-Disruptive Polymeric Carrier for Intracellular Delivery of Biomolecular Drugs. J. Control. Release 2003, 93 (2), 105–120. https://doi.org/https://doi.org/10.1016/j.jconrel.2003.06.001.

(16) Delcea, M.; Möhwald, H.; Skirtach, A. G. Stimuli-Responsive LbL Capsules and Nanoshells for Drug Delivery ☆. Adv. Drug Deliv. Rev. 2011, 63 (9), 730 – 747. https://doi.org/10.1016/j.addr.2011.03.010.

(17) Hester, J. F.; Olugebefola, S. C.; Mayes, A. M. Preparation of PH-Responsive Polymer Membranes by Self-Organization. J. Memb. Sci. 2002, 208 (1), 375–388. https://doi.org/https://doi.org/10.1016/S0376-7388(02)00317-4.

(18) Nunes, S. P.; Behzad, A. R.; Hooghan, B.; Sougrat, R.; Karunakaran, M.; Pradeep, N.; Vainio, U.; Peinemann, K.-V. Switchable PH-Responsive Polymeric Membranes Prepared via Block Copolymer Micelle Assembly. ACS Nano 2011, 5 (5), 3516–3522. https://doi.org/10.1021/nn200484v.

(19) Jochum, F. D.; zur Borg, L.; Roth, P. J.; Theato, P. Thermo- and Light-Responsive Polymers Containing Photoswitchable Azobenzene End Groups. Macromolecules 2009, 42 (20), 7854–7862. https://doi.org/10.1021/ma901295f.

(20) Feil, H.; Bae, Y. H.; Feijen, J.; Kim, S. W. Effect of Comonomer Hydrophilicity and Ionization on the Lower Critical Solution Temperature of N-Isopropylacrylamide Copolymers. Macromolecules 1993, 26 (10), 2496–2500. https://doi.org/10.1021/ma00062a016.

(21) Saeki, S.; Kuwahara, N.; Nakata, M.; Kaneko, M. Upper and Lower Critical Solution Temperatures in Poly (Ethylene Glycol) Solutions. Polymer (Guildf). 1976, 17 (8), 685–689. https://doi.org/https://doi.org/10.1016/0032-3861(76)90208-1.

(22) Ono, Y.; Shikata, T. Hydration and Dynamic Behavior of Poly(N-Isopropylacrylamide)s in Aqueous Solution: A Sharp Phase Transition at the Lower Critical Solution Temperature. J. Am. Chem. Soc. 2006, 128 (31), 10030–10031. https://doi.org/10.1021/ja063990i.

(23) Liu, H. Y.; Zhu, X. X. Lower Critical Solution Temperatures of N-Substituted Acrylamide Copolymers in Aqueous Solutions. Polymer (Guildf). 1999, 40 (25), 6985–6990. https://doi.org/https://doi.org/10.1016/S0032-3861(98)00858-1.

(24) Huo, M.; Yuan, J.; Tao, L.; Wei, Y. Redox-Responsive Polymers for Drug Delivery: From Molecular Design to Applications. Polym. Chem. 2014, 5 (5), 1519–1528. https://doi.org/10.1039/C3PY01192E.

(25) Minko, S. Responsive Polymer Brushes. J. Macromol. Sci. Part C 2006, 46 (4), 397–420. https://doi.org/10.1080/15583720600945402.

(26) Geniès, E. M.; Boyle, A.; Lapkowski, M.; Tsintavis, C. Polyaniline: A Historical Survey. Synth. Met. 1990, 36 (2), 139–182. https://doi.org/https://doi.org/10.1016/0379-6779(90)90050-U.

(27) Huang, J.; Virji, S.; Weiller, B. H.; Kaner, R. B. Polyaniline Nanofibers: Facile Synthesis and Chemical Sensors. J. Am. Chem. Soc. 2003, 125 (2), 314–315. https://doi.org/10.1021/ja028371y.

(28) Mantione, D.; Del Agua, I.; Sanchez-Sanchez, A.; Mecerreyes, D. Poly(3,4-Ethylenedioxythiophene) (PEDOT) Derivatives: Innovative Conductive Polymers for Bioelectronics. Polymers . 2017. https://doi.org/10.3390/polym9080354.

(29) Kumar, G. S.; Neckers, D. C. Photochemistry of Azobenzene-Containing Polymers. Chem. Rev. 1989, 89 (8), 1915–1925. https://doi.org/10.1021/cr00098a012.

(30) Beharry, A. A.; Woolley, G. A. Azobenzene Photoswitches for Biomolecules. Chem. Soc. Rev. 2011, 40 (8), 4422–4437. https://doi.org/10.1039/C1CS15023E.

(31) Bandara, H. M. D.; Burdette, S. C. Photoisomerization in Different Classes of Azobenzene. Chem. Soc. Rev. 2012, 41 (5), 1809–1825. https://doi.org/10.1039/C1CS15179G.

(32) Klajn, R. Spiropyran-Based Dynamic Materials. Chem. Soc. Rev. 2014, 43 (1), 148–184. https://doi.org/10.1039/C3CS60181A.

(33) Baker, R. W. Research Needs in the Membrane Separation Industry: Looking Back, Looking Forward. J. Memb. Sci. 2010, 362 (1), 134–136. https://doi.org/https://doi.org/10.1016/j.memsci.2010.06.028.

(34) Eriksson, P. Nanofiltration Extends the Range of Membrane Filtration. Environ. Prog. 1988, 7 (1), 58–62. https://doi.org/10.1002/ep.3300070116.

(35) Elimelech, M.; Phillip, W. A. The Future of Seawater Desalination: Energy, Technology, and the Environment. Science (80-.). 2011, 333 (6043), 712 LP-717. https://doi.org/10.1126/science.1200488.

(36) Khawaji, A. D.; Kutubkhanah, I. K.; Wie, J.-M. Advances in Seawater Desalination Technologies. Desalination 2008, 221 (1), 47–69. https://doi.org/https://doi.org/10.1016/j.desal.2007.01.067.

(37) Fair, J. C.; Osterle, J. F. Reverse Electrodialysis in Charged Capillary Membranes. J. Chem. Phys. 1971, 54 (8), 3307–3316. https://doi.org/10.1063/1.1675344.

(38) Turek, M.; Bandura, B. Renewable Energy by Reverse Electrodialysis. Desalination 2007, 205 (1), 67–74. https://doi.org/https://doi.org/10.1016/j.desal.2006.04.041.

(39) Vermaas, D. A.; Saakes, M.; Nijmeijer, K. Power Generation Using Profiled Membranes in Reverse Electrodialysis. J. Memb. Sci. 2011, 385–386, 234–242. https://doi.org/https://doi.org/10.1016/j.memsci.2011.09.043.

(40) Post, J. W.; Hamelers, H. V. M.; Buisman, C. J. N. Energy Recovery from Controlled Mixing Salt and Fresh Water with a Reverse Electrodialysis System. Environ. Sci. Technol. 2008. https://doi.org/10.1021/es8004317.

(41) Post, J. W.; Veerman, J.; Hamelers, H. V. M.; Euverink, G. J. W.; Metz, S. J.; Nymeijer, K.; Buisman, C. J. N. Salinity-Gradient Power: Evaluation of Pressure-Retarded Osmosis and Reverse Electrodialysis. J. Memb. Sci. 2007. https://doi.org/10.1016/j.memsci.2006.11.018.

(42) Katsuno, C.; Konda, A.; Urayama, K.; Takigawa, T.; Kidowaki, M.; Ito, K. Pressure-Responsive Polymer Membranes of Slide-Ring Gels with Movable Cross-Links. Adv. Mater. 2013, 25 (33), 4636–4640. https://doi.org/10.1002/adma.201301252.

(43) Meng, J.; Cao, Z.; Ni, L.; Zhang, Y.; Wang, X.; Zhang, X.; Liu, E. A Novel Salt-Responsive TFC RO Membrane Having Superior Antifouling and Easy-Cleaning Properties. J. Memb. Sci. 2014, 461, 123–129. https://doi.org/https://doi.org/10.1016/j.memsci.2014.03.017.

(44) Jeon, G.; Yang, S. Y.; Byun, J.; Kim, J. K. Electrically Actuatable Smart Nanoporous Membrane for Pulsatile Drug Release. Nano Lett. 2011, 11 (3), 1284–1288. https://doi.org/10.1021/nl104329y.

(45) Kato, S.; Aizawa, M.; Suzuki, S. Photo-Responsive Membranes: I. Light-Induced Potential Changes across Membranes Incorporating a Photochromic Compound. J. Memb. Sci. 1976, 1, 289–300. https://doi.org/https://doi.org/10.1016/S0376-7388(00)82273-5.

(46) Nicoletta, F. P.; Cupelli, D.; Formoso, P.; De Filpo, G.; Colella, V.; Gugliuzza, A. Light Responsive Polymer Membranes: A Review. Membranes . 2012. https://doi.org/10.3390/membranes2010134.

(47) Peng, T.; Cheng, Y.-L. Temperature-Responsive Permeability of Porous PNIPAAm-g-PE Membranes. J. Appl. Polym. Sci. 1998, 70 (11), 2133–2142.

https://doi.org/10.1002/(SICI)1097-4628(19981212)70:11<2133::AID-APP6>3.0.CO;2-P.

(48) Yang, Q.; Himstedt, H. H.; Ulbricht, M.; Qian, X.; Ranil Wickramasinghe, S. Designing Magnetic Field Responsive Nanofiltration Membranes. J. Memb. Sci. 2013, 430, 70–78. https://doi.org/https://doi.org/10.1016/j.memsci.2012.11.068.

(49) Manouras, T.; Vamvakaki, M. Field Responsive Materials: Photo-, Electro-, Magnetic- and Ultrasound-Sensitive Polymers. Polym. Chem. 2017, 8 (1), 74–96. https://doi.org/10.1039/C6PY01455K.

(50) Gordijo, C. R.; Shuhendler, A. J.; Wu, X. Y. Glucose-Responsive Bioinorganic Nanohybrid Membrane for Self-Regulated Insulin Release. Adv. Funct. Mater. 2010, 20 (9), 1404–1412. https://doi.org/10.1002/adfm.200901581.

(51) Ali, M.; Ahmed, I.; Nasir, S.; Duznovic, I.; Niemeyer, C. M.; Ensinger, W. Analytica Chimica Acta Potassium-Induced Ionic Conduction through a Single Nano Fl Uidic Pore Modi Fi Ed with Acyclic Polyether Derivative. Anal. Chim. Acta 2018, 1039, 132–139. https://doi.org/10.1016/j.aca.2018.07.056.

(52) Wandera, D.; Wickramasinghe, S. R.; Husson, S. M. Stimuli-Responsive Membranes. J. Memb. Sci. 2010, 357 (1), 6–35. https://doi.org/https://doi.org/10.1016/j.memsci.2010.03.046.

(53) Nakayama, H.; Kaetsu, I.; Uchida, K.; Sakata, S.; Tougou, K.; Hara, T.; Matsubara, Y. Radiation Curing of Intelligent Coating for Controlled Release and Permeation. Radiat. Phys. Chem. 2002, 63 (3), 521–523. https://doi.org/https://doi.org/10.1016/S0969-806X(01)00594-1.

(54) Do, K. N. T.; Kim, D. Synthesis and Characterization of Homogeneously Sulfonated Poly(Ether Ether Ketone) Membranes: Effect of Casting Solvent. J. Appl. Polym. Sci. 2008, 110 (3), 1763–1770. https://doi.org/10.1002/app.28150.

(55) M'Bareck, C. O.; Nguyen, Q. T.; Alexandre, S.; Zimmerlin, I. Fabrication of Ion-Exchange Ultrafiltration Membranes for Water Treatment: I. Semi-Interpenetrating Polymer Networks of Polysulfone and Poly(Acrylic Acid). J. Memb. Sci. 2006, 278 (1), 10–18. https://doi.org/https://doi.org/10.1016/j.memsci.2005.10.058.

(56) Liu, H.; Liao, J.; Zhao, Y.; Sotto, A.; Zhu, J.; van der Bruggen, B.; Gao, C.; Shen, J. Bioinspired Dual Stimuli-Responsive Membranes with Enhanced Gating Ratios and Reversible Performances for Water Gating. J. Memb. Sci. 2018, 564, 53–61. https://doi.org/https://doi.org/10.1016/j.memsci.2018.07.013.

(57) Choi, W. S.; Park, J.-H.; Koo, H. Y.; Kim, J.-Y.; Cho, B. K.; Kim, D.-Y. "Grafting-From" Polymerization inside a Polyelectrolyte Hollow-Capsule Microreactor. Angew. Chemie Int. Ed. 2005, 44 (7), 1096–1101. https://doi.org/10.1002/anie.200460971.

(58) Zdyrko, B.; Luzinov, I. Polymer Brushes by the "Grafting to" Method. Macromol. Rapid Commun. 2011, 32 (12), 859–869. https://doi.org/10.1002/marc.201100162.

(59) Matyjaszewski, K. Atom Transfer Radical Polymerization (ATRP): Current Status and Future Perspectives. Macromolecules 2012, 45 (10), 4015–4039. https://doi.org/10.1021/ma3001719.

(60) Gao, H.; Matyjaszewski, K. Synthesis of Star Polymers by a Combination of ATRP and the "Click" Coupling Method. Macromolecules 2006, 39 (15), 4960–4965. https://doi.org/10.1021/ma060926c.

(61) Robinson, K. L.; Khan, M. A.; de Paz Báñez, M. V; Wang, X. S.; Armes, S. P. Controlled Polymerization of 2-Hydroxyethyl Methacrylate by ATRP at Ambient Temperature. Macromolecules 2001, 34 (10), 3155–3158. https://doi.org/10.1021/ma0019611.

(62) Chiefari, J.; Chong, Y. K. (Bill); Ercole, F.; Krstina, J.; Jeffery, J.; Le, T. P. T.; Mayadunne, R. T. A.; Meijs, G. F.; Moad, C. L.; Moad, G.; et al. Living Free-Radical Polymerization by Reversible Addition−Fragmentation Chain Transfer: The RAFT Process. Macromolecules 1998, 31 (16), 5559–5562. https://doi.org/10.1021/ma9804951.

(63) Moad, G.; Chong, Y. K.; Postma, A.; Rizzardo, E.; Thang, S. H. Advances in RAFT Polymerization: The Synthesis of Polymers with Defined End-Groups. Polymer (Guildf). 2005, 46 (19), 8458–8468. https://doi.org/https://doi.org/10.1016/j.polymer.2004.12.061.

(64) Mayadunne, R. T. A.; Rizzardo, E.; Chiefari, J.; Chong, Y. K.; Moad, G.; Thang, S. H. Living Radical Polymerization with Reversible Addition−Fragmentation Chain Transfer

(RAFT Polymerization) Using Dithiocarbamates as Chain Transfer Agents. Macromolecules 1999, 32 (21), 6977–6980. https://doi.org/10.1021/ma9906837.

(65) Edmondson, S.; Osborne, V. L.; Huck, W. T. S. Polymer Brushes via Surface-Initiated Polymerizations. Chem. Soc. Rev. 2004, 33 (1), 14–22. https://doi.org/10.1039/B210143M.

(66) Lee, S. H.; Dreyer, D. R.; An, J.; Velamakanni, A.; Piner, R. D.; Park, S.; Zhu, Y.; Kim, S. O.; Bielawski, C. W.; Ruoff, R. S. Polymer Brushes via Controlled, Surface-Initiated Atom Transfer Radical Polymerization (ATRP) from Graphene Oxide. Macromol. Rapid Commun. 2010, 31 (3), 281–288. https://doi.org/10.1002/marc.200900641.

(67) Perruchot, C.; Khan, M. A.; Kamitsi, A.; Armes, S. P.; von Werne, T.; Patten, T. E. Synthesis of Well-Defined, Polymer-Grafted Silica Particles by Aqueous ATRP. Langmuir 2001, 17 (15), 4479–4481. https://doi.org/10.1021/la0102758.

(68) Stenzel, M. H.; Zhang, L.; Huck, W. T. S. Temperature-Responsive Glycopolymer Brushes Synthesized via RAFT Polymerization Using the Z-Group Approach. Macromol. Rapid Commun. 2006, 27 (14), 1121–1126. https://doi.org/10.1002/marc.200600223.

(69) Ranjan, R.; Brittain, W. J. Synthesis of High Density Polymer Brushes on Nanoparticles by Combined RAFT Polymerization and Click Chemistry. Macromol. Rapid Commun. 2008, 29 (12‐13), 1104‐1110. https://doi.org/10.1002/marc.200800085.

(70) Fan, X.; Lin, L.; Dalsin, J. L.; Messersmith, P. B. Biomimetic Anchor for Surface-Initiated Polymerization from Metal Substrates. J. Am. Chem. Soc. 2005, 127 (45), 15843–15847. https://doi.org/10.1021/ja0532638.

(71) Barbey, R.; Lavanant, L.; Paripovic, D.; Schüwer, N.; Sugnaux, C.; Tugulu, S.; Klok, H.-A. Polymer Brushes via Surface-Initiated Controlled Radical Polymerization: Synthesis, Characterization, Properties, and Applications. Chem. Rev. 2009, 109 (11), 5437–5527. https://doi.org/10.1021/cr900045a.

(72) Husseman, M.; Malmström, E. E.; McNamara, M.; Mate, M.; Mecerreyes, D.; Benoit, D. G.; Hedrick, J. L.; Mansky, P.; Huang, E.; Russell, T. P.; et al. Controlled Synthesis of Polymer Brushes by “Living” Free Radical Polymerization Techniques. Macromolecules 1999, 32 (5), 1424–1431. https://doi.org/10.1021/ma981290v.

(73) Matsuno, R.; Yamamoto, K.; Otsuka, H.; Takahara, A. Polystyrene- and Poly(3-Vinylpyridine)-Grafted Magnetite Nanoparticles Prepared through Surface-Initiated Nitroxide-Mediated Radical Polymerization. Macromolecules 2004, 37 (6), 2203–2209. https://doi.org/10.1021/ma035523g.

(74) Kobayashi, M.; Matsuno, R.; Otsuka, H.; Takahara, A. Precise Surface Structure Control of Inorganic Solid and Metal Oxide Nanoparticles through Surface-Initiated Radical Polymerization. Sci. Technol. Adv. Mater. 2006, 7 (7), 617–628. https://doi.org/10.1016/j.stam.2006.07.008.

(75) Zhao, X.; Lin, W.; Song, N.; Chen, X.; Fan, X.; Zhou, Q. Water Soluble Multi-Walled Carbon Nanotubes Prepared via Nitroxide-Mediated Radical Polymerization. J. Mater. Chem. 2006, 16 (47), 4619–4625. https://doi.org/10.1039/B609431G.

(76) Jordan, R.; Ulman, A.; Kang, J. F.; Rafailovich, M. H.; Sokolov, J. Surface-Initiated Anionic Polymerization of Styrene by Means of Self-Assembled Monolayers. J. Am. Chem. Soc. 1999, 121 (5), 1016–1022. https://doi.org/10.1021/ja981348l.

(77) Ingall, M. D. K.; Honeyman, C. H.; Mercure, J. V; Bianconi, P. A.; Kunz, R. R. Surface Functionalization and Imaging Using Monolayers and Surface-Grafted Polymer Layers. J. Am. Chem. Soc. 1999, 121 (15), 3607–3613. https://doi.org/10.1021/ja9833927.

(78) Advincula, R.; Zhou, Q.; Park, M.; Wang, S.; Mays, J.; Sakellariou, G.; Pispas, S.; Hadjichristidis, N. Polymer Brushes by Living Anionic Surface Initiated Polymerization on Flat Silicon (SiOx) and Gold Surfaces: Homopolymers and Block Copolymers. Langmuir 2002, 18 (22), 8672–8684. https://doi.org/10.1021/la025962t.

(79) Lambrinos, P.; Tardi, M.; Polton, A.; Sigwalt, P. The Mechanism of the Polymerization of n.Butyl Acrylate Initiated with N,N-Diethyl Dithiocarbamate Derivatives. Eur. Polym. J. 1990, 26 (10), 1125–1135. https://doi.org/https://doi.org/10.1016/0014-3057(90)90014-U.

(80) Otsu, T.; Yoshida, M. Role of Initiator-Transfer Agent-Terminator (Iniferter) in Radical Polymerizations: Polymer Design by Organic Disulfides as Iniferters. Die Makromol.

Chemie, Rapid Commun. 1982, 3 (2), 127–132. https://doi.org/10.1002/marc.1982.030030208.

(81) Nakayama, Y.; Matsuda, T. Surface Macromolecular Architectural Designs Using Photo-Graft Copolymerization Based on Photochemistry of Benzyl N,N-Diethyldithiocarbamate. Macromolecules 1996, 29 (27), 8622–8630. https://doi.org/10.1021/ma9606014.

(82) Matsuda, T.; Kaneko, M.; Ge, S. Quasi-Living Surface Graft Polymerization with Phosphorylcholine Group(s) at the Terminal End. Biomaterials 2003, 24 (24), 4507–4515. https://doi.org/https://doi.org/10.1016/S0142-9612(03)00349-1.

(83) Kim, N. Y.; Jeon, N. L.; Choi, I. S.; Takami, S.; Harada, Y.; Finnie, K. R.; Girolami, G. S.; Nuzzo, R. G.; Whitesides, G. M.; Laibinis, P. E. Surface-Initiated Ring-Opening Metathesis Polymerization on Si/SiO2. Macromolecules 2000, 33 (8), 2793–2795. https://doi.org/10.1021/ma000046c.

(84) Moon, J. H.; Swager, T. M. Poly(p-Phenylene Ethynylene) Brushes. Macromolecules 2002, 35 (16), 6086–6089. https://doi.org/10.1021/ma025539r.

(85) Jordan, R.; Ulman, A. Surface Initiated Living Cationic Polymerization of 2-Oxazolines. J. Am. Chem. Soc. 1998, 120 (2), 243–247. https://doi.org/10.1021/ja973392r.

(86) Husemann, M.; Mecerreyes, D.; Hawker, C. J.; Hedrick, J. L.; Shah, R.; Abbott, N. L. Surface-Initiated Polymerization for Amplification of Self-Assembled Monolayers Patterned by Microcontact Printing. Angew. Chemie Int. Ed. 1999, 38 (5), 647–649. https://doi.org/10.1002/(SICI)1521-3773(19990301)38:5<647::AID-ANIE647>3.0.CO;2-0.

(87) Decher, G.; Hong, J.-D. Buildup of Ultrathin Multilayer Films by a Self-Assembly Process, 1 Consecutive Adsorption of Anionic and Cationic Bipolar Amphiphiles on Charged Surfaces. Makromol. Chemie. Macromol. Symp. 1991, 46 (1), 321–327. https://doi.org/10.1002/masy.19910460145.

(88) Kovtyukhova, N. I.; Ollivier, P. J.; Martin, B. R.; Mallouk, T. E.; Chizhik, S. A.; Buzaneva, E. V; Gorchinskiy, A. D. Layer-by-Layer Assembly of Ultrathin Composite Films from

Micron-Sized Graphite Oxide Sheets and Polycations. Chem. Mater. 1999, 11 (3), 771–778. https://doi.org/10.1021/cm981085u.

(89) Kotov, N. A.; Dekany, I.; Fendler, J. H. Layer-by-Layer Self-Assembly of Polyelectrolyte-Semiconductor Nanoparticle Composite Films. J. Phys. Chem. 1995, 99 (35), 13065–13069. https://doi.org/10.1021/j100035a005.

(90) Sukhorukov, G. B.; Donath, E.; Lichtenfeld, H.; Knippel, E.; Knippel, M.; Budde, A.; Möhwald, H. Layer-by-Layer Self Assembly of Polyelectrolytes on Colloidal Particles. Colloids Surfaces A Physicochem. Eng. Asp. 1998, 137 (1), 253–266. https://doi.org/https://doi.org/10.1016/S0927-7757(98)00213-1.

(91) Tang, Z.; Wang, Y.; Podsiadlo, P.; Kotov, N. A. Biomedical Applications of Layer-by-Layer Assembly: From Biomimetics to Tissue Engineering. Adv. Mater. 2006, 18 (24), 3203–3224. https://doi.org/10.1002/adma.200600113.

(92) Borges, J.; Mano, J. F. Molecular Interactions Driving the Layer-by-Layer Assembly of Multilayers. Chem. Rev. 2014, 114 (18), 8883–8942. https://doi.org/10.1021/cr400531v.

(93) Gao, Y.; Kyratzis, I. Covalent Immobilization of Proteins on Carbon Nanotubes Using the Cross-Linker 1-Ethyl-3-(3-Dimethylaminopropyl)Carbodiimide—a Critical Assessment. Bioconjug. Chem. 2008, 19 (10), 1945–1950. https://doi.org/10.1021/bc800051c.

(94) Anderson, G. W.; Zimmerman, J. E.; Callahan, F. M. The Use of Esters of N-Hydroxysuccinimide in Peptide Synthesis. J. Am. Chem. Soc. 1964, 86 (9), 1839–1842. https://doi.org/10.1021/ja01063a037.

(95) Chang, M. C.; Douglas, W. H. Cross-Linkage of Hydroxyapatite/Gelatin Nanocomposite Using Imide-Based Zero-Length Cross-Linker. J. Mater. Sci. Mater. Med. 2007, 18 (10), 2045–2051. https://doi.org/10.1007/s10856-007-3152-0.

(96) Rasmussen, S. R.; Larsen, M. R.; Rasmussen, S. E. Covalent Immobilization of DNA onto Polystyrene Microwells: The Molecules Are Only Bound at the 5′ End. Anal. Biochem. 1991, 198 (1), 138–142. https://doi.org/https://doi.org/10.1016/0003-2697(91)90518-X.

(97) Lepoitevin, M.; Ma, T.; Bechelany, M.; Janot, J. M.; Balme, S. Functionalization of Single Solid State Nanopores to Mimic Biological Ion Channels: A Review. Advances in Colloid and Interface Science. 2017, pp 195–213. https://doi.org/10.1016/j.cis.2017.09.001.

(98) Tamada, K.; Nagasawa, J.; Nakanishi, F.; Abe, K.; Hara, M.; Knoll, W.; Ishida, T.; Fukushima, H.; Miyashita, S.; Usui, T.; et al. Structure of SAMs Generated from Functionalized Thiols on Gold. Thin Solid Films 1998, 327–329, 150–155. https://doi.org/https://doi.org/10.1016/S0040-6090(98)00618-X.

(99) Ganesh, V.; Pal, S. K.; Kumar, S.; Lakshminarayanan, V. Self-Assembled Monolayers (SAMs) of Alkoxycyanobiphenyl Thiols on Gold—A Study of Electron Transfer Reaction Using Cyclic Voltammetry and Electrochemical Impedance Spectroscopy. J. Colloid Interface Sci. 2006, 296 (1), 195–203. https://doi.org/https://doi.org/10.1016/j.jcis.2005.08.051.

(100) Xue, Y.; Li, X.; Li, H.; Zhang, W. Quantifying Thiol–gold Interactions towards the Efficient Strength Control. Nat. Commun. 2014, 5, 4348.

(101) Pevarnik, M.; Healy, K.; Davenport, M.; Yen, J.; Siwy, Z. S. A Hydrophobic Entrance Enhances Ion Current Rectification and Induces Dewetting in Asymmetric Nanopores. Analyst 2012, 137 (13), 2944–2950. https://doi.org/10.1039/C2AN16139G.

(102) Wei, R.; Gatterdam, V.; Wieneke, R.; Tampé, R.; Rant, U. Stochastic Sensing of Proteins with Receptor-Modified Solid-State Nanopores. Nat. Nanotechnol. 2012, 7, 257.

(103) Simons, K.; Ikonen, E. Functional Rafts in Cell Membranes. Nature 1997, 387 (6633), 569–572. https://doi.org/10.1038/42408.

(104) Takata, K.; Matsuzaki, T.; Tajika, Y. Aquaporins: Water Channel Proteins of the Cell Membrane. Prog. Histochem. Cytochem. 2004, 39 (1), 1–83. https://doi.org/https://doi.org/10.1016/j.proghi.2004.03.001.

(105) Krapivinsky, G.; Gordon, E. A.; Wickman, K.; Velimirović, B.; Krapivinsky, L.; Clapham, D. E. The G-Protein-Gated Atrial K+ Channel IKAch Is a Heteromultimer of Two

Inwardly Rectifying K+-Channel Proteins. Nature 1995, 374 (6518), 135–141. https://doi.org/10.1038/374135a0.

(106) Hilf, R. J. C.; Dutzler, R. X-Ray Structure of a Prokaryotic Pentameric Ligand-Gated Ion Channel. Nature 2008, 452, 375.

(107) Sackin, H. Mechanosensitive Channels. Annu. Rev. Physiol. 1995, 57 (1), 333–353. https://doi.org/10.1146/annurev.ph.57.030195.002001.

(108) Catterall, W. A. Structure and Regulation of Voltage-Gated Ca2+ Channels. Annu. Rev. Cell Dev. Biol. 2000, 16 (1), 521–555. https://doi.org/10.1146/annurev.cellbio.16.1.521.

(109) Consortium, T. I. T.; Giacomini, K. M.; Huang, S.-M.; Tweedie, D. J.; Benet, L. Z.; Brouwer, K. L. R.; Chu, X.; Dahlin, A.; Evers, R.; Fischer, V.; et al. Membrane Transporters in Drug Development. Nat. Rev. Drug Discov. 2010, 9, 215.

(110) Torres, G. E.; Gainetdinov, R. R.; Caron, M. G. Plasma Membrane Monoamine Transporters: Structure, Regulation and Function. Nat. Rev. Neurosci. 2003, 4 (1), 13–25. https://doi.org/10.1038/nrn1008.

(111) Niinuma, K.; Kato, Y.; Suzuki, H.; Tyson, C. A.; Weizer, V.; Dabbs, J. E.; Froehlich, R.; Green, C. E.; Sugiyama, Y. Primary Active Transport of Organic Anions on Bile Canalicular Membrane in Humans. Am. J. Physiol. Liver Physiol. 1999, 276 (5), G1153–G1164. https://doi.org/10.1152/ajpgi.1999.276.5.G1153.

(112) Accardi, A.; Miller, C. Secondary Active Transport Mediated by a Prokaryotic Homologue of ClC Cl- Channels. Nature 2004, 427 (6977), 803–807. https://doi.org/10.1038/nature02314.

(113) West, I. C. Energy Coupling in Secondary Active Transport. Biochim. Biophys. Acta - Biomembr. 1980, 604 (1), 91–126. https://doi.org/https://doi.org/10.1016/0005-2736(80)90586-6.

(114) Kasianowicz, J. J.; Brandin, E.; Branton, D.; Deamer, D. W. Characterization of Individual Polynucleotide Molecules Using a Membrane Channel. Proc. Natl. Acad. Sci. U. S. A. 1996, 93 (24), 13770–13773. https://doi.org/10.1073/pnas.93.24.13770.

(115) Howard, S. P.; Buckley, J. T. Activation of the Hole-Forming Toxin Aerolysin by Extracellular Processing. J. Bacteriol. 1985, 163 (1), 336 LP-340.

(116) Smart, O. S.; Goodfellow, J. M.; Wallace, B. A. The Pore Dimensions of Gramicidin A. Biophys. J. 1993, 65 (6), 2455–2460. https://doi.org/https://doi.org/10.1016/S0006-3495(93)81293-1.

(117) Collier, R. J.; Young, J. A. T. Anthrax Toxin. Annu. Rev. Cell Dev. Biol. 2003, 19 (1), 45–70. https://doi.org/10.1146/annurev.cellbio.19.111301.140655.

(118) Shogomori, H.; Kobayashi, T. Lysenin: A Sphingomyelin Specific Pore-Forming Toxin. Biochim. Biophys. Acta - Gen. Subj. 2008, 1780 (3), 612–618. https://doi.org/https://doi.org/10.1016/j.bbagen.2007.09.001.

(119) Yildiz, Ö.; Vinothkumar, K. R.; Goswami, P.; Kühlbrandt, W. Structure of the Monomeric Outer‐membrane Porin OmpG in the Open and Closed Conformation. EMBO J. 2006, 25 (15), 3702 LP-3713. https://doi.org/10.1038/sj.emboj.7601237.

(120) Manrao, E. A.; Derrington, I. M.; Laszlo, A. H.; Langford, K. W.; Hopper, M. K.; Gillgren, N.; Pavlenok, M.; Niederweis, M.; Gundlach, J. H. Reading DNA at Single-Nucleotide Resolution with a Mutant MspA Nanopore and Phi29 DNA Polymerase. Nat. Biotechnol. 2012, 30, 349.

(121) Derrington, I. M.; Butler, T. Z.; Collins, M. D.; Manrao, E.; Pavlenok, M.; Niederweis, M.; Gundlach, J. H. Nanopore DNA Sequencing with MspA. Proc. Natl. Acad. Sci. 2010, 107 (37), 16060 LP-16065. https://doi.org/10.1073/pnas.1001831107.

(122) Butler, T. Z.; Pavlenok, M.; Derrington, I. M.; Niederweis, M.; Gundlach, J. H. Single-Molecule DNA Detection with an Engineered MspA Protein Nanopore. Proc. Natl. Acad. Sci. 2008, 105 (52), 20647 LP-20652. https://doi.org/10.1073/pnas.0807514106.

(123) Jin, Q.; Fleming, A. M.; Johnson, R. P.; Ding, Y.; Burrows, C. J.; White, H. S. Base-Excision Repair Activity of Uracil-DNA Glycosylase Monitored Using the Latch Zone of α-Hemolysin. J. Am. Chem. Soc. 2013, 135 (51), 19347–19353. https://doi.org/10.1021/ja410615d.

(124) Kasianowicz, J. J.; Henrickson, S. E.; Weetall, H. H.; Robertson, B. Simultaneous Multianalyte Detection with a Nanometer-Scale Pore. Anal. Chem. 2001, 73 (10), 2268–2272. https://doi.org/10.1021/ac000958c.

(125) Henrickson, S. E.; DiMarzio, E. A.; Wang, Q.; Stanford, V. M.; Kasianowicz, J. J. Probing Single Nanometer-Scale Pores with Polymeric Molecular Rulers. J. Chem. Phys. 2010, 132 (13), 135101. https://doi.org/10.1063/1.3328875.

(126) Ying, Y.-L.; Li, D.-W.; Li, Y.; Lee, J. S.; Long, Y.-T. Enhanced Translocation of Poly(Dt)45 through an α-Hemolysin Nanopore by Binding with Antibody. Chem. Commun. 2011, 47 (20), 5690–5692. https://doi.org/10.1039/C0CC05787H.

(127) Sutherland, T. C.; Long, Y.-T.; Stefureac, R.-I.; Bediako-Amoa, I.; Kraatz, H.-B.; Lee, J. S. Structure of Peptides Investigated by Nanopore Analysis. Nano Lett. 2004, 4 (7), 1273–1277. https://doi.org/10.1021/nl049413e.

(128) Wloka, C.; Mutter, N. L.; Soskine, M.; Maglia, G. Alpha-Helical Fragaceatoxin C Nanopore Engineered for Double-Stranded and Single-Stranded Nucleic Acid Analysis. Angew. Chemie Int. Ed. 2016, 55 (40), 12494–12498. https://doi.org/10.1002/anie.201606742.

(129) Soskine, M.; Biesemans, A.; De Maeyer, M.; Maglia, G. Tuning the Size and Properties of ClyA Nanopores Assisted by Directed Evolution. J. Am. Chem. Soc. 2013, 135 (36), 13456–13463. https://doi.org/10.1021/ja4053398.

(130) Mohammad, M. M.; Iyer, R.; Howard, K. R.; McPike, M. P.; Borer, P. N.; Movileanu, L. Engineering a Rigid Protein Tunnel for Biomolecular Detection. J. Am. Chem. Soc. 2012, 134 (22), 9521–9531. https://doi.org/10.1021/ja3043646.

(131) Dekker, C.; Article, R.; Dekker, C. Solid-State Nanopores. Nat. Nanotechnol. 2007, 2 (4), 209–215. https://doi.org/10.1038/nnano.2007.27.

(132) Apel, P. Track Etching Technique in Membrane Technology. Radiat. Meas. 2001, 34 (1), 559–566. https://doi.org/https://doi.org/10.1016/S1350-4487(01)00228-1.

(133) Cornelius, T. W.; Apel, P. Y.; Schiedt, B.; Trautmann, C.; Toimil-Molares, M. E.; Karim, S.; Neumann, R. Investigation of Nanopore Evolution in Ion Track-Etched Polycarbonate Membranes. Nucl. Instruments Methods Phys. Res. Sect. B Beam

Interact. with Mater. Atoms 2007, 265 (2), 553–557. https://doi.org/https://doi.org/10.1016/j.nimb.2007.10.004.

(134) Apel, P. Y.; Korchev, Y. .; Siwy, Z.; Spohr, R.; Yoshida, M. Diode-like Single-Ion Track Membrane Prepared by Electro-Stopping. Nucl. Instruments Methods Phys. Res. Sect. B Beam Interact. with Mater. Atoms 2001, 184 (3), 337–346. https://doi.org/https://doi.org/10.1016/S0168-583X(01)00722-4.

(135) Mara, A.; Siwy, Z.; Trautmann, C.; Wan, J.; Kamme, F. An Asymmetric Polymer Nanopore for Single Molecule Detection. Nano Lett. 2004, 4 (3), 497–501. https://doi.org/10.1021/nl035141o.

(136) Iijima, S.; Ichihashi, T. Single-Shell Carbon Nanotubes of 1-Nm Diameter. Nature 1993, 363 (6430), 603–605. https://doi.org/10.1038/363603a0.

(137) Iijima, S. Helical Microtubules of Graphitic Carbon. Nature 1991, 354 (6348), 56–58. https://doi.org/10.1038/354056a0.

(138) Chopra, N. G.; Luyken, R. J.; Cherrey, K.; Crespi, V. H.; Cohen, M. L.; Louie, S. G.; Zettl, A. Boron Nitride Nanotubes. Science (80-.). 1995, 269 (5226), 966 LP-967. https://doi.org/10.1126/science.269.5226.966.

(139) Rubio, A.; Corkill, J. L.; Cohen, M. L. Theory of Graphitic Boron Nitride Nanotubes. Phys. Rev. B 1994, 49 (7), 5081–5084. https://doi.org/10.1103/PhysRevB.49.5081.

(140) Fernandez-Lima, F. A.; Henkes, A. V.; da Silveira, E. F.; Nascimento, M. A. C. Alkali Halide Nanotubes: Structure and Stability. J. Phys. Chem. C 2012, 116 (8), 4965–4969. https://doi.org/10.1021/jp208090j.

(141) Kang, D.-Y.; Zang, J.; Wright, E. R.; McCanna, A. L.; Jones, C. W.; Nair, S. Dehydration, Dehydroxylation, and Rehydroxylation of Single-Walled Aluminosilicate Nanotubes. ACS Nano 2010, 4 (8), 4897–4907. https://doi.org/10.1021/nn101211y.

(142) Zang, J.; Konduri, S.; Nair, S.; Sholl, D. S. Self-Diffusion of Water and Simple Alcohols in Single-Walled Aluminosilicate Nanotubes. ACS Nano 2009, 3 (6), 1548–1556. https://doi.org/10.1021/nn9001837.

(143) Li, J.; Stein, D.; McMullan, C.; Branton, D.; Aziz, M. J.; Golovchenko, J. A. Ion-Beam Sculpting at Nanometre Length Scales. Nature 2001, 412 (6843), 166–169. https://doi.org/10.1038/35084037.

(144) Storm, A. J.; Chen, J. H.; Ling, X. S.; Zandbergen, H. W.; Dekker, C. Fabrication of Solid-State Nanopores with Single-Nanometre Precision. Nat. Mater. 2003, 2 (8), 537–540. https://doi.org/10.1038/nmat941.

(145) Storm, A. J.; Chen, J. H.; Ling, X. S.; Zandbergen, H. W.; Dekker, C. Electron-Beam-Induced Deformations of SiO2 Nanostructures. J. Appl. Phys. 2005, 98 (1), 14307. https://doi.org/10.1063/1.1947391.

(146) Garaj, S.; Liu, S.; Golovchenko, J. A.; Branton, D. Molecule-Hugging Graphene Nanopores. Proc. Natl. Acad. Sci. 2013, 110 (30), 12192 LP-12196. https://doi.org/10.1073/pnas.1220012110.

(147) Russo, C. J.; Golovchenko, J. A. Atom-by-Atom Nucleation and Growth of Graphene Nanopores. Proc. Natl. Acad. Sci. 2012, 109 (16), 5953 LP-5957. https://doi.org/10.1073/pnas.1119827109.

(148) Siwy, Z. S.; Davenport, M. Graphene Opens up to DNA. Nat. Nanotechnol. 2010, 5, 697.

(149) Feng, J.; Liu, K.; Graf, M.; Lihter, M.; Bulushev, R. D.; Dumcenco, D.; Alexander, D. T. L.; Krasnozhon, D.; Vuletic, T.; Kis, A.; et al. Electrochemical Reaction in Single Layer MoS2: Nanopores Opened Atom by Atom. Nano Lett. 2015, 15 (5), 3431–3438. https://doi.org/10.1021/acs.nanolett.5b00768.

(150) Feng, J.; Graf, M.; Liu, K.; Ovchinnikov, D.; Dumcenco, D.; Heiranian, M.; Nandigana, V.; Aluru, N. R.; Kis, A.; Radenovic, A. Single-Layer MoS2nanopores as Nanopower Generators. Nature 2016, 536 (7615), 197–200. https://doi.org/10.1038/nature18593.

(151) Traversi, F.; Raillon, C.; Benameur, S. M.; Liu, K.; Khlybov, S.; Tosun, M.; Krasnozhon, D.; Kis, A.; Radenovic, A. Detecting the Translocation of DNA through a Nanopore Using Graphene Nanoribbons. Nat. Nanotechnol. 2013, 8, 939.

(152) Feng, J.; Liu, K.; Bulushev, R. D.; Khlybov, S.; Dumcenco, D.; Kis, A.; Radenovic, A. Identification of Single Nucleotides in MoS2 Nanopores. Nat. Nanotechnol. 2015, 10, 1070.

(153) Nicoli, F.; Verschueren, D.; Klein, M.; Dekker, C.; Jonsson, M. P. DNA Translocations through Solid-State Plasmonic Nanopores. Nano Lett. 2014, 14 (12), 6917–6925. https://doi.org/10.1021/nl503034j.

(154) Belkin, M.; Chao, S.-H.; Jonsson, M. P.; Dekker, C.; Aksimentiev, A. Plasmonic Nanopores for Trapping, Controlling Displacement, and Sequencing of DNA. ACS Nano 2015, 9 (11), 10598–10611. https://doi.org/10.1021/acsnano.5b04173.

(155) Li, Y.; Nicoli, F.; Chen, C.; Lagae, L.; Groeseneken, G.; Stakenborg, T.; Zandbergen, H. W.; Dekker, C.; Van Dorpe, P.; Jonsson, M. P. Photoresistance Switching of Plasmonic Nanopores. Nano Lett. 2015, 15 (1), 776–782. https://doi.org/10.1021/nl504516d.

(156) Wang, H.; Branton, D. Nanopores with a Spark for Single-Molecule Detection. Nat. Biotechnol. 2001, 19 (7), 622–623. https://doi.org/10.1038/90216.

(157) Clarke, J.; Wu, H.-C.; Jayasinghe, L.; Patel, A.; Reid, S.; Bayley, H. Continuous Base Identification for Single-Molecule Nanopore DNA Sequencing. Nat. Nanotechnol. 2009, 4, 265.

(158) Siria, A.; Poncharal, P.; Biance, A. L.; Fulcrand, R.; Blase, X.; Purcell, S. T.; Bocquet, L. Giant Osmotic Energy Conversion Measured in a Single Transmembrane Boron Nitride Nanotube. Nature 2013, 494 (7438), 455–458. https://doi.org/10.1038/nature11876.

(159) Kwok, H.; Briggs, K.; Tabard-Cossa, V. Nanopore Fabrication by Controlled Dielectric Breakdown. PLoS One 2014, 9 (3), e92880.

(160) Briggs, K.; Kwok, H.; Tabard-Cossa, V. Automated Fabrication of 2-Nm Solid-State Nanopores for Nucleic Acid Analysis. Small 2014, 10 (10), 2077–2086. https://doi.org/10.1002/smll.201303602.

(161) Lee, K.; Park, K.-B.; Kim, H.-J.; Yu, J.-S.; Chae, H.; Kim, H.-M.; Kim, K.-B. Recent Progress in Solid-State Nanopores. Adv. Mater. 2018, 30 (42), 1704680. https://doi.org/10.1002/adma.201704680.

(162) Noy, A.; Park, H. G.; Fornasiero, F.; Holt, J. K.; Grigoropoulos, C. P.; Bakajin, O. Nanofluidics in Carbon Nanotubes. Nano Today 2007, 2 (6), 22–29. https://doi.org/https://doi.org/10.1016/S1748-0132(07)70170-6.

(163) Baughman, R. H.; Zakhidov, A. A.; de Heer, W. A. Carbon Nanotubes--the Route Toward Applications. Science (80-.). 2002, 297 (5582), 787 LP-792. https://doi.org/10.1126/science.1060928.

(164) Holt, J. K.; Park, H. G.; Wang, Y.; Stadermann, M.; Artyukhin, A. B.; Grigoropoulos, C. P.; Noy, A.; Bakajin, O. Fast Mass Transport Through Sub-2-Nanometer Carbon Nanotubes. Science (80-.). 2006, 312 (5776), 1034 LP-1037. https://doi.org/10.1126/science.1126298.

(165) Secchi, E.; Marbach, S.; Niguès, A.; Stein, D.; Siria, A.; Bocquet, L. Massive Radius-Dependent Flow Slippage in Carbon Nanotubes. Nature 2016. https://doi.org/10.1038/nature19315.

(166) Mouterde, T.; Keerthi, A.; Poggioli, A. R.; Dar, S. A.; Siria, A.; Geim, A. K.; Bocquet, L.; Radha, B. Molecular Streaming and Its Voltage Control in Ångström-Scale Channels. Nature 2019, 567 (7746), 87–90. https://doi.org/10.1038/s41586-019-0961-5.

(167) Schneider, G. F.; Kowalczyk, S. W.; Calado, V. E.; Pandraud, G.; Zandbergen, H. W.; Vandersypen, L. M. K.; Dekker, C. DNA Translocation through Graphene Nanopores. Nano Lett. 2010, 10 (8), 3163–3167. https://doi.org/10.1021/nl102069z.

(168) Liu, S.; Lu, B.; Zhao, Q.; Li, J.; Gao, T.; Chen, Y.; Zhang, Y.; Liu, Z.; Fan, Z.; Yang, F.; et al. Boron Nitride Nanopores: Highly Sensitive DNA Single-Molecule Detectors. Adv. Mater. 2013, 25 (33), 4549–4554. https://doi.org/10.1002/adma.201301336.

(169) Fischbein, M. D.; Drndić, M. Electron Beam Nanosculpting of Suspended Graphene Sheets. Appl. Phys. Lett. 2008, 93 (11), 113107. https://doi.org/10.1063/1.2980518.

(170) Xu, X.; Li, C.; Zhou, Y.; Jin, Y. Controllable Shrinking of Glass Capillary Nanopores Down to Sub-10 Nm by Wet-Chemical Silanization for Signal-Enhanced DNA Translocation. ACS Sensors 2017, 2 (10), 1452–1457. https://doi.org/10.1021/acssensors.7b00385.

(171) Steinbock, L. J.; Bulushev, R. D.; Krishnan, S.; Raillon, C.; Radenovic, A. DNA Translocation through Low-Noise Glass Nanopores. ACS Nano 2013, 7 (12), 11255–11262. https://doi.org/10.1021/nn405029j.

(172) Sze, J. Y. Y.; Kumar, S.; Ivanov, A. P.; Oh, S.-H.; Edel, J. B. Fine Tuning of Nanopipettes Using Atomic Layer Deposition for Single Molecule Sensing. Analyst 2015, 140 (14), 4828–4834. https://doi.org/10.1039/C5AN01001B.

(173) Steinbock, L. J.; Steinbock, J. F.; Radenovic, A. Controllable Shrinking and Shaping of Glass Nanocapillaries under Electron Irradiation. Nano Lett. 2013, 13 (4), 1717–1723. https://doi.org/10.1021/nl400304y.

(174) Siwy, Z.; Dobrev, D.; Neumann, R.; Trautmann, C.; Voss, K. Electro-Responsive Asymmetric Nanopores in Polyimide with Stable Ion-Current Signal. Appl. Phys. A 2003, 76 (5), 781–785. https://doi.org/10.1007/s00339-002-1982-7.

(175) Kravets, L. I.; Dmitriev, S. N.; Apel, P. Y. The Properties and Porous Structure of Polypropylene Track Membranes. Radiat. Meas. 1995, 25 (1), 729–732. https://doi.org/https://doi.org/10.1016/1350-4487(95)00233-5.

(176) Shirkova, V. V; Tretyakova, S. P. Physical and Chemical Basis for the Manufacturing of Fluoropolymer Track Membranes. Radiat. Meas. 1997, 28 (1), 791–798. https://doi.org/https://doi.org/10.1016/S1350-4487(97)00186-8.

(177) Fleischer, R. L.; Price, P. B.; Symes, E. M. Novel Filter for Biological Materials. Science (80-.). 1964, 143 (3603), 249 LP-250. https://doi.org/10.1126/science.143.3603.249.

(178) Lück, H. B.; Matthes, H.; Gemende, B.; Heinrich, B.; Pfestorf, W.; Seidel, W.; Turuc, S. Production of Particle-Track Membranes by Means of a 5 MV Tandem Accelerator. Nucl. Instruments Methods Phys. Res. Sect. B Beam Interact. with Mater. Atoms 1990, 50 (1), 395–400. https://doi.org/https://doi.org/10.1016/0168-583X(90)90387-A.

(179) Barrat, J.-L.; Bocquet, L. Large Slip Effect at a Nonwetting Fluid-Solid Interface. Phys. Rev. Lett. 1999, 82 (23), 4671–4674. https://doi.org/10.1103/PhysRevLett.82.4671.

(180) Joly, L.; Ybert, C.; Trizac, E.; Bocquet, L. Liquid Friction on Charged Surfaces: From Hydrodynamic Slippage to Electrokinetics. J. Chem. Phys. 2006, 125 (20), 204716. https://doi.org/10.1063/1.2397677.

(181) Bocquet, L.; Charlaix, E. Nanofluidics, from Bulk to Interfaces. Chem. Soc. Rev. 2010, 39 (3), 1073–1095. https://doi.org/10.1039/B909366B.

(182) Balme, S.; Picaud, F.; Manghi, M.; Palmeri, J.; Bechelany, M.; Cabello-Aguilar, S.; Abou-Chaaya, A.; Miele, P.; Balanzat, E.; Janot, J. M. Ionic Transport through Sub-10 Nm Diameter Hydrophobic High-Aspect Ratio Nanopores: Experiment, Theory and Simulation. Sci. Rep. 2015, 5, 10135.

(183) Balme, S.; Picaud, F.; Lepoitevin, M.; Bechelany, M.; Balanzat, E.; Janot, J.-M. Unexpected Ionic Transport Behavior in Hydrophobic and Uncharged Conical Nanopores. Faraday Discuss. 2018, 210 (0), 69–85. https://doi.org/10.1039/C8FD00008E.

(184) Yusko, E. C.; An, R.; Mayer, M. Electroosmotic Flow Can Generate Ion Current Rectification in Nano- and Micropores. ACS Nano 2010, 4 (1), 477–487. https://doi.org/10.1021/nn9013438.

(185) Jorgenson, J. W.; Lukacs, K. D. High-Resolution Separations Based on Electrophoresis and Electroosmosis. J. Chromatogr. A 1981, 218, 209–216. https://doi.org/https://doi.org/10.1016/S0021-9673(00)82057-9.

(186) Hong, K. M.; Noolandi, J. Solution of the Smoluchowski Equation with a Coulomb Potential. I. General Results. J. Chem. Phys. 1978, 68 (11), 5163–5171. https://doi.org/10.1063/1.435636.

(187) Morgan, F. D.; Williams, E. R.; Madden, T. R. Streaming Potential Properties of Westerly Granite with Applications. J. Geophys. Res. Solid Earth 1989, 94 (B9), 12449–12461. https://doi.org/10.1029/JB094iB09p12449.

(188) Ohshima, H.; Ohki, S. Donnan Potential and Surface Potential of a Charged Membrane. Biophys. J. 1985, 47 (5), 673–678. https://doi.org/https://doi.org/10.1016/S0006-3495(85)83963-1.

(189) Stein, D.; Kruithof, M.; Dekker, C. Surface-Charge-Governed Ion Transport in Nanofluidic Channels. Phys. Rev. Lett. 2004, 93 (3), 35901. https://doi.org/10.1103/PhysRevLett.93.035901.

(190) Tagliazucchi, M.; Szleifer, I. 2 - Theoretical Basis for Structure and Transport in Nanopores and Nanochannels; Tagliazucchi, M., Szleifer, I. B. T.-C. M. N. and N., Eds.; William Andrew Publishing: Boston, 2017; pp 27–60. https://doi.org/https://doi.org/10.1016/B978-0-323-40182-1.00002-6.

(191) Vlassiouk, I.; Siwy, Z. S. Nanofluidic Diode. Nano Lett. 2007, 7 (3), 552–556. https://doi.org/10.1021/nl062924b.

(192) Tagliazucchi, M.; Szleifer, I. Chemically Modified Nanopores and Nanochannels; Elsevier Science, 2016.

(193) Hsu, J.-P.; Chen, Y.-M.; Yang, S.-T.; Lin, C.-Y.; Tseng, S. Influence of Salt Valence on the Rectification Behavior of Nanochannels. J. Colloid Interface Sci. 2018, 531, 483–492. https://doi.org/https://doi.org/10.1016/j.jcis.2018.07.012.

(194) Michelsen, K.; Schmid, V.; Metz, J.; Heusser, K.; Liebel, U.; Schwede, T.; Spang, A.; Schwappach, B. Novel Cargo-Binding Site in the β and δ Subunits of Coatomer. J. Cell Biol. 2007, 179 (2), 209 LP-217. https://doi.org/10.1083/jcb.200704142.

(195) Waldmann, R.; Lazdunski, M. H+-Gated Cation Channels: Neuronal Acid Sensors in the NaC/DEG Family of Ion Channels. Curr. Opin. Neurobiol. 1998, 8 (3), 418–424. https://doi.org/https://doi.org/10.1016/S0959-4388(98)80070-6.

(196) Govorunova, E. G.; Sineshchekov, O. A.; Janz, R.; Liu, X.; Spudich, J. L. Natural Light-Gated Anion Channels: A Family of Microbial Rhodopsins for Advanced Optogenetics. Science (80-.). 2015, 349 (6248), 647 LP-650. https://doi.org/10.1126/science.aaa7484.

(197) Patapoutian, A.; Peier, A. M.; Story, G. M.; Viswanath, V. ThermoTRP Channels and beyond: Mechanisms of Temperature Sensation. Nat. Rev. Neurosci. 2003, 4 (7), 529–539. https://doi.org/10.1038/nrn1141.

(198) Xia, F.; Guo, W.; Mao, Y.; Hou, X.; Xue, J.; Xia, H.; Wang, L.; Song, Y.; Ji, H.; Ouyang, Q.; et al. Gating of Single Synthetic Nanopores by Proton-Driven DNA Molecular Motors. J. Am. Chem. Soc. 2008, 130 (26), 8345–8350. https://doi.org/10.1021/ja800266p.

(199) Pérez-Mitta, G.; Burr, L.; Tuninetti, J. S.; Trautmann, C.; Toimil-Molares, M. E.; Azzaroni, O. Noncovalent Functionalization of Solid-State Nanopores via Self-

Assembly of Amphipols. Nanoscale 2016, 8 (3), 1470–1478. https://doi.org/10.1039/C5NR08190D.

(200) Nguyen, G.; Howorka, S.; Siwy, Z. S. DNA Strands Attached Inside Single Conical Nanopores: Ionic Pore Characteristics and Insight into DNA Biophysics. J. Membr. Biol. 2011, 239 (1), 105–113. https://doi.org/10.1007/s00232-010-9328-4.

(201) Yameen, B.; Ali, M.; Neumann, R.; Ensinger, W.; Knoll, W.; Azzaroni, O. Synthetic Proton-Gated Ion Channels via Single Solid-State Nanochannels Modified with Responsive Polymer Brushes. Nano Lett. 2009, 9 (7), 2788–2793. https://doi.org/10.1021/nl901403u.

(202) Yameen, B.; Ali, M.; Neumann, R.; Ensinger, W.; Knoll, W.; Azzaroni, O. Single Conical Nanopores Displaying PH-Tunable Rectifying Characteristics. Manipulating Ionic Transport With Zwitterionic Polymer Brushes. J. Am. Chem. Soc. 2009, 131 (6), 2070–2071. https://doi.org/10.1021/ja8086104.

(203) Pérez-Mitta, G.; Marmisolle, W. A.; Burr, L.; Toimil-Molares, M. E.; Trautmann, C.; Azzaroni, O. Proton-Gated Rectification Regimes in Nanofluidic Diodes Switched by Chemical Effectors. Small 2018, 14 (18), 1703144. https://doi.org/10.1002/smll.201703144.

(204) Buchsbaum, S. F.; Nguyen, G.; Howorka, S.; Siwy, Z. S. DNA-Modified Polymer Pores Allow PH- and Voltage-Gated Control of Channel Flux. J. Am. Chem. Soc. 2014, 136 (28), 9902–9905. https://doi.org/10.1021/ja505302q.

(205) Pérez-Mitta, G.; Marmisollé, W. A.; Trautmann, C.; Toimil-Molares, M. E.; Azzaroni, O. An All-Plastic Field-Effect Nanofluidic Diode Gated by a Conducting Polymer Layer. Adv. Mater. 2017, 29 (28), 1700972. https://doi.org/10.1002/adma.201700972.

(206) Pérez-Mitta, G.; Marmisollé, W. A.; Trautmann, C.; Toimil-Molares, M. E.; Azzaroni, O. Nanofluidic Diodes with Dynamic Rectification Properties Stemming from Reversible Electrochemical Conversions in Conducting Polymers. J. Am. Chem. Soc. 2015, 137 (49), 15382–15385. https://doi.org/10.1021/jacs.5b10692.

(207) Mal, N. K.; Fujiwara, M.; Tanaka, Y. Photocontrolled Reversible Release of Guest Molecules from Coumarin-Modified Mesoporous Silica. Nature 2003, 421 (6921), 350–353. https://doi.org/10.1038/nature01362.

(208) Liu; Dunphy, D. R.; Atanassov, P.; Bunge, S. D.; Chen, Z.; López, G. P.; Boyle, T. J.; Brinker, C. J. Photoregulation of Mass Transport through a Photoresponsive Azobenzene-Modified Nanoporous Membrane. Nano Lett. 2004, 4 (4), 551–554. https://doi.org/10.1021/nl0350783.

(209) Koçer, A.; Walko, M.; Meijberg, W.; Feringa, B. L. A Light-Actuated Nanovalve Derived from a Channel Protein. Science (80-.). 2005, 309 (5735), 755 LP-758. https://doi.org/10.1126/science.1114760.

(210) Vlassiouk, I.; Park, C.-D.; Vail, S. A.; Gust, D.; Smirnov, S. Control of Nanopore Wetting by a Photochromic Spiropyran: A Light-Controlled Valve and Electrical Switch. Nano Lett. 2006, 6 (5), 1013–1017. https://doi.org/10.1021/nl060313d.

(211) Li, P.; Xie, G.; Kong, X.-Y.; Zhang, Z.; Xiao, K.; Wen, L.; Jiang, L. Light-Controlled Ion Transport through Biomimetic DNA-Based Channels. Angew. Chemie Int. Ed. 2016, 55 (50), 15637–15641. https://doi.org/10.1002/anie.201609161.

(212) Zhang, M.; Hou, X.; Wang, J.; Tian, Y.; Fan, X.; Zhai, J.; Jiang, L. Light and PH Cooperative Nanofluidic Diode Using a Spiropyran-Functionalized Single Nanochannel. Adv. Mater. 2012, 24 (18), 2424–2428. https://doi.org/10.1002/adma.201104536.

(213) Nasir, S.; Ali, M.; Ensinger, W. Thermally Controlled Permeation of Ionic Molecules through Synthetic Nanopores Functionalized with Amine-Terminated Polymer Brushes. Nanotechnology 2012, 23 (22), 225502. https://doi.org/10.1088/0957-4484/23/22/225502.

(214) Liu, N.; Li, C.; Zhang, T.; Hou, R.; Xiong, Z.; Li, Z.; Wei, B.; Yang, Z.; Gao, P.; Lou, X.; et al. Fabrication of “Plug and Play” Channels with Dual Responses by Host–Guest Interactions. Small 2017, 13 (4), 1600287. https://doi.org/10.1002/smll.201600287.

(215) Zhang, Z.; Xie, G.; Xiao, K.; Kong, X. Y.; Li, P.; Tian, Y.; Wen, L.; Jiang, L. Asymmetric Multifunctional Heterogeneous Membranes for PH- and Temperature-Cooperative

Smart Ion Transport Modulation. Adv. Mater. 2016, 28 (43), 9613–9619. https://doi.org/10.1002/adma.201602758.

(216) Wang, R.; Sun, Y.; Zhang, F.; Song, M.; Tian, D.; Li, H. Temperature-Sensitive Artificial Channels through Pillar[5]Arene-Based Host–Guest Interactions. Angew. Chemie Int. Ed. 2017, 56 (19), 5294–5298. https://doi.org/10.1002/anie.201702175.

(217) Pérez-Mitta, G.; Albesa, A. G.; Knoll, W.; Trautmann, C.; Toimil-Molares, M. E.; Azzaroni, O. Host–guest Supramolecular Chemistry in Solid-State Nanopores: Potassium-Driven Modulation of Ionic Transport in Nanofluidic Diodes. Nanoscale 2015, 7 (38), 15594–15598. https://doi.org/10.1039/C5NR04645A.

(218) Wu, K.; Xiao, K.; Chen, L.; Zhou, R.; Niu, B.; Zhang, Y.; Wen, L. Biomimetic Voltage-Gated Ultrasensitive Potassium-Activated Nanofluidic Based on a Solid-State Nanochannel. Langmuir 2017, 33 (34), 8463–8467. https://doi.org/10.1021/acs.langmuir.7b01705.

(219) Liu, Q.; Xiao, K.; Wen, L.; Lu, H.; Liu, Y.; Kong, X.-Y.; Xie, G.; Zhang, Z.; Bo, Z.; Jiang, L. Engineered Ionic Gates for Ion Conduction Based on Sodium and Potassium Activated Nanochannels. J. Am. Chem. Soc. 2015, 137 (37), 11976–11983. https://doi.org/10.1021/jacs.5b04911.

(220) Ali, M.; Ahmed, I.; Ramirez, P.; Nasir, S.; Mafe, S.; Niemeyer, C. M.; Ensinger, W. Lithium Ion Recognition with Nanofluidic Diodes through Host–Guest Complexation in Confined Geometries. Anal. Chem. 2018, 90 (11), 6820–6826. https://doi.org/10.1021/acs.analchem.8b00902.

(221) Ali, M.; Ahmed, I.; Nasir, S.; Duznovic, I.; Niemeyer, C. M.; Ensinger, W. Potassium-Induced Ionic Conduction through a Single Nanofluidic Pore Modified with Acyclic Polyether Derivative. Anal. Chim. Acta 2018, 1039, 132–139. https://doi.org/https://doi.org/10.1016/j.aca.2018.07.056.

(222) Ali, M.; Ahmed, I.; Ramirez, P.; Nasir, S.; Cervera, J.; Mafe, S.; Niemeyer, C. M.; Ensinger, W. Cesium-Induced Ionic Conduction through a Single Nanofluidic Pore Modified with Calixcrown Moieties. Langmuir 2017, 33 (36), 9170–9177. https://doi.org/10.1021/acs.langmuir.7b02368.

(223) Hou, X.; Guo, W.; Xia, F.; Nie, F.-Q.; Dong, H.; Tian, Y.; Wen, L.; Wang, L.; Cao, L.; Yang, Y.; et al. A Biomimetic Potassium Responsive Nanochannel: G-Quadruplex DNA Conformational Switching in a Synthetic Nanopore. J. Am. Chem. Soc. 2009, 131 (22), 7800–7805. https://doi.org/10.1021/ja901574c.

(224) Tian, Y.; Hou, X.; Wen, L.; Guo, W.; Song, Y.; Sun, H.; Wang, Y.; Jiang, L.; Zhu, D. A Biomimetic Zinc Activated Ion Channel. Chem. Commun. 2010, 46 (10), 1682–1684. https://doi.org/10.1039/B918006K.

(225) Tian, Y.; Zhang, Z.; Wen, L.; Ma, J.; Zhang, Y.; Liu, W.; Zhai, J.; Jiang, L. A Biomimetic Mercury(Ii)-Gated Single Nanochannel. Chem. Commun. 2013, 49 (91), 10679–10681. https://doi.org/10.1039/C3CC42748J.

(226) Shang, Y.; Zhang, Y.; Li, P.; Lai, J.; Kong, X.-Y.; Liu, W.; Xiao, K.; Xie, G.; Tian, Y.; Wen, L.; et al. DNAzyme Tunable Lead(Ii) Gating Based on Ion-Track Etched Conical Nanochannels. Chem. Commun. 2015, 51 (27), 5979–5981. https://doi.org/10.1039/C5CC00288E.

(227) Xu, X.; Hou, R.; Gao, P.; Miao, M.; Lou, X.; Liu, B.; Xia, F. Highly Robust Nanopore-Based Dual-Signal-Output Ion Detection System for Achieving Three Successive Calibration Curves. Anal. Chem. 2016, 88 (4), 2386–2391. https://doi.org/10.1021/acs.analchem.5b04388.

(228) Li, P.; Kong, X.-Y.; Xie, G.; Xiao, K.; Zhang, Z.; Wen, L.; Jiang, L. Adenosine-Activated Nanochannels Inspired by G-Protein-Coupled Receptors. Small 2016, 12 (14), 1854–1858. https://doi.org/10.1002/smll.201503863.

(229) Wang, J.; Hou, J.; Zhang, H.; Tian, Y.; Jiang, L. Single Nanochannel-Aptamer-Based Biosensor for Ultrasensitive and Selective Cocaine Detection. ACS Appl. Mater. Interfaces 2018, 10 (2), 2033–2039. https://doi.org/10.1021/acsami.7b16539.

(230) Ali, M.; Ahmed, I.; Nasir, S.; Ramirez, P.; Niemeyer, C. M.; Mafe, S.; Ensinger, W. Ionic Transport through Chemically Functionalized Hydrogen Peroxide-Sensitive Asymmetric Nanopores. ACS Appl. Mater. Interfaces 2015, 7 (35), 19541–19545. https://doi.org/10.1021/acsami.5b06015.

(231) Sun, Z.; Liao, T.; Zhang, Y.; Shu, J.; Zhang, H.; Zhang, G.-J. Biomimetic Nanochannels Based Biosensor for Ultrasensitive and Label-Free Detection of Nucleic Acids. Biosens. Bioelectron. 2016, 86, 194–201. https://doi.org/https://doi.org/10.1016/j.bios.2016.06.059.

(232) Lepoitevin, M.; Nguyen, G.; Bechelany, M.; Balanzat, E.; Janot, J. M.; Balme, S. Combining a Sensor and a PH-Gated Nanopore Based on an Avidin-Biotin System. Chem. Commun. 2015, 51 (27), 5994–5997. https://doi.org/10.1039/c4cc10087e.

(233) Xu, X.; Zhao, W.; Gao, P.; Li, H.; Feng, G.; Zhao, Z.; Lou, X. Coordination of the Electrical and Optical Signals Revealing Nanochannels with an 'Onion-like' Gating Mechanism and Its Sensing Application. Npg Asia Mater. 2016, 8, e234.

(234) Ali, M.; Tahir, M. N.; Siwy, Z.; Neumann, R.; Tremel, W.; Ensinger, W. Hydrogen Peroxide Sensing with Horseradish Peroxidase-Modified Polymer Single Conical Nanochannels. Anal. Chem. 2011, 83 (5), 1673–1680. https://doi.org/10.1021/ac102795a.

(235) Xiao, K.; Wu, K.; Chen, L.; Kong, X.-Y.; Zhang, Y.; Wen, L.; Jiang, L. Biomimetic Peptide-Gated Nanoporous Membrane for On-Demand Molecule Transport. Angew. Chemie 2018, 130 (1), 157–161. https://doi.org/10.1002/ange.201708695.

(236) Ali, M.; Neumann, R.; Ensinger, W. Sequence-Specific Recognition of DNA Oligomer Using Peptide Nucleic Acid (PNA)-Modified Synthetic Ion Channels: PNA/DNA Hybridization in Nanoconfined Environment. ACS Nano 2010, 4 (12), 7267–7274. https://doi.org/10.1021/nn102119q.

(237) Liao, T.; Li, X.; Tong, Q.; Zou, K.; Zhang, H.; Tang, L.; Sun, Z.; Zhang, G.-J. Ultrasensitive Detection of MicroRNAs with Morpholino-Functionalized Nanochannel Biosensor. Anal. Chem. 2017, 89 (10), 5511–5518. https://doi.org/10.1021/acs.analchem.7b00487.

(238) Ali, M.; Yameen, B.; Neumann, R.; Ensinger, W.; Knoll, W.; Azzaroni, O. Biosensing and Supramolecular Bioconjugation in Single Conical Polymer Nanochannels. Facile Incorporation of Biorecognition Elements into Nanoconfined Geometries. J. Am. Chem. Soc. 2008, 130 (48), 16351–16357. https://doi.org/10.1021/ja8071258.

(239) Ali, M.; Ramirez, P.; Tahir, M. N.; Mafe, S.; Siwy, Z.; Neumann, R.; Tremel, W.; Ensinger, W. Biomolecular Conjugation inside Synthetic Polymer Nanopores Viaglycoprotein–lectin Interactions. Nanoscale 2011, 3 (4), 1894–1903. https://doi.org/10.1039/C1NR00003A.

(240) Ali, M.; Nasir, S.; Ramirez, P.; Cervera, J.; Mafe, S.; Ensinger, W. Carbohydrate-Mediated Biomolecular Recognition and Gating of Synthetic Ion Channels. J. Phys. Chem. C 2013, 117 (35), 18234–18242. https://doi.org/10.1021/jp4054555.

(241) Lepoitevin, M.; Jamilloux, B.; Bechelany, M.; Balanzat, E.; Janot, J. M.; Balme, S. Fast and Reversible Functionalization of a Single Nanopore Based on Layer-by-Layer Polyelectrolyte Self-Assembly for Tuning Current Rectification and Designing Sensors. RSC Adv. 2016, 6 (38), 32228–32233. https://doi.org/10.1039/c6ra03698h.

(242) Lepoitevin, M.; Bechelany, M.; Balanzat, E.; Janot, J.-M.; Balme, S. Non-Fluorescence Label Protein Sensing with Track-Etched Nanopore Decorated by Avidin/Biotin System. Electrochim. Acta 2016, 211. https://doi.org/10.1016/j.electacta.2016.06.079.

(243) Liu, N.; Jiang, Y.; Zhou, Y.; Xia, F.; Guo, W.; Jiang, L. Two-Way Nanopore Sensing of Sequence-Specific Oligonucleotides and Small-Molecule Targets in Complex Matrices Using Integrated DNA Supersandwich Structures. Angew. Chemie Int. Ed. 2013, 52 (7), 2007–2011. https://doi.org/10.1002/anie.201209162.

(244) Guo, W.; Hong, F.; Liu, N.; Huang, J.; Wang, B.; Duan, R.; Lou, X.; Xia, F. Target-Specific 3D DNA Gatekeepers for Biomimetic Nanopores. Adv. Mater. 2015, 27 (12), 2090–2095. https://doi.org/10.1002/adma.201405078.

(245) Pérez-Mitta, G.; Peinetti, A. S.; Cortez, M. L.; Toimil-Molares, M. E.; Trautmann, C.; Azzaroni, O. Highly Sensitive Biosensing with Solid-State Nanopores Displaying Enzymatically Reconfigurable Rectification Properties. Nano Lett. 2018, 18 (5), 3303–3310. https://doi.org/10.1021/acs.nanolett.8b01281.

(246) Achilli, A.; Cath, T. Y.; Childress, A. E. Power Generation with Pressure Retarded Osmosis: An Experimental and Theoretical Investigation. J. Memb. Sci. 2009. https://doi.org/10.1016/j.memsci.2009.07.006.

(247) Achilli, A.; Childress, A. E. Pressure Retarded Osmosis: From the Vision of Sidney Loeb to the First Prototype Installation — Review. Desalination 2010, 261 (3), 205–211. https://doi.org/https://doi.org/10.1016/j.desal.2010.06.017.

(248) Zhang, Z.; Wen, L.; Jiang, L. Bioinspired Smart Asymmetric Nanochannel Membranes. Chem. Soc. Rev. 2018, 47 (2), 322–356. https://doi.org/10.1039/C7CS00688H.

(249) Zhang, Z.; Kong, X. Y.; Xiao, K.; Liu, Q.; Xie, G.; Li, P.; Ma, J.; Tian, Y.; Wen, L.; Jiang, L. Engineered Asymmetric Heterogeneous Membrane: A Concentration-Gradient-Driven Energy Harvesting Device. J. Am. Chem. Soc. 2015, 137 (46), 14765–14772. https://doi.org/10.1021/jacs.5b09918.

(250) Zhang, Z.; Li, P.; Kong, X.-Y.; Xie, G.; Qian, Y.; Wang, Z.; Tian, Y.; Wen, L.; Jiang, L. Bioinspired Heterogeneous Ion Pump Membranes: Unidirectional Selective Pumping and Controllable Gating Properties Stemming from Asymmetric Ionic Group Distribution. J. Am. Chem. Soc. 2018, 140 (3), 1083–1090. https://doi.org/10.1021/jacs.7b11472.

Chapter 2:

Biomimetic stimuli-responsive ion channels

Introduction

This chapter is dedicated to the use of polyelectrolytes and polymers to functionalize track-etched nanopores in order to build biomimetic stimuli-responsive ion channels. As described in chapter 1, ion channels play a very important role in life of cells. They can respond to external stimuli to self-regulate intelligently. The transfer of these “smart” properties of ion channels to the artificial is of great interest for membranes industries. Selectivity and permeability are two factors to determine the performance of a membrane. They are principally controlled by pore size and surface properties. These two factors of traditional membranes are usually unchangeable thank to the membrane fouling or working-condition changes. Our objectives were to functionalize ionic-diodes to give them the ability to self-regulate their selectivity and permeability according to environment changes such as pH, light.

Here we investigated two channels of which one is pH-responsive and one is pH and light-responsive. For the first one we used layer-by-layer self-assembly pH-sensitive polyelectrolytes (poly-L-lysine/polyacrilic acid and polyethylenimine/polyacrilic acid). For the second one, we used more complex approach using chemical grafting of polymer functionalized with photo-switchable molecule (Polyethylene glycol-spiropyran). These macromolecules can change their structures, charges and hydrophylicity/hydrophobicity balance. Thus, they allow controlling the pore size and surface properties of the nanopore.

The experiments were performed in conical track-etched nanopores which has a diode-like behavior. Such property of asymmetrical nanopore can show an ion rectification because of the ion depletion/ion enrichment effect under electric fields. This ion rectification as well as ion conductance provides a visual characterization of the membrane changes described above.

The results presented in this chapter have been published as two articles:

Polyelectrolyte Multilayers on the Ionic Current Rectification of Conical Nanopores. Langmuir, 2018, 34 (11), pp 3405–3412.

Combining Light-Gated and pH-Responsive Nanopore Based on PEG-Spiropyran Functionalization. Adv. Mater. Interfaces, 2017, 5, 1701051.

Articles

Impact of polyelectrolyte multilayers on the ionic current rectification of conical nanopores

Tianji Ma, Paulius Gaigalas, Mathilde Lepoitevin, Ieva Plikusiene, Mikhael Bechelany, Jean-Marc Janot, Emmanuel Balanzat, and Sebastien Balme

Contribution: I performed nanopore experiments starting by P. Gaigalas and analyzed data. I contributed to the paper writing. .

Introduction

For the last two decades, single nanopore technology has contributed to the emergence and design of nano-fluidic responsive systems[1-4]. It has provided a deep understanding of the transport from simple electrolyte to (bio)macromolecule (DNA, polymer or protein) at the nano-scale and contributed to the development of new analytical devices[5-6]. Nanopores with a dissymmetry of charge or shape are also particularly fascinating for their ionic diode behavior[7-11]. They are usually obtained using polymer film (PET, PC or PI) by track-etched technique under dissymmetrical condition to ensure a conical shape[12]. In such nanopore, the ionic current rectification (ICR) comes from a depletion of anions or cations inside the nanopore[13-14]. It can be tuned by the functionalization of the nanopore inner surface walls. Following this strategy, numerous molecules or macromolecules were attached on the nanopore inner surface to develop stimuli channel such as pH-gate [15-16], light-responsive[17-18] as well as sensors[19-20].

The possibility to drive the ionic transport properties of a membrane in term of aperture and selectivity by the pH is one way to develop “smart” membranes. The first way is to graft molecules which exhibit different charges as a function of pH onto the reactive moieties induced by the chemical etching (typically carboxyl for PET). This allows a selective functionalization of the inner surface wall of the nanopore. Following this strategy, poly-protonic polymer brushes were used to drive the ICR with the pH[21]. Amphoteric molecules such as lysine or histidine were used to modify the nanopore selectivity[19]. At low pH, the

nanopore is positively charged and selective to anion, while at high pH it becomes negatively charged and thus selective to cation. Similar properties were also reported for a functionalization with poly(methacryoyl-L-lysine) brushes[20]. Spiropyran was also considered to drive the nanopore selectivity with the pH and control the aperture with the light. The second way to obtain pH responsive nanopore is the functionalization by layer-by-layer (LbL) deposition of polyelectrolyte[22]. This method is a fast and convenient. Indeed, it was reported that the adsorption of the poly-l-lysine on PET induce an inversion of ICR. This was used to monitor that the functionalization is occurred. The LbL deposition of polyelectrolyte were also considered to improve the ionic selectivity and reduces the fouling by proteins of membrane[23-24]. The deposition of multilayer of chitosan (CS)/ polyacrylic acid (PAA) creates a zwitterionic film onto the nanopore inner surface. This nanopore is thus selective to anion at low pH and cation at high pH as reported for the one functionalized by amphoteric molecule grafting[25]. However, this behavior cannot be generalized to all nanopore functionalized with polyelectrolyte. This was evidenced by nanopores functionalized with poly(ethylenimine) (PEI) and chondroitin-4-sulfate (ChS) multilayers[16]. At low salt concentration, the nanopore is close at pH > 4, while it is open and selective to anions at pH < 4. This phenomenon was interpreted by the swelling of ChS which occurs at low pH. The opposite behavior of nanopores functionalized with CS/PAA and with PEI/ChS is not totally understand and require further investigations. However, we can assume that the ICR properties is not mainly driven by the global charged of the nanopore but also by the reorganization and the swelling of polyelectrolyte layers. This assumption is supported by the inversion of ICR with pH that occurred for CS/PAA. Indeed the CS is not soluble at pH upper than 5 preventing the swelling of polyelectrolyte layers.

This work aims to investigate how the swelling and the polyelectrolyte reorganization influence the ICR of the conical nanopore which was not investigate in the previous paper. This work is also motivated to provide experimental solutions to fashion pH-gate and pH-responsive membrane which require understanding of all phenomena involved in the ionic transport inside the nanopore. To do so, we have functionalized single conical nanopore in PET, obtained by track-etched technique with two couples of polyelectrolytes: poly-l-lysine (PLL) /PAA and PEI/PAA. The influences of pH and ionic strength on ionic transport (conductance and ICR) were studied. Spectroscopic ellipsometry experiments were

performed on surface to characterize the influence of salt concentration and pH on the swelling of the polyelectrolyte multilayers. Finally, the impact of cross-linking of PLL/PAA was also considered to prevent the large structural modification of polyelectrolyte layers.

Material and Methods

Material

Poly(ethylene terephthalate) (PET) film (thickness 13 µm, biaxial orientation) was purchased from Goodfellow (ES301061). Sodium chloride (71380), potassium chloride (P3911), sodium hydroxide (30603), hydrogen chloride (30721), branched PEI (Mw 25 kD, 408727), PAA (Mw 100 kD, 523925), PLL (Mw 30 kD-60kD P2636), N-(3-Dimethylaminopropyl)-N'-ethylcarbodiimide hydrochloride (EDC) (03450) were purchased from Sigma-Aldrich. Ultra-pure water was produced from a Q-grad®-1 Milli-Q system (Millipore).

Track-etching nanopores and characterization

Single tracks were produced by Xe irradiation (8.98 MeV) in PET films (13 µm) (GANIL, SEM line, Caen, France). The PET films were exposed to UV light for 24h per side to activate the track (Fisher bioblock; VL215.MC, λ = 302 nm), before the chemical etching process. The etching of the conical nanopore was performed under dissymmetric conditions following the electro-stopping method[9]. The PET foil was mounted between the two compartments of a chemical cell in Teflon. The etchant solution (NaOH 9 M, 1.6 ml) was added on the base side and the stopping solution (KCl 1M and acetic acid 1M, 1.6 ml) on the tip side. A potential of 1 V was applied across the membrane; the reference electrode is immersed in the stop solution and the working one in the etchant solution. When the current reaches a value of several hundred pA, the etching process was stopped by the replacement of the etching solution by the stop one.

The conical nanopores are characterized as follow. The base diameter (*D*) is calculated as a function of the total etch time *t* (min) using the relationship determined in our lab $D = 2.5t$. The tip diameter (*d*) was calculated from the dependence of the conductance *G* to the NaCl concentration (equation 1)[26]. This calculation assumes a bulk-like ionic conductivity inside the nanopores. In order to correct the conductivity at high salt concentration, the diameter is calculated using the ionic conductivity of solution *κ*. The latter have been measured using

a conductimeter (Hanna HI 255 combined meter with conductivity and electrode HI 76310) after preparation.

$$G = \kappa \pi D d / 4L \quad (1)$$

where *L* is the nanopore length.

Current-voltage measurements

Electrical measurements were performed using a patch-clamp amplifier (EPC10 HEKA electronics, Germany). The current is measured by Ag/AgCl electrode. A single nanopore was mounted in the chemical Teflon cell containing an electrolyte solution. One electrode was plugged to the working end of the amplifier (*trans* chamber, base side) and the other electrode connected to the ground (*cis* chamber, tip side). Recorded currents were analyzed by Fitmaster (Heka Elektronik, Germany).

For I–V curves, the currents data were recorded as a function of the time under constant voltage from -1 V to 1 V by 100 mV step and from -100 mV to 100 mV by 10 mV steps. All current traces were recorded during 10 s at a frequency of 50 kHz. These measurements were performed 3 times. The conductance *G* is extracted from the linear zone of I-V curves from typically -75 mV to 75 mV.

Nanopore functionalization

PAA, PEI and PLL stock solutions at concentration of 1 mg ml^{-1} (pH 7) were prepared. The functionalization of the nanopores was performed under KCl 0.1 M pH 7 by addition of 16 µl of stock solution in the tip side of the nanopore (Fig. 1). First, the polycation (PEI or PLL) was added under voltage -1V for 5 minutes. Then PAA was added at the tip side during 5 minutes applying 1V. After each deposition, the cell was filled with KCl 0.1 M pH 7 to remove the excess of polyelectrolytes. The same procedure was repeated until the desired numbers of PEI/PAA or PLL/PAA bilayers was reached. During the deposition, the current was recorded at 5 kHz frequency in order to monitor the adsorption of the polyelectrolytes.

Nanopore	d	D	$(Polyelectrolyte)_{\#layers}$
NP-1	30	300	$(PLL)_3/(PAA)_3$
NP-2	28	475	$(PEI)_4/(PAA)_4$

NP-3	116	346	$(PLL)_{10}/(PAA)_{10}$
NP-4	91	460	$(PEI)_8/(PAA)_8$
NP-5	65.1	600	$(PLL)_2/(PAA)_2$crosslinked

Table 1 : list of the nanopores used in this work

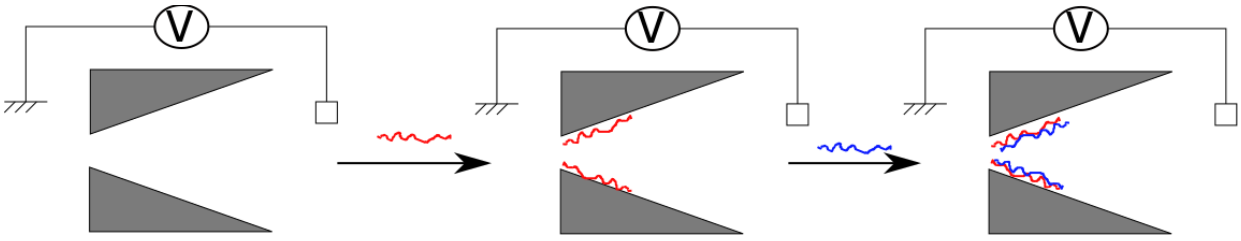

Fig. 1 Sketch to illustrate the nanopore functionalization with polyelectrolyte polycations (PLL or PEI) are in red and polyanions (PAA) are in blue.

Spectroscopic ellipsometry

Ellipsometric investigation of PLL/PAA and PEI/PAA bilayers were performed using spectral ellipsometer from J. A. Woollam M2000X on silicon wafer substrate. Firstly, a surface of the wafer was activated using piranha solution (H_2SO_4:H_2O_2 3:1) to form -OH groups at the surface which are necessary for the immobilization of the polyelectrolyte layers. Ellipsometric spectra were recorded from 200 nm to 1000 nm, angle of incident light was 70°. Cauchy dispersion function was applied for the regression analysis of the formed PEI, PAA and PLL layers. Optical constants and thicknesses of these layers were obtained using Complete EASE software.

Results and discussion

Polyelectrolyte deposition

Several single conical nanopores were obtained in PET film (thickness 13µm) by track-etched method (Table 1). For the one with a large tip diameter (d ~ 100 nm) more than 8 bilayers were deposited. For the ones with small tip diameter (d ~ 30 nm) less than 4 bilayers were used. After chemical etching, the inner surface of nanopore is covered by carboxylate groups and thus exhibits a negative surface charge at pH 8. In this case the I-V dependence recorded from -1 V to 1 V curves shows an ICR characterized by the rectification factor $f_{rec} =$

$|I_{(1V)}|/|I_{(-1V)}| < 1$ under our experimental condition. The polycation (PEI or PLL) or polyanion (PAA) deposition was performed by addition on the tip side of the nanopore. The applied voltage ±1V provides the energy required by the polyelectrolyte to overcome the barrier of entrance inside nanopore. Independently of the polyelectrolyte, the current recorded as a function of the time during the functionalization shows a strong decrease, which is induced by the charge inversion at the nanopore entrance [24]. Basically, after adsorption of the polycations, the nanopore becomes positively charged and thus the rectification factor increases above 1. Conversely, after the adsorption of the polyanions, the nanopore becomes negatively charged and the rectification factor decreases below 1. The inversion of the rectification factor evidences that each layer of polyelectrolytes has been deposited successfully (Fig. 2). According to previous work, we can assume that the polyelectrolyte deposition occurs at the narrow opening.

The evolution of f_{rec} with the number of polyelectrolyte layer strongly depends on the polycation. For $(PLL)_{10}/(PAA)_{10}$ with the increasing the number of bilayers, the addition of PLL does not induce a clear inversion of the rectification factor. The latter tends to an asymptotic value around 10^{-3}. Similar behavior was previously reported in the case of PEI/ChS deposition[16]. It can be assigned to partial charge compensation between either polyelectrolytes or an in-homogeneous surface charge patterns between the region close to the narrow opening and the rest of the nanopore. For $(PEI)_8/(PAA)_8$, the inversion of rectification occurs after each deposition likely due to a better charge compensation between polyelectrolytes. However, it is interesting to note that f_{rec} does not tend to 1 as reported for PAH/PSS[22].

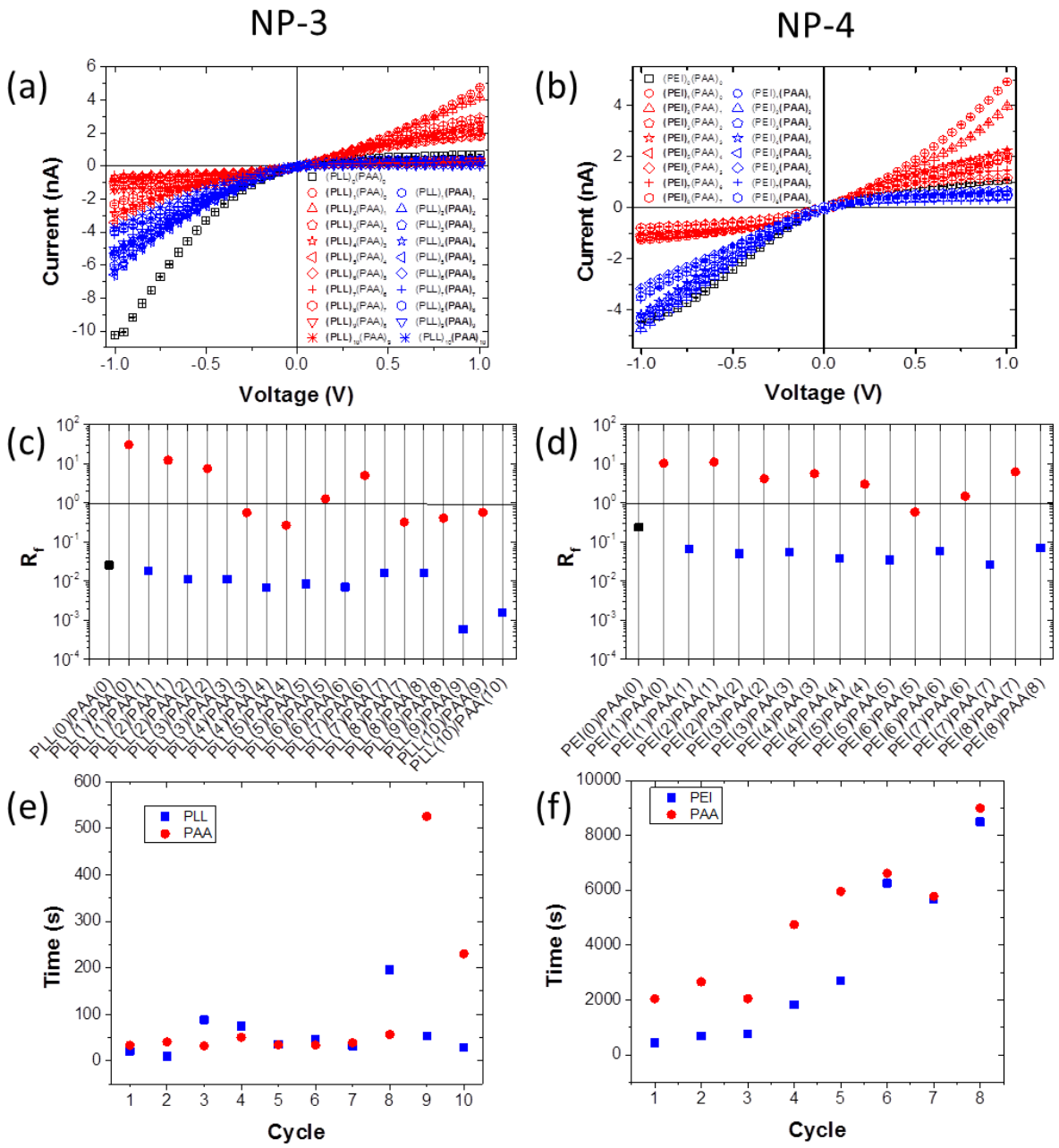

Fig. 2 Characterization of the nanopore functionalization. I-V dependence after polyelectrolyte deposition recorded at NaCl concentration of 0.1 M (a) NP-3 (b) NP-4. Rectification factor after the deposition of each electrolyte (c) NP-3 (d) NP-4. Time required to observe the inversion of current rectification induced by the polyelectrolyte deposition (e) NP-3 (f) NP-4

The time required to deposit the polyelectrolyte is very dependent on the nature of the polycation and the number of layers. In the case of PLL/PAA, the polyelectrolyte depositions

were achieved shorter than 120 s for the first seven bilayers. The disposition of bilayers 8 to 10 required more time. For PEI/PAA, the required deposition time was longer than the one for PLL/PAA. Typically the 3 first layers of PAA were achieved after more than 2000 s. In addition, the deposition time increased with the number of bilayers suggesting that it is probably due to steric hindrance. In order to confirm that, the thickness of PLL/PAA and PEI/PAA bilayers were investigated by spectroscopic ellipsometry. The obtained values of refraction index dispersion are presented in Fig. 3 and thicknesses of the layers are reported in Table 2. Figure SI-1 of raw Psi and Delta data shows that additional bilayers are formed on the top of the silicon substrate. Optical model well fits data for single PLL, PEI layers and for PLL/PAA and PEI/PAA bilayers only. The building of an optical model becomes very complicated when more bilayers are deposited on the substrate. Spectroscopic ellipsometry characterization evidences a difference of bilayer thickness which is 7.28 nm and 3.91 nm for PEI/PAA and PLL/PAA respectively. This difference is mainly due to the thickness of the PAA layer and thus its conformation which is more folded in presence of PEI. Thus, the longer deposition time reported for PEI/PAA can be interpreted by steric effects which make more complicated the penetration of the polyelectrolyte inside the nanopore. Another interpretation is the necessity to add more PAA chains to cover the PEI layers.

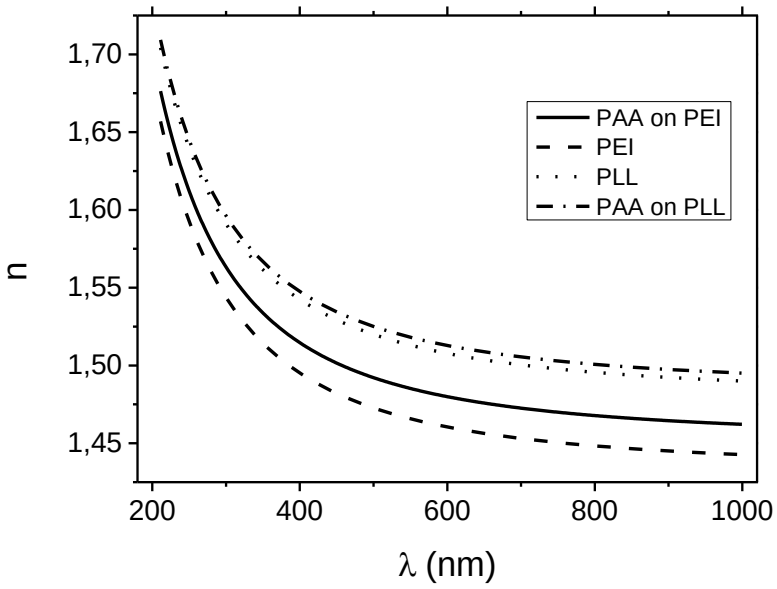

Fig. 3 Refractive indexes dispersion obtained for PAA, PEI and PLL layers deposited on silicon wafer substrate.

	PEI/PAA		PLL/PAA	
	PEI	PAA	PLL	PAA
Thickness (nm)	2.14	5.14	1.68	2.23

Table 2: Thicknesses of PLL, PAA, PEI layers on silicon wafer

Ionic transport through nanopores modified by LbL deposition

The ionic transport properties of the nanopore decorated with the polyelectrolyte were studied for different NaCl concentrations (from 10^{-3} M until 1 M) at various pH (Fig. 4). Because the pKa of PAA is 4.5, we can expect that at pH 3 the nanopore will be globally positively charged inducing an inversion of the rectification factor.

PEI/PAA LbL functionalization of a nanopore

In Fig. 4 are reported the I-V dependence at pH 3 and 7 for two nanopores with large (d>90 nm) and small (d~30 nm) tip diameters. For the nanopore (d= 91 nm) functionalized with 8 bilayers of PEI/PAA, the I-V dependence shown a rectification factor below 1 at pH 7.

Interestingly, at pH 3, the inversion of the rectification factor occurs at low salt concentration (NaCl = 0.01 and 0.05 M). With the increase of the salt concentration, the nanopore seems closed and the rectification factor is about 1. Such pH-gating properties under acidic conditions were previously reported for nanopore decorated with PEI/ChS [16]. However in that case, the pH-gate property disappeared with the increase of the salt concentration. For the PEI/PAA, the interesting result is that the nanopore is selective to anion at low salt concentration at pH 3. To confirm this property, the same study was performed in a conical nanopore with a smaller tip diameter (d=29 nm) decorated with 4 bilayers of PEI/PAA. The I-V dependences reported on Figure 3 reveal the same behavior. For these two nanopores, the enclosure at pH 3 arises for a NaCl concentration of 0.1 M. It should be notice here that the behavior observed at pH 3 is totally reversible with the increase of pH.

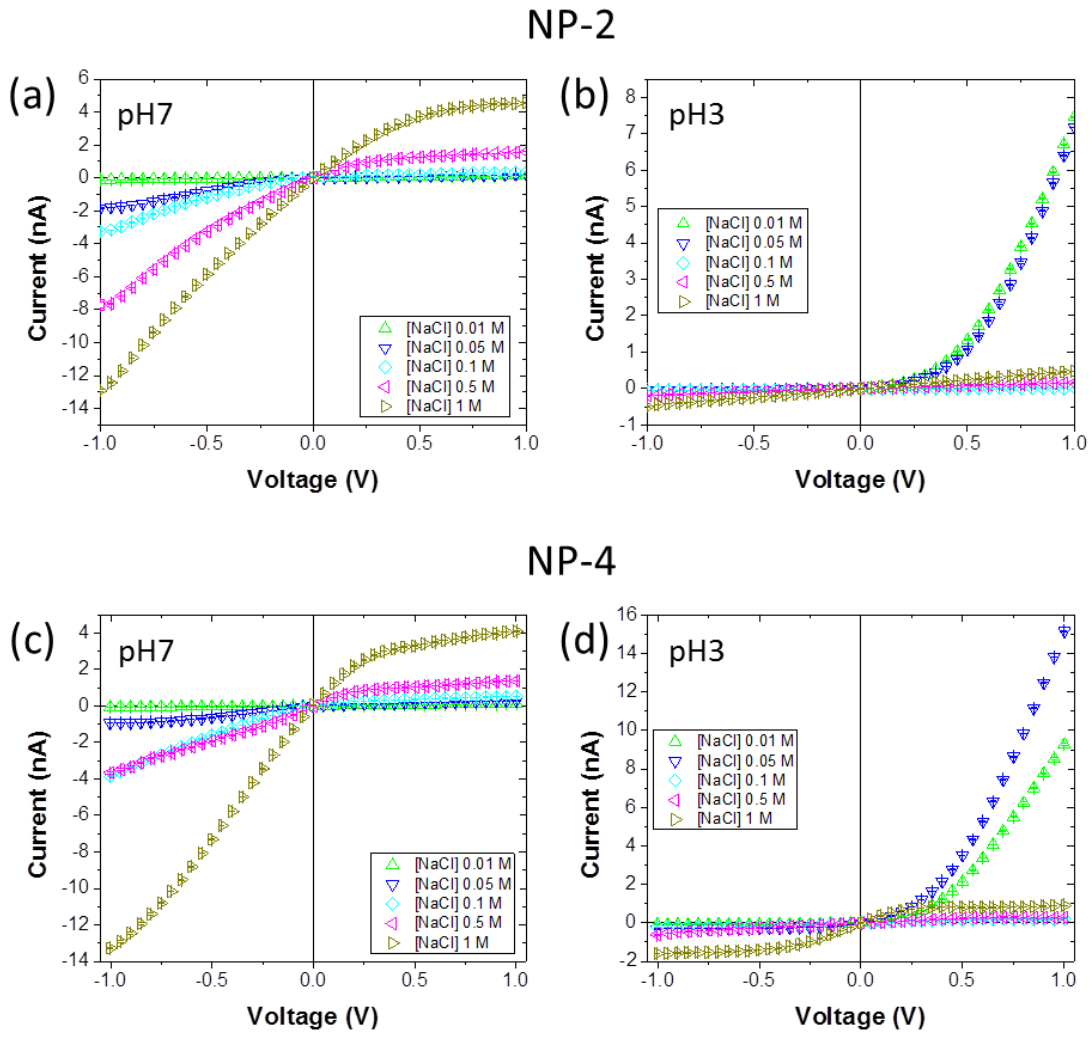

Fig. 4 I-V dependance of NP functionalized with PEI/PAA LbL at pH 7 and pH 3

To go further in our investigations, we studied the evolution of the nanopore conductance as a function of the NaCl concentration for different pH (Fig. 5). Inside a charged nanopore, the ionic conductance decreases with the salt concentration until a plateau. This constant conductivity is due to the mobile counter ions which shield the surface charge and the slippage[27-29]. At pH above 4, the conductance decreases with the salt concentration without reaching clearly a plateau. This result suggests a global compensation of charges between the polycations and polyanions. This is also consistent with the charge inversion observed after each polyelectrolyte deposition. At pH 3, the conductance exhibits an unusual dependence with the salt concentration. At salt concentration below 0.1 M, the conductance decreases with the salt concentration, however, the values are higher than the one obtained at pH >3. This can be explained by the disequilibrium of charge induced by the protonation of the carboxylate groups of PAA. In order, to counterbalance the excess of positive charges or PEI, Cl^- ions are "pumped" from the reservoir into the nanopore, increasing the concentration of mobile ions. For salt concentration above 0.1 M, the conductance decreases due to nanopore enclosure. This could be assigned to the reorganization of the polyelectrolyte layers.

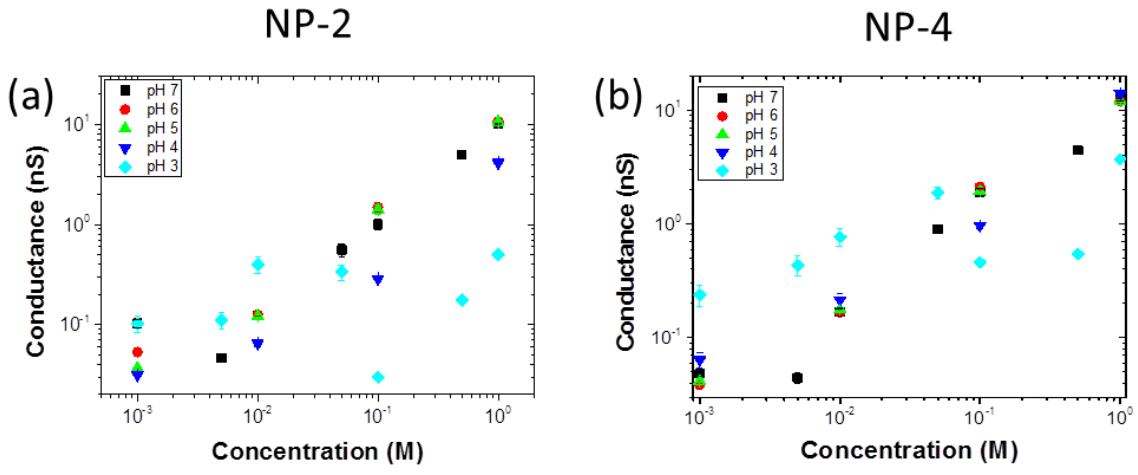

Fig. 5 Dependence of the conductance vs the NaCl concentration of NP functionalized with PEI/PAA LbL from pH 7 to pH 3

Conical nanopores decorated with PLL/PAA LbL

The NaCl transport though nanopore functionalized with PLL/PAA LbL exhibits a completely different behaviors (Fig. 6). The rectification is lower than 1 at pH 7. The conductance as function of the NaCl concentration reveals a plateau at low salt concentration as usually reported in the case of charged nanopore. This constant conductance is attributed to a partial compensation of charge between PLL and PAA. This is consistent with the fact that the PLL deposition did not induce an inversion of ICR previously shown. The value of the conductance plateau at low salt concentration is higher at pH 4 and 3. This could be explained by the protonation of PAA which breaks the partial balance of charge between both polyelectrolytes. In this case, the global charge of the polyelectrolyte layers should become globally positive and, thus, we could expect an inversion of ICR. The I-V curves recorded at pH 3 for two nanopores with different diameters exhibit rectification factor below 1 that is on opposition with the expected result (Figure 5). This can be interpreted by two assumptions. The first one is the modification of PAA pKa in nanopore as predicted by theoretical model[30] and supported by previous work[20]. The second one is a modification of the polyelectrolyte conformation as occurs for PEI/PAA or PEI/ChS.

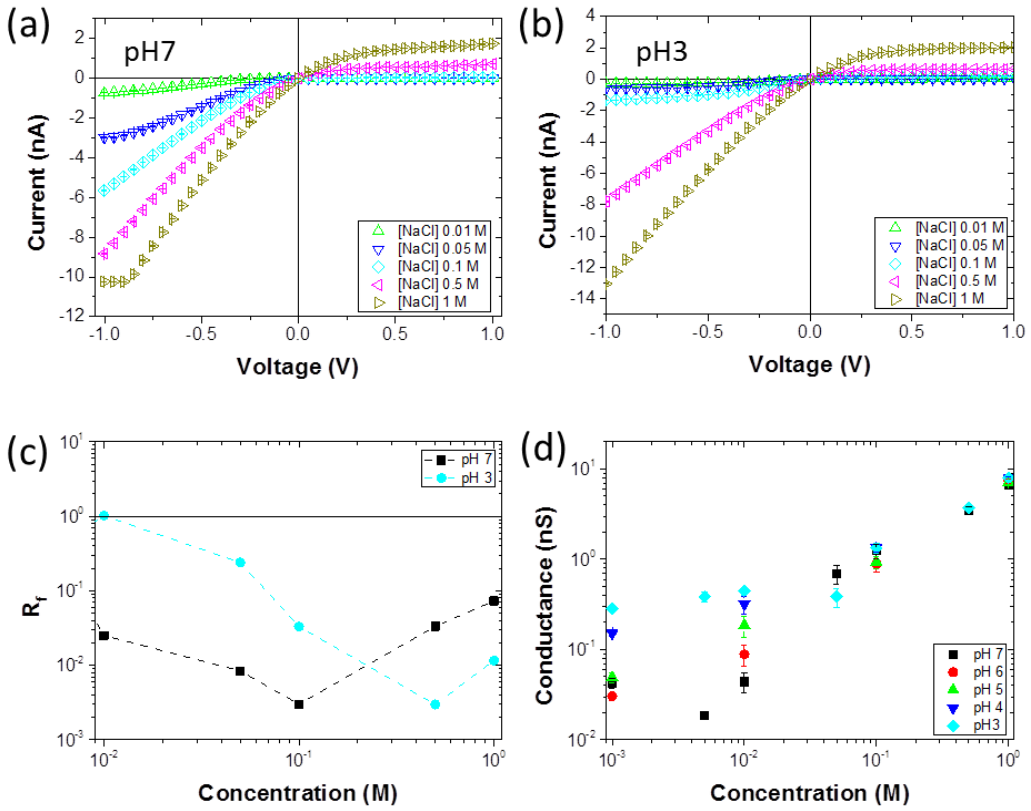

Fig. 6 I-V dependence (a-b), rectification factor (c) at ph 7 and pH 3 and conductance as a function of NaCl concentration (d) of NP functionalized with PLL/PAA LbL from pH 7 to pH 3.

We have investigated how pH and the NaCl concentration affect the PLL/PAA bilayers structure by total internal reflection spectroscopic ellipsometry (TIRE) (Fig. 7). When increasing the NaCl concentration from 0.01 M to 1 M, the ellipsometry parameters shift to the longer wavelength. This indicates a swelling of the polyelectrolyte bilayers. For a fixed NaCl concentration (0.01 M or 1 M), the ellipsometry spectra are quite similar at pH 3 and 7. This means that the pH does not influence the bilayer swelling. Usually, weak polyelectrolyte layers like PAA swell at pH below their pKa[31]. According to the TIRE results, the non-inversion of the ICR at pH 3 could be attributed to a displacement of the pKa of PAA. However this interpretation does not take in account the effect of confinement and the possible displacement of polyelectrolyte chains.

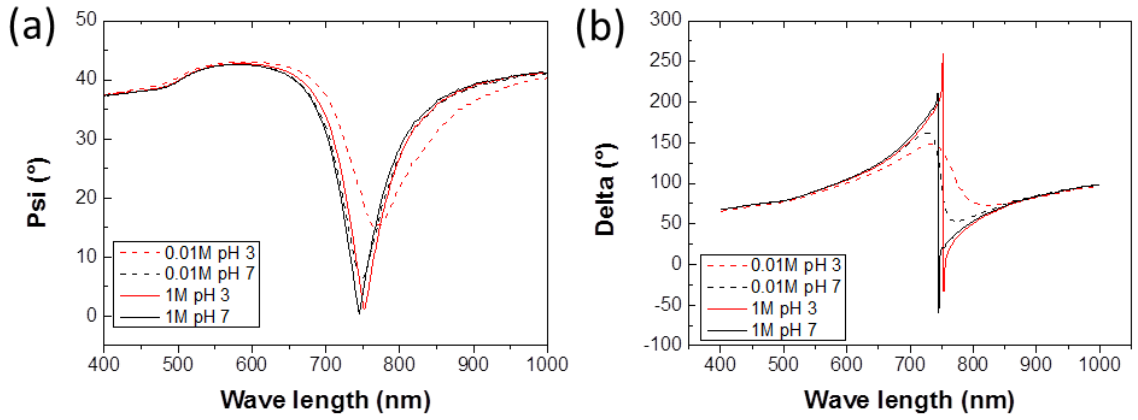

Fig. 7 Real time monitoring of ellipsometric parameters Psi and Delta using pH and NaCl concentration.

To go further in our investigation, we have evaluated if the modification of PLL/PAA bilayer structure is involved in the non-inversion of the ICR at pH 3. In order to stabilize the polyelectrolyte bilayer, the amine of PLL and carboxylic moieties of PAA were cross-linked after deposition using N-(3-Dimethylaminopropyl)-N'-ethylcarbodiimide. The evidence of each steps of functionalization was characterized by the modification of the ICR. The I-V response were recorded at different NaCl concentrations from 10^{-3} M to 1 M at pH 8 and 3 (Fig. 8). At pH 8, the current rectification is below 1 whatever the salt concentration. This means that the nanopore enhances the transport of cation (here Na^+) compared to Cl^-. This is confirmed by the permeation ratio P_{Na+}/P_{Cl-} = 8 measured under dissymmetrical condition. This result is assigned to a charge globally negative of the nanopore. This is reasonable because the last layer is polyanion and the nanopore surface is totally deprotonated. At pH 3, an inversion of the current rectification occurs. The factor is above than 1. In this case, the transport of Cl^- is favored compared to the Na^+ as confirmed by a permeation ratio P_{Na+}/P_{Cl-} = 0.01. This result is assigned to a global positive charge of the region close to the narrow opening where are located the polyelectrolyte layers. The inversion of ICR is reversible with the increase of pH.

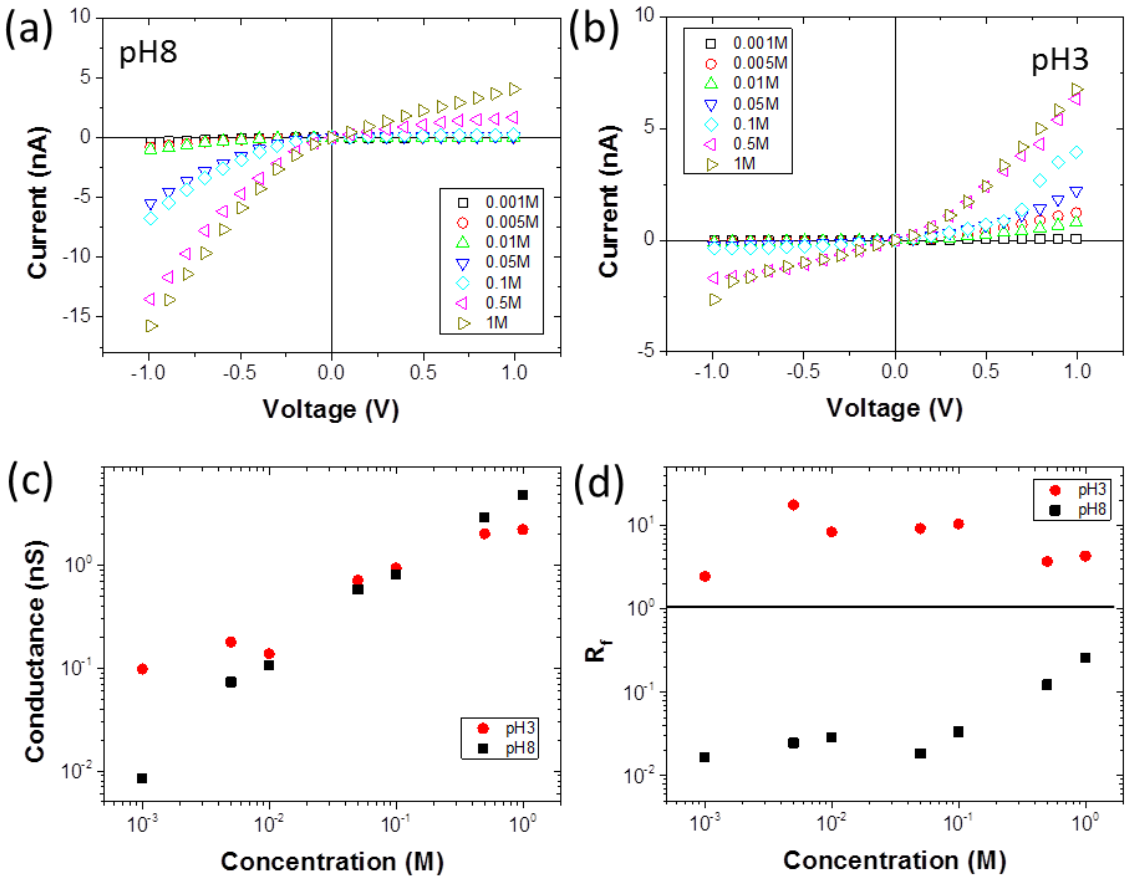

Fig. 8 I-V dependence (a-b), rectification factor (c) and conductance as a function of NaCl concentration (d) of NP functionalized with PLL/PAA LbL at pH 8and pH 3.

The conductance dependence with the salt concentration does not follow the same behavior at pH 3 and pH 8. At pH 3, the conductance decreases with the salt concentration until reaching a plateau at NaCl 0.01 M. The constant conductance is assigned to the counter mobile anions present inside the nanopore to shield the excess of positive charges in the polyelectrolyte layers. At pH 8, the constant value at low concentration is not observed suggesting charge compensation between the electrolytes and eventually counter ions trapped inside layer. This interpretation seems in contradiction with the rectification below 1 which suggests a preferential transport of cation. But, it has to be stressed out that the functionalization occurs only close to the narrow aperture, the rest of the nanopore is negatively charged. This dissymmetry of charges along the nanopore explains the current rectification. These results confirm that the structure modification of polyelectrolyte induced by the pH and/or salt concentration is involved in the ICR properties. For PLL/PAA only deposited on the inner surface of the nanopore, the pH effect does not induced and

expected inversion of ICR. However after crosslinking, the polyelectrolyte layers are stabilized and cannot easily move. In this case, the nanopore exhibits similar properties than if it is functionalized with zwitterionic molecules. This is also consistent with the properties previously reported for a conical nanopore functionalized with chitosan/PAA. Indeed, the chitosan is not soluble at pH upper than 5, and thus, the bilayer cannot move as after crosslinking.

Conclusion

To sum up, our work aimed to investigate the impact of the polyelectrolyte swelling and reorganization on the ICR properties of the conical nanopore. The starting assumption was those polyelectrolyte multilayers create a zwitterionic film on nanopore surface where the charges and thus the IRC can be inversed by the pH. The simple deposition of PLL/PAA and PEI/PAA does not follow this trend. For the nanopore functionalized with PEI/PAA, interesting ionic transport properties were obtained because at pH 3 the nanopore is selective to anion and open only at low salt concentration. Conversely at pH 7, it is selective to cation and already open whatever the salt concentration. For the nanopore functionalized with PLL/PAA, the ICR inversion does not occurred at pH 3. The effect of polyelectrolyte reorganization is confirmed because after crosslinking to prevent the swelling, the ICR is consistent with the expected global charge of the nanopore. Globally, our work highlights how the control of the polyelectrolyte behavior is a key point to fashion pH-responsive nanopore as well as membrane because the track-etched technique allows obtaining a single pore as well as multipore.

Reference

1. Lepoitevin, M.; Ma, T. J.; Bechelany, M.; Janot, J. M.; Balme, S., Functionalization of single solid state nanopores to mimic biological ion channels: A review. Adv Colloid Interfac 2017, 250, 195-213.

2. Zhang, H. C.; Tian, Y.; Jiang, L., Fundamental studies and practical applications of bio-inspired smart solid-state nanopores and nanochannels. Nano Today 2016, 11 (1), 61-81.

3. Ali, M.; Ahmed, I.; Ramirez, P.; Nasir, S.; Niemeyer, C. M.; Mafe, S.; Ensinger, W., Label-Free Pyrophosphate Recognition with Functionalized Asymmetric Nanopores. Small 2016, 12 (15), 2014-2021.

4. Ali, M.; Ahmed, I.; Ramirez, P.; Nasir, S.; Cervera, J.; Mafe, S.; Niemeyer, C. M.; Ensinger, W., Cesium-Induced Ionic Conduction through a Single Nanofluidic Pore Modified with Calixcrown Moieties. Langmuir 2017, 33 (36), 9170-9177.

5. Hou, X.; Guo, W.; Jiang, L., Biomimetic smart nanopores and nanochannels. Chem Soc Rev 2011, 40 (5), 2385-2401.

6. Shi, W. Q.; Friedman, A. K.; Baker, L. A., Nanopore Sensing. Anal Chem 2017, 89 (1), 157-188.

7. Constantin, D.; Siwy, Z. S., Poisson-Nernst -Planck model of ion current rectification through a nanofluidic diode. Phys Rev E 2007, 76 (4), 041202.

8. Siwy, Z.; Heins, E.; Harrell, C. C.; Kohli, P.; Martin, C. R., Conical-nanotube ion-current rectifiers: The role of surface charge. J Am Chem Soc 2004, 126 (35), 10850-10851.

9. Apel, P. Y.; Korchev, Y. E.; Siwy, Z.; Spohr, R.; Yoshida, M., Diode-like single-ion track membrane prepared by electro-stopping. Nucl Instrum Meth B 2001, 184 (3), 337-346.

10. Jiang, Y. N.; Feng, Y. P.; Su, J. J.; Nie, J. X.; Cao, L. X.; Mao, L. Q.; Jiang, L.; Guo, W., On the Origin of Ionic Rectification in DNA-Stuffed Nanopores: The Breaking and Retrieving Symmetry. J Am Chem Soc 2017, 139 (51), 18739-18746.

11. Ali, M.; Ramirez, P.; Nasir, S.; Cervera, J.; Mafe, S.; Ensinger, W., Tetraalkylammonium Cations Conduction through a Single Nanofluidic Diode: Experimental and Theoretical Studies. Electrochim Acta 2017, 250, 302-308.

12. Harrell, C. C.; Siwy, Z. S.; Martin, C. R., Conical Nanopore Membranes: Controlling the Nanopore Shape. Small 2006, 2 (2), 194-198.

13. Cervera, J.; Schiedt, B.; Ramirez, P., A Poisson/Nernst-Planck model for ionic transport through synthetic conical nanopores. Europhys Lett 2005, 71 (1), 35-41.

14. Cervera, J.; Schiedt, B.; Neumann, R.; Mafe, S.; Ramirez, P., Ionic conduction, rectification, and selectivity in single conical nanopores. J Chem Phys 2006, 124 (10), 104706.

15. Lepoitevin, M.; Nguyen, G.; Bechelany, M.; Balanzat, E.; Janot, J. M.; Balme, S., Combining a sensor and pH-gated Nanopore based on an Avidin-biotin system Chem Commun 2015, 51, 5994-5997

16. Zhao, Y.; Janot, J. M.; Balanzat, E.; Balme, S., Mimicking pH-gated ionic channel by polyelectrolyte complex confinement inside single nanopore. Langmuir 2017, 33, 3484–3490.

17. Ma, T. J.; Walko, M.; Lepoitevin, M.; Janot, J. M.; Balanzat, E.; Kocer, A.; Balme, S., Combining Light-Gated and pH-Responsive Nanopore Based on PEG-Spiropyran Functionalization. Adv Mater Interfaces 2018, 5 (2).

18. Zhang, M. H.; Hou, X.; Wang, J. T.; Tian, Y.; Fan, X.; Zhai, J.; Jiang, L., Light and pH Cooperative Nanofluidic Diode Using a Spiropyran-Functionalized Single Nanochannel. Adv Mater 2012, 24 (18), 2424-2428.

19. Ali, M.; Ramirez, P.; Mafe, S.; Neumann, R.; Ensinger, W., A pH-Tunable Nanofluidic Diode with a Broad Range of Rectifying Properties. Acs Nano 2009, 3 (3), 603-608.

20. Yameen, B.; Ali, M.; Neumann, R.; Ensinger, W.; Knoll, W.; Azzaroni, O., Single Conical Nanopores Displaying pH-Tunable Rectifying Characteristics. Manipulating Ionic Transport With Zwitterionic Polymer Brushes. J Am Chem Soc 2009, 131 (6), 2070-2071.

21. Yameen, B.; Ali, M.; Neumann, R.; Ensinger, W.; Knoll, W.; Azzaroni, O., Proton-regulated rectified ionic transport through solid-state conical nanopores modified with phosphate-bearing polymer brushes. Chem Commun 2010, 46 (11), 1908-1910.

22. Ali, M.; Yameen, B.; Cervera, J.; Ramirez, P.; Neumann, R.; Ensinger, W.; Knoll, W.; Azzaroni, O., Layer-by-Layer Assembly of Polyelectrolytes into Ionic Current Rectifying Solid-State Nanopores: Insights from Theory and Experiment. J Am Chem Soc 2010, 132 (24), 8338-8348.

23. Alem, H.; Blondeau, F.; Glinel, K.; Demoustier-Champagne, S.; Jonas, A. M., Layer-by-layer assembly of polyelectrolytes in nanopores. Macromolecules 2007, 40 (9), 3366-3372.

24. Lepoitevin, M.; Jamilloux, B.; Bechelany, M.; Balanzat, E.; Janot, J. M.; Balme, S., Fast and reversible functionalization of a single nanopore based on layer-by-layer polyelectrolyte self-assembly for tuning the current rectification and designing sensors. RSC Advances 2016, 6, 32228.

25. Balme, S.; Ma, T.; Balanzat, E.; Janot, J. M., Large osmotic energy harvesting from functionalized conical nanopore suitable for membrane applications J Membrane Sci 2017, 544, 18-24.

26. Harrell, C. C.; Lee, S. B.; Martin, C. R., Synthetic single-nanopore and nanotube membranes. Anal Chem 2003, 75 (24), 6861-6867.

27. Balme, S.; Picaud, F.; Manghi, M.; Palmeri, J.; Bechelany, M.; Cabello-Aguillar, S.; Abou-Chaaya, A.; Miele, P.; Balanzat, E.; Janot, J. M., Ionic transport through sub 10 nm hybrophobic nanopore : experiment, theory and simulation. Sci Rep-UK 2015, 5, 10135.

28. Secchi, E.; Marbach, S.; Nigues, A.; Stein, D.; Siria, A.; Bocquet, L., Massive radius-dependent flow slippage in carbon nanotubes. Nature 2016, 537 (7619), 210-213.

29. Siria, A.; Poncharal, P.; Biance, A.-L.; Fulcrand, R.; Blase, X.; Purcell, S. T.; Bocquet, L., Giant osmotic energy conversion measured in a single transmembrane boron nitride nanotube. Nature 2013, 494 (7438), 455-458.

30. Tagliazucchi, M.; Azzaroni, O.; Szleifer, I., Responsive Polymers End-Tethered in Solid-State Nanochannels: When Nanoconfinement Really Matters. J Am Chem Soc 2010, 132 (35), 12404-12411.

31. Shiratori, S. S.; Rubner, M. F., pH-dependent thickness behavior of sequentially adsorbed layers of weak polyelectrolytes. Macromolecules 2000, 33 (11), 4213-4219.

Combining Light-Gated and pH-responsive nanopore based on PEG-spiropyran functionalization

*Tianji Ma, Martin Walko, Mathilde Lepoitevin, Jean-Marc Janot, Emmanuel Balanzat, Armagan Kocer and Sebastien Balme**

Contribution: I design the study with Sebastien Balme, did the nanopore experiments and analyzed the data and contributed to the paper writing

Introduction

The ion channels and pumps are involved in diverse biological processes such as neuron communication, regulation processes, water transport, energy production.[1] Most of them exhibit a preferential transport of ions, which is characterized by a current rectification as well as reversible gating properties in response to external stimuli. One example of stimuli responsive channels is the light responsive ones which are involved in vision processes.[2] The gating is regulated by a photo-switch molecule: the retinal, which isomerizes when absorbing a photon.[3]

Inspired by this process, many synthetic photo-switch molecules were synthetized to develop new types of materials [4] or to trigg the nanopore aperture [5]. Among them, spiropyran is particularly interesting because its photoinduced change is not only a simple stereo-isomerisation but induces a modification of both its chemical structure and physical properties (figure 1).[6] Under visible light, the spiropyran (SP) is uncharged and not soluble in water. Under UV irradiation, spiropyran changes to a merocyanine (MC) form which is zwitterionic and soluble in water. These exceptional properties have been used to functionalize both inorganic and polymer material.[7] Spiropyrans were immobilized on inorganic surfaces to tune their wettability[8], the binding of metal ions[9], or DNP antibody[10] and their electrochemical properties[11]. They allow controlling the aggregation and the solubility of nanoparticles with light[12]. When grafted to polymers, they form reversible micelles[13]. Spiropyrans were also successfully used to functionalize biomacromecules to control their enzymatic activity[14], DNA hybridation[15], and folding.[16] To mimic light responsive channels, spiropyrans were linked to biological mechanical channel such as MscL. [17]

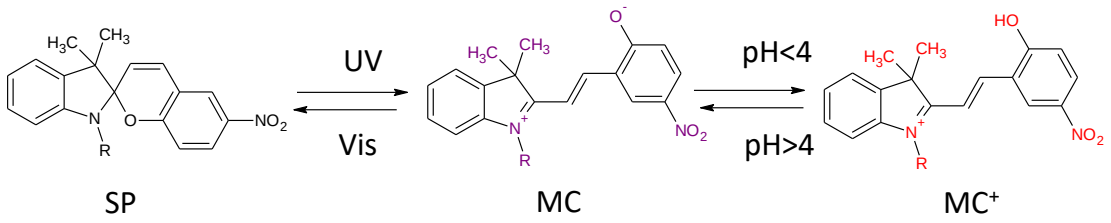

Fig. 9 Chemical structure of spiropyran.

In membrane science, spiropyrans are particularly interesting because ionic transport across the membrane can be tuned by simply using light.[18] It can be done with polymeric as well as inorganic membranes. In the case of the polymeric membranes, the light-gating is mainly due to the reorganization of polymers and/or their swelling. In the case of inorganic membranes, the properties are due to the modification of the wettability of the surface.[19] Using this concept, spiropyrans were grafted inside nanoporous membranes. Vlassiouk and co-workers have functionalized alumina membranes with an alkoxysilane ended by amine groups.[20] Following a similar idea, Zhang et al. have grafted spiropyrans inside single conical nanopores.[21] These nanopores were obtained by the track-etched technique in PET films and exhibited unique properties of an ionic diode. In this case, depending on the isomer of the spiropyrans, a modification of the current rectification was observed. Since the spiropyrans are directly grafted onto the nanopore surface wall, only their charge (uncharged or zwitterionic or positively charged) plays a role in the ionic transport. However, the characterization of such effect required a high voltage rate (typically +/- 5 V). In addition to the light responsiveness, spiropyrans also react to the pH and can modify the ionic transport accordingly. This is of particular interest in the design of multifunctional membranes.[22]

In this work, we generated a nanopore that is responsive to both light and pH. To do that, conical nanopores obtained by the track-etched technique were functionalized with spiropyrans. In order to amplify the gating properties of the conical nanopore, the spiropyran was linked to a long polymer chain of PEG. According to previous works on copolymer micelles, such a system facilitates a self-assembly inside the nanopore.[13,18] Then, we studied the ionic transport properties of NaCl and KCl through these nanopores. We intended to determine the conformation adopted by the PEG-spiropyran inside the

nanopore depending on the irradiation type. We discuss also the impact of PEG chain on the reversibility of this photo-switch. The power generated by the nanopore under salt gradients was also evaluated. Beside the influence of light irradiation, the pH was also investigated mainly to drive and determine the ionic selectivity of the nanopore.

Materials and methods

Material

13 µm thick PET films, with biaxial orientations were purchased from Goodfellow (ref ES301061). 1-ethyl-3-(3-dimethylaminopropyl)-carbodiimide (EDC, 03449), HCl (ref 30721), NaOH (30620), MES (M8250), NaCl (S7653), Dithiothreitol (D9163) DMSO (41640) and Phosphate-buffered saline (PBS, Sigma-Aldrich ref P4417) were purchased from Sigma-Aldrich. Ortho-pyridyldisulfide-polyethyleneglycol-amine (OPSS-PEG-NH2, Mw 3400 D, ref PG2-AMOS-3K) was purchased from Nanocs. KCl (POCL-00A) were purchased from Labkem. 3',3'-dimethyl-1'-(2-iodoacetyloxyethyl)-6-nitrospiro[2H-1-benzopyran-2,2'-indoline] (I-SP) were synthetized following the procedure detailed in ref [17a].

Track-etching nanopores

Single conical nanopores were obtained by track-etched methods. The single tracks were produced by Xe irradiation (8.98 MeV u^{-1}) of PET film at GANIL, SME line (Caen, France). The tracks were activated by UV exposition (Fisher bioblock; VL215.MC, l= 312 nm) for 12 hours for the base side and 6 hours for the tip side. Shortly after the UV activation, the PET film was mounted between the two chambers of a Teflon cell. The conical shape was obtained using the electro-stopping method. One chamber was filled with the etchant solution (9 M NaOH) and the other chamber was filled with the stopping solution (1 M KCl and 1 M acetic acid). The reference and working electrodes are placed in the stopping and the etchant solution, respectively. Then, 1 V potential was applied. The nanopore opening was characterized by the current as a function of time recorded by a patch-clamp amplifier (HEKA EPC-10). The etching process was stopped by replacing the etchant solution with the stopping solution when the current was rised to several hundreds of pAs. The nanopore was then rinsed in ultrapure water for 24 h hours. The tip diameter d of the conical nanopore was determined from the dependence of the conductance G measured in the linear zone of the I–V curve.

$$G = \frac{\kappa d D \pi}{4L} \quad (1)$$

Where, κ is the ionic conductivity of the solution assuming a bulk like transport, L is the nanopore length (13 µm) and D is the base diameter which was calculated from the total etching time t using the relationship D = 2.5t (the factor 2.5 was determined in our experimental set up using multipore track-etched membranes Figure 2).

Table 3: Properties of the nanopores used in this study.

Pore	d_{UV} nm) ()	d_{VIS} (nm)	D (nm)
NP-1	5.3	1.1	1200
NP-2	12.7	1.3	555
NP-3	10.3	1.9	290

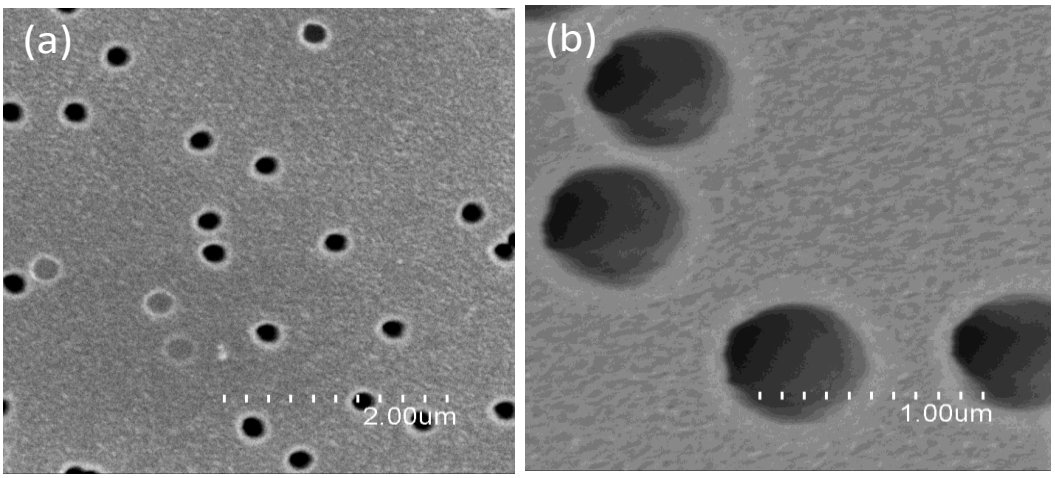

Fig. 10 SEM image of base side of conical nanopore after etching time close to the ones for NP-3 (a) and NP2 (b).

Functionalization of the nanopore

2.3.1 PEGylation

A reactive solution of Ortho-pyridyldisulfide-polyethyleneglycol-amine was prepared with 0.1 M KCl, 0.1 M MES, pH 4.7. The pH was adjusted with HCl and NaOH solutions using a pH meter (Hanna HI 221 pH meter, pH electrode HI 1131). This solution was added inside each chamber of the cell. 1-Ethyl-3-(3-dimethylaminopropyl) carbodiimide solution was added to reach 50 mM and let equilibrate for 2 hours.

2.3.1 Reduction by dithiothreitol

A 16.8 mg of dithiothreitol was dissolved in 5 ml of ultra-pure water. 200 µl of that solution was added to the tip side of the cell in a 800 µl phosphate-buffered saline solution and the base side was filled with only 800 µl of PBS solution. The reaction ran for 2 hours.

2.3.1 Spiropyran attachment

40 µl of stock solution of I-SP (1 mg ml^{-1}) in DMSO was added in the tip side of the nanopore into 800 µl DMSO. The other side was filled with 800 µl DMSO. The incubation lasted 2h.

Current-voltage measurement

Current-voltage measurements were performed with a patch-clamp amplifier (EPC10 HEKA electronics, Germany). The current was measured by Ag/AgCl, 1 M KCl electrodes. The working and ground electrodes were connected to the trans (base aperture of nanopore) and the cis side (tip aperture of the nanopore) of the cell, respectively (Figure 2). The two chambers of the cell were filled with the same electrolyte solution for the symmetric measurements. For asymmetric measurements, the cis side had the same concentration while the concentration varied on the trans side. Current traces were recorded as a function of time from 1 V to -1 V by 100 mV steps for 2 s and from 100 mV to -100 mV by 10 mV steps for 2s. Except when it is specifically mentioned, the I-V curves were recorded in darkness.

The nanopore irradiation was performed by focusing the light provided by an arc lamp (HXP R 120 W/45C). UV and visible light were selected by a single-band bandpass filter 375/110 nm (Semrock BrightLine® FF01) and long-pass filter 500 nm (Thorlabs FELH), respectively.

Absorbance spectra

The absorbance spectra was perfomed on multipore membrane (density 10^6 pore cm^{-2}) using a spectrophotometer JASCO equiped with an integration sphere.

Results and discussion

Nanopore functionalization

For this work, we selected conical nanopores with tip diameters from 5 to 9 nm obtained by track-etching under dissymmetrical conditions (Figure 3). The nanopore functionalization by PEG-spiropyran was done following the three steps procedure. First, the OPSS-PEG-NH2 was attached onto the carboxylate groups present at the surface of the inner wall of the nanopore, by EDC activation. Then, the ortho-Pyridyldisulfide-Polyethylene was reduced by dithiothreitol. The last step was a nucleophilic substitution of the iodine moieties of spiropyrans by thiol groups terminated by PEG chain. The result was the attachment of the spiropyran to the PEG via a thioether bond. Each step of the nanopore functionalization was evidenced by the modification of the I-V response in 100 mM KCl as shown in Figure 3c. The PEGylation induced a decrease of the conductance, likely due to the reduction of the nanopore diameter. The rectification factor is defined as $rf = \left|I_{(1V)}/I_{(-1V)}\right|$. Because, its value depends on the surface charge density, it is a simple and efficient method to confirm the functionalisation of the conical nanopore after each step (Figure 2c). For the raw nanopore, *rf*< 1 due to the carboxylate groups which induce selectivity to cation. After grafting of the ortho-pyridyldisulfide-polyethylene, we observed an inversion of rectification factor (*rf* > 1). The latter is assigned to the protonation of pyridyl moieties which confers a global positive surface charge of the nanopore inner wall. The reduction of ortho-pyridyldisulfide groups induces a *rf*< 1 which evidences the loss of pyridyl moieties. Finally, after the grafting of spiropyran, we observe a lower current and a rectification factor close to 1 confirming the grafting of an uncharged molecule. We attempted to confirm the nanopore functionalisation by an alternative method. To do so, the PEG-SP was grafted inside a multipore membrane (density 10^6 pores cm^{-2}) using the same method. The absorbance spectrum recorded with the the functionalized membrane after UV irradiation reveals a peak around 550 nm which is characteristic of the MC form (Figure 3e). This confirms that our method allows us to graft PEG-SP inside nanopore.

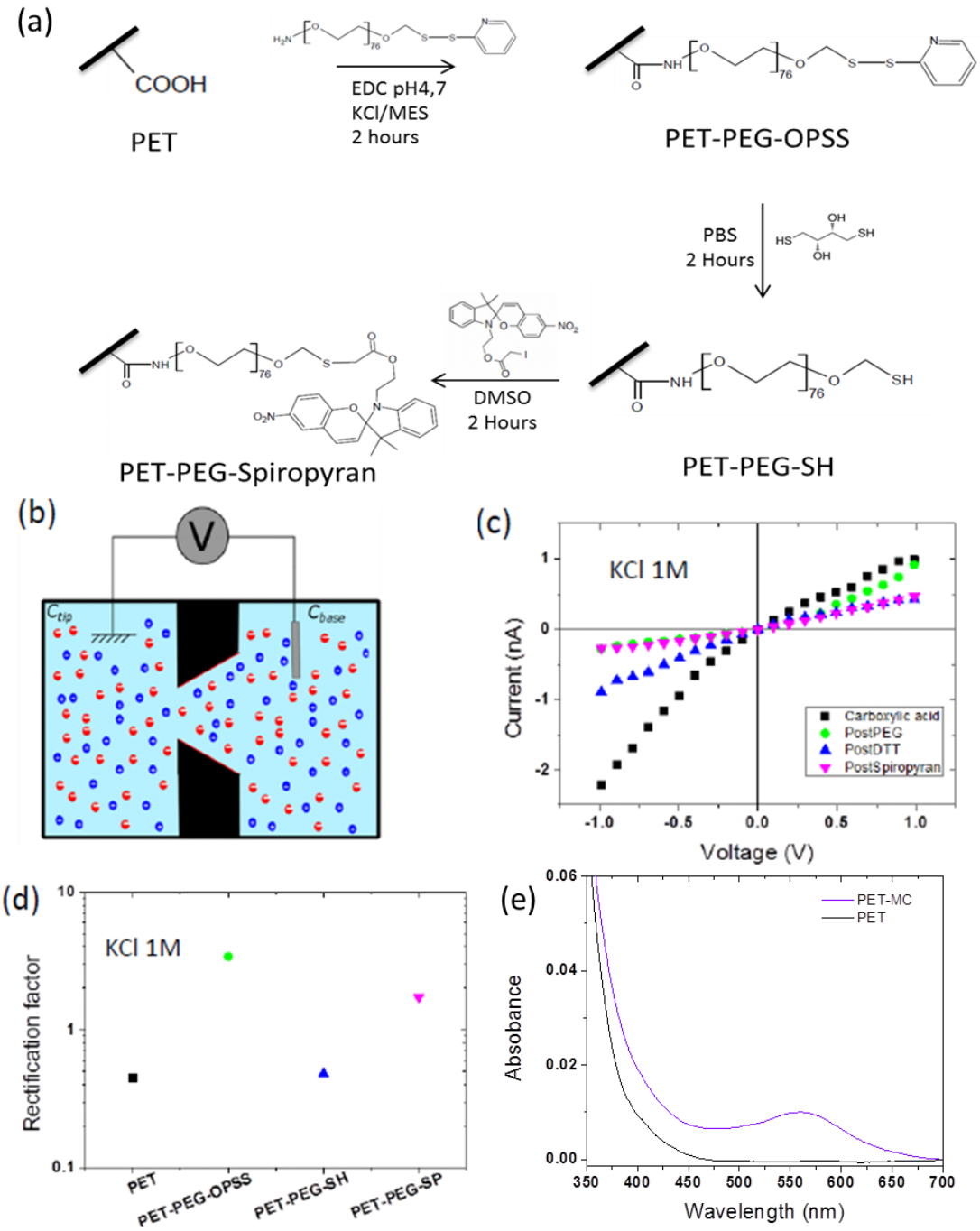

Fig. 11 (a) scheme of the nanopore functionalization. (b) Sketch of the setup for the I-V curve measurements. (c) I-V response under 1 M KCl and (d) rectification factors obtained after each step of the functionalization for NP-3(d_{UV} =10.3nm/ d_{VIS} = 11.9nm) (e) absorbance spectra of PET multipore membrane before (black line) and after functionalization with PEG-SP following UV irradiation on dried sample (violet line).

Light-responsive ionic diode

After the functionalization was completed, the influence of light irradiation on ionic diode properties was characterized by the I-V dependence. In figure 4a the I-V responses of the nanopore after the PEG-spiropyran grafting in 0.1 M and 0.01 M KCl at pH 7 are reported. The first experiment was performed under visible light directly after functionalization. Then, the nanopore was irradiated with UV light for 30 minutes and the I-V curve was measured in the same solution (Figure 4). We observed that I-V responses were different, confirming the presence of photochromic molecule inside the nanopore. In the first experiment, the I-V curves were almost linear. Under VIS irradiation, the spiropyran is neutral explaining the loss of current rectification. After irradiation by UV light, an increase of current and a nonlinear I-V response is observed. This can be explained by the transformation of spiropyran molecule into merocyanine, which is a zwitterionic molecule. In this case, the current rectification was induced by the presence of charges on the nanopore inner wall. At this stage, our results were in good agreement with the one previously reported by Zhang and co-workers.[21] However, two points have to be discussed (i) the reversibility of the photo-switch and (ii) the influence of the PEG chains.

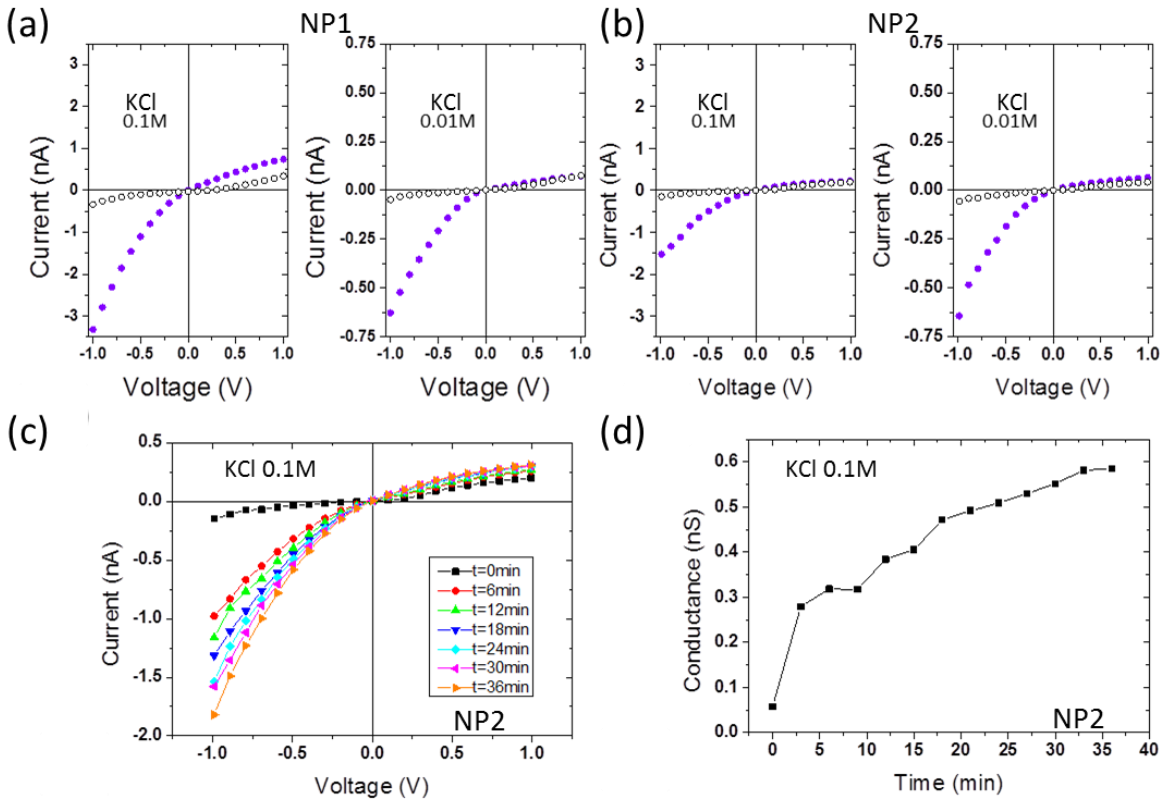

Fig. 12 Typical I-V response obtained after VIS irradiation (open black circle) and after UV irradiation (full violet circle) for NP-1(d_{UV} =5.3nm/ d_{VIS} =1.1nm) (a) and NP-2(d_{UV} =12.7nm/ d_{VIS} =1.3nm) (b) at different KCl concentrations, i.e. 0.1M and 0.01 M. Kinetics of the nanopore (NP-2) opening under UV irradiation (c) evolution of the I-V response regarding the time of the visible irradiation (d) evolution of the nanopore conductance as a function of the irradiation time (here the I-V curve were recorded under light).

First, the switching from the SP to the MC form took a couple of seconds in water solution while it takes more than 30 min inside the nanopore. This should be assigned to the low transmittance of PET in UV. We focused then, on the reversibility of this photo-switch. After UV switching, the irradiation by visible light did not show a significant modification of the I-V response. This could be because the molecules are blocked in their merocyanine configuration. In previous works, authors have also reported the difficulty to switch from MC to SP form in water. Vlassiouk et al. repported that the photo-switching occurs in water when the spiropyrans are attached directly to the inner surface of the nanopore.[20] However, the photoswitching was only monitored in ethanol. Zhang et al. reported that the nanopore has to be dried to switch from MC to SP form. The authors assigned this non-reversibity in

water to a high activation barrier, which is accompanied by the dewetting process inside a nanopore.[21] We propose another mechanism which takes into account the PEG chain.The spiropyran form of the molecule is not soluble in water. Thus, when it is grafted at the surface of the inner wall of the nanopore, it will minimize its interaction with water molecule by increasing its interaction with the surface, especially if the latter is hydrophobic. In our case, the functionalization involves a PEG chain between the PET and the photo-switchable molecule. These PEG could stabilize the molecule in its merocyanine form because they are highly hydrophilic. In this case, we suppose that the merocyanine form is favored in this environment and cannot switch back to its SP form because they are surrounded by too many water molecules.

In order to confirm this hypothesis, we modified the polarity of the solvent, to facilitate switching from the MC to the SP form. With a mixture EtOH/water at different ratios, the photoswitching did not occur. However, by using pure EtOH, we could observe that after VIS irradiation, the nanopore conductance dramatically decreased, confirming the switching from MC to SP form. This experiment was repeated several times (Figure 5). Thus, the reversible gating of the nanopore requires the use of ethanol to switch from the MC to SP form.

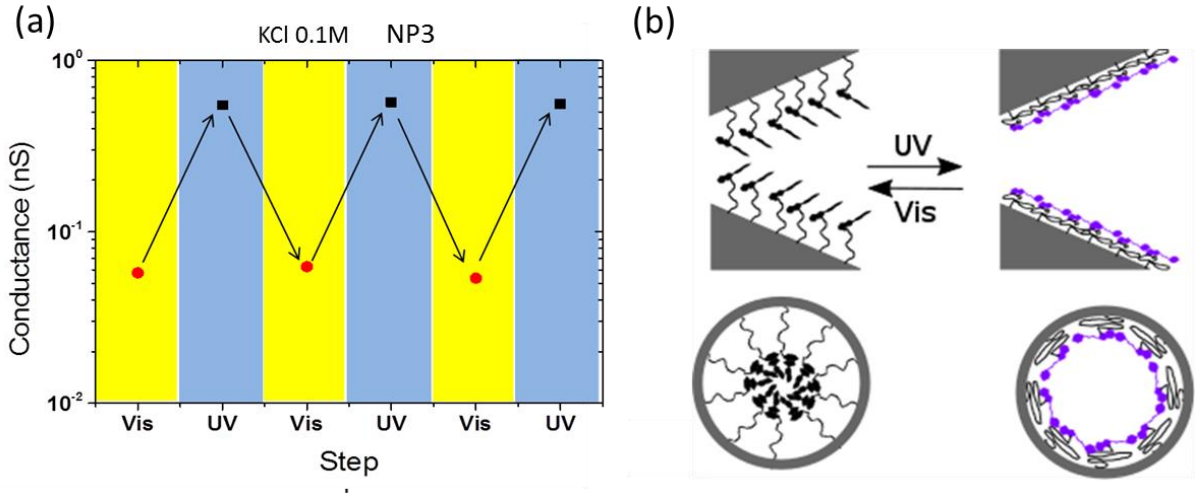

Fig. 13 Reversibility of the photo-switchable properties of NP 3 (d_{UV} =10.3 nm/ d_{VIS} =1.9 nm) (a) nanopore conductance in 100 mM KCl. The photoswitch from VIS to UV and from UV to VIS was performed in water and ethanol respectively. (b) Sketch of the PEG-SP and PEG-MC conformations inside the nanopore.

As previously mentioned, single conical nanopores behave as an ionic diode due to a preferential ionic transport,[23] which is commonly characterized by the current rectification. The origin of this phenomenon has been extensively studied by PNP simulations.[5b,24] It appears that the nanopore dissymmetry induces a depletion of ionic concentration of co-ions compared to counter-ions. It has been shown that in the case of conical nanopores, the current rectification is more pronounced with the increase of surface charges.[25] Thus, the analysis of current rectification should emphasize the configuration of the photo-switch molecule. Figure 14 reports the rectification factor calculated from equation 2 as a function of the salt concentration after VIS and UV irradiation at pH 7. According to our experimental protocol, a rectification lower than 1 means that the transport of cations is favored. This is the case when the photo-switchable molecule is in its merocyanine configuration. With the increase of the salt concentration, the rectification tends to approach 1, as usually observed for charged nanopore. After switching to spiropyran isomer, since the surface is uncharged, it is not surprising that the rectification factor is around 1 for both NaCl and KCl independently of the salt concentration.

To go further in the investigation of the ionic transport inside nanofluidic diode functionalized by PEG-spiropyran, we studied the I-V- response under different salt concentrations (0.001 M, 0.01 M, 0.1 M, and 1 M) for KCl and NaCl. From the linear part of I-V response typically between -60 mV to 60 mV, we calculated the conductance G and plotted it as a function of the salt concentration as shown in figure 14. Regardless of the type of salt, the conductance under VIS was lower than the conductance after UV irradiation (table 1). This difference could be explained by the wetting/dewetting of the nanopore depending on the photoswitch molecule isomerization state. Interestingly, for spiropyran isomer, the nanopores exhibit a similar apparent tip diameter around 1.3 nm. The decrease of the amplitude of the conductance and the similar diameter after VIS irradiation suggest that other mechanisms occurred, such as self-assembly.[26] We have shown previously that the PEG chains play a role in the photoswitch reversibility and should be taken into account. In our case, it is likely due to self-assembly of spiropyrans inside the nanopore, which induce a modification of the PEG conformation. This scenario presumes that PEG can adopt a mushroom and a brush-like conformation, which depends on the density of the polymer chain on the nanopore inner walls. The surface charge of PET conical nanopore is commonly

estimated about 0.10 C m^{-2} corresponding to a distance of 1.48 nm between two carboxylate moieties. The mushroom radius of PEG estimated by Flory law is 3.8 nm. Since these two values are very close and that it is likely that all carboxylate moieties are not functionalized, we can assume that a mushroom conformation of PEG is possible. In this case, under VIS irradiation the self-assembly of spiropyranes stretches the PEG chain to a brush-like conformation; while merocyanine is well solvated in water and thus the PEG chains adopt a mushroom conformation to minimize the energy of the system. This interpretation reinforces the fact that the transformation of merocyanine into spiropyran does not occur in water.

Usually, at the nanoscale, the conductance follows two regimes.[27] At high concentration, it increases with the salt concentration in order to reach a bulk-like ionic transport. At low salt concentration, the conductance reaches a plateau. Usually, this conductance is assigned to the transport of counter-ions which shield the nanopore surface charges. However, this plateau was reported also in the case of hydrophobic and uncharged nanopores.[28] In this case, it was partially assigned to the slip length and the water organization close to the surface. After VIS irradiation, when the spiropyran is uncharged, we can extrapolate a "plateau- like" behavior at very low salt concentrations, likely at concentrations lower than 1 mM. More interestingly, the plateau was not clearly observed after UV irradiation when the photo-switch molecule is in the zwitterionic state. This suggested that the surface charges induced by merocyanine are not shielded by the counter-ions in solution. The charge compensation is between ammonium and phenolate from the same molecule or two neighbor molecules. It should be noticed that a similar behavior is observed for both KCl and NaCl even at high concentrations when the potassium should chelate the PEG.[29]

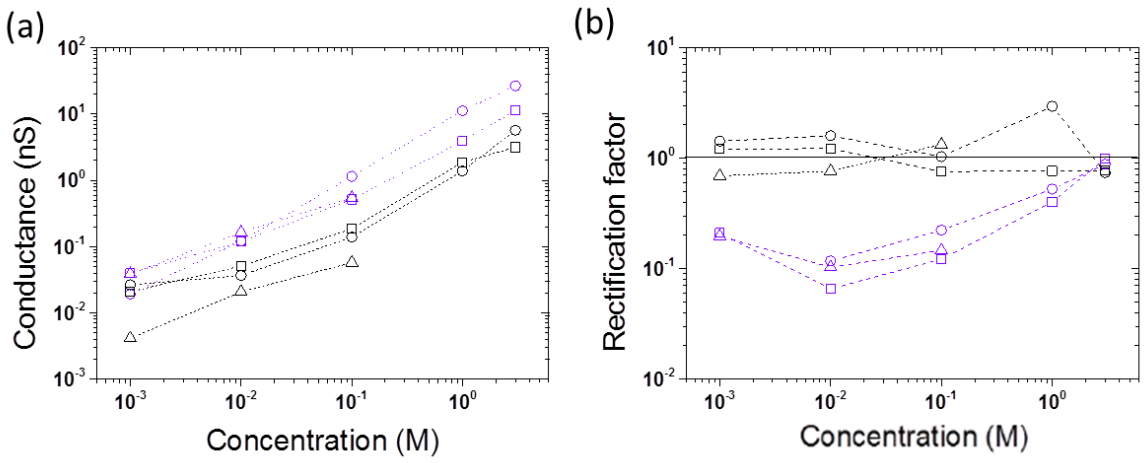

Fig. 14 Nanopore conductance (a) and rectification factor (b) as a function of KCl and NaCl concentration of NP-1 (square and circle respectively) and NP-3 (d_{UV} =10.3nm/ d_{VIS} =1.9 nm) (triangle) after VIS (open black symbol) and after UV (open violet symbol).

To investigate the nanopore charges after VIS and UV irradiation, we measured the power generated by a single nanopore under a salt concentration gradient from the tip side to the base side. Indeed, it has been shown that the maximum power P_{Max} generated by a nanopore is strongly dependent on its surface charge density and its shape.[30] This power is obtained from the zero-volt current (I_0) and the open circuit potential (V_{rev}). These values were obtained from the I-V dependence measured under dissymmetrical salt concentrations (Figure 15).

$$P_{Max} = I_0 . V_{res} \quad (2)$$

The current I_0 is extracted from the current at V=0 when the concentration (c_{Tip}) in the tip and the base side (c_{Base}) of the nanopore were 1 M and between 1 - 100 mM, respectively. As expected, under the SP form, the current was lower (between 50 pA to 90 pA) than under the MC form (500 pA to 620 pA). These values are in the same range as the one reported for a conical nanopore.[31] The difference of current is assigned to the increase of surface charges due to the zwitterionic character of MC and the fact that the nanopore is open. The P_{Max} after UV and VIS irradiation follows a linear dependence with the $\log(c_{Tip}/c_{Base})$. To compare the efficiency in terms of energy harvesting of both isomers of the photoswitch molecule, we can assume that $P_{Max} = k \log(c_{Tip}/c_{Base})$ where, k is a coefficient of

efficiency. After UV irradiation, this coefficient was 5 times larger than after VIS irradiation (45.48 pW^{-1} against 5.97 pW^{-1}).

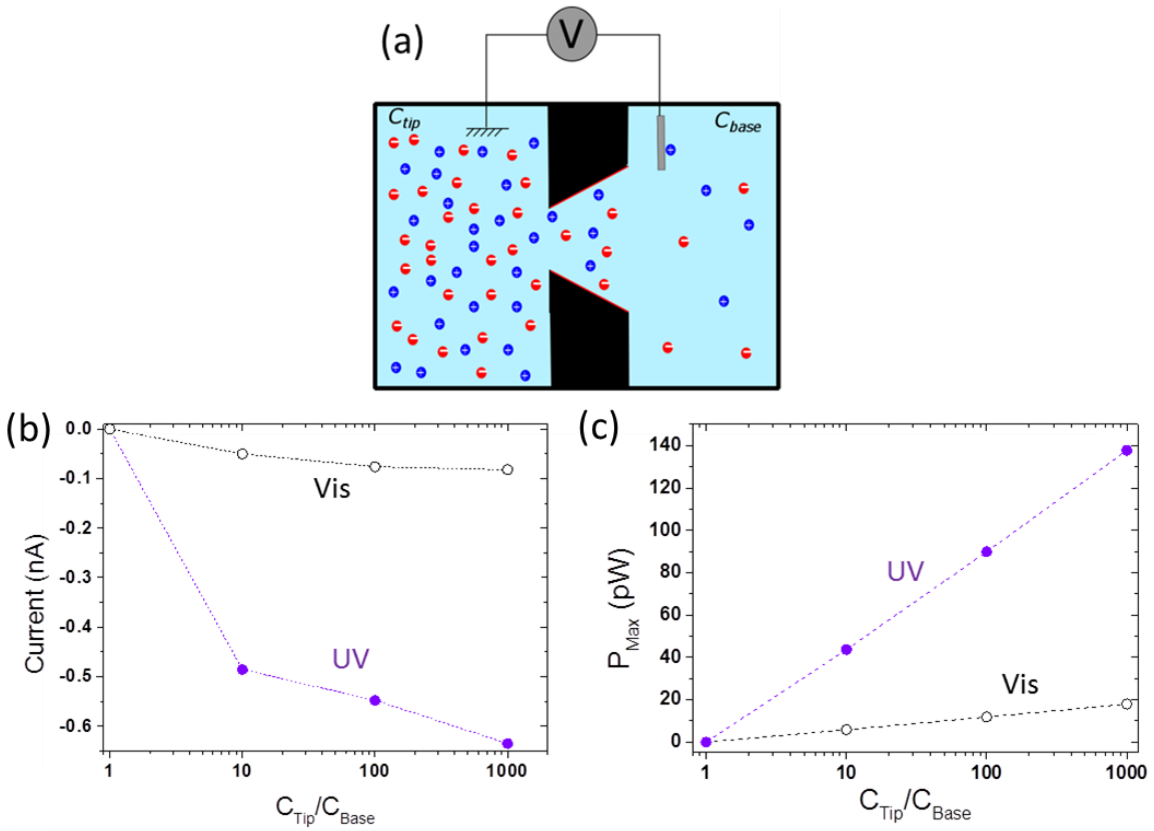

Fig. 15 (a) sketch of the experiment performed under an ionic gradient. For NP-1(d_{UV} =5.3 nm/ d_{VIS}= 1.1nm), (b) zero-volt current and (c) power generated under ionic gradient after VIS irradiation (open black circles) and after UV irradiation (violet circles).

pH controlled ionic diode and nanopore selectivity

In the MC form the photo-switchable molecule has a phenol group that can be protonated at low pH. Thus, at low pH, we should expect an inversion of nanopore selectivity. To confirm it, the ionic transport was studied at pH 3 and 7 (Figure 8). The results show an inversion of the current rectification at pH 3. In terms of selectivity, the current rectification is greater than 1 showing that the anion transport is favored. This is easily explained by the modification of surface charge due to the protonation of the phenolate moieties of the merocyanine. It can be noticed that at pH 7 the rectification factor tends to be 1 when the salt concentration increases. In order to evaluate the selectivity of the nanopore, we measured the reverse

voltage under dissymmetrical concentration (Figure 16). At pH 7, the P_{K+}/P_{Cl-} is 3 and 10 for nanopores with tip diameter 5 and 9 nm, respectively, while at pH 3 it is 0.5 and 0.05. This result confirms the preferential transport of ions.

At pH 3, the dependence of the conductance to the salt concentration exhibits a plateau of conductance at low concentrations as opposed to pH 7. The lack of plateau at pH 7 was interpreted by the internal charge compensation as the merocyanine is zwitterionic. At pH 3, the protonation of phenolate moieties breaks the internal charge compensation. The positive charges of ammonium moieties are shielded by chlorines, which are the mobile charges inside the nanopore explaining the plateau of conductance observed at low concentrations.

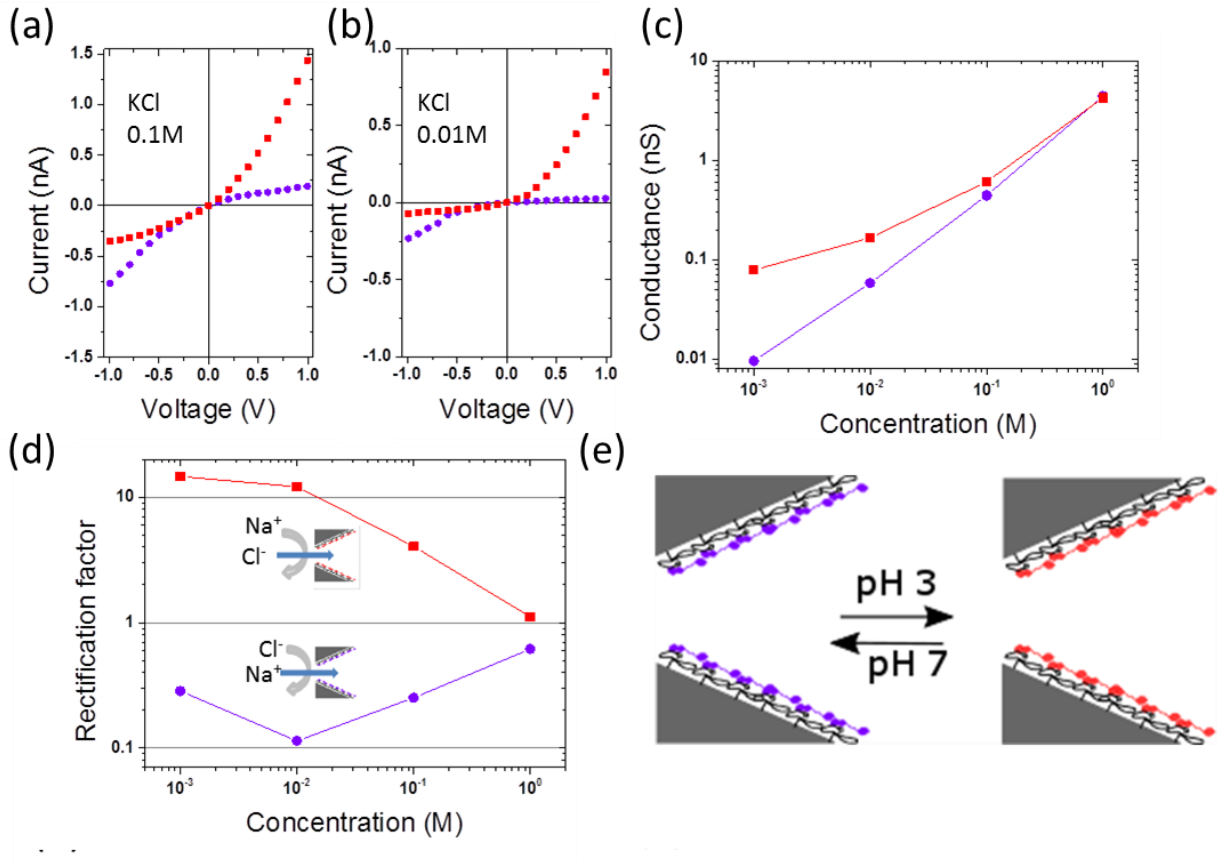

Fig. 16 Influence of the pH on NP-2 (d_{UV} =12.7 nm) conductance after UV irradiation. (a) and (b) are the I-V response at pH 7 (violet, circle) and at pH 3 (red square) recorded at concentration 100 mM and 10 mM. (c) Conductance and (d) rectification factor as a function of KCl concentration at pH 7 (violet, circle) and at pH 3 (red square) (e) sketch of PEG-MC and PEG-MC+ organization inside the nanopore.

Conclusion

To sum up, we have successfully designed a light responsive nanopore by grafting PEG-SP chains inside conical nanopores. We have studied the ionic transport as a function of both the pH and light irradiation. After UV irradiation, the nanopore is open, while after VIS irradiation, the nanopore is closed. The reversible switching from MC to SP isomer cannot be done in water and requires a solvent with a lower polarity such as ethanol. Our results provide a direct evidence of the ability of PEG to block the photo-switch under its zwitterionic form. Besides the light gating properties, it is possible to modulate the nanopore selectivity with pH. This work shows the possibility to design multifunctional nanopores that combine both diode and gating behavior. Such nanopores could be interesting for many applications from nano-valves to sensing properties using a single pore. Because the nanopores obtained by track-etched method can be upscaled to multipore membranes, these properties could also bring new opportunities to develop adaptive membranes for separation or energy conversion.

Reference

[1] D. C. Gadsby Nat Rev Mol Cell Bio 2009, 10, 344.

[2] a) G. Nagel,T. Szellas,W. Huhn,S. Kateriya,N. Adeishvili,P. Berthold,D. Ollig,P. Hegemann,E. Bamberg P Natl Acad Sci USA 2003, 100, 13940; b) G. Nagel,D. Ollig,M. Fuhrmann,S. Kateriya,A. M. Mustl,E. Bamberg,P. Hegemann Science 2002, 296, 2395.

[3] J. Kuhne,K. Eisenhauer,E. Ritter,P. Hegemann,K. Gerwert,F. Bartl Angew Chem Int Edit 2015, 54, 4953.

[4] a) A. A. Beharry,G. A. Woolley Chem Soc Rev 2011, 40, 4422; b) H. Tian,S. J. Yang Chem Soc Rev 2004, 33, 85; c) N. Ma,Y. P. Wang,Z. Q. Wang,X. Zhang Langmuir 2006, 22, 3906.

[5] a) M. Ali,S. Nasir,P. Ramirez,I. Ahmed,Q. H. Nguyen,L. Fruk,S. Mafe,W. Ensinger Adv Funct Mater 2012, 22, 390; b) S. Nasir,P. Ramirez,M. Ali,I. Ahmed,L. Fruk,S. Mafe,W. Ensinger J Chem Phys 2013, 138.

[6] B. S. Lukyanov,M. B. Lukyanova Chemistry of Heterocyclic Compounds 2005, 41, 281.

[7] R. Klajn Chem Soc Rev 2014, 43, 148.

[8] a) D. Dattilo,L. Armelao,G. Fois,G. Mistura,M. Maggini Langmuir 2007, 23, 12945; b) D. Kessler,F. D. Jochum,J. Choi,K. Char,P. Theato Acs Appl Mater Inter 2011, 3, 124.

[9] K. Fries,S. Samanta,S. Orski,J. Locklin Chem Commun 2008, 6288.

[10] R. Blonder,S. Levi,G. L. Tao,I. BenDov,I. Willner J Am Chem Soc 1997, 119, 10467.

[11] T. Niazov,B. Shlyahovsky,I. Willner J Am Chem Soc 2007, 129, 6374.

[12] D. B. Liu,W. W. Chen,K. Sun,K. Deng,W. Zhang,Z. Wang,X. Y. Jiang Angew Chem Int Edit 2011, 50, 4103.

[13] H. I. Lee,W. Wu,J. K. Oh,L. Mueller,G. Sherwood,L. Peteanu,T. Kowalewski,K. Matyjaszewski Angew Chem Int Edit 2007, 46, 2453.

[14] Y. Ito,N. Sugimura,O. H. Kwon,Y. Imanishi Nat Biotechnol 1999, 17, 73.

[15] C. Beyer,H. A. Wagenknecht Synlett 2010, 1371.

[16] A. Fissi,O. Pieroni,G. Ruggeri,F. Ciardelli Macromolecules 1995, 28, 302.

[17] a) A. Kocer,M. Walko,B. L. Feringa Nat Protoc 2007, 2, 1426; b) A. Kocer,M. Walko,W. Meijberg,B. L. Feringa Science 2005, 309, 755.

[18] K. Xiao,X. Y. Kong,Z. Zhang,G. H. Xie,L. P. Wen,L. Jiang J Photoch Photobio C 2016, 26, 31.

[19] G. L. Wang,A. K. Bohaty,I. Zharov,H. S. White J Am Chem Soc 2006, 128, 13553.

[20] I. Vlassiouk,C. D. Park,S. A. Vail,D. Gust,S. Smirnov Nano Lett 2006, 6, 1013.

[21] M. H. Zhang,X. Hou,J. T. Wang,Y. Tian,X. Fan,J. Zhai,L. Jiang Adv Mater 2012, 24, 2424.

[22] a) M. Lepoitevin,G. Nguyen,M. Bechelany,E. Balanzat,J. M. Janot,S. Balme Chem Commun 2015, 51, 5994; b) Y. Zhao,J. M. Janot,E. Balanzat,S. Balme Langmuir 2017.

[23] Z. Siwy,E. Heins,C. C. Harrell,P. Kohli,C. R. Martin J Am Chem Soc 2004, 126, 10850.

[24] J. Cervera,B. Schiedt,R. Neumann,S. Mafe,P. Ramirez J Chem Phys 2006, 124.

[25] J. Cervera,B. Schiedt,P. Ramirez Europhys Lett 2005, 71, 35.

[26] N. G. Liu,D. R. Dunphy,P. Atanassov,S. D. Bunge,Z. Chen,G. P. Lopez,T. J. Boyle,C. J. Brinker Nano Lett 2004, 4, 551.

[27] R. B. Schoch,J. Y. Han,P. Renaud Rev Mod Phys 2008, 80, 839.

[28] S. Balme,F. Picaud,M. Manghi,J. Palmeri,M. Bechelany,S. Cabello-Aguillar,A. Abou-Chaaya,P. Miele,E. Balanzat,J. M. Janot scientific reports 2015, 5, 10135.

[29] M. Boukhet,F. Piguet,H. Ouldali,M. Pastoriza-Gallego,J. Pelta,A. Oukhaled Nanoscale 2016, 8, 18352.

[30] a) J. Cervera,P. Ramirez,S. Mafe,P. Stroeve Electrochim Acta 2011, 56, 4504; b) W. Guo,L. X. Cao,J. C. Xia,F. Q. Nie,W. Ma,J. M. Xue,Y. L. Song,D. B. Zhu,Y. G. Wang,L. Jiang Adv Funct Mater 2010, 20, 1339.

[31] a) L. X. Cao,W. Guo,W. Ma,L. Wang,F. Xia,S. T. Wang,Y. G. Wang,L. Jiang,D. B. Zhu Energ Environ Sci 2011, 4, 2259; b) S. Balme,T. Ma,E. Balanzat,J. M. Janot Journal of Membrane Science 2017, 544, 18.

Discussions

To control ion transport in response to external stimuli inside a track etched nanopore, the crucial task is to decorate the pore by suitable function. To achieve this purpose, various available methods were described in chapter 1 including *in situ* polymerization from the surface and anchoring already prepared molecules to the surface. As shown in the two articles, two systems of stimuli-responsive are constructed in track-etched nanopore. We utilized method known as “grafting to” for the functionalization in the two studies. For two systems, conical nanopores were used to get diode-like behaviors resulting from the asymmetric geometry. Diode-like nanopores have a current rectification behavior that ion current is large at one direction and small at the other direction under electrical bias. These properties from the asymmetry (charge, geometry) can directly characterize the ion selectivity of the pore. In this shape, the ion transport properties are mainly controlled by the tip side of the pore because of the small aperture. Thus, small changes of chemical structures at tip involved a large change of ion transport.

The first work aimed to give pH-responsive property by depositing layer-by-layer polyelectrolytes which are sensible to pH because of the weak acid and base groups on the chains. Three different cases were investigated by depositing PLL/PAA, PLL/PAA crosslinked and PEI/PAA. These three polyelectrolytes have different charge densities regarding their formula: $\sigma_{PAA}>\sigma_{PEI}>\sigma_{PLL}$. This different density of charges makes the essential difference between PLL/PAA and PEI/PAA functionalized ion channels. As PLL has much less charges than PAA, partial charge compensation between PLL and PAA makes an accumulation of negative charges. As a result, with increasing the number of layers, the nanochannel is more and more selective to cations even with PLL as the last layer. For the case of PEI/PAA, higher charge density of PEI than PAA ensures a more complete charge compensation. This result in that the previous layers rather than the last can hardly influence the ion transport. Thus, the ion selectivity essentially depends on the last layer. These are confirmed by the R_f change during the layer-by-layer desposition.

With the complete charge compensation effect, PEI/PAA modified nanopore has global negative charges at pH 7, while it has global positive charges at pH 3 because of protonation of carboxylate moities. This makes an inversion of I-V curve due to the different ion

selectivity between pH 3 and pH 7. At pH above 3, conductance at low salt concentration does not form a plateau which means that no enough high counter-ion concentration is inside the pore. When the pH reach 3, protonation of polyelectrolytes makes the pore containing a high concentration of anions, such a high conductance plateau appears at low concentration. Besides the charge effect, polyelectrolytes swelling behavior also plays a role in controlling ion transport. At high salt concentration at pH 3, a decrease of conductance was observed. This can be assumed that the swelling of polyelectrolytes partially blocks the pore by steric effect. On the contrary than PEI/PAA, the PLL/PAA exhibits a negatively charged behavior from pH 3 to pH 7 and a plateau of conductance at low salt concentration. In this case, the ion transport of the pore is almost dominated by the excess of negative charges of PAA. This flexible polyelectrolyte structure can be fixed by cross-linking of amine and carboxylic acid moieties. After the crosslinking, the self-assembled layers get the same behavior of zwitterionic molecules. The arrangement of molecular structures responding to pH and salt concentration becomes negligible. So the ion transport of the pore is totally dominated by protonation/deprotonation according to pH.

Globally, the ion transport is regulated by two parameters the charge and the swelling in this work and the ion transport can be divided in two regimes: “bulk” and “surface” depending on the electrolyte concentration in the reservoir. These properties of polyelectrolytes functionalized nanopore can be very useful to design ion selective membranes for osmotic energy harvesting that will be discussed in the next chapter. Ion transport at high concentration is essentially achieved by electrolytes in pore with surface phenomenon neglected. In this regime, charges on the surface are largely screened so ion selectivity is induced. At low concentration, ion transport through counter ions in electrical double layers become dominant. If the polyelectrolytes swell a lot, a more loose structure allows ion transport inside the polyelectrolyte layers. This transport phenomenon due to polyelectrolytes swelling should be avoided because of the transport difficulty inside and conductance reduction due to steric effect.

The second work used another type of “grafting to” method. Spiropyran modified PEG are chemically grafted on the pore surface by EDC chemistry. As a consequence, the nanopore can then control ion transport properties in response to light wavelength because of the isomerization of spiropyran molecule in such conditions. When this photo-switchable

molecule is under visible light, it will take the non-charged form which is hydrophobic. If it is irradiated by UV light, it will be switched into a zwitterionic form known as merocyanine. Due to the charges, this form is hydrophilic. Thus, light responsive ion channel can be achieved by directly grafting spiropyran on the surface. In this case, ion transport regulation is only controlled by surface charge. The PEG-spiropyran functionalized nanopore is modulated by both charges and conformational changes. Hydrophobic spiropyrans can self-assemble together to close the pore by steric effect and at the same time, hydrophobic form decreases the counter-ion concentrations in the pore. The two effects contribute together to close the pore at both low concentration and high concentration. When the pore is under UV light, zwitterionic merocyanines will capture counter-ions. This will increase ion conductance at low salt concentration. Because of the charges of merocyanines, electrical repulsion makes the PEG-merocyanines collapse on the pore surface, such conformational change lead to an increase of effective pore diameter. More interestingly, the pore under UV light can respond also to pH because of the protonation/deprotonation of charged groups in merocyanines. Thus, a light and pH double controlled ion valve is constructed.

As for switching procedure, due to the hydrophobicity of spiropyran molecules, molecular switching from merocyanines to spiropyrans meets difficulty in aqueous solution. Ethanol or other less polar solvent are necessary to provide a less hydrophilic environment for the switching in visible light. To solve this problem, another strategy has been tried which is not included in this manuscript by using a more hydrophobic chain based on polypeptides to link spiropyrans. These hydrophobic polypeptides can provide a less polar environment for the molecule switching in visible light that it can be hoped to achieve a solvent free light controlled ion channel based on spiropyran.

Through this chapter, polyelectrolytes and modified polyelectrolytes are interesting strategies to functionalize track etched nanopores to design stimuli-responsive ion channels. Because they can have stimuli-responsive functions, suitable molecular size and various possibility of immobilization in track etched nanopore.

Chapter 3:

Osmotic energy harvesting

Introduction

In this chapter, the generation of osmotic energy of polyelectrolytes functionalized track-etched nanopore was investigated. The osmotic energy also called blue energy has the highest energy density among numerous energy forms in ocean. It takes the advantages of chemical potential difference between brine/sea water and river water mixing through ion selective membranes. However the low performance of ion selective membranes limits the maximum power density more or less 1 W m^{-2}, it is still interesting to develop this technique to get back a part of energy from the desalination industry which is necessary to reduce the high energetic cost of this process.

By now, ion selective membranes suffer from high membrane cost, low ion selectivity and high membrane resistances. Track etched membranes based on polymer films as long-time used classical membranes have advantages of low cost and easy functionalization. More interestingly, track etching techniques also allow fabricating single nanopores that is useful to study the membrane behavior from single pores to multipores scale. Here we proposed to enhance the membrane ion selectivity by introducing more charges in the pore to capture more counter-ions by immobilizing polyelectrolytes. The first work was achieved by layer-by-layer depositing of polyacrilic acid/chitosan on pore surface. Then, ion transport and power generation properties were studied. The second work involved *in situ* synthesis of crosslinked highly charged hydrogel inside track etched nanopore. This study was done from single nanopore to multipore membrane. Finally, we have stacked cation and anion selective membranes.

The results presented in this chapter have been published as two articles:

Large osmotic energy harvesting from functionalized conical nanopore suitable for membrane applications. J. Membr. Sci. 2017, 544, 18.

Nanopore Functionalized By Highly Charged Hydrogels For Osmotic Energy Harvesting. ACS Appl. Mater. Interfaces, 2019, 11, 13, 12578-12585.

Articles

Large osmotic energy harvesting from functionalized conical nanopore suitable for membrane applications

Sébastien Balme, Tianji Ma, Emmanuel Balanzat and Jean-Marc Janot

Contribution : I did the experiments with Sebastien Balme.

Introduction

Access to energy from renewable natural resources at low cost is a major challenge to deal with energy dependence. In this area, a remarkable amount of energy due to the difference in salinity between seawater and river water is available [1-3]. In order to capture such osmotic energy, so-called "blue energy", two main methods are currently under development. The first ones are based on the Pressure-Retarded Osmosis (PRO) [4]. They allow reaching a power density until 10 W m^{-2} [5]. The second ones, the Reverse Electro Dialysis (RED), permit the capture directly from the salinity gradient [6-10]. Until now, the main limitation of this technology comes from its low energetic efficiency, less than 1 W m^{-2} when using stacks of cation-exchange and anion-exchange membranes [11] or 3.46 W m^{-2} in the case of a membrane composed by ionic diodes [5]. However it is conceptually possible to improve this energetic yield by the use of membranes composed of nanopores with a high surface charge σ and/or a low thickness L.[12]

$$I_{osm} \approx \frac{2\pi R\sigma}{L}\frac{k_B T}{\eta \lambda_B}\log(C_s) \qquad \text{(eq. 1)}$$

where I_{osm} osmotic current, R the nanopore radius, η the viscosity, λ_B the Bjerrum length and C_s the ratio of salt concentrations on either side of membrane.

This consideration has been supported by two recent publications. In the first one, Siria et al. have highlighted a giant osmotic current through a unique boron nitride nanotube [12]. This current is generated by a important surface charge and likely by a long slip length due to the crystallinity of the nanotube [13]. In the second one, Feng and his coworkers used a MoS_2 nanopore with a very low thickness of three atoms [14]. From these two studies, the extrapolation of the results obtained on a single nanopore to a multipore membrane let think of a possible production of several kW m^{-2}. However, the limiting factor of both MoS_2

and BN nanotube is the difficulty to produce membranes of several m^2 or cm^2 with a high density of these nanopores. Thus the challenge is to prove that it is possible to generate a giant osmotic current from the properties of a particular single nanopore and that is reproduced several times within a multipore membrane [15]. In order to reach this goal, two ways seem suitable. The first one is the deposition of BN by atomic layer deposition [16]. The second one is to use nanopores which present ionic diode properties [17-19]. The latters are usually obtained for asymmetric nanopore such as conical or semi-cigar shape. The diode effect depend on the nanopore tip diameter [20, 21] and on the density of surface charges [22, 23]. It was explained by ion-enrichment and ion-depletion inside the nanopore [24, 25]. Such nanopore was previous considered for osmotic energy harvesting [18, 26, 27]. They permit to generate from few to several hundred pW per nanopore which is very promises. A theoretical study has shown that both charge distribution and shape play a role in power generation. It predicts that a nanopore with a short effective length of the narrow tip should improve the osmotic energy production [28].

In this study, we decided to use nanopores obtained by the track-etched method because they are easily functionalizable and up-scalable to multipore membranes [29-32]. In addition, this method allows obtaining of ionic diode when using a pore of conical shape [33, 34]. In order to increase the surface charge, we have functionalized the nanopore using a deposition, layer-by-layer, of polyelectrolytes [35-38]. Here, the idea is to deposit a couple of polyelectrolytes; one neutral and the other charged at the operating pH, between 7.4 and 8.4. In addition, the structure of the polyelectrolyte layers must not be modified with the concentration of salt and should remain stable over time. Accordingly, we have functionalized the conical nanopores by alternating deposits, layer after layer, of chitosan (CH) and poly(acrylic acid) (PAA) . The PAA provides the negative surface charge of the nanopore; the chitosan with a pKa around 5.6 is neutral to the operating pH. In addition, chitosan is not soluble in water at pH above 6. It confers to the CH/PAA multilayers a good stability. In addition these bilayers do not swell with the ionic strength [39]. The proof of concept and the ionic transport properties will be shown on a single nanopore, then we will demonstrate the possible upscale to multipore membranes.

Materials and methods

Materials

Poly(ethylene terephthalate) (PET) film (thickness 6 µm, biaxial orientation) was purchased from Goodfellow (ES301061). Sodium chloride (71380), $CuCl_2$ (751944) and $CoCl_2$ (769495) and sodium hydroxide (30603), Chitosan (448869), Poly(acrylic acid) solution Mw 100000 (523925) were purchased from Sigma-Aldrich. Potassium chloride (POCL-00A) was purchased from LabKem. Ultra-pure water was produced from a Q-grad®-1 Milli-Q system (Millipore). Artificial seawater was obtained by dissolution of Coral Pro salt (Read Sea) in distillated water.

Current-voltage measurements on single nanopore

The single nanopore was mounted in the Teflon cell containing an electrolyte solution. The current is measured by Ag/AgCl, wires directly immersed in electrolyte solution. One electrode was plugged to the working end of the amplifier (trans chamber, base side) and the other electrode connected to the ground (cis chamber, tip side). Electrical measurements were achieved by a patch-clamp amplifier (EPC10 HEKA electronics, Germany). Recorded currents were analyzed by Fitmaster (Heka Elektronik, Germany).

For IV curves, the currents data were recorded as a function of time under constant voltages from -1 V to 1 V by step of 100 mV and from -100 mV to 100 mV by step of 10 mV. All current traces were recorded during 5 s at a frequency of 50 kHz. These measurements were repeated 3 times.

For the power measurement, we used reference electrode Ag/AgCl 1 M KCl electrodes connected to electrolyte solution by agar–agar bridges. Before measurements, the eventual difference of electrode potential was calibrated using symmetrical concentration of salt in both compartments.

Power measurement on multipore membrane

The power measurement of multipore membrane (0.37 cm^{-2}) was performed using reference electrode Ag/AgCl 1 M KCl electrodes connected to electrolyte solution by agar–agar bridges. A 1 Ohm resistance closes the circuit. The current and voltage were recorded using multimeters Keithley 617 and Agilent 344110A respectively.

Track-etching nanopores and characterization

Single tracks were produced by Xenon irradiation (8.98 MeV u^{-1}) of the PET film (6 µm) (GANIL, SEM line, Caen, France). The PET film was exposed to UV light for 12 h per side to activate the track (Fisher bioblock; VL215.MC, λ = 302 nm) just before the chemical etching. The etching of the conical nanopore was performed under dissymmetric conditions. The PET foil was mounted between two compartments of a chemical cell in Teflon. The etchant solution (NaOH 9M, 1.6 ml) was added on base side and the stopping solution (KCl 1M and acetic acid 1M, 1.6 ml) on tip side. The etching process was performed at 23°C. A potential of 1 V was applied across the membrane. When the current reaches a value around 400 pA, the etching process was stopped by the replacement of the etching solution by the stop one.

The single conical nanopores are characterized in two steps. At first the base diameter (d_{base}) is deduced from the SEM image of a multipore membrane etched under the same condition (shining exposition, etching time, NaOH concentration). The tip diameter (d_{tip}) is calculated, from the dependence of the conductance G with NaCl concentration (eq. 2) (from 0.1 M to 1 M) assuming a bulk-like ionic conductivity inside the nanopores. In order to correct the conductivity at high salt concentration the ionic conductivity of solution κ have been measured using a conductimeter (Hanna HI 255 combined meter with conductivity and electrode HI 76310) after preparation [40].

$$G = \kappa \, \pi d_{base} d_{tip} / 4L \qquad \text{(eq. 2)}$$

where L is the nanopore length.

In our experiment the etching time provides base diameters between 750 nm to 640 nm, which corresponds to tip diameters from 12 to 14 nm.

The multipore membranes were obtained following the same procedure using a PET film irradiated with a fluency of 10^7 ions cm^{-2}. The final density of nanopore on the tip side, obtained by SEM imaging, is 2 10^6 pore cm^{-2}.

Nanopore functionalisation

The PAA stock solution with a concentration 1mg ml^{-1} was prepared at pH 5. The CH stock solution, concentration 1mg ml^{-1}, was prepared at pH 3. The nanopore functionalization was performed under buffer condition KCl 0.1 M MES 10mM pH 5.4. The sorption of CH was

performed by addition of 16 µl of stock solution in tip side. A voltage -1V was applied during 5 minutes. The cell was then rinsed with buffer to remove the excess of polyeletrolyte. Then 16 µl of PAA solution was added on tip side during 5 minutes under voltage 1V. The procedure was repeated until the desired numbers of CH/PAA bilayers.

Results and discussions

The single nanopores traces were obtained by irradiation of PET films. The conical shape was achieved by a chemical etching under dissymmetrical conditions using electro-stopping method [41, 42]. An estimation of base diameter is given by SEM (figure 1) on a multipore membrane etched under the same conditions. The tip diameter is deduce from the conductance measurements of a 1M KCl solution [40]. The nanopore functionalization was performed by alternate deposition of CH/PAA under voltage to drive their entrance inside the pore. The success of the functionalization was characterized by the modification of the IV curves after each layer deposition of polyelectrolyte (Figure 1).

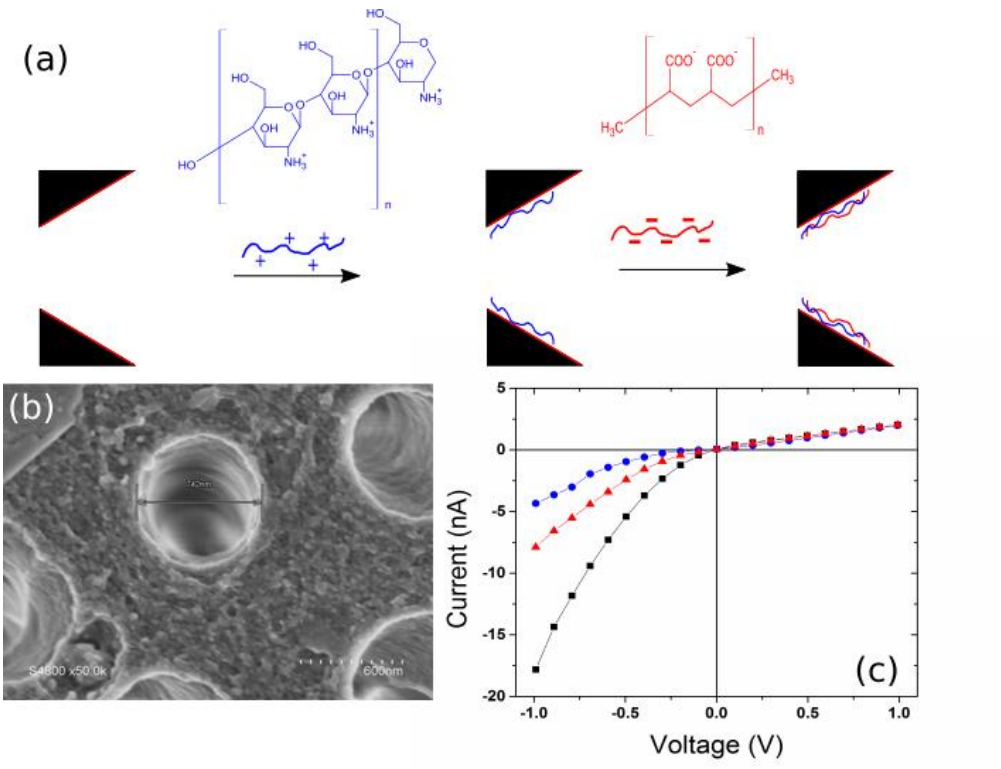

Fig. 1 (a) Sketch of single conical nanopore functionalization (b) SEM image of base side of track-etched membrane after 180 minutes of chemical etching. (c) IV curves measured at KCl 0.1 M MES 10mM pH 5.4 of single nanopore after chemical etching (black, square), chitosan adsorption (blue circle) and PAA adsorption (red triangle) .

We studied the ionic transport, under symmetrical conditions using NaCl solutions at various concentrations from 10^{-3} mol.l^{-1} to 1 mol.l^{-1} and for different pH. This salt was chosen because it represents 85% of the ionic composition of the sea water. The nanopore conductance was obtained by the fit of the linear part of IV curve, typically between -75 mV and 75 mV. The results reported in Figure 2 show that the conductance *G* decreases of one order of magnitude when the bulk concentration of NaCl *c* decreases from 1 M to 10^{-3} mol l^{-1}. This range is in the same order than the one reported for the BN nanotube at pH 11 suggesting a high surface charge of the nanopore [12]. It can be also noticed that the nanopore conductance is higher at pH 7.6 than at pH 3. Thus, the high surface charge can be explained by the high density of COO^- due to PAA layer which are not shielded by CH which is neutral at pH upper than 7. In order to study the influence of the pH on the NaCl transport, we introduce a rectification factor defined as $rf = \left|I_{(1V)}/I_{(-1V)}\right|$ (Figure 2). This rectification factor is currently used to characterize the diode effect. Its value depends on the surface charge density and the ionic selectivity of the nanopore [43, 44]. For a pH below the pKa of the PAA the *rf* factor is greater than 1, the nanopore is positively charged and selective to the anion. For a pH above the pKa of the CH the *rf* factor is less than 1, in this case, the nanopore is negatively charged and selective to the cation. For pH around 4.3 the *rf* factor is close to 1. The value (higher or lower than 1) depends on the balance of the charges between the two polyelectrolytes. The clear correlation between the rectification factor and the pKa of the two polyelectrolytes confirms the success of the functionalization.

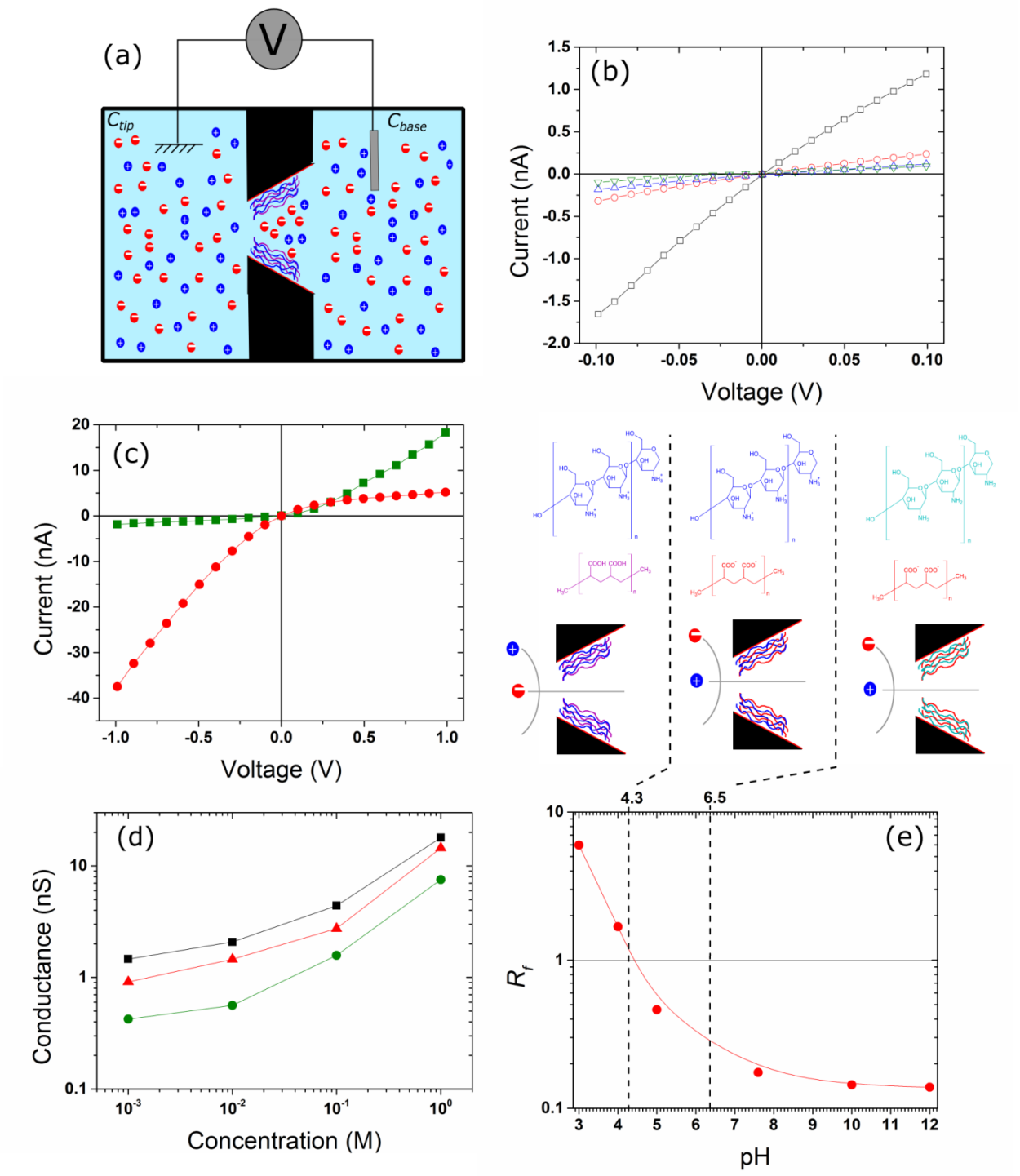

Fig. 2 (a) Illustration of an experiment performed under symmetrical salt concentrations (b) Dependence of IV curves of conical nanopore recorded at different NaCl concentrations, 1M (black, square), 0.1 M (red, circle), 0.01 M (blue, up triangle) and 0.001 (green, down triangle) (pH 7.6) (c) IV curves obtained for NaCl 1M at pH 3 (green, square) and pH7.6 (red, circle), (d) nanopore conductivity as function of NaCl concentration at pH 3 (green, circle) pH 7.6 (red, triangle) and pH 10 (black, square) (e) evolution of the rectification factor with the

pH for NaCl 1 M and illustration of ion flux at the origin of the current rectification with respect to the charge of each polyelectrolyte.

The CH is well known as chelating agent to remove metal ions from water.[45] In order to confirm the functionalization by another way, we have evaluated the impact of the metal ions on the nanopore surface charge. The addition of Cu^{2+} or Co^{2+} on the tip side of the nanopore induces an increase of the rectification factor (Figure 3). An inversion of this factor occurs for 2 mM of Cu^{2+} or 10 mM of Co^{2+}. These results are explained by the adsorption of the metal ion on the CH/PAA layer. The metal ion adsorption is reversible by washing at pH 3. This behavior has been previously reported in the case of nanopipettes functionalized by PAA/CH.[46]

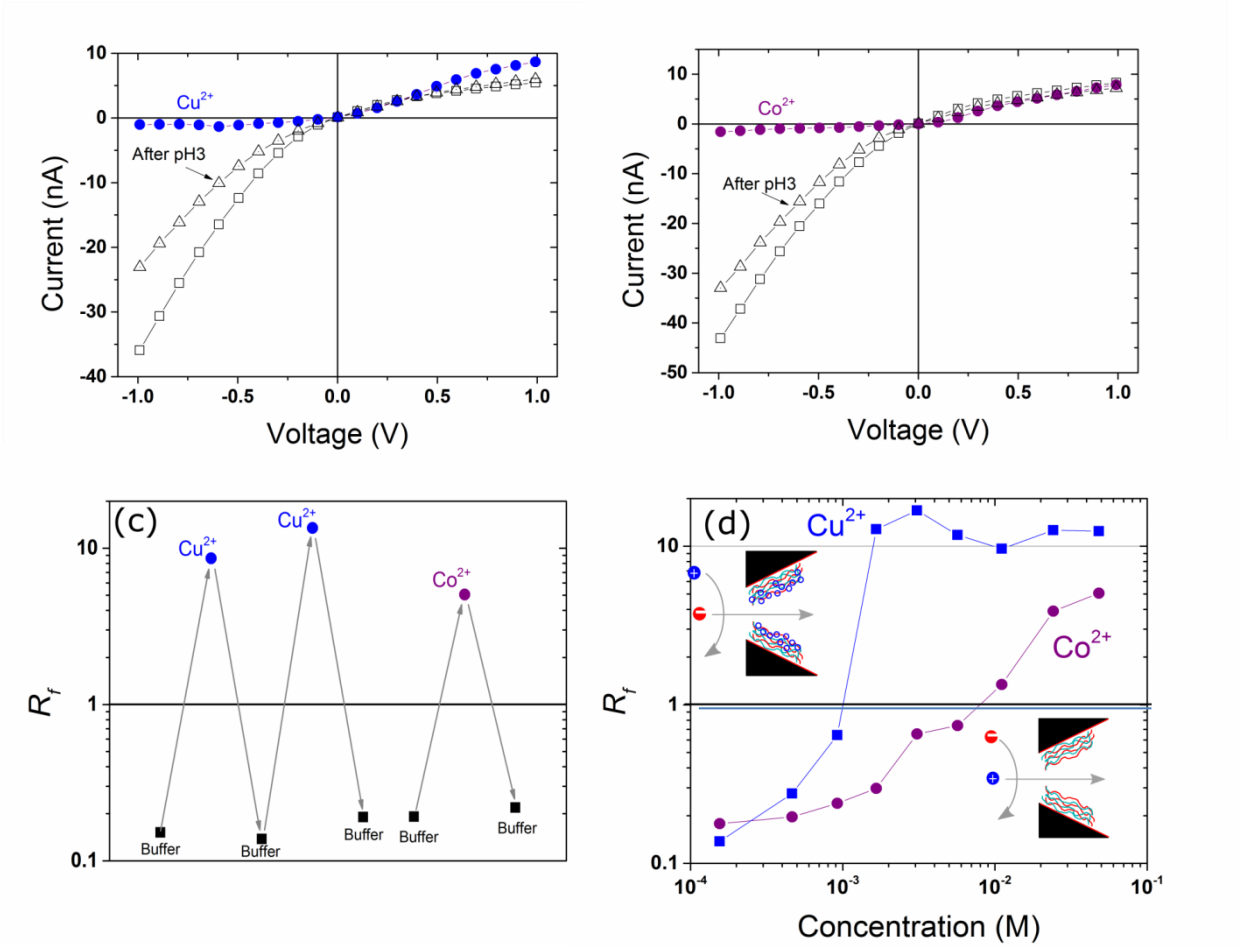

Fig. 3 Influence of metal ion on ionic transport. (a-b) I-V response recorded under NaCl 1M at pH 8 (open square), after addition of Cu^{2+} (a) or Co^{2+} (b) (full, circle) and after rince at pH 3 to remove the metal ion (open triangle). (c) Rectification factor after cycle of metal ion

adsorption (circle)/desorption (square). (d) Evolution of the rectification as a function of Cu^{2+} (bleu, square) or Co^{2+} (purple, circle) concentrations added in tip side.

To go further in our investigations and to evaluate the osmotic current generated by the single nanopore, the ionic transport of NaCl was studied under dissymmetrical salt conditions (Figure 4a). The concentration ($c_{,Tip}$) in the tip side of the nanopore was set to 1M and the concentration in the base side ($c_{,Base}$) varied from 10^{-3} M to 1 M. From the IV curves (Figure 4 and SI), we extract two types of informations. The first is the permeation ratio between Na^+ and Cl^- P_{Na}/P_{Cl} which is obtained from the V_{res} using the Goldman-Hodgin-Katz equation; at pH 7.6 this ratio P_{Na}/P_{Cl} is equal to 1.74. The second, is the osmotic current I_{osm} which is extract from the current at V=0 [5, 27, 28]. As shown in Figure 4b the osmotic current depends on the pH. For a $c_{,Tip}/c_{,Base}$ = 1000, I_{osm} reaches very large values, -0.6 nA and -0.9 nA for pH 7.6 and 10 respectively. Without functionalization the I_{osm} is lower (typically -0.2 nA for a nanopore with à d_{tip} =27).We can calculate the transport coefficient K_{osm} in the nanopore.

$$|I_{osm}| = K_{osm}\log\left(c_{Tip}/c_{Base}\right) \quad \text{(eq. 3)}$$

From equation 3 we obtained K_{osm} ≈0.06 nA, 0.12 nA and 0.21 nA for pH 3, 7.6 and 10 respectively. We the maximum power density calculated from $P_{max} = I^2_{osm}/4G$ for a single nanopore are reported on Figure 5a. Interestingly, we obtain 25 pW at pH 7.6 for c_{Tip}/c_{Base}= 1000 which is in the same range than the one reported in the case the BN nanotube at pH 9.5 [12] and in conical nanopore in polyimide film [27]. Without the functionalization, the energy provides by single nanopore is about 5.2 pW for c_{Tip}/c_{Base} =1000. This confirms that PAA/CH layers improve the production of osmotic energy. In ionic diode, the mechanism of energy conversion was previously explained using model calculations based on coupled Poisson-Nernst–Planck equations [18]. It is due the counter-ions which spontaneously and preferentially diffuse across the nanopore. This process does not require an extern electrical voltage. The diffusion current comes from the separation of cation and anion within the electrical double layer close to the inner nanopore wall. Thus a high density of surface charge favors to the generation of diffusion current and thus the

energy production [47]. According the previous theoretical prediction, the osmotic current is enhanced when the surface charge is high and the effective nanopore length is short [12, 28]. However, if the nanopore length is below 400 nm, the strong ion concentration polarization decreases the nanopore selectivity [48, 49]. In our case, these both conditions are gathered. As previously mentioned, the nanopore functionalization provides a high density of COO- which is not shielded at neutral at pH by CH. In addition, the polyelectrolyte deposition was performed during only 5 minutes. Thus, we can consider that PAA and CH are adsorbed at the region close to the narrow opening [38]. This induces a partial enclosure of tip which modifies the nanopore geometry by a decreasing of effective length in narrow tip. We observe also that P_{max} values are similar at pH 7.6 and 10 when PAA is negatively charged and CH unsoluble on water. At pH 3, the P_{max} is very low. In the same time, both conductance and osmotic current are lower. This is surprising because only CH is charged and thus we could expect large of osmotic current as in pH upper 7. This discrepancy can be explained by a modification of PAA conformation due to the protonation and CH because it is soluble in water at low pH.

At this stage, our nanopore can be considered as a good candidate for generating osmotic energy. However the stability of nanopore has to be verified. The ionic transport under both symmetrical and dissymmetrical conditions was studied after 6 days in order to prove that this system is suitable for application purposes. The results show that both conductivity (SI) and osmotic current (Figure 4c) are similar, confirming the stability of the nanopore and the of PAA/CH layers.

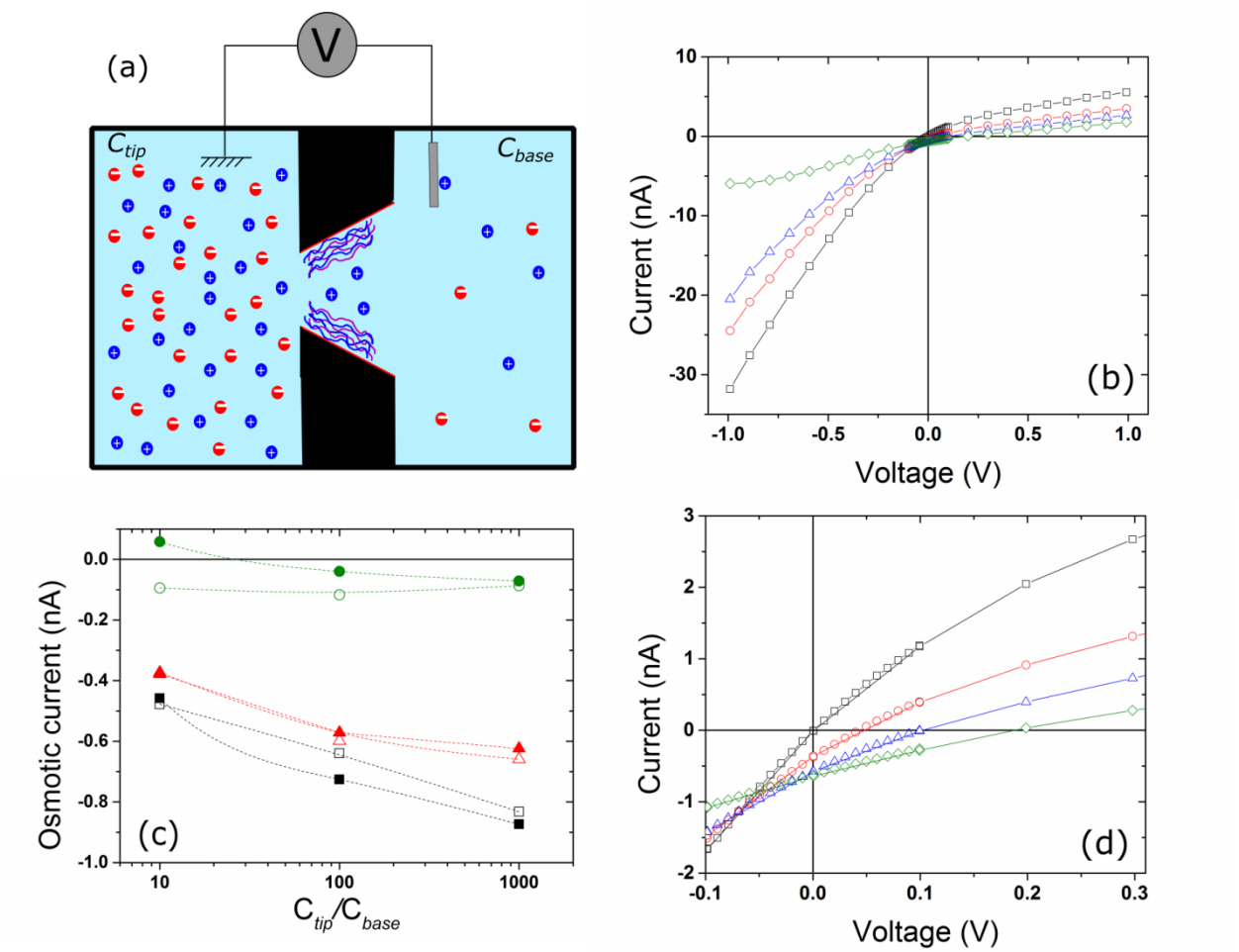

Fig. 4 (a) illustration of an experiment performed under dissymmetrical salt concentrations (b/d) IV curves obtained at pH 7.6 for NaCl C_{Ttp} = 1M and C_{base} = 1M (black, square), 0.1 M (red, circle), 0.01 M (blue, triangle) and 0.001 (green, diamond) (pH 7.6). (c) Evolution of the osmotic current as a function of the concentration ratio of salt on either side of nanopore pH 3 (green, circle) , pH 7.6 (red, triangle) and pH 10 (black, square), day 1 (full symbols) and after 6 day (open symbols).

In order to consider a realistic use of these nanopores, we have to prove the possibility to extend the properties obtained on a single nanopore to a multipore membrane. To do that, we etched 0.37 cm^{-2} of a PET film irradiated with a fluency of 10^7 ions cm^{-2} under dissymmetrical conditions. After the chemical etching, we obtained a membrane with a density of nanopore on the tip side of 2 10^6 pores cm^{-2} and a pore diameter between 30 to 300 nm. Then, the membrane is functionalized with 5 CH/PAA bilayers using the same protocol as for the single nanopore membrane. The I_{osm} was measured under dissymmetrical

NaCl conditions by the Ag/AgCl electrodes directly connected to a resistance of 1 Ohm. From the simple extrapolation of the results obtained on the single nanopore to a membrane with a surface 0.37 cm^2 and density of 2 10^6 pores cm^{-2}, we can expect to measure a current for a ratio c_{Tip}/c_{Base} = 1000 at pH 7.6 around 350 µA. The experimental measurement shows a value of 34 µA and a voltage of 120 mV corresponding to 0.1 W m^{-2}. This energy density can be increased until 0.45 W m^{-2} using a 1 M NaCl solution against the distillated water. We also performed a more realistic test using artificial seawater and tap water. In this case, the power density obtained is 0.078 W m^{-2}. This power density seems to be weak compared to 0.97 W m^{-2} reported in the literature [11], however, 50 stacks of anion and cation exchange membranes were used to reach this performance. In our experiments we used a single membrane with a low density and a large polydispersity of nanopores. In order to improve the performance of ionic diode membrane, different ways could be considered. The density of nanopore can be increased. However, regarding the conical shape it is not possible to used membrane with a density of nanopore 10^{10} pores cm^{-2} as suggest in the case of BN nanopore [12]. However with a better control of nanopore dispersity and a density of nanopore 10^7, an improvement by a factor 10 is realistic. A concave bullet-like tip geometry can be considered to increase the power generate by the nanopore as predicted by Cervera et al. [28].

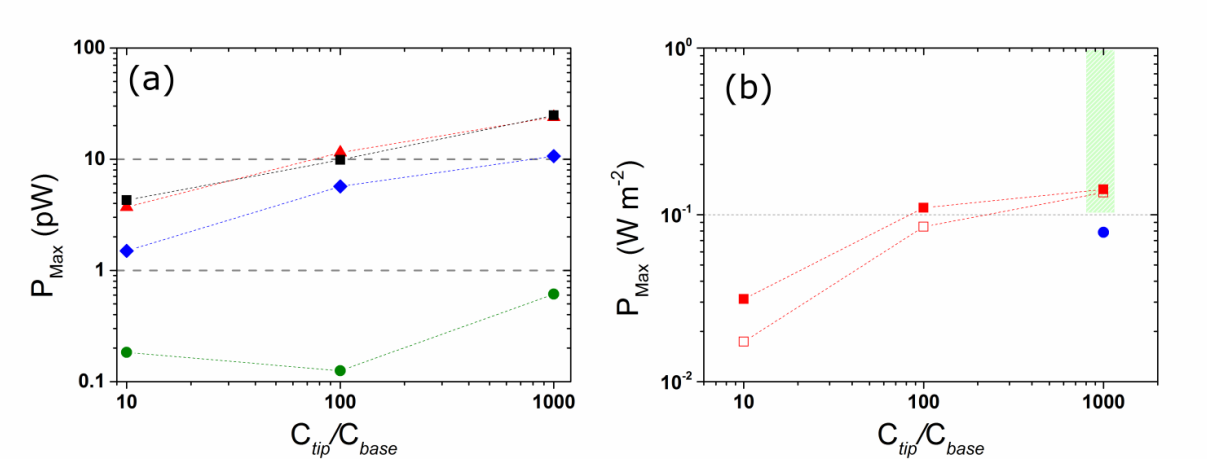

Fig. 5 (a) Power generated by a single nanopore as a function of the NaCl concentration ratio at pH 3 (green, circle), 5 (blue, diamond), 7.6 (red, triangle) and 10 (black, square). (b) Power density generated by a multipore membrane of 2 10^6 pores cm^{-2} as the function of the NaCl c_{Tip}/c_{Base} (red open square day 1 and red full square day 3). The blue circle corresponds to

experiment performed using artificial seawater and tap water. The rectangle areas correspond to the energy reported for classical RED membrane [5] (light green).

Conclusion

To summarize, we have demonstrated that a conical nanopore functionalized by layers of CH/PAA is a simple and efficient route to design a membrane used for osmotic current generation. The accessible performance for a single nanopore is in the same order of magnitude as for a single BN nanotube. Compare to the latter the upscale to multipore membrane is suitable as demonstrated in the case of low density membrane. From this proof of concept, we can expect to substantially improve the performance of the membrane for the production of a power density reaching several W m^{-2}. We guess that the present strategy permits to consider the manufacturing at large scale of membranes and therefore a real-life application for the production of “blue energy”.

Reference

[1]. B.E. Logan and M. Elimelech, Membrane-based processes for sustainable power generation using water. Nature, 488 (2012) 313-319.

[2]. Z.J. Jia, et al., Blue energy: Current technologies for sustainable power generation from water salinity gradient. Renewable & Sustainable Energy Reviews, 31 (2014) 91-100.

[3]. N.Y. Yip, et al., Thermodynamic, Energy Efficiency, and Power Density Analysis of Reverse Electrodialysis Power Generation with Natural Salinity Gradients. Environmental Science & Technology, 48 (2014) 4925-4936.

[4]. F. Helfer, C. Lemckert, and Y.G. Anissimov, Osmotic power with Pressure Retarded Osmosis: Theory, performance and trends - A review. Journal of Membrane Science, 453 (2014) 337-358.

[5]. J. Gao, et al., High-Performance Ionic Diode Membrane for Salinity Gradient Power Generation. Journal of the American Chemical Society, 136 (2014) 12265-12272.

[6]. J.W. Post, et al., Towards implementation of reverse electrodialysis for power generation from salinity gradients. Desalination and Water Treatment, 16 (2010) 182-193.

[7]. J.W. Post, et al., Salinity-gradient power: Evaluation of pressure-retarded osmosis and reverse electrodialysis. Journal of Membrane Science, 288 (2007) 218-230.

[8]. J.G. Hong, et al., Potential ion exchange membranes and system performance in reverse electrodialysis for power generation: A review. Journal of Membrane Science, 486 (2015) 71-88.

[9]. M. Turek and B. Bandura, Renewable energy by reverse electrodialysis. Desalination, 205 (2007) 67-74.

[10]. D.A. Vermaas, M. Saakes, and K. Nijmeijer, Power generation using profiled membranes in reverse electrodialysis. Journal of Membrane Science, 385 (2011) 234-242.

[11]. J. Veerman, et al., Reverse electrodialysis: Performance of a stack with 50 cells on the mixing of sea and river water. Journal of Membrane Science, 327 (2009) 136-144.

[12]. A. Siria, et al., Giant osmotic energy conversion measured in a single transmembrane boron nitride nanotube. Nature, 494 (2013) 455-458.

[13]. E. Secchi, et al., Massive radius-dependent flow slippage in carbon nanotubes. Nature, 537 (2016) 210-213.

[14]. J.D. Feng, et al., Single-layer MoS2 nanopores as nanopower generators. Nature, 536 (2016) 197-+.

[15]. J.Z. Ji, et al., Osmotic Power Generation with Positively and Negatively Charged 2D Nanofluidic Membrane Pairs. Advanced Functional Materials, 27 (2017).

[16]. M. Weber, et al., Boron Nitride Nanoporous Membranes with High Surface Charge by Atomic Layer Deposition. ACS Appl Mater Interfaces, (2017) doi: 10.1021/acsami.7b02883.

[17]. C.B. Picallo, et al., Nanofluidic Osmotic Diodes: Theory and Molecular Dynamics Simulations. Physical Review Letters, 111 (2013).

[18]. W. Guo, et al., Energy Harvesting with Single-Ion-Selective Nanopores: A Concentration-Gradient-Driven Nanofluidic Power Source. Advanced Functional Materials, 20 (2010) 1339-1344.

[19]. Z. Zhang, et al., Engineered Asymmetric Heterogeneous Membrane: A Concentration-Gradient-Driven Energy Harvesting Device. Journal of the American Chemical Society, 137 (2015) 14765-14772.

[20]. P.Y. Apel, et al., Effect of nanopore geometry on ion current rectification. Nanotechnology, 22 (2011) 175302.

[21]. M.L. Kovarik, K.M. Zhou, and S.C. Jacobson, Effect of Conical Nanopore Diameter on Ion Current Rectification. Journal of Physical Chemistry B, 113 (2009) 15960-15966.

[22]. D. Constantin and Z.S. Siwy, Poisson-Nernst -Planck model of ion current rectification through a nanofluidic diode. Physical Review E, 76 (2007).

[23]. G. Nguyen, I. Vlassiouk, and Z.S. Siwy, Comparison of bipolar and unipolar ionic diodes. Nanotechnology, 21 (2010).

[24]. Q. Liu, et al., Asymmetric properties of ion transport in a charged conical nanopore. Physical Review E, 75 (2007).

[25]. J. Cervera, B. Schiedt, and P. Ramirez, A Poisson/Nernst-Planck model for ionic transport through synthetic conical nanopores. Europhysics Letters, 71 (2005) 35-41.

[26]. L.X. Zhang, et al., Modulating ion current rectification generating high energy output in a single glass conical nanopore channel by concentration gradient. Chinese Chemical Letters, 26 (2015) 43-46.

[27]. L.X. Cao, et al., Towards understanding the nanofluidic reverse electrodialysis system: well matched charge selectivity and ionic composition. Energy & Environmental Science, 4 (2011) 2259-2266.

[28]. J. Cervera, et al., Asymmetric nanopore rectification for ion pumping, electrical power generation, and information processing applications. Electrochimica Acta, 56 (2011) 4504-4511.

[29]. P. Apel, Track etching technique in membrane technology. Radiation Measurements, 34 (2001) 559-566.

[30]. M. Ali, et al., Tuning nanopore surface polarity and rectification properties through enzymatic hydrolysis inside nanoconfined geometries. Chemical Communications, 49 (2013) 8770-8772.

[31]. M. Ali, et al., A pH-Tunable Nanofluidic Diode with a Broad Range of Rectifying Properties. Acs Nano, 3 (2009) 603-608.

[32]. M. Lepoitevin, et al., Combining a sensor and pH-gated Nanopore based on an Avidin-biotin system Chemical Communications, 51 (2015) 5994-5997

[33]. P.Y. Apel, et al., Accurate characterization of single track-etched, conical nanopores. Physical Chemistry Chemical Physics, 16 (2014) 15214-15223.

[34]. I. Vlassiouk and Z.S. Siwy, Nanofluidic diode. Nano Letters, 7 (2007) 552-556.

[35]. M. Ali, et al., Layer-by-Layer Assembly of Polyelectrolytes into Ionic Current Rectifying Solid-State Nanopores: Insights from Theory and Experiment. Journal of the American Chemical Society, 132 (2010) 8338-8348.

[36]. Y. Zhao, et al., Mimicking pH-gated ionic channel by polyelectrolyte complex confinement inside single nanopore. Langmuir, (2017).

[37]. Y.X. Zhao, et al., Mimicking pH-Gated Ionic Channels by Polyelectrolyte Complex Confinement Inside a Single Nanopore. Langmuir, 33 (2017) 3484-3490.

[38]. M. Lepoitevin, et al., Fast and reversible functionalization of a single nanopore based on layer-by-layer polyelectrolyte self-assembly for tuning current rectification and designing sensors. Rsc Advances, 6 (2016) 32228-32233.

[39]. C.K.S. Pillai, W. Paul, and C.P. Sharma, Chitin and chitosan polymers: Chemistry, solubility and fiber formation. Progress in Polymer Science, 34 (2009) 641-678.

[40]. C.C. Harrell, S.B. Lee, and C.R. Martin, Synthetic single-nanopore and nanotube membranes. Analytical Chemistry, 75 (2003) 6861-6867.

[41]. P.Y. Apel, et al., Diode-like single-ion track membrane prepared by electro-stopping. Nuclear Instruments & Methods in Physics Research Section B-Beam Interactions with Materials and Atoms, 184 (2001) 337-346.

[42]. J.E. Wharton, et al., A method for reproducibly preparing synthetic nanopores for resistive-pulse biosensors. Small, 3 (2007) 1424-1430.

[43]. Z. Siwy, et al., Conical-nanotube ion-current rectifiers: The role of surface charge. Journal of the American Chemical Society, 126 (2004) 10850-10851.

[44]. J. Cervera, et al., Ionic conduction, rectification, and selectivity in single conical nanopores. Journal of Chemical Physics, 124 (2006).

[45]. A. Gamage and F. Shahidi, Use of chitosan for the removal of metal ion contaminants and proteins from water. Food Chemistry, 104 (2007) 989-996.

[46]. P. Actis, et al., Voltage-Controlled Metal Binding on Polyelectrolyte-Functionalized Nanopores. Langmuir, 27 (2011) 6528-6533.

[47]. Y. Feng, et al., Bioinspired Energy Conversion in Nanofluidics: A Paradigm of Material Evolution. Advanced Materials, (2017) 10.1002/adma.201702773.

[48]. L.X. Cao, et al., Anomalous Channel-Length Dependence in Nanofluidic Osmotic Energy Conversion. Advanced Functional Materials, 27 (2017).

[49]. S.J. Kim, et al., Concentration polarization and nonlinear electrokinetic flow near a nanofluidic channel. Physical Review Letters, 99 (2007).

Nanopore Functionalized by Highly Charged Hydrogels for Osmotic Energy Harvesting

Tianji Ma, Emmanuel Balanzat, Jean-Marc Janot, Sébastien Balme

Contribution: I designed the work with Sebastien Balme, did experiments, analyse data and wrote the manuscript.

Introduction

Energy and environment are currently two of the main topics for modern society thanks to the global warming. Until today, fossil fuels are used as the primary energy source to support human life and also generate both environmental and ecological problems[254–256]. Although, a variety of sustainable energy sources are being exploited such as biofuel[257], solar[258], wind[259], geothermal electricity[260] and water[261]. In this context, the osmotic energy (called also blue energy) which takes advantage of the salinity difference between sea water and river water could be a good candidate thanks to the renewability of the resource, the pollution free, relatively low cost and rich reserves[167]. The estimated production of blue energy is closed to 2 TW which can fulfill the electricity demand today[262].

To practically make use of this large energy from water, the efforts were made to develop two methods based on membrane separation processes[41]: pressure retarded osmosis (PRO) and reversed electro-dialysis (RED). For the PRO facilities, a semipermeable membrane is placed between river water (feed solution with low osmotic pressure) and sea water (draw solution with high osmotic pressure). Water pass from feed to draw solution driven by the osmotic pressure difference[249,263]. By equipping a turbine to the reservoirs of draw solution, the energy of this water flow is converted to electricity. In RED technology, stacked ion exchange membranes (IEMs) are used. The ions move selectively from concentrated salt solution to diluted one driven by salinity gradient[40,264]. The charge flow of the ion separation is converted into electric current by redox reaction of electrodes. The energy harvested by this technology is relatively low and to make it suitable for real application an effort is essential to improve the performance of membranes.

To develop both anion exchange membranes and cation exchange membranes, many materials were used to improve the power density, the energy efficiency and the cost of membranes[261,265]. Recently the investigation at single nanopore level has allowed major fundamental breakthrough for further application. Indeed, Siria, A. et al. measured giant osmotic energy through a single boron nitride nanotube with a diameter between 100 nm and 200 nm, providing a power generation of 20 pW pore^{-1} (C_{max}/C_{min} = 1000)[158]. Feng, J. et al. synthesized a single sheet of MoS_2 nanopore with a diameter of 5 nm and a membrane thickness of only 0.65 nm. This single sheet structure generates an osmotic current at more than 8 nA and a single pore power at almost 0.5 nW (C_{max}/C_{min} = 1000)[150]. Despite impressive result at single pore scale, these nanopores cannot be scaled up on large area of multipore membranes for practical uses by now. Besides of these, 2D materials based on graphene oxides have also been considered for RED application J. Ji et al. utilized a negative/positive charge graphene oxide membrane to get a power density of 0.77 W m^{-2} [266]. As nanotube, these 2D materials are particularly efficient since they combine both surface charge and/or large slippage to generate osmotic energy[165,267]. Beside the surface charge, the asymmetrical structure of nanopore generates also the ionic selectivity[194,268,269]. Recently, L. Jiang's group has developed a package of asymmetrical heterogeneous membranes which take advantage of both charge and membrane asymmetry. They used mesoporous carbon/macroporous alumina membrane[270] to achieve a power density at 3.46 W cm^{-2}. Two block copolymers[271] are synthesized to get a power density of 2.04 W cm^{-2}.is from combining porous block copolymer with track-etched PET membrane a power density of 0.35 W cm^{-2} was reached [252]. While they suffer from fragility of alumina support, complexity of fabricating composite membranes or the low pore density of conical nanopore.

In this work, we want to tackle the main issue related to conical nanopore obtained by track-etched method to propose a membrane stack with high nanopore density taking the advantage to a polymer support. Indeed the fabrication and physical-chemistry properties of such membranes have been well exploited[97,272–275]. It is thus possible to play with both asymmetrical geometry and surface charges to develop an ionic diode like ion exchange membranes from single pore scale to high density multipore membranes. The control of pore number, their shape and their surface properties allows many applications such as biosensing[235,244,276–278], stimulus responsive ionic channels[9,218,279,280], energy harvesting[281]

and so on. To involve high charge density, the functionalization with polyelectrolytes seems a good solution regarding previous study[8,281]. However another option could be more efficient. Recently by learning from electric-eel, M. Mayer's group obtain an open-circuit potential differences of over 100 V by stacking thousands of highly charged and salinity-containing hydrogel cells[282]. But limited by the current density, the power density at 27 mW m^{-2} can be improvable. Following this work, we synthesize in-situ a cation-selective gel using 3-sulfopropyl acrylate and an anion-selective gel using (3-acrylamidopropyl)trimethylammonium directly inside nanopore. Due to the high densities of sulfonic and quaternary ammonium groups, we assume that these hydrogels will involve a high concentration of counter-ions inside the nanopore generating a high ionic selectivity. On the same time, we consider two nanopore geometries: conical and cylindrical. As the conical pore has ionic diode propertied, we expect that the ionic selectivity will be enhanced; meanwhile this shape limits the membrane at low pore density due to the large diameter of base side. Conversely, the cylindrical pore does not have a broken symmetry and thus the performance could be lower, but it can be scaled up to a high pore density.

So our investigation will begin with conical and cylindrical single nanopores filled with hydrogels. Through these nanopores the ionic transport properties, ionic selectivity and energy conversion ability are studied. Then hydrogel functionalized conical and cylindrical multipore membranes are studied to evaluate the power generation. Finally, the power density is measured on a stacked of membranes. A clear relationship between single nanopore and a stack of high density membranes is shown.

Materials and methods

Materials

13 µm thick PET films, with biaxial orientations were purchased from Goodfellow (ref ES301061). 3-sulfopropyl acrylate potassium salt (SPAK) (251631), (3-acrylamidopropyl)-trimethylammonium chloride (APTAC) (448281), acrylamide (01700), 2-Hydroxy-4'-(2-hydroxyethoxy)-2-methyl-propiophenone (photoinitiator) (410895), N,N'-Methylenebisacrylamide (BIS) (M7279), tetramethyl-ethylenediamine (TEMED) (T7024), ammonium persulfate (APS) (A3678), sodium chloride (71380) are purchased from Sigma-Aldrich. Chloride acid (20248.290) and sodium hydroxide (28245.298) are purchased from

VWR Chemicals. Water used in these experiments was purified by Q-grad®-1 Milli-Q system (Millipore).

Synthesis of ion selective gels

Anionic gel: Chemicals are weighed and dissolved in water to prepare a precursor solution at 2 ml with 2.0 M 3-sulfopropyl acrylate (potassium salt), 0.045 M photoinitiator, 1.9 M acrylamide and 0.055 M BIS. For the experiments with different amounts of BIS to compare the effect of different gel reticulation degrees, three concentrations of BIS are used as R_3 = 0.055 M, R_2 = 0.037 M and R_1 = 0.018 M. Then 0.005 M APS and 0.033 M TEMED were added to the solutions as catalyst. Very quickly the nanopore membrane is immerged into the solution and make sure that both sides of membrane are well infiltrated. The solution is well isolated from air and the reaction is during overnight. Cationic gel: The same procedure is applied with a different precursor solution with 2.0 M (3-acrylamidopropyl)trimethylammonium chloride, 2.75 M acrylamide and 0.034 M BIS.

Track-etched nanopores

Single nanopores and multipore membranes were obtained by track-etched methods. The tracks were produced by Xe irradiation (8.98 MeV u^{-1}) in PET film at GANIL, SME line (Caen, France). For single track, a hole (diameter 1 mm) with a shutter was placed on ion beam path. The control of track number was provided by a detector placed behind the sample. For multipore membrane the beam directly irradiates the sample. For conical single and multipore membrane, after being activated by UV irradiation (Fisher bioblock; VL215.MC, l= 312 nm) during 9 hours for the tip side and 15 hours for the base side, the PET film was mounted in a Teflon cell with two chambers. An etchant solution (9 M NaOH) and a stopping solution (1 M KCl and 1 M acetic acid) were used for each side to have an asymmetrical conical shape. A reference was placed in the stopping solution and a working electrode the etchant solution. A potential 1 V was applied across the film to control the pore opening by measuring the current as a function of time using an amplifier (HEKA EPC10). Then the etching process was stopped by replacing the etchant solution with stopping solution and finally the membrane was immerged in 18.2 MΩ cm pure water for 24 hours.

For cylindrical single and multipore, the same UV treatment was performed then the PET film was immerged in an etchant solution (3 M NaOH) at 50°C during 10 minutes to obtain a

pore diameter about 100 nm. Finally, the membrane was also let in 18.2 MΩ cm pure water for the next use.

The diameter of single nanopore is calculated from the dependence of the conductance G measured in the linear zone of the I–V curve (-60mV to 60mV) in 1 M NaCl solution.

$$G = \frac{\kappa d D \pi}{4L} \quad (1)$$

where, κ is the ionic conductivity of the solution assuming a bulk like transport, L is the nanopore length (13 µm). For cylindrical nanopore $d = D$, meanwhile, for conical nanopore d and D are the tip and base diameter respectively. D is calculated from the total etching time t using the relationship $D = 2.5\ t$ (the factor 2.5 is determined in our experimental set up using multipore track-etched membranes).

Current-voltage measurement

Current-voltage measurements for single nanopore were performed using a patch-clamp amplifier (EPC10 HEKA electronics, Germany) with Ag/AgCl, 1 M KCl electrodes. As shown in figure S2 the pore is in the same Teflon cell of etching procedure. The two chambers of the cell were filled with the same electrolyte solution for the symmetric measurements. For asymmetric measurements, the cis side (ground electrode) had the same concentration while the concentration varied on the trans side (working electrode). For conical nanopore, tip side is always with cis side. Current traces were recorded as a function of time from 1 V to -1 V by steps of 100 mV during 2 s each and from 100 mV to -100 mV by steps of 10 mV during 2 s each.

The current and voltage measurement for multipore membrane were performed by an electrometer (Kethley 610) and a multimeter (Agilent 34410A) with Ag/AgCl electrodes. The unitary membrane is measured in the same Teflon cell as single pore while stacked membranes are mounted in a Plexiglas cell. The solution flow is driven by peristaltic pump mimipuls 3 (Gilson)

Results and discussions

Single nanopore design and characterization

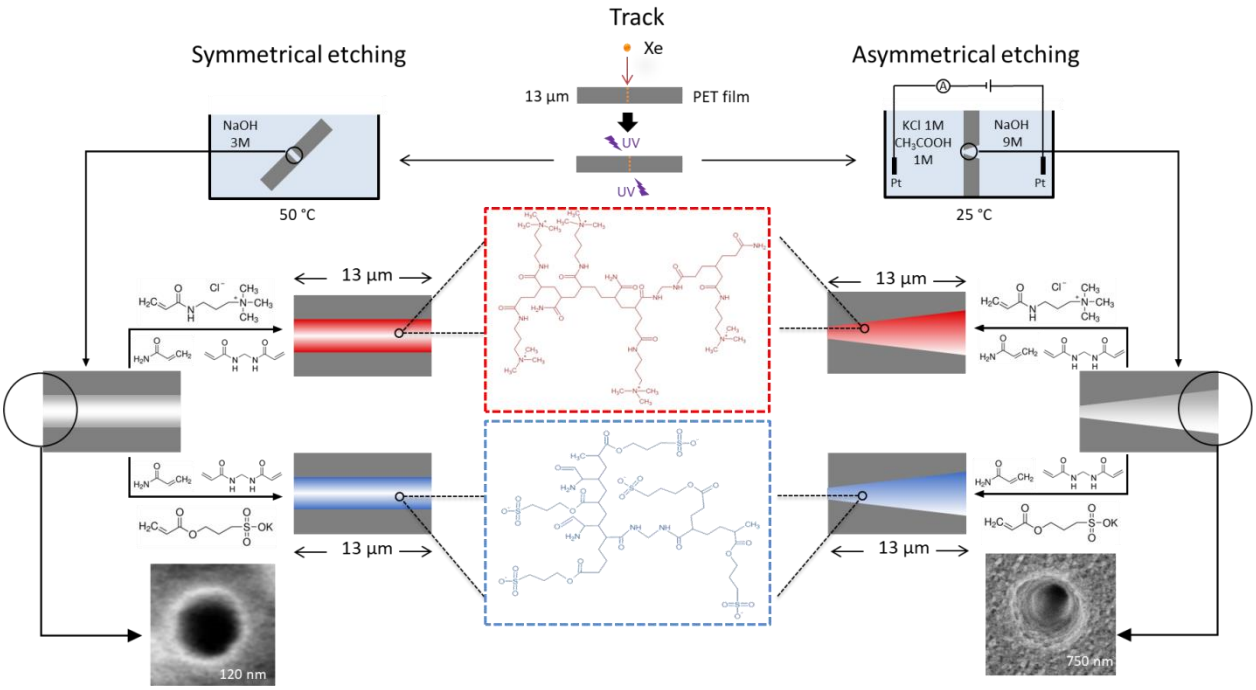

Fig. 1 Schematic representation of cylindrical and conical track-etched nanoporefabrication and functionalization by polyacrylamide hydrogels.

For nanopore functionalization with anionic or cationic polyacrylamide hydrogel, the gelation procedure inside the pore was carried out by adding the precursor solution and catalyst directly at both sides of nanopores. As showed in figure 1, for cationic hydrogel, a quaternary ammonium containing molecule APTAC is polymerized with acrylamide and cross-linked with BIS, while for anionic hydrogel, a sulfonic acid terminated molecule SPAK is used for negative charges. The reactions were let during whole night well protected from air which can destroy the polymerization.

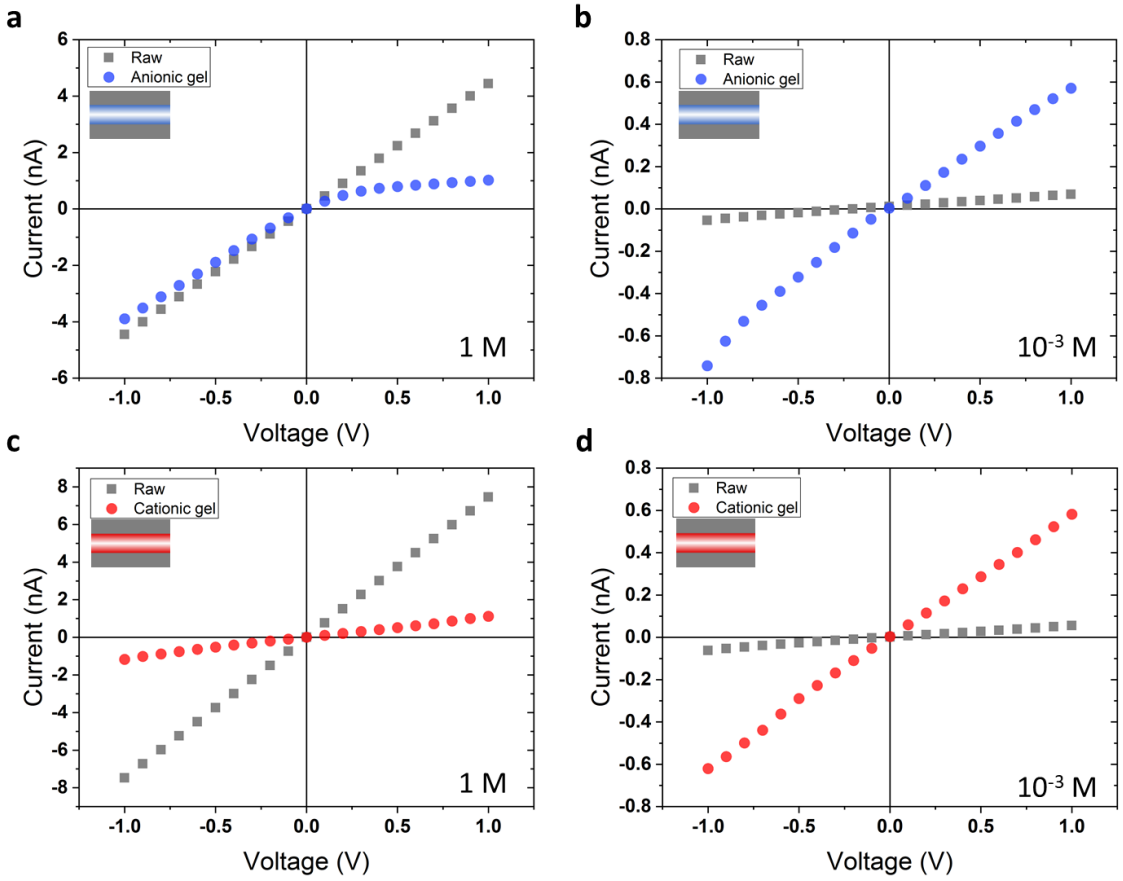

Fig. 2 I-V curves of single cylindrical nanopore (diameter D = 92 nm) before (raw) and after being filled by anionic polyacrylamide hydrogel (a) measured in 1M NaCl solution pH 7.0 (b) measured in 10^{-3} M NaCl solution pH 7.0. I-V curves of single cylindrical nanopore (diameter *D* = 101 nm) before (raw) and after being filled by cationic polyacrylamide hydrogel (c) measured in 1M NaCl solution pH 7.0 (d) measured in 10^{-3} M NaCl solution pH 7.0.

First of all, we have to prove that our protocol to synthetize the gel inside the nanopore works. To do so, current–voltage (I–V) measurements were performed before and after filling gels to show the changes of ionic transport properties for each single nanopore. For cylindrical nanopores, the experiments were first performed with NaCl solution at high concentration (1 M). After gel addition, the I-V curve (figure 2, a and c) show a decrease of slope which means a decrease of electrical conductance. In the case of nanopore with a diameter about 100 nm at 1 M of NaCl, the Debye distance is negligible. Thus the conductance can be assimilating to the bulk solution. So the decrease of conductance can be assigned to a reduction of the pore volume which is occupied by polymer chain of the gel. For the pore with anionic gel (figure 2 a), additionally to a decrease of conductance, we

observe a rectification lower than 1 which means that the nanopore is selective to cation as conical one. Conversely to 1 M, the I-V curve slope measured at low NaCl concentration (10^{-3} M) increase a lot after filling with gel. This can be assigned to the presence of a large amount of counter-ions inside the pore which shield the polymer charge, these evidences confirm that the pores is filled with gel functions.

For conical nanopore (figure S1), the rectification is observed for both two gel functionalized nanopore at high concentration as shown in figure S1. The pore with anionic gel is selective to cations with a rectification factor ($R_f = |I_{+1V}/I_{-1V}|$) smaller than 1. On the contrary the cationic gel is selective to anion and thus the R_f higher than 1. In dilute solution, cationic gel conical pore has always a high rectification because of the highly charged gel at the entrance of the tip side and anionic pore shows a high conductance which confirms the large amount of counter-ions for another time.

Ionic transport properties

To better investigate the effect of gel on the nanopore charges, we investigate the conductance for a series of NaCl concentration from 10^{-4} M to 1 M (figure 3). For functionalized nanopores with anionic and cationic gel, we can find a cross between conductance-concentration curves before and after gel addition. At low salt concentration the counter ions that ensure the nanopore electroneutrality drive the conductance. With the increase of salt concentration the steric effect becomes dominant and the conductance with gel is lower than the one without gel. For the positive charged pore, the ionic conductance slightly changes from 10^{-4} M to 1 M compared with the pore without gel. This suggests that the gel makes the nanopore highly charged due to a dense framework. In this case, the ionic transport is strongly dominated by counter ions rather than bulk solution. For anionic pore, we synthesized the gels with different amounts of crosslinker ($R_3 > R_2 > R_1$). We can observe at low salt concentration a higher conductance with the increase of crosslink degree (figure 3, b). In this case, the gel becomes denser increasing the concentration of counter ion. For the conical nanopore (figure S2), cationic gel has the same effect as in cylindrical one. The ionic conductance raises a lot at low salt concentration with the presence of charges and decrease at high concentration due to the steric effect.

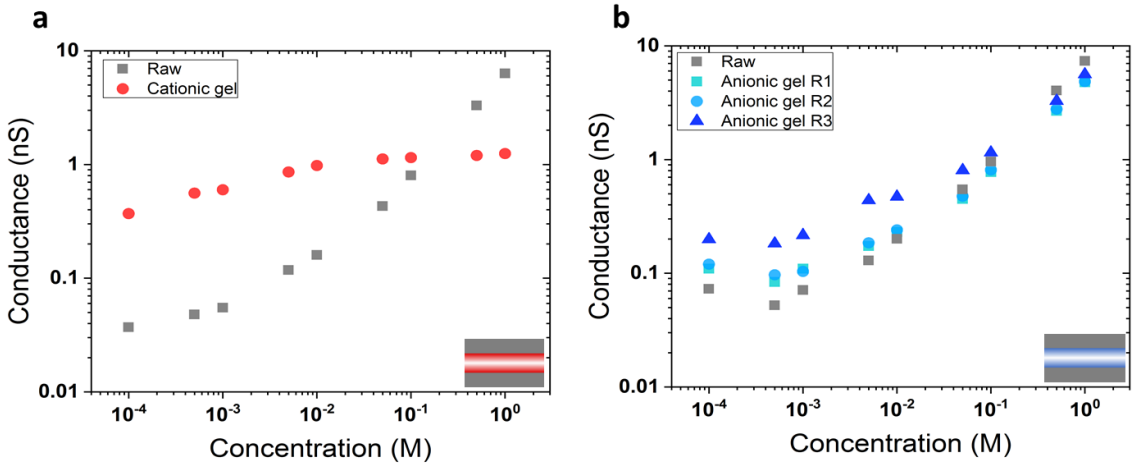

Fig. 3 Conductance of cylindrical nanopore (a) with cationic gel (D = 101 nm) and (b) with anionic gel (BIS concentration $R_3 > R_2 > R_1$) according to salt concentration (D_{R1} = 95 nm, D_{R2} = 92 nm, D_{R3} = 92 nm.).

With the high charge density inside the pore and a conductivity driven by the counter ion, the nanopore should be highly selective especially with the conical shape. The first indication of that comes from the property of ionic current rectification characterized by the rectification factor (R_f). Figure 4 shows the rectification factors varying with NaCl concentrations for cylindrical and conical pores filled with cationic and anionic gel. For the cylindrical pore filled with cationic gel (figure 4, a), the R_f closed to 1 regardless of the electrolytes concentration with and without gel. This means that even if the gel charges governed ionic transport regime, ionic accumulation and depletion do not occurs inside the membrane. On the contrary, the anionic gel induces an ionic current rectification. The R_f lower than 1 between 10^{-3} M and 1 M show a selectivity to cation that is consistent with the negative charge of the gel. We observe also that with a higher crosslink degree R_f value decrease. This means that when the gel is more dense and thus the nanopore more charged the ionic rectification factor is closer than 1. This agrees the behavior observe for the nanopore functionalized with cationic gel. The origin of current rectification is not well elucidated. However one assumption can be expressed. An inhomogeneity of gel distribution along the nanopore could create some ion depletion zone inducing rectification behavior.

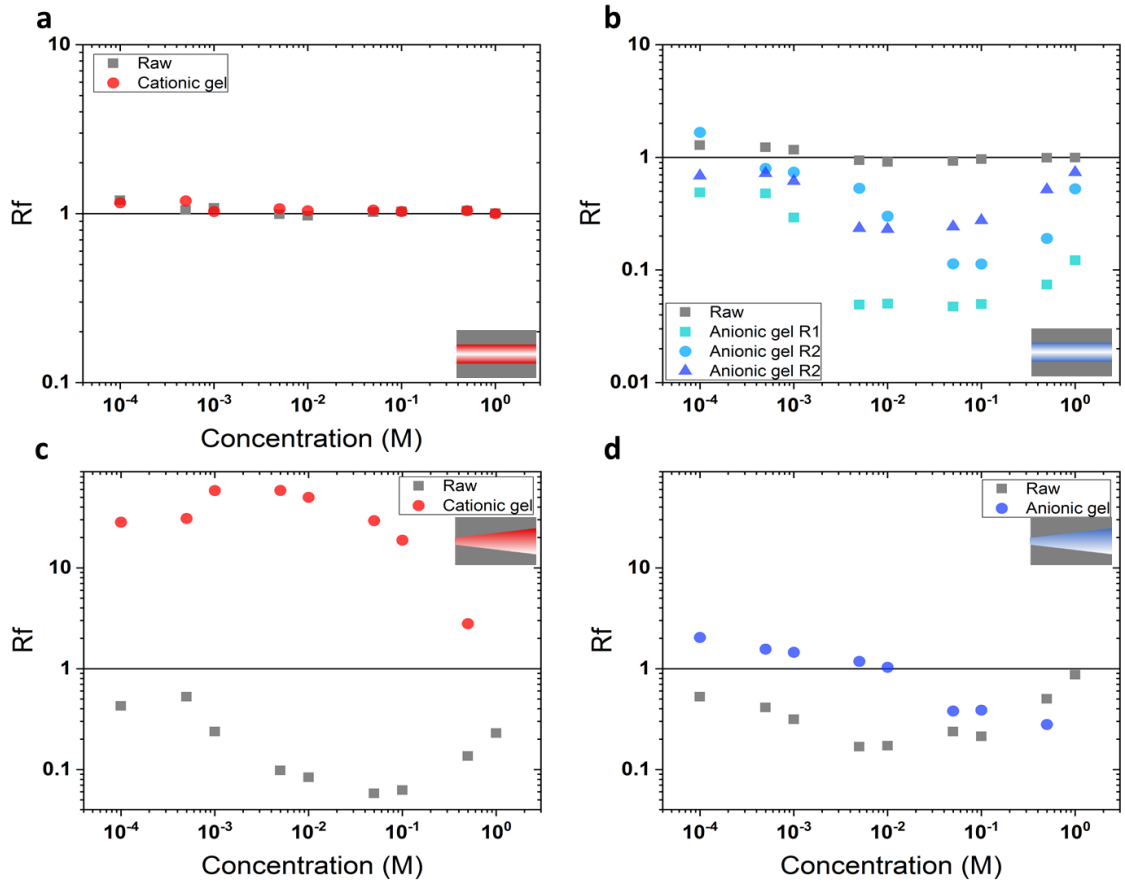

Fig. 4 Rectification of cylindrical nanopore with (a) cationic gel (D = 101 nm) (b) anionic gel (D_{R1} = 95 nm, D_{R2} = 92 nm, D_{R3} = 92 nm.), of conical nanopore with (c) cationic gel (d = 79 nm, D = 497 nm) (d) anionic (d = 70 nm, D = 412 nm) gel in terms of salt concentration, with C_{max}/C_{min} = 1000.

For the conical nanopore, a very distinct R_f change is observed after functionalization with cationic gel (figure 4, c). With the conical geometry, ionic depletion occurs near the positive charge dominated membrane which involves high selectivity to anion. While with anionic gel, rectification behavior takes place only at high concentration selective to cations. At low concentration, a high ionic conductance reduces impact of the ionic accumulation and ionic depletion, thus the rectification becomes negligible.

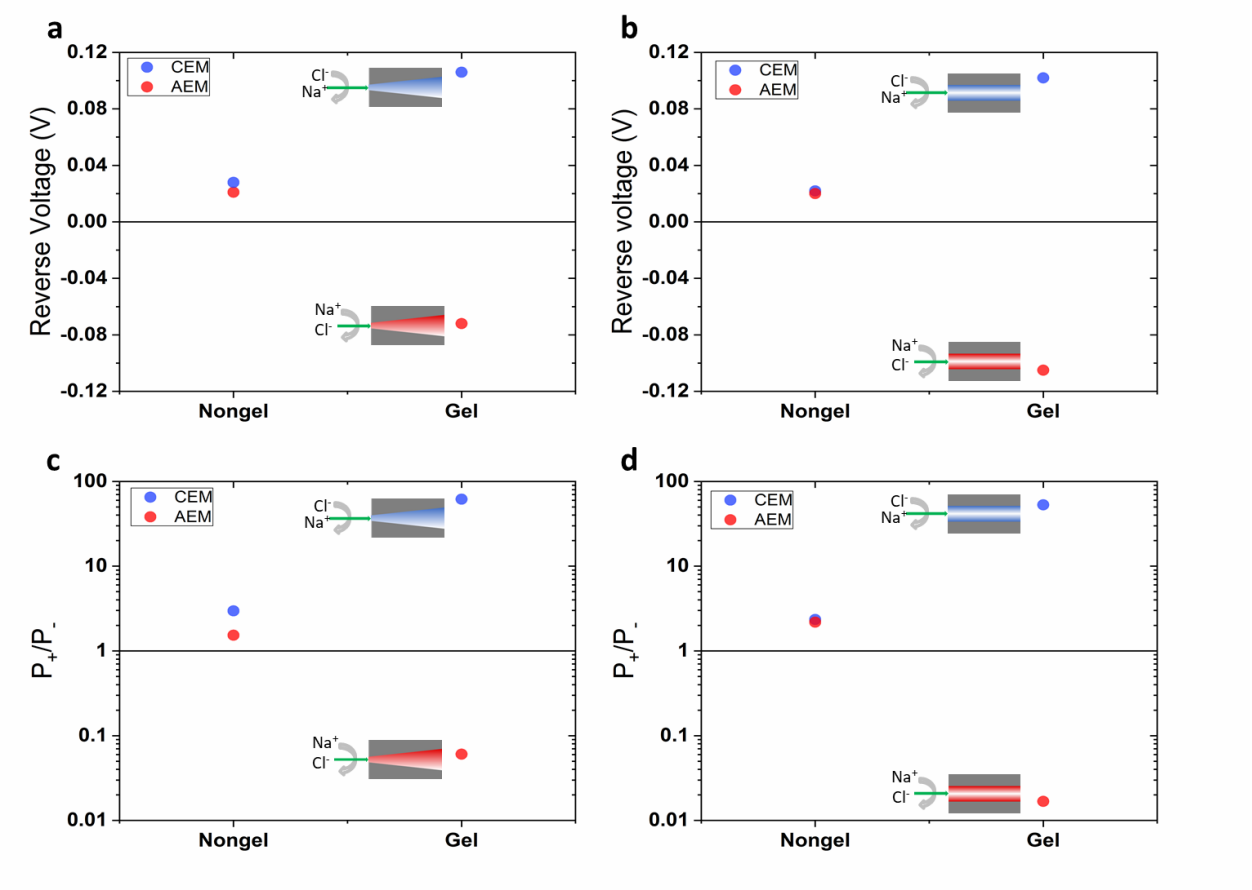

Fig. 5 Reverse voltage generated by gel functionalization in (a) conical nanopore (b) cylindrical nanopore and ionic selectivity corresponding in (c) conical nanopore (d) cylindrical nanopore, with C_{max}/C_{min} = 1000. Cylindrical pore $D_{anionic}$ = 92 nm, $D_{cationic}$ = 101 nm, conical anionic d = 70 nm, D = 412 nm and conical cationic d = 79 nm, D = 497 nm.

The nanopore selectivity can be directly obtained from the reverse voltage under transmembrane concentration gradient. To do so a NaCl solution of 1 M at pH 7.0 and a NaCl solution of 10^{-3} M at pH 7.0 are added in each side of the cell, for cylindrical nanopores. For conical nanopores, the high concentration is placed on the tip side; and the low one to the base side. From the I-V curves, we can directly get the intercepts on the current and voltage axes which present short-circuit current (I_{SC}) and open-circuit voltage (V_{OC}). The V_{OC} has two contributions: one is from the osmotic diffusion effect and the other one is from redox Nernst potential on the electrodes. For all results showed here, this second term is subtracted by using $V_{rev} = V_{oc} - E_{redox}$.

Figure 5, a and b show the reversal voltage measured for nanopore filled with gels. From this value, we calculate the corresponding ionic selectivity calculated via the Goldman–Hodgkin–Katz voltage equation[283]:

$$V_{rev} = \frac{k_B T}{e} \ln\left(\frac{P_{Na^+}/P_{Cl^-} \times C_{high} + C_{low}}{P_{Na^+}/P_{Cl^-} \times C_{low} + C_{high}}\right) \quad (2)$$

where P_{Na^+}/P_{Cl^-} is the selectivity, C_{high} and C_{low} are the electrolytes concentrations, k_B is the Boltzmann constant, T is the solution temperature and e is the electron charge.

As the non-functionalized PET nanopore has –COOH groups on the inner surface wall, at pH 7.0 the surface has negative charged. This gives to the nanopore a cationic selectivity confirmed by the reversal voltage at around 0.02 – 0.03 V. After filling with anionic hydrogels, the nanopore charges increase, so a significant higher reverse voltage is obtained up to 0.10 V which also present a cation selectivity about 50-70. Meanwhile, with cationic gel, the nanopore gets inversed selectivity characterized by a negative reversal voltage. In this case the anions can be much easier to pass through the nanopore). It is interesting to notice that the ratios P_{Na^+}/P_{Cl^-} are close for the conical and the cylindrical nanopore. This result was totally unexpected, however, it is relatively consistent with the fact that the ionic transport though the nanopore is governed by the gel. In this case, the effect of geometry on the conductance and the selectivity seem shield.

Energy generated from single nanopore

The energy conversion performance is also investigated by applying a transmembrane concentration gradient under salinity gradient of C_{max}/C_{min} = 1000.

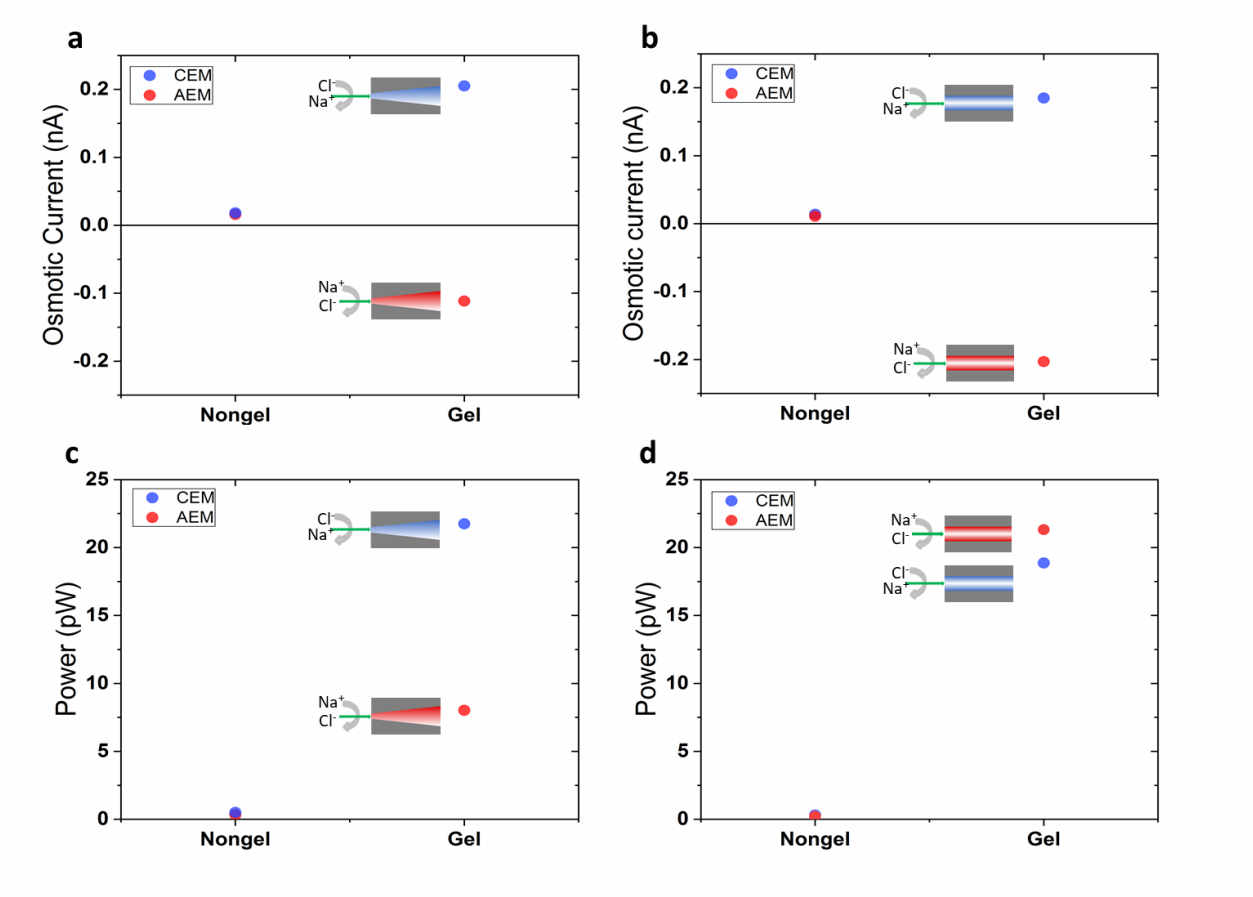

Fig. 6 Osmotic current generated by gel functionalization in (a) conical nanopore (b) cylindrical nanopore, and single pore power corresponding in (c) conical nanopore (d) cylindrical nanopore. C_{max}/C_{min} = 1000. Cylindrical pore $D_{anionic}$ = 92 nm, $D_{cationic}$ = 101 nm, conical anionic d = 70 nm, D = 412 nm and conical cationic d = 89 nm, D =497 nm.

The osmotic currents (I_{oms}) are calculated using $I_{osm}=I_{mes}$ - $G\times E_{redox}$, where I_{mes} is the intercepts on the current axes which present short-circuit current (I_{SC}).Like reversal potentials, the raw PET pore has a small osmotic current due to the presence of –COO- groups at pH 7.0 (figure 6). After filling with gel, we observe a huge increase of osmotic current from about 10 pA up to about +/-200 pA. Together with the reversal potential, we calculate the power generated with a single nanopore. The single pore power is obtained at around 20 pW regardless of the pore shape or gel charge. It is competitive compared with other single nanopores such as boron nitride nanotube (20 pW)[158] and monolayer molybdenum disulfide (500 pW)[150].

Energy generated from multipore membranes and membranes stacks

To go further on harvesting of osmotic energy, the gel inclusion process was implemented on multipore membranes (Figure 7). First, the experiments were carried out on membranes with low pore density (5.10^5 pores cm^{-2}). The same track-etching procedure is adopted for multipore membrane fabrication. The membrane thickness is always 13 µm . Two geometries are tested to compare their performance. Cylindrical membrane has a pore size of 156 nm ± 22 nm and 172 nm ± 29 nm for each side while conical nanopore has a pore size of 753 nm ± 42 nm for base side and 77 nm ± 11 nm for tip side. The transmembrane voltage under per multipore membrane equals to 0.1 V as the same of the single nanopore. The membrane surface measured here is 0.28 cm2. For anionic cylindrical and conical membranes, the current density is measured as 0.29 A m^{-2} and 0.23 A m^{-2}. Multiplied by voltage, we get a power density as 0.03 W m^{-2} and 0.02 W m^{-2}. If we calculate the theoretical power density based on the values of single nanopore (20 pW $pore^{-1}$), we can get it as 0.1 W m^{-2}. It has an obvious loss on power density for multipore membrane.

With stack of four membranes the transmembrane voltage generated by the difference of salinity are summed to reach about 0.4 V. Another time we get quite similar results between cylindrical and conical pores as cylindrical membranes get 0.41 V and 0.86 µA while conical membranes get 0.81 µA. This result confirms again that the ionic transport is governed by gel charges rather than the nanopore geometry. According to that the cylindrical pore can be used as conical one to generate osmotic current. The interest of cylindrical pore is the possibility to fabricate membranes with higher pore densities. By using the membrane surface as 0.28 cm^2 of each cell, the power density is calculated as 0.01 W m^{-2}. By stacking membranes, global power density decreases almost two third because of the high resistance which comes from the long distance between two cells and the low concentration at 10^{-3} M.

The same procedure was used to design membrane with a pore density of 3.10^9 cm^{-2} of cylindrical nanopore. By stacking 4 membranes, the voltage stays at 0.39 V and the current reach at 107 µA so the total power is obtained as 37.7 µW (each membrane surface 0.28 cm^2). The power density is calculated as 0.37 W m^{-2}. From 2.10^5 to 3.10^9 the pore density becomes 15000 times larger while the current increases only 51 times. With this high pore density, the tracks can be crossed and the pore shapes can be non-regular, so when the pore density becomes large enough, there will not be a linear relation between the pore density and the current density. However this can be improved using a low fluency coupled with a

large number of ion beam passage to perform track. In addition, one limit of our stack is the distance inter-membrane of 1 cm that involves a very large resistance decreasing the performance.

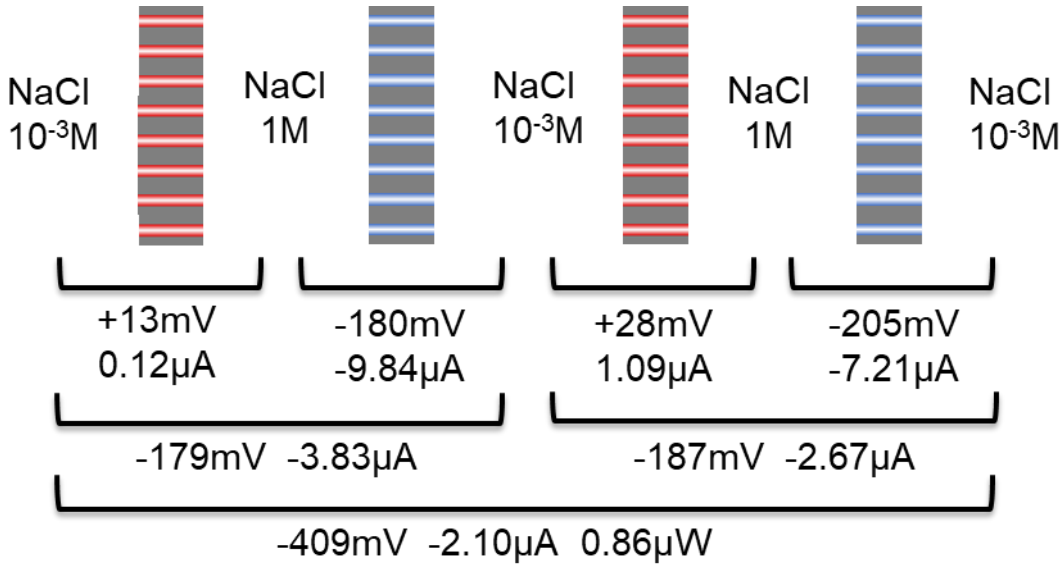

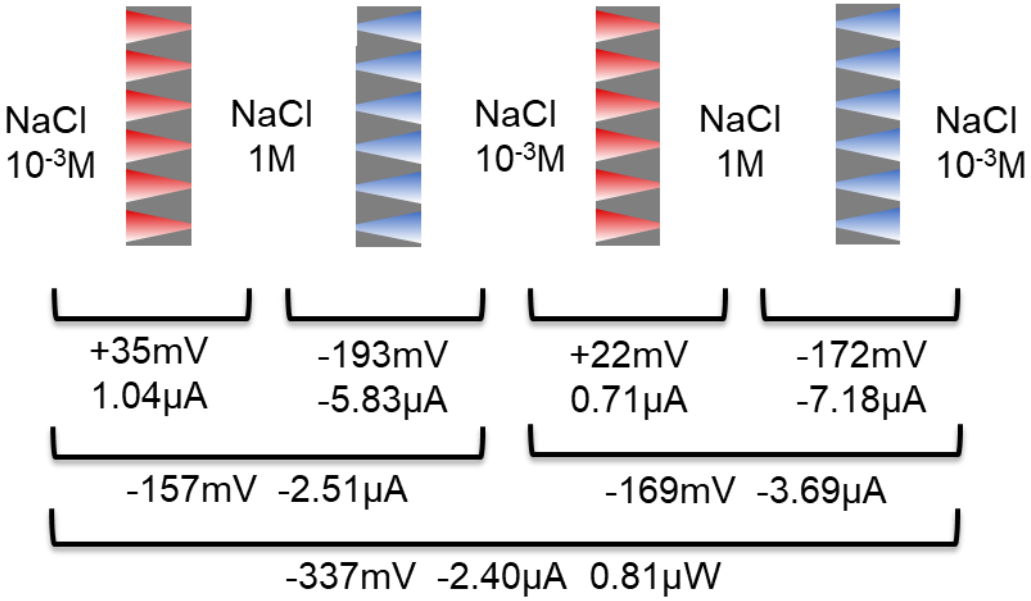

Fig. 7 Voltage and current measured across the functionalized multipore membranes with a pore density of 2.10^5 cm^{-2}. Membrane thickness = 13µm.

Conclusions

In summary, in this work we demonstrate the use of a track etched polymer nanopore membrane for harvesting the osmotic energy. The nanopores were functionalized by filling with highly charged hydrogels. The ionic transport properties investigate at single nanopore scale show that it is governed essentially by the gel charge shielding the effect of geometry. Because the performance of energy conversion is almost independent of the nanopore shape, the cylindrical geometry is proved as a good candidate for high pore density membranes. The functionalized nanopores show high ionic selectivity and good energy conversion ability with a power density of about 0.37 W m^{-2} working in pH 7. By improving the direction of tracks and the inter membrane distances we could improve the energy yield and thus consider such membrane for real application.

References

1. Chu, S. & Majumdar, A. Opportunities and challenges for a sustainable energy future. Nature 488, 294–303 (2012).

2. Stocker, T. F. et al. Climate change 2013 the physical science basis: Working Group I contribution to the fifth assessment report of the intergovernmental panel on climate change. Climate Change 2013 the Physical Science Basis: Working Group I Contribution to the Fifth Assessment Report of the Intergovernmental Panel on Climate Change 9781107057, (2013).

3. Roemmich, D. et al. Unabated planetary warming and its ocean structure since 2006. Nat. Clim. Chang. 5, 240–245 (2015).

4. Fargione, J., Hill, J., Tilman, D., Polasky, S. & Hawthorne, P. Land clearing and the biofuel carbon debt. Science (80-.). (2008). doi:10.1126/science.1152747

5. Lewis, N. S. Research opportunities to advance solar energy utilization. Science (2016). doi:10.1126/science.aad1920

6. Joselin Herbert, G. M., Iniyan, S., Sreevalsan, E. & Rajapandian, S. A review of wind energy technologies. Renewable and Sustainable Energy Reviews (2007). doi:10.1016/j.rser.2005.08.004

7. Bertani, R. Geothermal power generation in the world 2010-2014 update report. Geothermics (2016). doi:10.1016/j.geothermics.2015.11.003

8. Logan, B. E. & Elimelech, M. Membrane-based processes for sustainable power generation using water. Nature (2012). doi:10.1038/nature11477

9. Siria, A., Bocquet, M.-L. & Bocquet, L. New avenues for the large-scale harvesting of blue energy. Nat. Rev. Chem. (2017). doi:10.1038/s41570-017-0091

10. Ramon, G. Z., Feinberg, B. J. & Hoek, E. M. V. Membrane-based production of salinity-gradient power. Energy and Environmental Science (2011). doi:10.1039/c1ee01913a

11. Post, J. W. et al. Salinity-gradient power: Evaluation of pressure-retarded osmosis and reverse electrodialysis. J. Memb. Sci. (2007). doi:10.1016/j.memsci.2006.11.018

12. She, Q., Jin, X. & Tang, C. Y. Osmotic power production from salinity gradient resource by pressure retarded osmosis: Effects of operating conditions and reverse solute diffusion. J. Memb. Sci. (2012). doi:10.1016/j.memsci.2012.02.014

13. Achilli, A., Cath, T. Y. & Childress, A. E. Power generation with pressure retarded osmosis: An experimental and theoretical investigation. J. Memb. Sci. (2009). doi:10.1016/j.memsci.2009.07.006

14. Post, J. W., Hamelers, H. V. M. & Buisman, C. J. N. Energy recovery from controlled mixing salt and fresh water with a reverse electrodialysis system. Environ. Sci. Technol. (2008). doi:10.1021/es8004317

15. Tedesco, M., Cipollina, A., Tamburini, A. & Micale, G. Towards 1 kW power production in a reverse electrodialysis pilot plant with saline waters and concentrated brines. J. Memb. Sci. (2017). doi:10.1016/j.memsci.2016.09.015

16. Veerman, J., Saakes, M., Metz, S. J. & Harmsen, G. J. Electrical power from sea and river water by reverse electrodialysis: A first step from the laboratory to a real power plant. Environ. Sci. Technol. 44, 9207–9212 (2010).

17. Siria, A. et al. Giant osmotic energy conversion measured in a single transmembrane boron nitride nanotube. Nature 494, 455–458 (2013).

18. Feng, J. et al. Single-layer MoS2nanopores as nanopower generators. Nature 536, 197–200 (2016).

19. Ji, J. et al. Osmotic Power Generation with Positively and Negatively Charged 2D Nanofluidic Membrane Pairs. Adv. Funct. Mater. 27, (2017).

20. Secchi, E. et al. Massive radius-dependent flow slippage in carbon nanotubes. Nature (2016). doi:10.1038/nature19315

21. Vlassiouk, I. & Siwy, Z. S. Nanofluidic diode. Nano Lett. 7, 552–556 (2007).

22. Siwy, Z. S. Ion-current rectification in nanopores and nanotubes with broken symmetry. Adv. Funct. Mater. 16, 735–746 (2006).

23. Ma, T. et al. Impact of Polyelectrolyte Multilayers on the Ionic Current Rectification of Conical Nanopores. Langmuir 34, 3405–3412 (2018).

24. Gao, J. et al. High-performance ionic diode membrane for salinity gradient power generation. J. Am. Chem. Soc. 136, 12265–12272 (2014).

25. Zhang, Z. et al. Ultrathin and Ion-Selective Janus Membranes for High-Performance Osmotic Energy Conversion. J. Am. Chem. Soc. 139, 8905–8914 (2017).

26. Zhang, Z. et al. Engineered Asymmetric Heterogeneous Membrane: A Concentration-Gradient-Driven Energy Harvesting Device. J. Am. Chem. Soc. 137, 14765–14772 (2015).

27. Lepoitevin, M., Ma, T., Bechelany, M., Janot, J. M. & Balme, S. Functionalization of single solid state nanopores to mimic biological ion channels: A review. Advances in Colloid and Interface Science 250, 195–213 (2017).

28. Ali, M., Schiedt, B., Healy, K., Neumann, R. & Ensinger, W. Modifying the surface charge of single track-etched conical nanopores in polyimide. Nanotechnology 19, (2008).

29. Apel, P. Y., Ramirez, P., Blonskaya, I. V., Orelovitch, O. L. & Sartowska, B. A. Accurate characterization of single track-etched, conical nanopores. Phys. Chem. Chem. Phys. 16, 15214–15223 (2014).

30. Siwy, Z. et al. Ion transport through asymmetric nanopores prepared by ion track etching. in Nuclear Instruments and Methods in Physics Research, Section B: Beam Interactions with Materials and Atoms 208, 143–148 (2003).

31. Siwy, Z. & Fuliński, A. Fabrication of a Synthetic Nanopore Ion Pump. Phys. Rev. Lett. 89, (2002).

32. Giamblanco, N. et al. Amyloid Growth, Inhibition, and Real-Time Enzymatic Degradation Revealed with Single Conical Nanopore. Anal. Chem. 90, 12900–12908 (2018).

33. Lepoitevin, M. et al. Fast and reversible functionalization of a single nanopore based on layer-by-layer polyelectrolyte self-assembly for tuning current rectification and designing sensors. RSC Adv. 6, 32228–32233 (2016).

34. Lepoitevin, M. et al. Combining a sensor and a pH-gated nanopore based on an avidin-biotin system. Chem. Commun. 51, 5994–5997 (2015).

35. Hou, X. et al. A biomimetic asymmetric responsive single nanochannel. J. Am. Chem. Soc. 132, 11736–11742 (2010).

36. Cabello-Aguilar, S. et al. Slow translocation of polynucleotides and their discrimination by α-hemolysin inside a single track-etched nanopore designed by atomic layer deposition. Nanoscale 5, 9582–9586 (2013).

37. Zhao, Y., Janot, J. M., Balanzat, E. & Balme, S. Mimicking pH-Gated Ionic Channels by Polyelectrolyte Complex Confinement Inside a Single Nanopore. Langmuir 33, 3484–3490 (2017).

38. Tomicki, F., Krix, D., Nienhaus, H. & Ulbricht, M. Stimuli-responsive track-etched membranes via surface-initiated controlled radical polymerization: Influence of grafting density and pore size. J. Memb. Sci. 377, 124–133 (2011).

39. Zhang, Z. et al. Asymmetric Multifunctional Heterogeneous Membranes for pH- and Temperature-Cooperative Smart Ion Transport Modulation. Adv. Mater. 28, 9613–9619 (2016).

40. Ma, T. et al. Combining Light-Gated and pH-Responsive Nanopore Based on PEG-Spiropyran Functionalization. Adv. Mater. Interfaces 5, (2018).

41. Balme, S., Ma, T., Balanzat, E. & Janot, J. M. Large osmotic energy harvesting from functionalized conical nanopore suitable for membrane applications. J. Memb. Sci. 544, 18–24 (2017).

42. Schroeder, T. B. H. et al. An electric-eel-inspired soft power source from stacked hydrogels. Nature 552, 214–218 (2017).

43. Rollings, R. C., Kuan, A. T. & Golovchenko, J. A. Ion selectivity of graphene nanopores. Nat. Commun. 7, (2016).

44. Guerrini, M. et al. Orthogonal analytical approaches to detect potential contaminants in heparin. Proc. Natl. Acad. Sci. 106, 16956–16961 (2009).

45. Sasisekharan, R. & Shriver, Z. From crisis to opportunity: A perspective on the heparin crisis. Thromb. Haemost. 102, 854–858 (2009).

46. Beni, S., Limtiaco, J. F. K. & Larive, C. K. Analysis and characterization of heparin impurities. Anal. Bioanal. Chem. 399, 527–539 (2011).

47. Liu, Z. et al. Mass balance analysis of contaminated heparin product. Anal. Biochem. 408, 147–156 (2011).

48. Kalita, M. et al. A nanosensor for ultrasensitive detection of oversulfated chondroitin sulfate contaminant in heparin. J. Am. Chem. Soc. 136, 554–557 (2014).

49. Ding, Y., Shi, L. & Wei, H. A ‘turn on’ fluorescent probe for heparin and its oversulfated chondroitin sulfate contaminant. Chem. Sci. 6, 6361–6366 (2015).

50. Wang, Y. J. et al. Selective, switchable fluorescent probe for heparin based on aggregation-induced emission. Anal. Biochem. 514, 48–54 (2016).

51. Hu, Y., Guo, W., Ding, Y., Cheng, H. & Wei, H. Modulating luminescence of Tb3+with biomolecules for sensing heparin and its contaminant OSCS. Biosens. Bioelectron. 86, 858–863 (2016).

52. Kasianowicz, J. J., Brandin, E., Branton, D. & Deamer, D. W. Characterization of individual polynucleotide molecules using a membrane channel. Proc. Natl. Acad. Sci. U. S. A. 93, 13770–3 (1996).

53. Dekker, C., Article, R. & Dekker, C. Solid-state nanopores. Nat. Nanotechnol. 2, 209–215 (2007).

54. Karawdeniya, B. I., Bandara, Y. M. N. D. Y., Nichols, J. W., Chevalier, R. B. & Dwyer, J. R. Surveying silicon nitride nanopores for glycomics and heparin quality assurance. Nat. Commun. 9, 1–8 (2018).

55. Roman, J. et al. Solid-state nanopore easy chip integration in a cheap and reusable microfluidic device for ion transport and polymer conformation sensing. ACS Sensors under revision (2018). doi:10.1021/acssensors.8b00700

56. Roman, J. et al. Functionalized Solid-State Nanopore Integrated in a Reusable Microfluidic Device for a Better Stability and Nanoparticle Detection. ACS Appl. Mater. Interfaces acsami.7b14717 (2017). doi:10.1021/acsami.7b14717

57. Giamblanco, N. et al. Sensors and Actuators B : Chemical Detection of protein aggregate morphology through single antifouling nanopore. Sensors Actuators B. Chem. 260, 736–745 (2018).

58. Lepoitevin, M., Bechelany, M., Balanzat, E., Janot, J.-M. & Balme, S. Non-Fluorescence label protein sensing with track-etched nanopore decorated by avidin/biotin system. Electrochim. Acta 211, (2016).

59. Lepoitevin, M., Ma, T., Bechelany, M., Janot, J.-M. & Balme, S. Functionalization of single solid state nanopores to mimic biological ion channels: A review. Adv. Colloid Interface Sci. 250, 195–213 (2017).

60. Ali, M. et al. Label-Free Pyrophosphate Recognition with Functionalized Asymmetric Nanopores. Small 12, 2014–2021 (2016).

61. Ali, M., Nasir, S. & Ensinger, W. Bioconjugation-induced ionic current rectification in aptamer-modified single cylindrical nanopores. Chem. Commun. 51, 3454–3457 (2015).

62. Ali, M., Neumann, R. & Ensinger, W. Sequence-specific recognition of DNA oligomer using peptide nucleic acid (PNA)-modified synthetic ion channels: PNA/DNA hybridization in nanoconfined environment. ACS Nano 4, 7267–7274 (2010).

63. Ali, M., Nguyen, Q. H., Neumann, R. & Ensinger, W. ATP-modulated ionic transport through synthetic nanochannels. Chem. Commun. 46, 6690 (2010).

64. Lepoitevin, M. et al. Fast and reversible functionalization of a single nanopore based on layer-by-layer polyelectrolyte self-assembly for tuning current rectification and designing sensors. RSC Adv. 6, (2016).

65. Lepoitevin, M. et al. Combining a sensor and a pH-gated nanopore based on an avidin-biotin system. Chem. Commun. 51, (2015).

66. Fennouri, A. et al. Kinetics of enzymatic degradation of high molecular weight polysaccharides through a nanopore: Experiments and data-modeling. Anal. Chem. 85, 8488–8492 (2013).

Discussions

This chapter focuses on the track-etched nanopore for application in osmotic energy harvesting. This energy takes advantage from difference of chemical potentials between sea water and river water. It can be collected by membrane processing including pressure retarded osmosis and reversed electrodialysis. In the case of charged porous membranes, the ion transport is dominated by electrical double layer close to the surface. The thickness of this layer depends on the salt concentration. When the membrane is mounted between two reservoirs of different concentrations, a selective diffusio-osmotic ion flow driven by salinity gradient will generate an electron flow if two redox electrodes are immersed in these reservoirs. There are several methods to improve the membrane performance including increasing membrane porosity, increasing surface charge density, decreasing membrane thickness and decreasing membrane resistance. In this chapter, we aimed to improve the ion selective membrane by increasing charge density using polyelectrolytes. This functionalization in track etched nanopore can give it anion or cation selectivity and increases both osmotic current and reversed voltage.

The first work used chitosan (ChS) and poly(acrylic acid) (PAA) in conical nanopores. This functionalization method was performed by layer-by-layer of polyelectrolytes has been studied in the previous chapter. ChS is chosen here because of its non-solublility are pH upper than 6. This property avoids polyelectrolytes swelling in different salt concentrations that reduce the pore conductance as discussed in chapter 2. PAA has a very high density of negative charges, so it is a good candidate to couple with ChS to dope the nanopore with negative surface charge. Conical nanopores have diode-like behaviors due to their asymmetrical geometry. The ion selectivity can enhance the membrane performance. Other than that, compared to symmetrical nanopore, the asymmetric geometry decreases the concentration polarization inside the pore improving the salinity gradient. As ChS has less charge density than PAA, the pore surface has an excess of negative charges after 5 bilayers of deposition. The weak base and acid groups on the polyelectrolytes make this kind on nanopores sensible to pH. The charge density is much higher at pH 10 rather than pH 7.6 or pH 3. Besides of pH, this nanopore is also sensitive to specific metal ions because of the specific chelating effect of ChS to Cu^{2+} and Co^{2+}. The existence of these bivalent cations can be captured by ChS and block the pore leading to a small ion conductance.

The asymmetric measurement of the functionalized nanopore was carried out under salinity gradient. Under 1M NaCl at tip side and 1mM NaCl at base side (C_{tip}/C_{base}=1000), the maximum of extractable power of one single nanopore is obtained as around 20 pW at pH 7.6 and pH 10. This value has the same amplitude of previously reported boron nitride nanotubes which are limited as single nanopore level. The single nanopore can be easily scaled up as the ion fluency can be easily controlled during the track process. The same functionalization was achieved in multipore membranes with a pore density of 2 10^6 cm^{-2}. A power density of 0.1 W m^{-2} was obtained. If we calculate the theoretical power output for a multipore membrane according to power provided by a single pore, the power density should be 0.4 W m^{-2}. This energy lose can be attributed to the uncompleted pore openings and uncompleted pore functionalization. The real power output is relatively high regarding to the low pore density; however, the pore density is limited by the large base side of the conical pore. The pore diameters used in this experiment is around 30 nm. As we know that larger the pore diameter, larger the power density. A higher pore diameter can generate higher osmotic current, but it is limited by the thickness of EDL. As the generation of diffusion-osmotic current is an interfacial phenomenon and happened within the EDL, a larger pore diameter will cause low ion selectivity. These limitations seem to need to be solved with a stereoscopic functionalization in order to create a larger EDL space inside the pore.

Keeping in mind this purpose, the second work focused on 3D hydrogel functionalization in track-etched nanopores. This pore filling functionalization makes it possible for higher pore diameters. So in this work, cylindrical pores of about 100 nm and conical pore of 80 nm at tip and 400 nm to 700 nm at base were utilized. These freshly fabricated membranes were immersed in the solution containing monomers, crosslinkers, precursors and catalyzers so that the polymerization was achieved directly inside the pore. Two hydrogels containing anionic groups and cationic groups are separately synthesized to design cation selective membrane and anion selective membrane. Energy generation measurements show that hydrogel functionalized conical and cylindrical nanopores have similar performance and the power generated under salinity gradient of C_{tip}/C_{base}=1000 is quite close to that of boron nitride nanotubes and ChS/PAA functionalized conical nanopore. This result confirms the essential role of hydrogel functions for osmotic energy generation; moreover the equal

performances of cylindrical and conical pore indicate that the ion selectivity is dominated by high charge density instead of pore geometry. This conclusion gives the possibility of up scaling the hydrogel functionalized track etched membrane with -high pore density. The functionalization was carried out in low pore density membrane of 2 10^5 cm^{-2}. Power density of one membrane is obtained at 0.02 to 0.03 W m^{-2}. This value can be compared with the theoretical power calculated according to pore density and single pore power which is 0.04 W m^{-2}. Like the ChS/PAA functionalized nanopore, an energy lose always presents; but it is clear that energy lose in hydrogel functionalized membrane is less than that of ChS/PAA. This information indicates a higher pore opening rate and functionalization rate with hydrogels because of the larger pore diameter. As in real electricity generation a high voltage is required, so the accumulation of reversed voltage is important. To test this feasibility, two anionic membranes and two cationic membranes were stacked alternatively on series. A global voltage about 0.4 V was obtained as a linear sum of each membrane. However, if we measure the global power density of the stacked 4 membranes, the value is 0.01 W m^{-2} which is smaller than one single membrane. It is essentially because of the long inter-membrane distance where 1 mM NaCl solutions give high resistance in our experimental devices.

As the cylindrical pores and conical pores are confirmed having the same performance, a membrane of very high pore density in cylindrical shape is possible. So two membranes functionalized by both two hydrogels at 3 10^9 pores m^{-2} were stacked on series. A final global power density of 0.37 W m^{-2} was gained. From 2 10^5 to 3 10^9 pore m^{-2}, pore density becomes 15000 times higher while current density increases only 50 times. This non-linear relation should be attributed to the overlap of nanopores at such a high pore density. This result can be then improved by better oriented and distributed tracks in experimental devices with shorter distances.

In this chapter, functionalization of polyelectrolytes from 2D to 3D has been studied to give track-etched membranes higher ion selectivity. The experiments from single nanopore to multipore membranes until stacked membranes show relations along the scaling-up. Such research gives a new strategy to develop ion selective membranes for osmotic energy harvesting even still many aspects remain to be improved such as pore size distribution unifying and entering resistance eliminating.

Chapter 4

Biosensors

Introduction

In this chapter, we take the advantage to conical track-etched nanopore for biosensors using polyelectrolytes/biomacromolecules functionalization. The two methods of nanopores sensing were used: ion current rectification and resistive pulse have been served to detect biomolecules.

Oversulfated chondroitin sulfate (OSCS) is a contaminant found in heparin samples 10 years ago. It caused hundreds of death in US. Its simple detection has been still a problem to ensure the security of heparins because of their similar chemical structures. By analysing the ion current rectification changes, a nanopore functionalized with poly-L-lysine (PLL) allows to quantitatively detect oversulfated chondroitin sulfate (OSCS) from the inhibition of heparinase. It also allows quantifying the heparin degradation with the time. This simple, low-cost and stable biosensor filled in the blank of OSCS detection with a good detection sensitivity and low global cost.

Resistive pulse techniques based on Coulter counter principles were also investigated for single hyaluronic acid (HA) molecule detection. In a long conical nanopore, the translocation behavior of large HA molecules of more than 10^6 Da have been investigated thank to the blob models as well as the de Gennes' scaling principles and following researchers. By grafting hyaluronidases in base side of nanopore, the enzymes did not lose their activity that allows real time analyzing the degradation products. More interestingly, by immobilizing hyaluronidases in tip side of nanopore with a diameter of several nanometers, the duration of intermediate complexion substrate-enzyme was measured for the first time inside a nanopore.

The results presented in this chapter have been published as two articles:

Conical track-etched Nanopore for a free-label detection of OSCS contaminants in heparin. Biosens. Bioelectron.137, 2019, 207-212

Dynamics of Long Hyaluronic Acid Chains through Conical Nanochannel for Characterizing Enzyme Reactions in Confined Space, submitted.

Articles

Single conical track-etched Nanopore for a free-label detection of OSCS contaminants in heparin

Tianji Ma, Emmanuel Balanzat, Jean-Marc Janot, Sébastien Balme

Contribution: I design the work with Sebastien Balme. I, did the experiments, the data analysis and the figures. I also participated to write the paper..

Introduction

Heparin (HEP) is a commonly used anticoagulant to treat several clotting disorders. 10 years ago, a sanitary problem from contamination of oversulfated chondroitin (OSCS) has caused the death of about 200 patients around the world[284,285]. Since this event, an effort was made to detect small amount of OSCS from heparin mixture that is not easy due to their close structures[286]. To this end, the classical methods based on chromatography were the first considered. However they are limited to a detection limit around 0.3 % in weight and required expensive instruments such as mass spectrometer or NMR to identify the OSCS[287]. More recently, the fluorescence based sensors allow to improve the detection limit until from 10^{-2} % until 10^{-9} % weight[288]. The OSCS detection is usually indirect since they used ability to inhibit the HEP degradation by Heparinase. Despite their low detection limits, the major weakness of these fluorescence sensors is that they require fluorescent probe[289,290], nanoparticle[288] and/or biomolecule[291] engineering for the specific detection of heparin as well as fluorescence spectrometer microscope equipment. Thus provide a simple and cheap technology to detect OSCS from HEP sample is still highly challenging.

The single nanopore is versatile method for macromolecule sensing that emerged last two decades[114,131]. Using the resistive pulse technique through solid-state nanopore, a sample of HEP contaminated by OSCS can be identified[292]. However, the concentration cannot be obtained by this way. In addition, the major problems of solid-state nanopore are the short lifetime and the low success rate of experiments which limit the real application, despite recent improvement by PEG functionalization[6,293,294]. The conical track-etched nanopore is a good alternative to design label-free sensor based on the modulation of ionic current rectification (ICR)[245,295]. Based on that, small molecules as well as protein can be specifically

detected by a ligand/receptor systems[239,296–298]. However, these sensors are often one-off especially when the ligand binding is not totally reversible. Recently, we have shown that the reversible functionalization with poly-L-lysine (PLL) could be promised for biosensing applications[299]. Another, advantage to use polyelectrolytes (PE) inside nanopore is that the layer-by-layer deposition can be monitored and the kinetic depends on their properties (size and charge) [269]. Following our previous investigations in this field, we propose here to design a reusable sensor for OSCS contained in a HEP sample. Our strategy is based on (i) the reversibility of PLL/HEP functionalization of a conical nanopore and (ii) the degradation of the HEP by heparinase which is inhibited by the OSCS. Here, we assume that action of enzyme will decrease the affinity between degraded HEP and the PLL. This would impact the nanopore surface charge and thus the ICR.

In order to prove the concept that conical nanopore could be a suitable alternative to detect the HEP contamination by OSCS, we present our work in several following step. First, we will demonstrate the reversibility of the PLL/HEP deposition as well as their impact on the IRC. Then, we will evaluate the impact of the HEP concentration on the IRC in order to evidence a dose-response curve. The OSCS contained in HEP solution will be detected using heparinase. Thus, we will follow the kinetic of degradation of HEP by heparinase by nanopore and compared the result with classical methods. Then, using this strategy, we will study the relationship OSCS concentration ICR to establish the dose-response dependence. The last sections will be dedicated to discuss the reproducibility of sensing experiments and the nanopore sensor lifetime. This last step will aim to validate our sensor.

Material and methods

Materials

Poly(ethylene terephthalate) (PET) film (thickness 13 µm, biaxial orientation) was purchased from Goodfellow (ES301061). Sodium chloride (71380), potassium chloride (P3911), sodium hydroxide (30603), hydrogen chloride (30721), trizma hydrochloride (T3253), CAPS (C2632), sodium acetate (W302406), ethylenediaminetetraacetic acid (EDTA) (E5513), Poly-L-lysine hydrobromide (PLL) (30 kD-70kD P2636), Heparin sodium salt from porcine intestinal mucosa (HEPep) (H4784), Heparinase I and III Blend from Flavobacterium heparinum (H3917), Heparinase II from Flavobacterium heparinum (H6512) were purchased from Sigma-Aldrich.

Over Sulfated Chondroitin Sulfate (OSCS) Standard (3125401) was purchased from SERVA. Ultra-pure water was produced from a Q-grad®-1 Milli-Q system (Millipore).

Track-etching nanopores and current –voltage measurements

The PET films (13 µm) were irradiated by a single Xe irradiation (8.98 MeV) (GANIL, SEM line, Caen, France) to create single tracks and thus a single nanopore. Then, the latter was exposed to UV irradiation during 9 hours for tip side and 15 hours for base side (Fisher bioblock; VL215.MC, λ = 302 nm). The activated PET film was mounted between two chambers of a Teflon cell. The etchant solution (NaOH 9 M, 1.6 ml) was added on the base side and the stopping solution (KCl 1M and CH3COOH 1M, 1.6 ml) on the tip side. An electrode (Pt) is immersed in the stop solution and the working one (Pt) in the etchant solution and then a potential of 1 V was applied across the membrane. The nanopore opening was characterized by the current as a function of time recorded by a patch-clamp amplifier (EPC-10 HEKA electronics, Germany). The etching process was stopped by replacement of the etching solution by the stop one when the current reach a value of several hundred pA.

The tip diameter *d* of the conical nanopore was determined from the dependence of the conductance G measured in the linear zone of the I–V curve (typically between - 60 mV to 60 mV) assuming a bulk-like ionic conductivity inside the nanopores (equation 1).

$$G = \frac{\kappa d D \pi}{4L} \qquad (1)$$

Where, κ is the ionic conductivity of the solution, L is the nanopore length (13 µm) and D is based diameter which was calculated from the total etching time t using the relationship D = 2.5t (the factor 2.5 was determined in our experimental set up using multipore track-etched membranes).

The I-V curve were obtained from the current traces recorded as a function of time from 1 V to -1 V by 100 mV steps for 2 s and from 100 mV to -100 mV by 10 mV steps for 2s using a sampling rate 50 kHz.

Nanopore functionalization and reversibility of PLL/HEP layer

The same buffer solution (50 mM Tris-HCl, 75 mM CH_3COONa, 100 mM NaCl) was used for polyelectrolyte adsorption and enzymatic degradation. The pH is adjusted to 7.5 by addition

of chloride acid and sodium hydroxide. For the functionalization with PLL, 10 µl of the polyelectrolyte solution (1mg/ml) was added in the tip side of the nanopore. A voltage -1V was applied from the tip side to the base one during 3 minutes. Then a various volume of HEP (1mg/ml) was added in 1.6 ml buffer solution at tip side of the cell. The 1 V for HEP was applied for 3 min. The I-V curves were recorded after replacing polyelectrolyte solution by buffer. After each detection of HEP, the PLL-HEP layer was desorbed using a buffer at pH 12 containing 100 mM KCl, 5 mM Trizma-HCl and 1 mM EDTA.

Enzymatic degradation

50 U of Heparinase I and III was dissolved in 2.5 ml of storage solution containing 20 mM Tris-HCl, 100 mM NaCl, 1 mM EDTA at pH 7.5. 10 U of Heparinase II is dissolved in 1 ml of the same buffer. 0.25 ml of Heparinase I and III at 20 U/ml and 0.5 ml off Heparinase II at 10 U/ml are mixed and then diluted 10 times. So the final solution has a concentration of 1.33 U/ml of total enzyme.

The enzymatic reaction is carried out at ambient temperature ~25°C during time from 0 to 250 min in the buffer solution pH 7.5 containing 50 mM Tris-HCl, 75 mM (CH3COO)Na, 100 mM NaCl . For each essay, 3 µl of HEP (1 mg/ml) and 5 µl of enzyme cocktail solution (1.33 U/ml) are added in 1.5 ml of the reaction buffer solution. So the concentrations of HEP and Heparinase for reaction are 2 µg/ml and 4.43 mU/ml respectively.

For OSCS detection, 2 mg OSCS is dissolved in 20 ml storage solution described above. Then 1 ml of this solution is dissolved by 10 times (10 µg/ml) and 1 ml dissolved by 1000 times (0.1 µg/ml). To obtained the OSCS/heparin ratio 10%, 1%, 0.1%, 0.01% w/w, 30 µl, 3 µl of OSCS (10 µg/ml) or 30 µl, 3 µl of OSCS (0.1 µg/ml) was added in 1.5 ml of reaction solution containing HEP at 2 µg/ml. Then 4.43 mU/ml of enzyme solution was added. The enzymatic reaction was carried out at 25 °C during 200 min.

Results and discussions

The strategy to obtain the nanopore sensor is illustrated on the figure 1. It consists to open a single conical nanopore on a PET film and decorated it by adsorption of PLL. Then, as mention in introduction, our methodology has follow three steps of detection (i) the HEP (ii) the HEP degraded by heparinase and (iii) the the HEP degraded by heparinase in presence of OSCS.

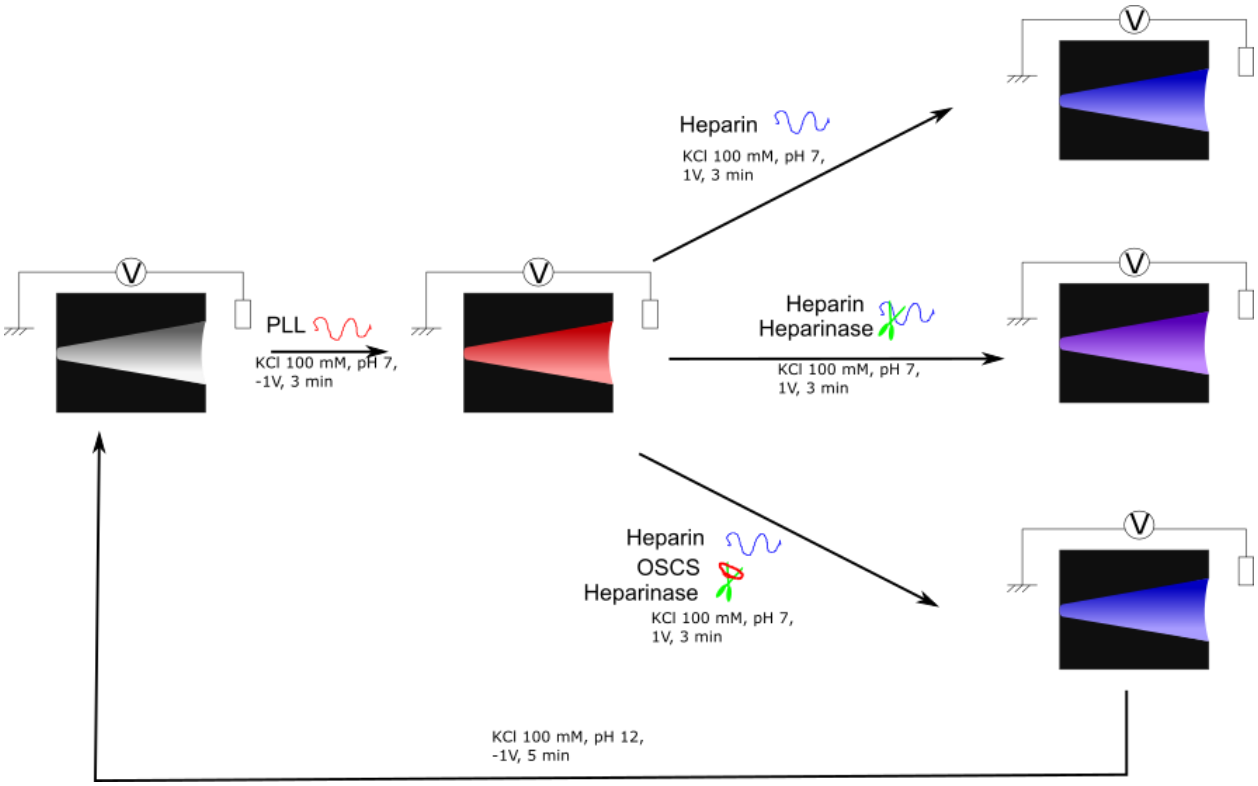

Fig. 1 Sketch of experimental methodology follows in this work. The first step is the nanopore functionalization by PLL. The second step is the different experiments performed to detect HEP and OSCS.

Heparin detection by conical nanopore decorated with PLL

The PET single conical nanopores were obtained by track-etched methods under dissymmetrical condition as previously described[300]. Shortly, we used the electrostopping method. The D_{base} is deduced from the etching time. In order to confirm the factor used is suitable and evaluate the impact of the dispersity of the base diameter, we performed the same experiment on low density membrane (10^5 pores/cm$^{2)}$ to avoid the nanopores overlap. In Figure S1 are reported the SEM of several nanopores obtained after etching time 156 min. From the etching time and conductance measured on a single nanopore performed in the same condition, we obtained a D_{base} = 390 nm and a d_{tip} = 22.5 nm. Accoring to the dispersity observed on the multipore membrane (Figure S1) the error on the d_{tip} about 1.5 nm. After alkaline etching, the nanopore inner wall exhibits carboxylate moieties which confer it a negative surface charge. The I-V dependence recorded at pH 7 NaCl 100 mM shows ICR behavior characterized by the rectification factor Rf = |I(1V)/I(-1V)| < 1 (Figure 2). The first set of experiment is dedicated to show the nanopore functionalization by PLL and the HEP

detection. To do so, the PLL was added in the tip chamber and a voltage -1 V was applied until inversion of I-V curve that is characteristic to the inversion of the nanopore surface charge (Figure 2 and S2). After washing, the heparin was added to the tip chamber under 1 V during 3 min.

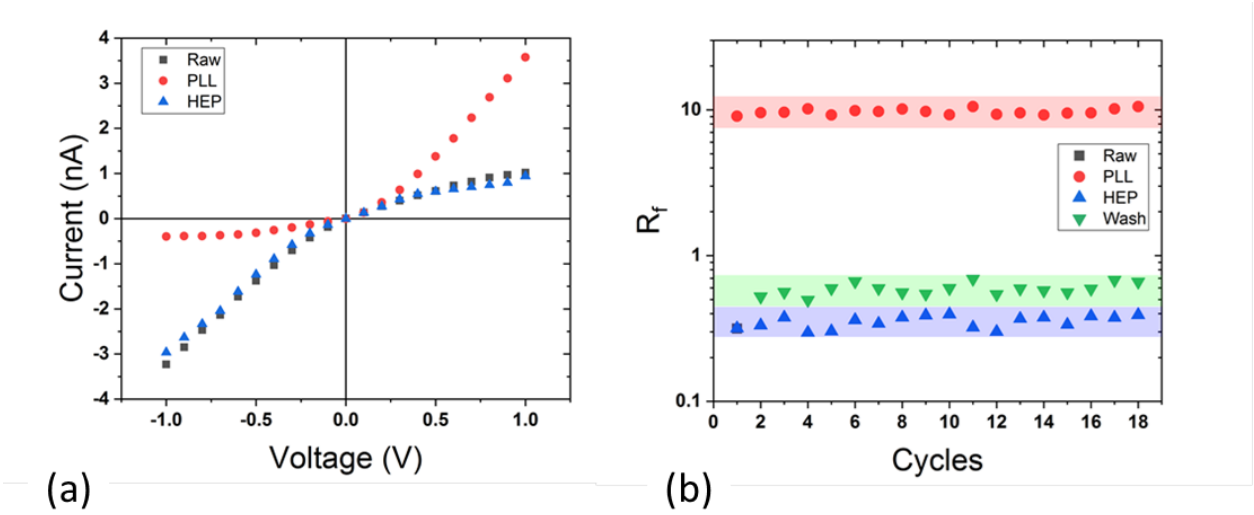

Fig. 2 (a) Sketch of experimental functionalization and heparin detection using conical nanopore, (a) I-V curve of raw single nanopore (black, square), after PLL deposition (red, circle) and after heparin deposition (blue, triangle), (b) Rectification factor obtained for raw single nanopore (black, square), after PLL deposition (red, circle), heparin deposition (blue, triangle) and washing at pH 12 (green triangle). The experiments were performed on a single nanopore d_{tip} = 22.5 nm and D_{base} =390 nm.

The I-V curve was again inversed due to the excess of negative charge from heparin. This evidences that each polyectrolyte can be detected by the conical nanopore. The first targeted property of our nanopore sensor is its reusability. To prove that, we have performed several cycles of PLL/HEP adsorption followed by a washing at pH 12 under 1V during 5 min to remove the PE layers on different nanopores with similar size. The *Rf* as well as the conductance recorded after each step are similar for the 18 cycles (Figure 2 and S3) and 4 cycles (SI-3). This confirms as expected that conical nanopore is reusable for the heparin detection.

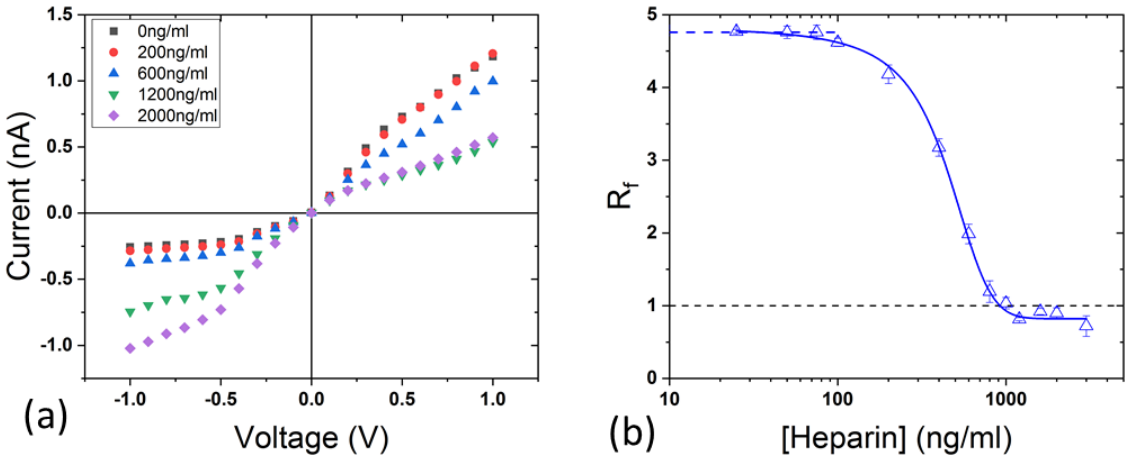

Fig. 3 (a) I-V dependence after HEP adsorption at different bulk concentrations (b) R_f as a function of HEP bulk concentration. The blue dash line corresponds to the R_f measured after PLL adsorption and the full line to non-linear fit by equation 1. The experiments were performed on a single nanopore d_{tip} = 35 nm and D_{base} = 300 nm for a total number of cycle n = 28.

Our nanopore is suitable to detect HEP using the IRC. We have to demonstrate if the value of *Rf* is dependent on the HEP concentration in order to establish a dose-response curve. We can notice that at low concentration, the adsorption of PE onto a charged surface is usually described by a Langmuir model. Here, the detection method by ICR does not give the exact interfacial concentration of PE but it is sensitive to the modification of the global surface charge. We measured the I-V dependence after adsorption of HEP for different bulk concentrations following the cycle PLL/HEP adsorption and washing at pH 12 (Figure 3). The rectification factor after each step for two consecutive quantitative analyses was reported on figure S54 to confirm the constant values after PLL adsorption and after washing. Conversely, the rectification factor decreases with the heparin concentration in the bulk. This means that the positive charges of PLL are counterbalanced by the increase of HEP amount adsorbed inside the nanopore. Assuming that the HEP adsorption on PLL is mainly governed by the electrostatic interactions, the amine groups of PLL layer can be seen as binding sites for acidic moieties of the HEP. In this case the rectification factor can be assimilated to the bound fraction of HEP on PLL as following equilibrium.

[PLL] + [HEP] ⇄ [PLL - HEP]

The plot of rectification factor as a function of HEP concentration in the bulk can be fitted by a classical sigmoidal equation (eq. 2) equation where the asymptotic values are the rectification factor induced by only the PLL (Rf_{PLL}) and after saturation by HEP (Rf_{HEP}). The sigmoidal curve comes from the fact that to modify the IRC a sufficient amount of HEP has to be adsorbed to impact the nanopore surface charge. At low concentration, the amount of HEP adsorbed is not sufficient to significantly modify the nanopore surface charge and thus the IRC. In this case, the transport is mainly dominated by the PLL charge. With the increase of HEP concentration, more and more HEP are adsorbed and thus affect the IRC. In this range, the nanopore sensor is suitable to obtain the dose-response of HEP based on the *Rf*. Finally, when HEP concentration reaches a certain value the adsorption is very fast and the *Rf* become constant.

$$Rf = Rf_{PLL} + \frac{Rf_{HEP} - Rf_{PLL}}{1+10^{(logEC50-c)p}} \quad (2)$$

where the half maximal effective concentration EC50 is the bulk concentration where HEP reaches 50% of PLL coverage, *c* the concentration of HEP in the solution and *p* the equivalent of Hill coefficient which gives information about degree of interaction between the binding sites of PLL and the HEP. The non-linear fit (Figure 3b) gives an EC50 = 435.9 ng/ml and a p= -2.79 10^{-3}. The p value below 1 means that when a HEP is bound on PLL its affinity for another HEP molecule decrease. This result highlights that the HEP adsorption inside the nanopore should not be described by a Langmuir isotherm since this model assumes that binding sites are completely independent. This result opens numerous questions about our basic conception of polyelectrolyte adsorption under confinement that is crucial for the understanding the membrane functionalization using such macromolecules.

OSCS detection by conical nanopore decorated with PLL

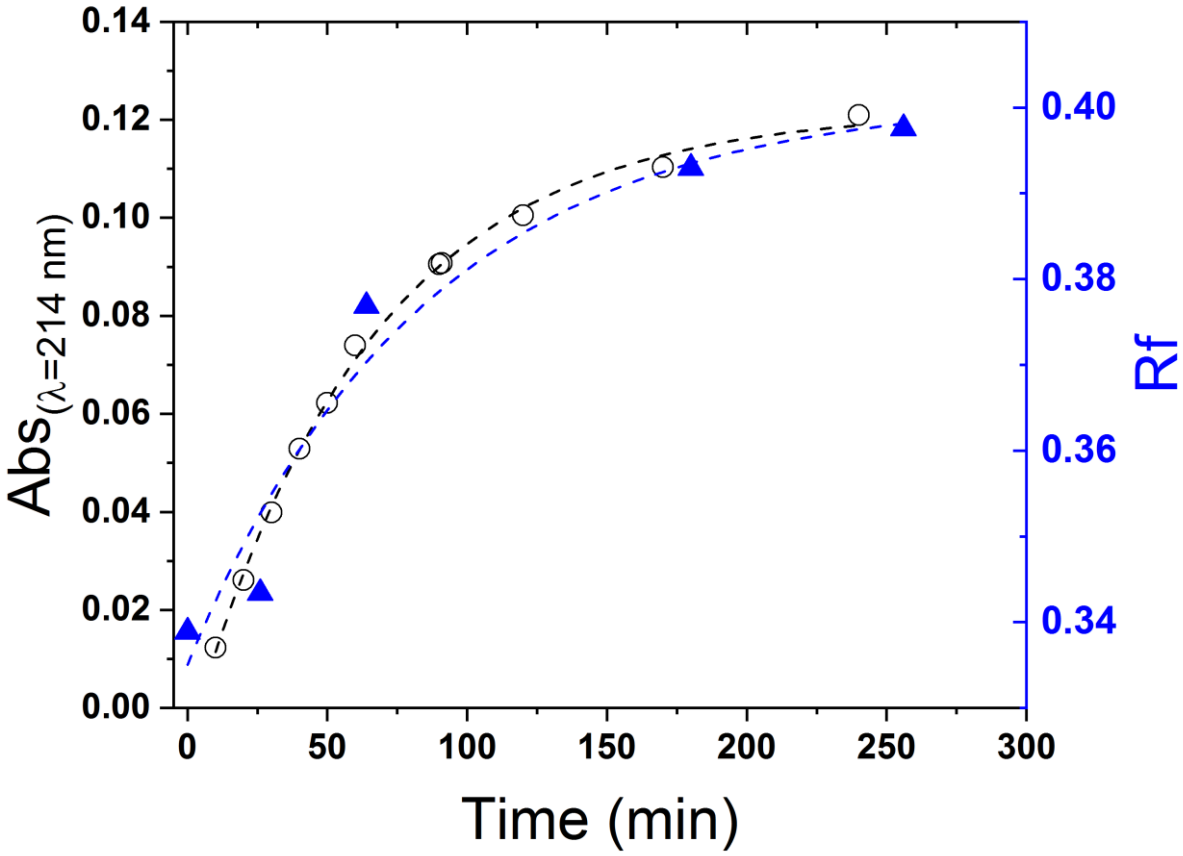

Fig. 4 Enzymatic degradation of HEP by heparinase follows by absorbance-based methods (black, circle) and nanopore functionalized by PLL. The experiments was performed on one nanopore d_{tip} = 29 nm and D_{base} =340 nm following 5 cycles of PLL-HEP adsorption/washing at pH12.

Our concept for OSCS sensing is based on its ability to inhibit the HEP degradation by heparinase. As first step, we have to establish a correlation between the IRC and the degradation degree of HEP. To do so, we adsorbed the HEP after different degradation time by heparinase.. As shown on figure 4, the rectification factor increases with the degradation time of HEP. This can be explained by a weaker affinity of oligosaccharide from the HEP with the PLL due to their lower molecular weight. The kinetic of HEP degradation obtained by nanopore experiment is compared with the one obtained by a classical method which consists of dose the oligosaccharide by absorbance at 214 nm (Figure 4 and SI-6). It follows an order 1 kinetic law (eq. 3).

$$[P] = [P_0]\exp(-kt) \qquad (3)$$

where *P* is the product of Hep degradation. The value of kinetic constant *k* obtained by nanopore detection (k =1.12 10^{-2}±0.6 10^{-2}) and absorbance (k =1.56 10^{-2}±0.06 10^{-2}) are very close proving that the nanopore functionalized with PLL is a good candidate to follow easily the enzymatic degradation of PE. It could be noticed that using a single nanopore, the enzymatic degradation was only characterized by resistive pulse method[276,301].

Because the IRC depends on the degree of heparin degradation, we expected that the inhibition by OSCS can be also detected by nanopore. The first experiment was to compare the I-V curves after addition of heparine degraded by heparinase after 200 min incubation at 25°C with and without 10 % weight of OSCS (Figure 5a). Without the inhibitor, the rectification factor decreases from 5.22 to 1.86 because the affinity of oligosaccharides with PLL is too weak to provide efficient charge compensation. In presence of OSCS the heparinase is inhibited and the HEP is less degraded. The long chains of heparin have a better affinity with the PLL inducing more efficient charge compensation characterized by a decrease of *Rf* until 0.9. The range of OSCS dose-response is reported on Figure 5b and S7. The experiments conducted on two individual nanopores with tip diameter 12 nm and 36 nm show the same trend. The value *Rf* decreases with the OSCS concentration. For both nanopores the *Rf* is boundary between two asymptotic values the one obtained after heparin degradation without inhibitor and the one obtained after adsorption of non-degraded heparin. For all tested nanopores, the detection range where the *Rf* is dependent on the OSCS concentration is found from 0.1 to 10^{-4} w/w.

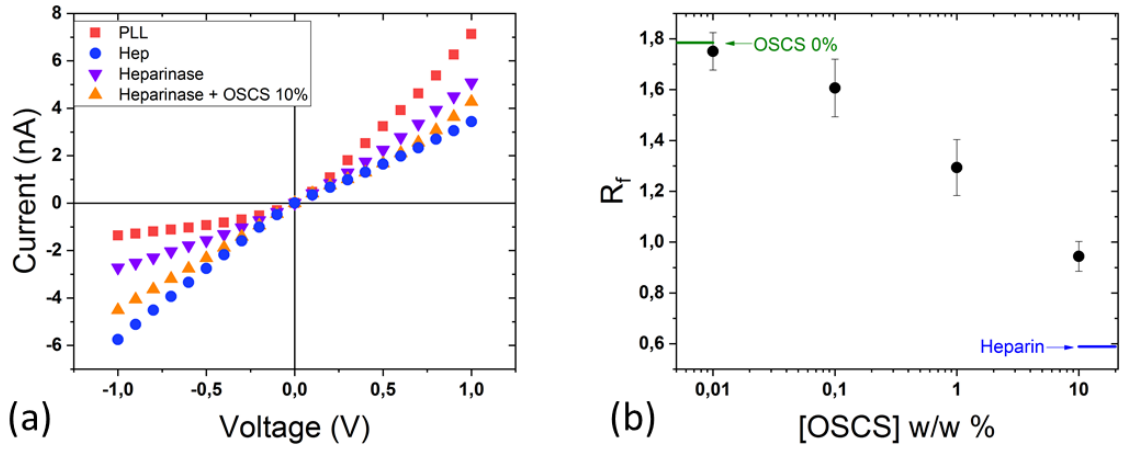

Fig. 5 (a) Sketch of the OSCS detection using single PLL functionalized nanopore (b) I-V curves recorded after PLL adsorption (red, square), after HEP (blue, circle) degraded by

heparinase in presence (orange, triangle) or not (violet, triangle) of OSCS 0.1 % weight (c) Rectification factor as a function of OSCS concentration (black, circle), in green and blue line are reported the two asymptotic values obtained without addition of OSCS and for non-degradated heparin. The results were obtained with a single conical nanopore d_{tip} = 12 nm and D_{base} =540 nm.

Stability and reproducibility of nanopore sensor

As mentioned in introduction, the main bottlenecks to use solid-state nanopore as sensor are their short lifetime and the difficulties to reproduce similar experiments several consecutive days without constraining experiments. We discuss now about the stability and the lifetime of our nanopore. For the heparin sensing, the experiments shown in figures 2, S-2 and S3 where 18 cycles performed in the same day are reported. For the dose response experiments (Figure S5), 28 cycles was performed during two consecutive days. These results confirm that approach based on the reversible functionalization with PLL allows using the same nanopore for several experiments with a good reproducibility of results. The experiments about the OSCS sensing (Figure 5b and S7) were performed during two consecutive days. In order to provide a clear proof of the nanopore stability, we show in figure 6, a series of HEP and HEP after degradation with by heparinase in presence of OSCS 1% detection experiments performed during 18 days. Between each experiment the nanopore was conserved in milliQ water. The result show that a good reproducility of results. Typically after each step the rectification factor stay comparable along the day. We notice also that after 18 days the nanopore is still working.

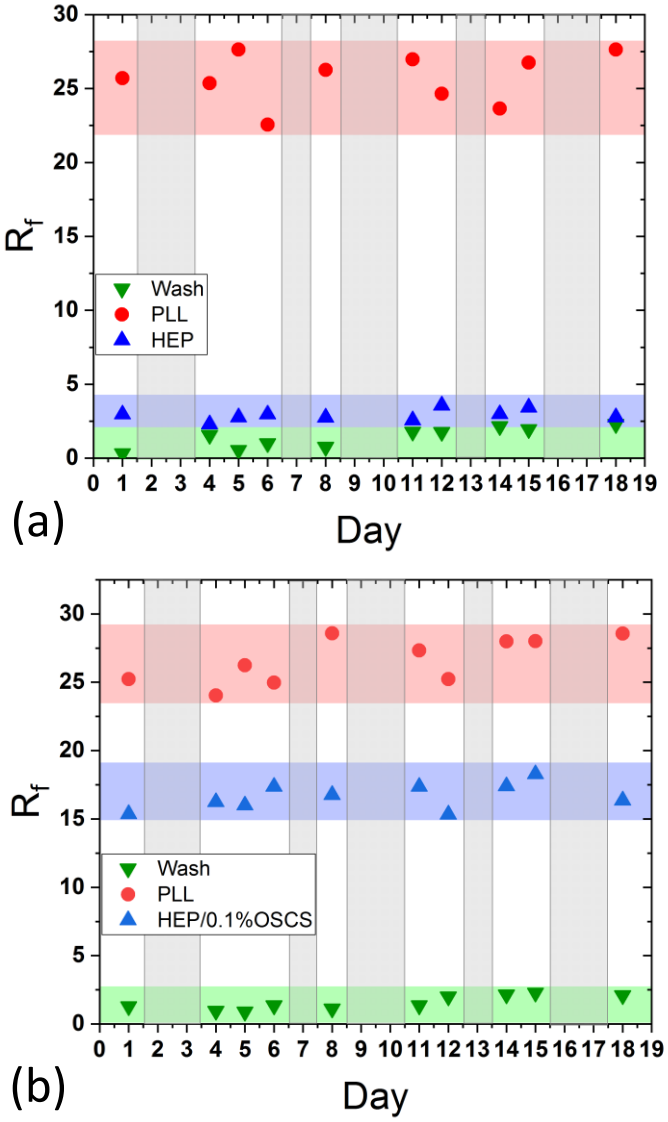

Fig. 6 Nanopore sensor stability and reproducibility: Rectification factor obtained for single nanopore, after PLL deposition (red, circle), and washing at pH 12 (green triangle) and (a) after HEP (blue, triangle) and (b) after HEP degradated by heparinase in presence of OSCS 0.1 % weight (blue, triangle). The experiments were performed at different day on the same nanopore d_{tip} = 29 nm and D_{base} =340 nm. The gray zone correspond to storage period without experiment (1 or 2 days)

Conclusion

To sum up, the single nanopore sensor described herein can be used to detect easily a wide range of OSCS concentration contained in heparin sample. The detection limit about 0.01 % weights that is less sensitive compared methods based on fluorescence but in the good range for the characterization of contaminated sample of heparin. In addition, our approach

does not require the synthesis of fluorescent dyes, specific DNA ligands or nanoparticles nor expensive instrumentation. Indeed, the nanopore functionalization requires a couple of minutes and it is totally reversible which allows quantifying the OSCS after performed a calibration curve. It is also perfectly conceivable the integration of the nanopore inside a microfluidic device and use a miniaturized amplifier to build a portable system to analyze heparin sample. So, we could expect that this nanopore sensor will enhance the quality control chain of heparin allowing avoiding the risk of patients' death. Beside the detection of heparin contaminant, two other applications are possible with our nanopore: the characterization of enzymatic degradation of PE and the mechanism of PE layer formation. Globally, this study highlight that a conical nanopore simply functionalized with PLL is powerful for many applications from enzymology to controlling quality of drug.

Reference

(1) Guerrini, M.; Zhang, Z.; Shriver, Z.; Naggi, A.; Masuko, S.; Langer, R.; Casu, B.; Linhardt, R. J.; Torri, G.; Sasisekharan, R. Orthogonal Analytical Approaches to Detect Potential Contaminants in Heparin. Proc. Natl. Acad. Sci. 2009, 106 (40), 16956–16961. https://doi.org/10.1073/pnas.0906861106.

(2) Sasisekharan, R.; Shriver, Z. From Crisis to Opportunity: A Perspective on the Heparin Crisis. Thromb. Haemost. 2009, 102 (5), 854–858. https://doi.org/10.1160/TH09-02-0083.

(3) Beni, S.; Limtiaco, J. F. K.; Larive, C. K. Analysis and Characterization of Heparin Impurities. Anal. Bioanal. Chem. 2011, 399 (2), 527–539. https://doi.org/10.1007/s00216-010-4121-x.

(4) Liu, Z.; Xiao, Z.; Masuko, S.; Zhao, W.; Sterner, E.; Bansal, V.; Fareed, J.; Dordick, J.; Zhang, F.; Linhardt Robert J., R. J. Mass Balance Analysis of Contaminated Heparin Product. Anal. Biochem. 2011, 408 (1), 147–156. https://doi.org/10.1016/j.ab.2010.09.015.

(5) Kalita, M.; Balivada, S.; Swarup, V. P.; Mencio, C.; Raman, K.; Desai, U. R.; Troyer, D.; Kuberan, B. A Nanosensor for Ultrasensitive Detection of Oversulfated Chondroitin Sulfate Contaminant in Heparin. J. Am. Chem. Soc. 2014, 136 (2), 554–557. https://doi.org/10.1021/ja409170z.

(6) Ding, Y.; Shi, L.; Wei, H. A “Turn on” Fluorescent Probe for Heparin and Its Oversulfated Chondroitin Sulfate Contaminant. Chem. Sci. 2015, 6 (11), 6361–6366. https://doi.org/10.1039/c5sc01675d.

(7) Wang, Y. J.; Lin, L.; Zhang, X.; Schultz, V.; Zhang, F.; Sun, J. Z.; Linhardt, R. J. Selective, Switchable Fluorescent Probe for Heparin Based on Aggregation-Induced Emission. Anal. Biochem. 2016, 514, 48–54. https://doi.org/10.1016/j.ab.2016.09.007.

(8) Hu, Y.; Guo, W.; Ding, Y.; Cheng, H.; Wei, H. Modulating Luminescence of Tb3+with Biomolecules for Sensing Heparin and Its Contaminant OSCS. Biosens. Bioelectron. 2016, 86, 858–863. https://doi.org/10.1016/j.bios.2016.07.085.

(9) Kasianowicz, J. J.; Brandin, E.; Branton, D.; Deamer, D. W. Characterization of Individual Polynucleotide Molecules Using a Membrane Channel. Proc. Natl. Acad. Sci. U. S. A. 1996, 93 (24), 13770–13773. https://doi.org/10.1073/pnas.93.24.13770.

(10) Dekker, C.; Article, R.; Dekker, C. Solid-State Nanopores. Nat. Nanotechnol. 2007, 2 (4), 209–215. https://doi.org/10.1038/nnano.2007.27.

(11) Karawdeniya, B. I.; Bandara, Y. M. N. D. Y.; Nichols, J. W.; Chevalier, R. B.; Dwyer, J. R. Surveying Silicon Nitride Nanopores for Glycomics and Heparin Quality Assurance. Nat. Commun. 2018, 9 (1), 1–8. https://doi.org/10.1038/s41467-018-05751-y.

(12) Roman, J.; Français, O.; Jarroux, N.; Patriarche, G.; Pelta, J.; Bacri, L.; Le Pioufle, B. Solid-State Nanopore Easy Chip Integration in a Cheap and Reusable Microfluidic Device for Ion Transport and Polymer Conformation Sensing. ACS Sensors 2018, 3 (10), 2129–2137. https://doi.org/10.1021/acssensors.8b00700.

(13) Roman, J.; Jarroux, N.; Patriarche, G.; Français, O.; Pelta, J.; Le Pioufle, B.; Bacri, L. Functionalized Solid-State Nanopore Integrated in a Reusable Microfluidic Device for a Better Stability and Nanoparticle Detection. ACS Appl. Mater. Interfaces 2017, acsami.7b14717. https://doi.org/10.1021/acsami.7b14717.

(14) Giamblanco, N.; Coglitore, D.; Janot, J.; Eugène, P.; Charlot, B.; Balme, S. Sensors and Actuators B : Chemical Detection of Protein Aggregate Morphology through Single

Antifouling Nanopore. Sensors Actuators B. Chem. 2018, 260, 736–745. https://doi.org/10.1016/j.snb.2018.01.094.

(15) Lepoitevin, M.; Bechelany, M.; Balanzat, E.; Janot, J.-M.; Balme, S. Non-Fluorescence Label Protein Sensing with Track-Etched Nanopore Decorated by Avidin/Biotin System. Electrochim. Acta 2016, 211. https://doi.org/10.1016/j.electacta.2016.06.079.

(16) Lepoitevin, M.; Ma, T.; Bechelany, M.; Janot, J.-M.; Balme, S. Functionalization of Single Solid State Nanopores to Mimic Biological Ion Channels: A Review. Adv. Colloid Interface Sci. 2017, 250, 195–213. https://doi.org/10.1016/j.cis.2017.09.001.

(17) Ali, M.; Ahmed, I.; Ramirez, P.; Nasir, S.; Niemeyer, C. M.; Mafe, S.; Ensinger, W. Label-Free Pyrophosphate Recognition with Functionalized Asymmetric Nanopores. Small 2016, 12 (15), 2014–2021. https://doi.org/10.1002/smll.201600160.

(18) Ali, M.; Nasir, S.; Ensinger, W. Bioconjugation-Induced Ionic Current Rectification in Aptamer-Modified Single Cylindrical Nanopores. Chem. Commun. 2015, 51 (16), 3454–3457. https://doi.org/10.1039/C5CC00257E.

(19) Ali, M.; Neumann, R.; Ensinger, W. Sequence-Specific Recognition of DNA Oligomer Using Peptide Nucleic Acid (PNA)-Modified Synthetic Ion Channels: PNA/DNA Hybridization in Nanoconfined Environment. ACS Nano 2010, 4 (12), 7267–7274. https://doi.org/10.1021/nn102119q.

(20) Ali, M.; Nguyen, Q. H.; Neumann, R.; Ensinger, W. ATP-Modulated Ionic Transport through Synthetic Nanochannels. Chem. Commun. 2010, 46 (36), 6690. https://doi.org/10.1039/c0cc01632b.

(21) Lepoitevin, M.; Jamilloux, B.; Bechelany, M.; Balanzat, E.; Janot, J.-M.; Balme, S. Fast and Reversible Functionalization of a Single Nanopore Based on Layer-by-Layer Polyelectrolyte Self-Assembly for Tuning Current Rectification and Designing Sensors. RSC Adv. 2016, 6 (38). https://doi.org/10.1039/c6ra03698h.

(22) Ma, T.; Gaigalas, P.; Lepoitevin, M.; Plikusiene, I.; Bechelany, M.; Janot, J. M.; Balanzat, E.; Balme, S. Impact of Polyelectrolyte Multilayers on the Ionic Current Rectification of Conical Nanopores. Langmuir 2018, 34 (11), 3405–3412. https://doi.org/10.1021/acs.langmuir.8b00222.

(23) Lepoitevin, M.; Nguyen, G.; Bechelany, M.; Balanzat, E.; Janot, J.-M.; Balme, S. Combining a Sensor and a PH-Gated Nanopore Based on an Avidin-Biotin System. Chem. Commun. 2015, 51 (27). https://doi.org/10.1039/c4cc10087e.

(24) Fennouri, A.; Daniel, R.; Pastoriza-Gallego, M.; Auvray, L.; Pelta, J.; Bacri, L. Kinetics of Enzymatic Degradation of High Molecular Weight Polysaccharides through a Nanopore: Experiments and Data-Modeling. Anal. Chem. 2013, 85 (18), 8488–8492. https://doi.org/10.1021/ac4020929.

(25) Giamblanco, N.; Coglitore, D.; Gubbiotti, A.; Ma, T.; Balanzat, E.; Janot, J. M.; Chinappi, M.; Balme, S. Amyloid Growth, Inhibition, and Real-Time Enzymatic Degradation Revealed with Single Conical Nanopore. Anal. Chem. 2018, 90, 12900–12908. https://doi.org/10.1021/acs.analchem.8b03523.

Dynamics of Long Hyaluronic Acid Chains through Conical Nanochannel for Characterizing Enzyme Reactions in Confined Space

Tianji Ma, Jean-Marc Janot, Sébastien Balme

Contribution: I designed the work with Sébastien Balme, did experiments, analyse data and wrote the manuscript**.**

Introduction

Enzymes as a biological catalyst play a vital role in living cells to accelerate chemical reactions in life conditions. The efficiency of enzymes comes from their highly precise and complex structures as well-designed machines. They find numerous applications in food industries, fine chemical synthesis and waste treatment from lab to industrial scale[1]. The enzymatic reactions can be performed under porous materials to design enzymatic membrane reactors (EMR)[2]. To this purpose, the enzymes were immobilized via physical adsorption, entrapment or covalent bonding in numerous porous materials[3,4] such as silica[5], clay minerals[6], double layered hydroxides[7], aluminum oxide[8], celites[9], agarose[10], polyelectrolytes[11] and metal-organic frameworks[12,13] according to enzyme properties and reaction conditions. The enzymatic reactions have been proved to be well carried out in porous membranes by confirming satisfied products output[1]. However, much effort has to be done to understand what exactly happens when an enzyme is immobilized in a confined space. More than 100 years ago, Leonor Michaelis and Maud Leonora Menten proposed an equation (so-called Michaelis-Menten) to describe enzymatic reaction kinetics[14]: $E + S \underset{k_{-1}}{\overset{k_1}{\rightleftarrows}} E \times S \xrightarrow{k_{cat}} E + P$ where k_1 and k_{-1} are the forward and reverse rate constants for substrate binding and k_{cat} is the catalytic rate constant. The k_{cat} is well confirmed by ensemble experiments, whereas, for each enzyme reaction, it should be different because of the general existence of fluctuations which is hidden at the ensemble level[15]. The recent advanced techniques based on fluorescence imaging microscopy and spectroscopy, as well as molecule manipulations make it possible to further characterization of the enzymatic reactions at single molecule level[16–18]. These techniques allow the real time observation of

each step and intermediates involved during enzymatic reaction. However, spectroscopy based techniques are limited to study enzymes under confined space.

Nanopore technology is found as good way to investigate biochemical reaction[19,20]. On the one hand, the kinetic of enzymatic reactions have been characterized by ensemble experiments using both proteins and solid-state nanopores. Fennouri et *al*. achieved the characterization of enzyme activity by study of the translocation of degraded hyaluronic acid through biological nanopore[21,22]. Using track-etched nanopore, our group followed the enzymatic degradation of β-lactoglobulin amyloid by resistive pulse technique[23] and heparin by ionic current rectification[24]. On the other hand, by immobilizing proteins inside single solid-state nanopores several groups achieved to detect specific bindings using resistive pulse technique. Wei et *al*. immobilized protein A (his-6-tragged) on nitrilotriacetic acid (NTA)-moieties attached to a gold-coated silicon nitride (SiN) nanopore and the kinetics of IgG antibody binding to Protein A was observed[25]. Yusko EC et *al*. immobilized biotin molecules on a lipid bilayer coated SiN nanopore[26]. Then, streptavidin was detected through the pore, resulting from the specific biotin-avidin interaction. Inspired by these previous works, we can hypothesize that nanopore approach is a suitable way to study enzyme activity directly inside a nanopore. We expect combine (i) the real-time analysis of enzymatic degradation products and (ii) characterization of enzyme-substrate interaction by measuring translocation duration change.

Before characterizing the enzymatic reaction, inside a nanopore we should well understand the whole process of the flexible polymers flowing into a confined space. This was investigated by theoretical studies and simulations since more than 40 years[27]. De Gennes and co-workers have proposed scaling theory for describing flexible polymers under confined space using Pincus' blob model. This called Gennes' regime is different from Odijk's where channel/pore diameter h is smaller than twice of persistence length of the molecule a ($h < 2a$)[28]. De Gennes' regime describes the cases where channel (or pore) diameter D is larger than $2a$ but still smaller than the coil diameter of polymers in bulk D ($2a < h < D$). In this regime, polymers can be considered as a series of blobs which contain a number of monomers. Peterlin, de Gennes and Pincus successively proposed and calculated a critical volumetric flow where a coil-like polymer would change to a stretched form in a nanopore[29–31]. Based on that, Daoudi et *al*. described flexible polymers flowing inside conical channels by

identifying dilute regime and semi-dilute regime according to a possible overlap of polymer coils in bulk solution[32]. On the same way in developing de Gennes' regime in conical nanochannel, relations between the number of monomers and the axis distance occupied in a defined conical channel was established[33,34]. Theoretical studies are far ahead of related experimental research due to the difficulty in preparing well-defined samples providing related confined space in nanoscale[35]. From 1990s, the progress in single nanopore technology[36] for single molecule sensing[37] draws more research interests on that especially to investigate voltage driven translocations. Numerous experiments of voltage-driven polymer translocations through different kinds of asymmetric nanopore such as proteins[14,15,18,38–40], nanocapillaries[41–43] and polymer track-etched[44] have been done However, there was never reported the experiments of translocating a large enough macromolecule in a conical channel with small enough tip aperture under de Gennes' regime which are similar to conditions of above theoretical studies.

This paper aims to investigate the enzymatic degradation of the polymer (the hyaluronic acid noted as HA) with high molecular weight (1.5 MDa < M < 1.8 MDa) directly inside the conical nanochannel at single molecule level. We first investigate the translocation of HA through conical track-etched nanochannels under dilute and semi-dilute regimes since such study is still missing. In that case, we aim to make an experimental evidence of the blobs model of flexible polymer inside conical channel. Then hyaluronidase was immobilized on the channel inner wall by a one-step chemical bonding. By controlling enzyme positions only in base side of the conical channel, a real-time analysis of enzymatic degradation was achieved. Finally, the grafting of enzymes in the narrowest of the channel (tip side) made possible to by measurement of the translocation duration changes to identification of the enzyme-substrate complexions.

Results and discussions

Influence of the regime on HA translocation through conical nanochannel

The single conical nanochannel in polymer film was fabricated by track-etching method under asymmetric condition [45]. It was mounted in a cell composed by two chambers filled with phosphate saline buffer (PBS) where NaCl concentration was adjusted to 1 M. For experiments in the dilute regime and semi-dilute regime, two similar conical nanochannels

(L= 13 µm) were used with base and tip diameters at D_{base} = 715 nm, D_{tip} = 23.5 nm (α = 1.52°) (noted as nanochannel 1) and at D_{base} = 750 nm D_{tip} = 35.4 nm (α = 1.57°) (noted as nanochannel 2) respectively. Hyaluronic acid with a high molar weight between 1.5 to 1.8 10^6 g mol^{-1} has a large hydrodynamic diameter which was estimated between 280 nm to 310 nm under physiological saline solution according to literature[46]. Their chain length is estimated 4000 nm (monomer length at 1.1 nm). To switch from dilute to semi-dilute regime, hyaluronic acid should have a strong interaction between each other. Under 1 M NaCl and according to the polymer size, the critical concentration of hyaluronic acid is estimated 500 nM from de Gennes' and Cowman's theories[33,46]. Considering that, we performed translocation experiments at 120 nM or 600 nM of hyaluronic acid for nanochannel 1 (dilute regime) and nanochannel 2 (semi-dilute regime) respectively. The hyaluronic acid was added on the base side and transmembrane biases from 300 mV to 900 mV were applied to drive polymers approaching, being captured and passing through the nanochannel. As our nanochannels have a conical shape and a base diameter more than twice larger than the hydrodynamic diameter of polymers, we can assume that the polymer entrance inside the channel requires overcoming a low energy barrier[47,48].

Figure 1a and b depict the schematic representations of the polymers inside the conical nanochannels. Examples of current traces recorded at 700 mV during 10 s for polymers in two different regimes are shown in Figure 1c and d with a zoom of several current blockades (Figure 1e and f). We can observe that the shapes of current blockades are different for the two regimes. In dilute one, the blockades show a clear asymmetric shape with a ΔI_{max} value at the end of the event. This shape-depending signal can be referring to the chain coil compression from base side to tip side in a conical channel (Figure S1). In other words, the density of the coil gets increased during compression leading to a progressive increase of current blockade. More interestingly, the signals have double peaks each: a current blockade followed to an enhancement during the polymer expulsion outside the nanochannel. This current enhancement could be attributed to the ion concentration modulation when the polymer get out of the channel[49,50]. For the semi-dilute regime, the translocation is carried out in a channel with similar pore diameters and cone angle (α = 1.57°). The current blockade events are found much more symmetrical (Figure 1f). The lack of a compression under similar nanopore size as in dilute regime can be assigned to the existence of a polymer

matrix due to the overlap of coils. Indeed, under crowded environment the volume of a polymer chain is reduced. These observations agree with the theoretical studies of Daoud and de Gennes using a scaling method[51].

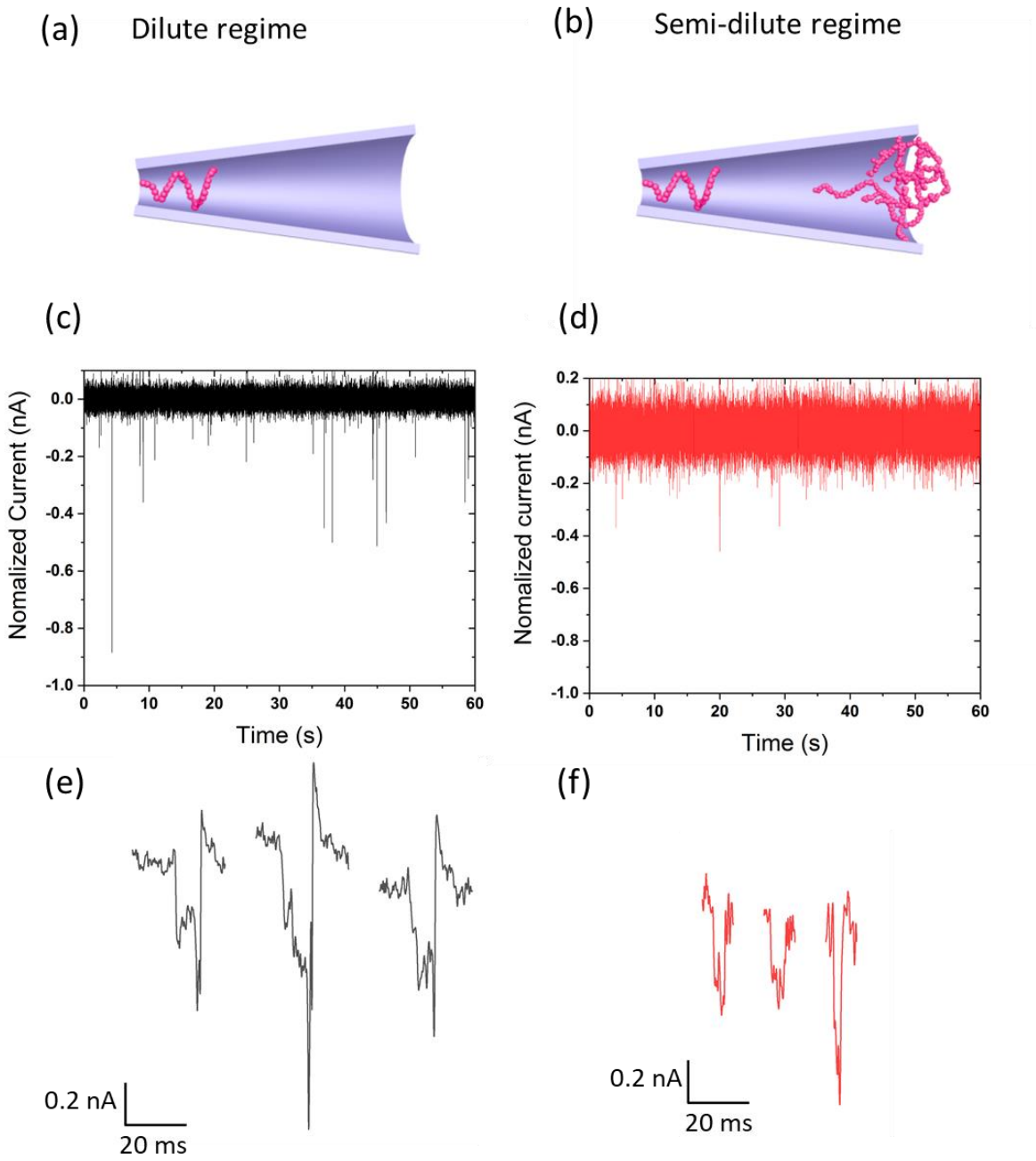

Figure 1. Sketch representations of hyaluronic acid through conical channel in dilute regime (a) and in semi-dilute regime (b). The sketches are not to scale. Examples of current trace recorded in dilute regime (c) and semi-dilute regime (d). Zoom of current blockade in dilute regime (e) and in the semi-dilute regime (f). Channel 1 in black: D_{base} = 715 nm, D_{tip} = 23.5 nm and Channel 2 in red: D_{base} = 750 nm, D_{tip} = 35.4 nm.

Figure 2a shows an event map of hyaluronic acid translocation in two regimes under 700 mV presenting two populations clearly. The different regimes of polymer solution induce in a different relative current blockade ratio $\Delta I_{max}/I_0$ (Figure 2b obtained from Figure S3 amd S4). The de Gennes' blob model has been used to describe flexible polymers in a long cone-shaped channel by Nikoofard and Fazli[34,52]. The linear density of the monomers along the channel axis *x* can be written as:

$$\lambda(x) \sim \frac{1}{b}\left(\frac{\xi(x)}{b}\right)^{\frac{1}{v}-1} \quad (1)$$

where *b* is the monomer size, $\frac{1}{v}-1$ equals to 0.7 as the Flory component v equals to 0.6 in this case[33,52] and ξ(x) is the blob size: $\xi(x) \sim D_0 + 2(x+a)\tan\alpha$. D_0 is the pore diameter of the tip side, α is the channel apex angle and a is the distance between beginning of the channel and the position of molecule beginning that can be fixed to 0. Thus, by integrating $\lambda(x)$ along the distance *L* occupied by polymer in the channel, we can get the total number of the polymer *N* as:

$$N \sim \frac{b^{-\frac{1}{v}}}{\tan\alpha}\left[(D_0 + 2(a+L)\tan\alpha)^{\frac{1}{v}} - (D_0 + 2a\tan\alpha)^{\frac{1}{v}}\right]. \quad (2)$$

From the equation 2, we can calculate *L* for hyaluronic acid in nanochannel 1 setting molar mass at 1.65 Mg mol^{-1}, $\tan\alpha$ at 0.027, D_0 at 13.5 nm, *b* at 0.75 nm^3 and a at 0. The *L* is obtained as 81 nm. Then, the ratio *η* of the volume occupied by the hyaluronic acid in this section can be calculated to be 7.7% using 1.1 nm as the length of a disaccharide unit and 0.68 nm^2 as the cross section of polymer chain. If we consider now that the channel contains two parts: one section is filled with one polymer and one section is full of electrolyte solution, we can define the nanochannel as a sum of two resistances R_1 where the HA and R_2 (Figure S2).

As the electrolyte solution has a NaCl concentration as high as 1 M, we neglect the conductance contribution of electrical double layer in the channel and the charge density of hyaluronic acid screened. Considering 7.7 % of the volume occupied by the molecule in R_1, the relative current blockade $\Delta G/G_0 = \Delta I/I_0$ is calculated to be 1.16 % (Figure S2). This value is quite close to average experimental data at about 1 % as shown in Figure 2b. As the channel has a length of 13 µm and a D_{Base} of 715 nm, we cannot claim that only one molecule is inside the channel. However the relative good agreement $\Delta G/G_0$ between calculation and

experiment let think that in such dilute regime, only one molecule is strongly confined close to the tip side leading to the unique contribution of current blockade. Other hyaluronic acid molecules could be located in the channel but they are too far from the tip aperture and not compressed enough to contribute to the current blockade considering the large gyration diameter of HA. Therefore the de Gennes' blob model as well as the calculation by Fazli et al.[33,52] are perfectly suitable in the case of polymer translocation under dilute regime. If we do the same calculation in the case of a semi-dilute regime, 0.7% of conductance decrease is obtained. This value is far from experimental one from 3% to 4%. This can be explained by the polymer matrix that fills the channel and takes more space inside.

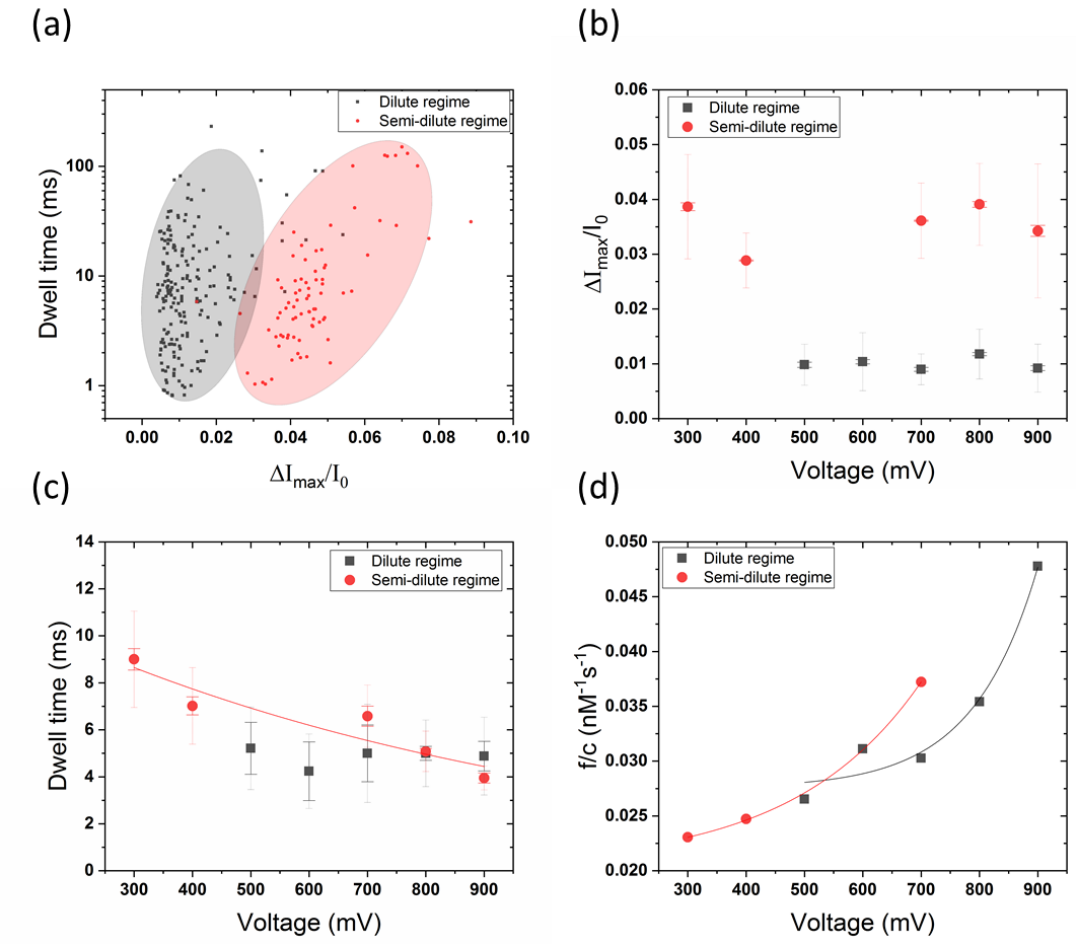

Figure 2. (a) Event map for two regimes obtained under V = 700 mV. Blockade rate (b), dwell time (c) and frequency of events (d) of HA under dilute regime (black square) and semi-dilute regime (red circle) against applied voltage. (d) Event map for two regimes obtained under V = 700 mV. Channel 1 in black: D_{base} = 715 nm, D_{tip} = 23.5 nm and Channel 2 in red: D_{base} = 750 nm, D_{tip} = 35.4 nm. The transparent error bars represent the full width at

half maximum of the Gaussian distributions and the solid error bars represent the standard error. In Figure d, the lines are the exponential fitting of equation (3).

Now, we investigate the dynamic aspects of HA translocation through conical nanochannel. The dwell time of translocations in two regimes in responding applied voltage increase is given Figure 2c. In the semi-dilute regime, the dwell time decreases exponentially in with the voltage. The exponential dependence can be described by the function $f(V) = Aexp(-V/V_c)$ where A = 12074 µs and V_c = 900 mV. This means that the dwell time measured in the semi-dilute regime could be considered as a transport time. It has been found by Oukhaled et al. that the dwell time of translocation of poly(ethylene glycol) chains (>35 kDa) in the semi-dilute regime is governed by the reptation time in a protein pore with small aspect ratio. It means that the extraction of one single chain of the polymer network into a small protein takes more time than the transport time[40]. This is contrary to our case where the nanochannel length scale is much larger than the polymer size. The reptation time of the polymer being extracted from the matrix is relatively short compared to the transport time. So this procedure is highly dependant on aspect ratio of the nanopore/nanochannel. In dilute regime, dwell time keeps almost constant when the electrical bias increases until to 900 mV.

Then we compare translocations in two regimes in terms of energy. This difference of free energy barrier can be obtained from the frequency of blockade events as a function of applied voltage according to Van't Hoff-Arrhenius law reading:

$$f = f_0 \exp\left[-\frac{V}{V_0}\right], \quad (3)$$

where f_0 is the frequency of blockades without applied electric bias

$$f_0 = k\frac{CDA}{L} exp\left[-\frac{U}{k_B T}\right], \quad (4)$$

where, k is a probability factor, *C* the polymer concentration, *D* the diffusion coefficient, *A* the cross-section area of the channel, *L* the channel length, $k_B T$ are the Boltzmann constant and the temperature and U the energy barrier. By fitting the data in Figure 2d with equation (3), f_0/C is obtained as 5.8 10^{-6} Hz nM^{-1} for dilute regime and 6.8 10^{-4} Hz nM^{-1} for the semi-dilute regime. The calculation of the absolute value is relatively uncertain because of the lack

of precise values for k, L and D[39]. Thus, we can calculate the difference of activation energy by removing these factors and assuming the same diffusion coefficient:

$$\frac{f_{0\,D}/C_D}{f_{0\,SD}/C_{SD}} = \exp\left[\frac{U_{SD}-U_D}{k_BT}\right]. \quad (5)$$

$U_{SD} - U_D$ is obtained as -0.16k_BT. The value is still not precise because the diffusion coefficient of HA is not the same in two regimes (D_{SD} is slightly smaller than D_D). However the qualitative relation remains the same meaning as the energy barrier of translocation of hyaluronic acid through conical nanochannel in dilute regime is higher than that in semi-dilute regime. Comparing these two regimes, the confinement energy of the polymer stretching in the elongation shear is relatively low because of the stretch conformation of polymers in the network of the semi-dilute regime. For dilute regime, the required energy to deform the large polymer coil under confined environment should be larger but it is still negligible when the pore angle is small[32]. Thus the different energy barriers could be explained by the friction between polymer coils and channel surface during the compression procedure to reach the tip aperture in such a long nanochannel. Thereof, the energy from the interaction with the surface becomes dominant.

Influence of the tip aperture on HA translocation through conical nanochannel

Another key factor which influences polymer translocation is the nanochannel diameter. For our conical nanochannels, the tip diameter plays a more important role rather than the base due to the location of the sensing zone. First, we had to choose one regime for following investigations. When the polymer solution flows in the channel with the shrinking of the channel diameter, dilute solutions may be concentrated inside the channel into the semi-dilute regime. So to avoid this unexpected transition, we choose to conduct experiments under the same semi-dilute regime. To compare with the results obtained in the nanochannel 2 (D_{base} = 750 nm, D_{tip} = 35.4 nm α = 1.57°), we supply another set of experiments in nanochannel 3 (D_{base} =1185 nm and D_{tip} = 6.1 nm α = 2.59°) (Figure 3a). In this experiment set, the tip diameter is close to 2a of the hyaluronic acid molecule (where *a* is its persistence length with a value around 4 nm to 9 nm[53,54]).

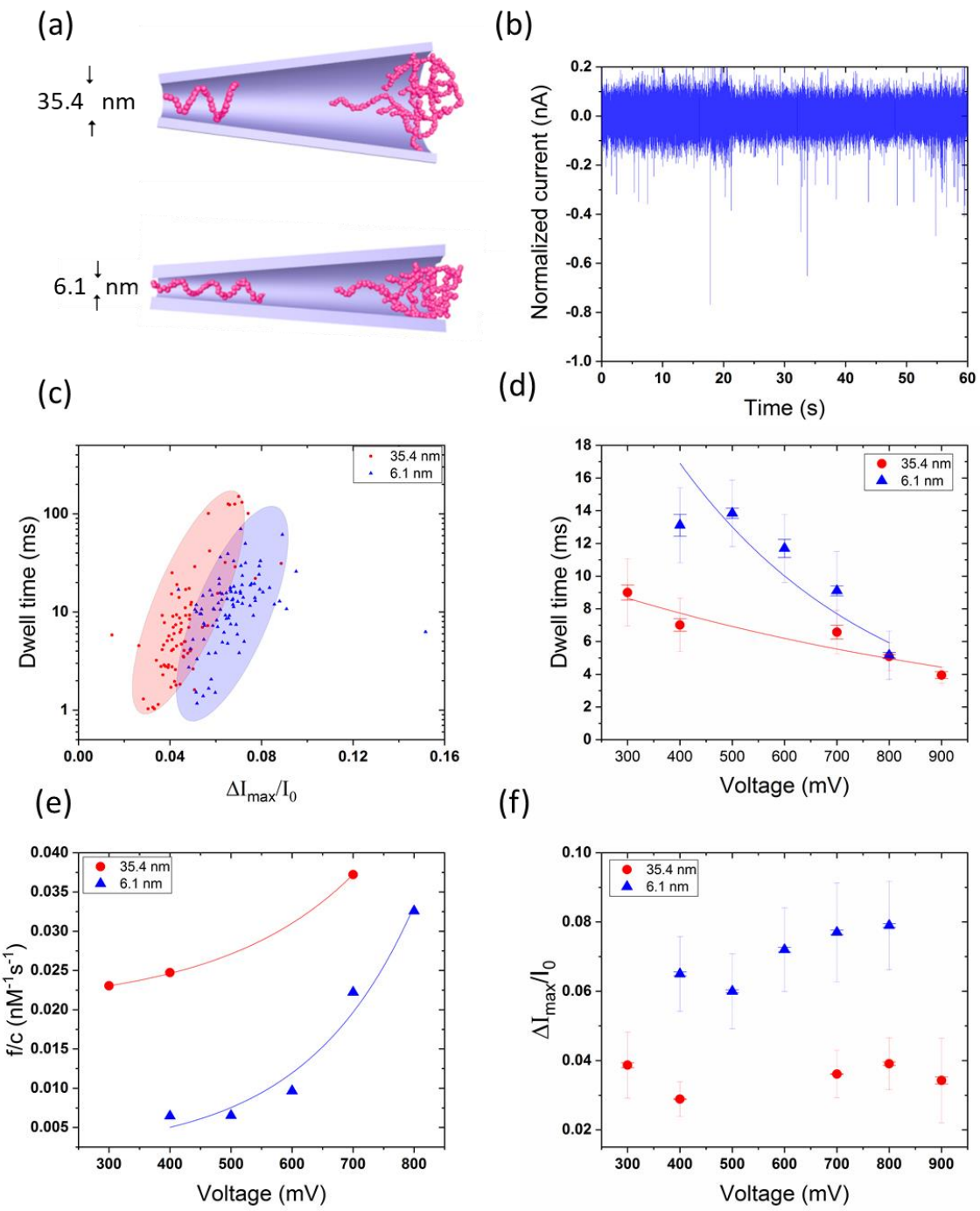

Figure 3. (a) Sketches of hyaluronic acid translocation through long conical channel with different diameters. The sketches are not to scale. (b) Example of current trace for channel 3. (c) Event map for two channels under 400 mV. Dwell time (d) event frequency (e) and blockade rate (f) of HA in channel 2 (red circle) and in channel 3 (blue triangle) against applied voltage. Channel 2 in red: D_{base} = 750 nm, D_{tip} = 35.4 nm and channel 3 in blue: D_{base} = 1185 nm, D_{tip} = 6.1 nm. The transparent error bars represent the full width at half maximum

of the Gaussian distributions and the solid error bars represent the standard error. In Figure e, the lines are the exponential fitting of equation (3).

Figure 3b shows a recorded current trace for nanochannel 3 and Figure 3c shows an event map for two channels under 400 mV. The dwell time in the channel of 35.4 nm seems shorter meanwhile its current blockade is higher than that in the channel of 6.1 nm. Details of dwell time as a function of applied voltage are shown in Figure 3d (obtained from Figure S4 amd S5). Translocation duration of HA in both two nanochannels follows exponential dependence ($f(V) = Aexp(-V/V_c)$ with A = 48177 µs and V_c = 382 mV. This indicates that transport time has a dominating contribution to dwell time for the polyelectrolyte translocation in long conical nanochannel in the semi-dilute regime whatever the tip aperture diameter.

The difference of energy barrier between two nanochannels has been calculated by fitting event frequency as a function of applied voltage (Figure 3e). From this figure, we can see that the frequency of blockade events is higher for the larger nanochannel. From the equation (5), we calculate the difference of free energy barrier:

$$\frac{f_{0\,35.4}/C_{35.4}}{f_{0\,6.1}/C_{6.1}} = \exp\left[\frac{U_{6.1}-U_{35.4}}{k_BT}\right], \qquad (6)$$

The value $U_{6.1} - U_{35.4}$ is obtained as 0.66 k_BT. Here, the higher energy barrier for the small nanopore can be assigned to the friction as the interaction between molecules and the nanochannel surface is strong. This difference of friction in two regimes could be explained by the scaling law of de Gennes using blob models. The ratio of frictional forces for the semi-dilute regime and dilute regime can be described by the ratio of the effective monomer mobility B^{-1} that includes the hydrodynamic interactions between monomers in confined space. Thus according to Daoudi and Brochard[32], we have:

$$\frac{B_{SD}^{-1}}{B_D^{-1}} = \frac{\eta_s(\xi_{SD}/g_{SD})}{\eta_s(\xi_D/g_D)} \qquad (7)$$

where η_s is the solution viscosity, for the semi-dilute regime, ξ is the mesh size of the polymer network which can be calculated as $\xi = ac^{-0.75}$, a is the monomer size, c the concentration, g the number of monomers inside a blob of diameter ξ[40]. This ratio can be simplified by substituting $g = \left(\frac{\xi}{a}\right)^{5/3}$ into Eq. (7) as:

$$\frac{B_{6.1}^{-1}}{B_{35.4}^{-1}} = \left(\frac{\xi_{35.4}}{\xi_{6.1}}\right)^{2/5} \quad (8)$$

The ξ is calculated using $\xi = ac^{-0.75}$ with a of 1 nm and c the volume fraction of polymers assuming that hyaluronic acid has similar density of water. The volume fraction of a polymer in confined nanochannel (close to tip) can be obtained by calculating the distance L occupied by the molecule in nanochannel using equation (2). For the nanochannel with tip aperture of 6.1 nm, its blob diameter ξ is obtained to be 3.6 nm as volume fraction is 18.4%; for the nanochannel with tip aperture of 35.4 nm, its blob diameter ξ is obtained to be 9.8 nm as volume fraction is 4.8%. Therefore, the friction coefficient in nanochannel of 6.1 nm is higher than in nanochannel of 35.4 nm. This is in accordance with the different energy barriers obtained previously that reduction of tip aperture of nanochannels will increase the frictions between polymers and the channel wall leading to a higher energy barrier. This difference in volume fraction due to the occupation of the polymer close to the tip aperture (18.4% for nanochannel of 6.1 nm and 4.8% for nanochannel of 35.4 nm) can also well explain the difference of current blockade rates in Figure 3f: with more occupation by the polymer, it has a higher current drop. So the equation (2) and (7) based on scaling law can be a good tool to predict quantitatively or qualitatively the translocation of large flexible polyelectrolytes through a long conical nanochannel.

Detection of HA with nanochannels decorated with enzyme in tip

After studying the polymer translocation through our conical nanochannels, we performed experiments involving grafted enzymes. Besides the shape controllability, PET track-etched nanochannels have also advantages on simplicity of surface modification due to carboxylic acid moieties. In the first set of experiments, we use conical nanochannel of D_{base}=1000 nm, D_{tip}=4.3 nm, α = 2.19° (noted nanochannel 4). The hyaluronidase was grafted using EDC under MES buffer by addition on base side. The chemical grafting lasts for the whole night to assure a maximum enzyme immobilization. Regarding to the size of the tip diameter (4.3 nm smaller than the size of enzyme), we can assume that enzymes fill the nanopore but do not reach the tip end. After being washed and stabilized by PBS buffer, the functionalized nanochannel was used for hyaluronic acid translocation experiments. We notice that we used in the same condition as the previous experiment performed in the semi-dilute regime.

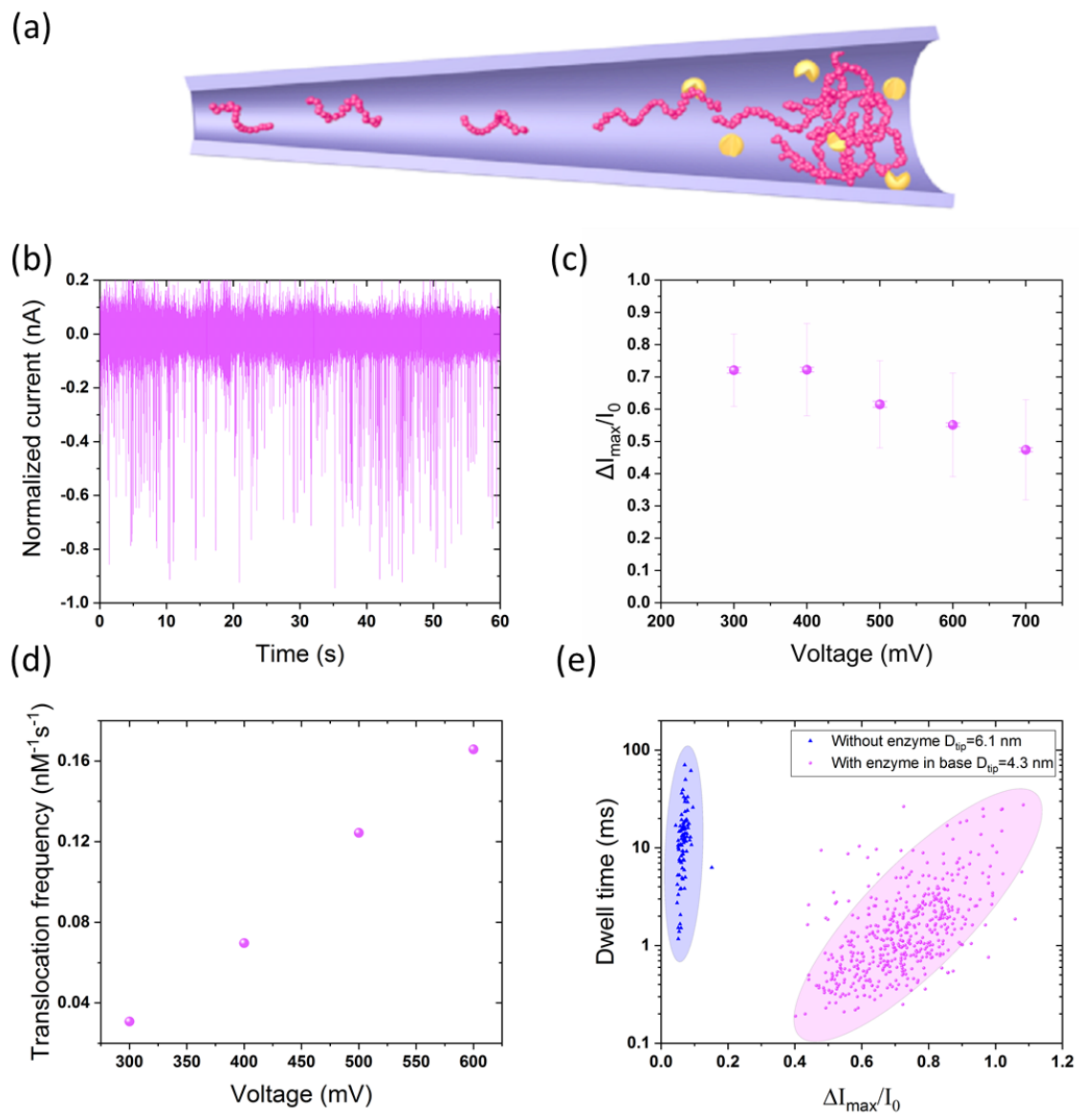

Figure 4. (a) Sketch of hyaluronic acid flowing into the long conical channel with hyaluronidase immobilized on the base side. The sketch is not to scale. (b) Example of a current trace recorded. Frequency (c), dwell time (d) and blockade rate (e) of translocation events against applied voltage. Channel 4: D_{base}=1000 nm, D_{tip}=4.3nm. The transparent error bars represent the full width at half maximum of the Gaussian distributions and the solid error bars represent the standard error.

Figure 4a is a schematic representation of enzymes immobilized in the nanochannel with small tip diameter. After enzymes immobilization, a slight diminution of effective channel diameter was measured (Figure S6) due to steric block of hyaluronidase close to the tip side of the nanopore. This allows confirming the success of functionalization. Effective tip diameter becomes 2.2 nm instead of 4.3 nm of the channel without enzymes resulting in

higher amplitude of relative current blockade (Figure 4c). Sporadic attachment of hyaluronidase is suggested in the light of the crosslinking conditions[4]. The HA driven into the channel by electrical bias will be bound and hydrolyzed by hyaluronidase, thus we could expect that more events will be detected. The experimental results show that translocation frequency gets an increase of a factor about 20 compared to the experiment in the channel of 6.1 nm without enzymes (Figure 4d and Figure 3e). We also observe a larger distribution of relative current blockades meaning that varieties of chain length are recorded (Figure 4 and Figure S7). In addition, dwell times recorded here are much shorter than those of un-degraded HA because the degraded polymers are shorter (Figure 4e). With this base-hyaluronidase-functionalized nanochannel, it could be possible to analyze the size distributions as of the enzymatic reaction products in real time after a calibration. The successful detection of enzymatic degradation products by immobilized hyaluronidase confirms that it remains reactivity after crosslinking conditions, under confinement and electrical bias. This evidence can allow us to further observing the direct interaction between HA and enzymes in order to measure the duration of the intermediate complexion at single molecule level in our channel.

Detection of HA-Hyaluronidase interaction with nanochannels decorated with enzyme in base

To do so, we functionalized the nanochannel 2 (D_{tip} =35.4 nm) with hyaluronidase following the same procedure as the one used for nanochannel 4 previously. The current-voltage curves before and after enzyme grafting was measured in PBS, 1M NaCl also showing clear reduction of the tip size and surface charge (Figure S8). This can be an evidence of the successful enzyme grafting inside the nanochannel. According to the large tip diameter, enzyme can be located on the tip entrance. The translocation experiments in the semi-dilute regime were repeated in this nanochannel and impressive long events were observed for the first time in our work (Figure 5a). The current trace show several events with mean duration of 1022 ± 78 ms. Compared to our previous experiments, no relationship between the event duration and applied voltages was found indicating a static behavior of the polymer instead of a kinetic process. In addition, the duration of about 1 s is in agreement with a enzymatic reaction time scale usually reported between some hundreds milliseconds to several seconds[55]. Thus, these long events can be assigned to the enzymatic reactions

between hyaluronic acid and hyaluronidase. More interestingly, some peaks inside these long blockades were observed as shown in Figure 5a. This could be explained by the presence of another HA that passes through the nanochannel when a polymer is bound to the enzyme. The dwell time of this peak is longer than the events without enzymes. This should be due to the reduction of the channel diameter by enzymes and/or interactions between polymers and enzymes.

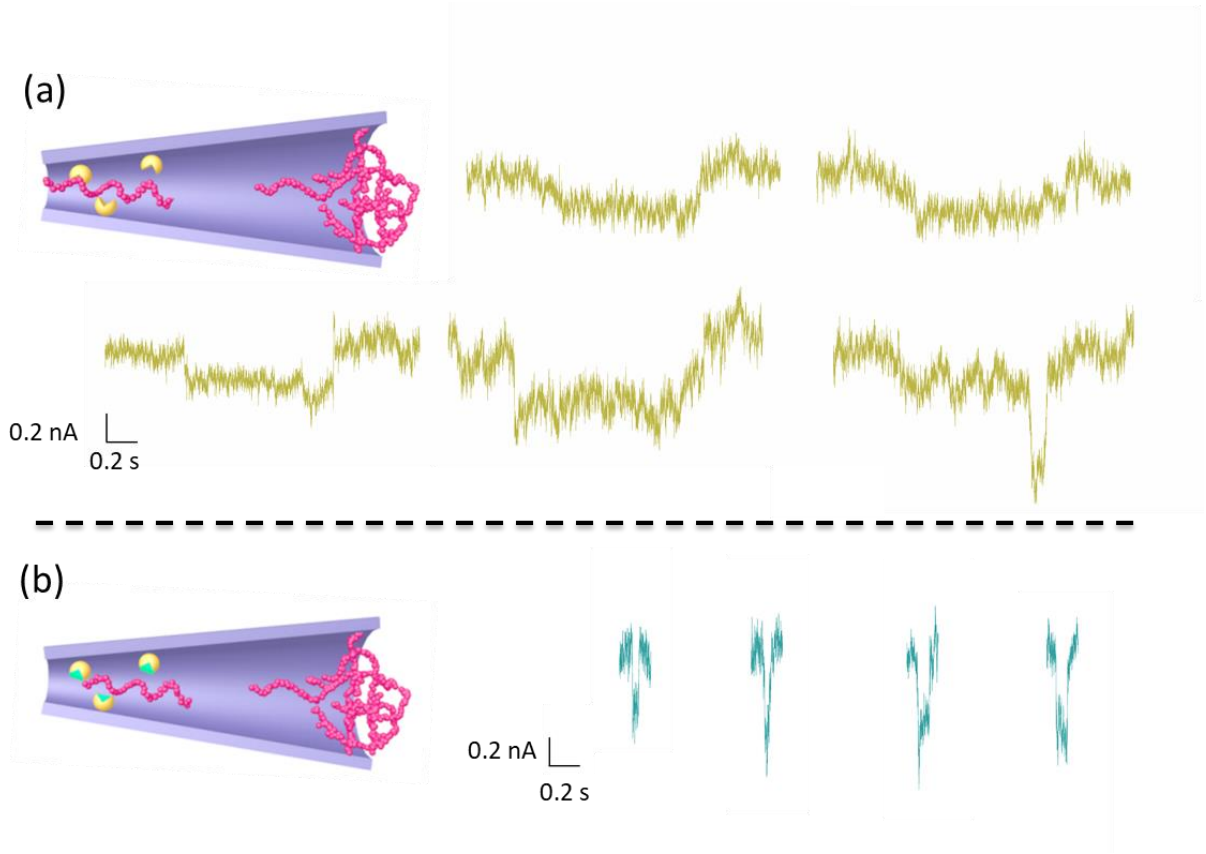

Figure 5. (a) Sketch of translocating hyaluronic acid through the channel 2 with hyaluronidase in the tip side and examples of current blockades. (b) Sketch of translocating hyaluronic acid through the channel 3 with inhibited hyaluronidase in the tip side and examples of current blockades. The sketches are not to scale.

To confirm the origin of these two kinds of events, we have added a hyaluronidase inhibitor (quercetin) to the tip side of the channel and then we continue to record the current traces. After addition of quercetin, long events (second time scale) have not been recorded but only short ones (tens millisecond time scale). As shown in Figure 5b, these events have very similar shape, amplitudes and duration of the peak inside long current blockade. This result confirms our assumption that the long events can be assigned to the specific binding of

substrate-enzyme and the short one to the passage of the polymer chain when an enzyme is working. This draws a very clear image describing what is going on in the channel when an enzyme is grafted inside. Thus, for first time, a direct measurement of off-rate duration of enzymatic reaction is achieved at single molecule level under condition commonly used in membrane science for enzymatic reactor membrane.

Conclusion

The translocation of hyaluronic acid with a molar weight at about 1.5 to 1.8 MDa was directly observed for the first time through a conical nanochannel using resistive pulse technique. The inner-channel behaviors can be well explained by the de Gennes's scaling theory. We studied the effect of the solution regime (dilute and semi-dilute) and pore diameter to better understand how these conditions control the transport and the polymer conformation inside the narrow aperture of the nanopore. Conversely than protein pores, the conical nanochannel the surface energy is predominant than the confinement. Then, hyaluronidase was immobilized inside the conical nanochannel for characterizing degradations of hyaluronic acid. Playing with the nanochannel diameter, a real time analyze of degradation products can be feasible after a simple calibration. Finally, by grafting the enzymes at the tip side of a larger nanochannel, the duration of enzyme-substrate intermediate complex was measured for the first time under confinement at single molecule scale. This work opens a new gate in three distinct research and application fields. Firstly, the direct observation and validation of theory of polymers inside conical nanochannel will allow answering numerous questions in basic description of polymer translocation. We can expect that it will help the membrane design involving polymer filtration application. Secondly, the nanochannel is a suitable platform to investigate protein-protein/molecule interactions at single molecule level. Lastly, the nanochannel can provide answers to questions related to the impact of immobilization and the confinement on enzymatic activity. We can expect that this new approach to characterize individual enzymatic reactions will help researchers to understand the involvement of confinement on enzymatic degradation. This will allow optimizing the enzymatic grafting in numerous applications in material or membrane science.

Experimental Section

Materials:

13 µm thick PET films, with biaxial orientations were purchased from Goodfellow (ref ES301061). Hyaluronic acid (53747), Hyaluronidase (H3631), phosphate buffer saline

(PBS) (P4417), 2-(N-morpholino) ethanesulfonic acid (MES) (M8250), potassium chloride (P3911) and sodium chloride (71380) were purchased from Sigma-Aldrich. Chloride acid (20248.290) and sodium hydroxide (28245.298) were purchased from VWR Chemicals. N-(3-dimethylaminopropyl)-N'-ethylcarbodiimide (EDC) (AS-29855) was purchased from AnaSpec. Water used in these experiments was purified by Q-grad®-1 Milli-Q system (Millipore).

Track etched single nano-channel fabrication:

Single tracks are produced by Xe irradiation (8.98 MeV u^{-1}) in PET film at GANIL, SME line (Caen, France). A hole (diameter 1 mm) with a shutter is placed on ion beam path. The control of track number is provided by a detector placed behind the sample. After producing tracks in PET films, they are sealed and stock away from light. The day before the experiment, the track is activated under UV irradiation (Fisher bioblock; VL215.MC, l= 312 nm) during 9 hours for the tip side and 15 hours for the base side. Then, it is mounted in a Teflon cell with two chambers. An etching solution of 9M NaOH is added to the base side chamber and a stopping solution of 1M KCl and 1M acetic acid is added to the tip side chamber to inhibit the reaction by neutralizing NaOH. Pt electrodes connected to an amplifier (HEKA EPC10) are used to apply an electric field. An electrical bias of 1V is applied to provide electrostopping and monitor the pore opening by measuring the current as a function of time. When, we get an appropriate current level, the etching solution is replaced by stopping solution to completely stop the etching. After 10 minutes, the pore is washed by Milli-Q water several times and is stabilized in Milli-Q water during the night. In such an asymmetric etching condition at room temperature, a long conical channel with a small angle can be obtained.

The tip diameter D_{tip} of the conical channel was determined from the dependence of the conductance G measured in the linear zone of the current–voltage curve from - 60 mV to 60 mV assuming a bulk-like ionic conductivity inside channels (equation 13).

$$G = \frac{\kappa d D \pi}{4L} \qquad (13)$$

where, κ is the ionic conductivity of the solution, L is the channel length (13 µm) and D_{base} is the base diameter which was calculated from the total etching time t using the relationship D_{base} = 2.5t (the factor 2.5 was determined in our experimental set up using multipore track-etched membranes).

The current-voltage curves were obtained from the current traces recorded as a function of time from 1 V to -1 V by steps of 100 mV for 2 s and from 100 mV to -100 mV by steps of 10 mV for 2 s using a sampling rate 50 kHz. Ag/AgCl electrodes were used for the measurements. For conductance measurement to determine tip diameter, a solution of NaCl at 1 M was used.

Recording of hyaluronic acid translocation:

Hyaluronic acid translocations were recorded using the same amplifier (HEKA EPC10). The sampling rate is 100 kHz and a built-in low-pass filter at 10 kHz is used. Data analysis for event detection is performed using a custom-made LabView software with butterworth filter of 5 KHz, 3 orders and Savitzky-Golay filter of 1200 side points, 1 order. We take 5σ to detect events.

Enzyme immobilization:

The hyaluronidase immobilization inside the channel was performed in situ. The two chambers of the cell containing the channel membrane were filled with a solution containing 0.1 M KCl, 0.1 M MES at pH 4.7. The pH of the solution was adjusted using HCl and NaOH solutions. The hyaluronidase was then added in cis chamber (tip side of the channel) or in the trans-chamber (base side of the channel) according to the need. At the end, 50 mM of EDC was added in both two chambers. The reaction was during the whole night for a maximum grafting. Then, the channel was well rinsed by Milli-Q water and then stabilized in PBS buffer for 1 hour.

I-V curves of the channel before and after enzyme immobilization was recorded in PBS buffer with 1M of NaCl shown in Figure S1. The change of rectification and conductance can be the evidence of the enzyme grafting.

References

1. Kirk, O., Borchert, T. V. & Fuglsang, C. C. Industrial enzyme applications. *Curr. Opin. Biotechnol.* **13,** 345–351 (2002).

2. Rios, G. M., Belleville, M. P., Paolucci, D. & Sanchez, J. Progress in enzymatic membrane reactors – a review. *J. Memb. Sci.* **242,** 189–196 (2004).

3. Coglitore, D., Janot, J.-M. & Balme, S. Protein at liquid solid interfaces: Toward a new

paradigm to change the approach to design hybrid protein/solid-state materials. *Adv. Colloid Interface Sci.* **270,** 278–292 (2019).

4. Hanefeld, U., Cao, L. & Magner, E. Enzyme immobilisation: fundamentals and application. *Chem. Soc. Rev.* **42,** 6211–6212 (2013).

5. Luckarift, H. R., Spain, J. C., Naik, R. R. & Stone, M. O. Enzyme immobilization in a biomimetic silica support. *Nat. Biotechnol.* **22,** 211–213 (2004).

6. Kim, J., Grate, J. W. & Wang, P. Nanostructures for enzyme stabilization. *Chem. Eng. Sci.* **61,** 1017–1026 (2006).

7. Bouaziz, Z. *et al.* Structure and antibacterial activity relationships of native and amyloid fibril lysozyme loaded on layered double hydroxide. *Colloids Surfaces B Biointerfaces* **157,** 10–17 (2017).

8. Md Jani, A. M., Losic, D. & Voelcker, N. H. Nanoporous anodic aluminium oxide: Advances in surface engineering and emerging applications. *Prog. Mater. Sci.* **58,** 636–704 (2013).

9. Chang, S.-F., Chang, S.-W., Yen, Y.-H. & Shieh, C.-J. Optimum immobilization of Candida rugosa lipase on Celite by RSM. *Appl. Clay Sci.* **37,** 67–73 (2007).

10. Zucca, P., Fernandez-Lafuente, R. & Sanjust, E. Agarose and its derivatives as supports for enzyme immobilization. *Molecules* **21,** 1577 (2016).

11. Ndour, N. *et al.* Impact of polyelectrolytes on lysozyme properties in colloidal dispersions. *Colloids Surfaces B Biointerfaces* **183,** 110419 (2019).

12. Gkaniatsou, E. *et al.* Metal–organic frameworks: a novel host platform for enzymatic catalysis and detection. *Mater. Horizons* **4,** 55–63 (2017).

13. Mehta, J., Bhardwaj, N., Bhardwaj, S. K., Kim, K.-H. & Deep, A. Recent advances in enzyme immobilization techniques: Metal-organic frameworks as novel substrates. *Coord. Chem. Rev.* **322,** 30–40 (2016).

14. Michaelis, L. & Menten, M. Kinetik der Invertinwirkung. *Biochem. Z.* **49,** 333–369 (1913).

15. Xie, X. S. Enzyme Kinetics, Past and Present. *Science (80-.).* **342,** 1457 LP-1459 (2013).

16. Xie, X. S. & Trautman, J. K. OPTICAL STUDIES OF SINGLE MOLECULES AT ROOM TEMPERATURE. *Annu. Rev. Phys. Chem.* **49,** 441–480 (1998).

17. Funatsu, T., Harada, Y., Tokunaga, M., Saito, K. & Yanagida, T. Imaging of single fluorescent molecules and individual ATP turnovers by single myosin molecules in aqueous solution. *Nature* **374,** 555–559 (1995).

18. Neuman, K. C. & Nagy, A. Single-molecule force spectroscopy: optical tweezers, magnetic tweezers and atomic force microscopy. *Nat. Methods* **5,** 491 (2008).

19. Sakmann, B. *Single-Channel Recording*. (Springer US, 2013).

20. Kherim, W., Veerle, V. M., Carsten, W. & Giovanni, M. Single-molecule nanopore enzymology. *Philos. Trans. R. Soc. B Biol. Sci.* **372,** 20160230 (2017).

21. Fennouri, A. *et al.* Kinetics of enzymatic degradation of high molecular weight polysaccharides through a nanopore: Experiments and data-modeling. *Anal. Chem.* **85,** 8488–8492 (2013).

22. Fennouri, A. *et al.* Single Molecule Detection of Glycosaminoglycan Hyaluronic Acid Oligosaccharides and Depolymerization Enzyme Activity Using a Protein Nanopore. *ACS Nano* **6,** 9672–9678 (2012).

23. Giamblanco, N. *et al.* Amyloid Growth, Inhibition, and Real-Time Enzymatic Degradation Revealed with Single Conical Nanopore. *Anal. Chem.* **90,** 12900–12908 (2018).

24. Ma, T., Balanzat, E., Janot, J.-M. & Balme, S. Single conical track-etched nanopore for a free-label detection of OSCS contaminants in heparin. *Biosens. Bioelectron.* **137,** 207–212 (2019).

25. Wei, R., Gatterdam, V., Wieneke, R., Tampé, R. & Rant, U. Stochastic sensing of proteins with receptor-modified solid-state nanopores. *Nat. Nanotechnol.* **7,** 257 (2012).

26. Yusko, E. C. *et al.* Controlling protein translocation through nanopores with bio-inspired fluid walls. *Nat. Nanotechnol.* **6,** 253 (2011).

27. De Gennes, P. G. Scaling concepts in polymer physics. Cornell university press. *Ithaca*

N.Y., 324 (1979).

28. Odijk, T. The statistics and dynamics of confined or entangled stiff polymers. *Macromolecules* **16,** 1340–1344 (1983).

29. Hydrodynamics of linear macromolecules . *Pure and Applied Chemistry* **12,** 563 (1966).

30. De Gennes, P. G. Coil-stretch transition of dilute flexible polymers under ultrahigh velocity gradients. *J. Chem. Phys.* **60,** 5030–5042 (1974).

31. Pincus, P. Excluded Volume Effects and Stretched Polymer Chains. *Macromolecules* **9,** 386–388 (1976).

32. Daoudi, S. & Brochard, F. Flows of Flexible Polymer Solutions in Pores. *Macromolecules* **11,** 751–758 (1978).

33. Colby, R. H. & Rubinstein, M. Polymer physics. *New-York Oxford Univ.* **100,** 274 (2003).

34. Nikoofard, N., Khalilian, H. & Fazli, H. Directed translocation of a flexible polymer through a cone-shaped nano-channel. *J. Chem. Phys.* **139,** 74901 (2013).

35. Li, L., Chen, Q., Jin, F. & Wu, C. How does a polymer chain pass through a cylindrical pore under an elongational flow field? *Polymer (Guildf).* **67,** A1–A13 (2015).

36. Dekker, C., Article, R. & Dekker, C. Solid-state nanopores. *Nat. Nanotechnol.* **2,** 209–215 (2007).

37. Kasianowicz, J. J., Brandin, E., Branton, D. & Deamer, D. W. Characterization of individual polynucleotide molecules using a membrane channel. *Proc. Natl. Acad. Sci. U. S. A.* **93,** 13770–3 (1996).

38. Johnson, K. A. & Goody, R. S. The Original Michaelis Constant: Translation of the 1913 Michaelis–Menten Paper. *Biochemistry* **50,** 8264–8269 (2011).

39. Henrickson, S. E., Misakian, M., Robertson, B. & Kasianowicz, J. J. Driven DNA Transport into an Asymmetric Nanometer-Scale Pore. *Phys. Rev. Lett.* **85,** 3057–3060 (2000).

40. Oukhaled, A. G., Biance, A. L., Pelta, J., Auvray, L. & Bacri, L. Transport of long neutral polymers in the semidilute regime through a protein nanopore. *Phys. Rev. Lett.* **108,**

(2012).

41. Steinbock, L. J., Lucas, A., Otto, O. & Keyser, U. F. Voltage-driven transport of ions and DNA through nanocapillaries. *Electrophoresis* **33,** 3480–3487 (2012).

42. Bell, N. A. W., Muthukumar, M. & Keyser, U. F. Translocation frequency of double-stranded DNA through a solid-state nanopore. *Phys. Rev. E* **93,** 22401 (2016).

43. Bell, N. A. W., Chen, K., Ghosal, S., Ricci, M. & Keyser, U. F. Asymmetric dynamics of DNA entering and exiting a strongly confining nanopore. *Nat. Commun.* **8,** 380 (2017).

44. Harrell, C. C. *et al.* Resistive-Pulse DNA Detection with a Conical Nanopore Sensor. *Langmuir* **22,** 10837–10843 (2006).

45. Apel, P. Track etching technique in membrane technology. *Radiat. Meas.* **34,** 559–566 (2001).

46. Cowman, M. K., Schmidt, T. A., Raghavan, P. & Stecco, A. Viscoelastic Properties of Hyaluronan in Physiological Conditions. *F1000Research* **4,** 622 (2015).

47. Balme, S., Lepoitevin, M., Dumée, L. F., Bechelany, M. & Janot, J.-M. Diffusion dynamics of latex nanoparticles coated with ssDNA across a single nanopore. *Soft Matter* **13,** 496–502 (2017).

48. Cabello-Aguilar, S. *et al.* Dynamics of polymer nanoparticles through a single artificial nanopore with a high-aspect-ratio. *Soft Matter* **10,** 8413–8419 (2014).

49. Goyal, G., Freedman, K. J. & Kim, M. J. Gold Nanoparticle Translocation Dynamics and Electrical Detection of Single Particle Diffusion Using Solid-State Nanopores. *Anal. Chem.* **85,** 8180–8187 (2013).

50. Chen, K. *et al.* Biphasic Resistive Pulses and Ion Concentration Modulation during Particle Translocation through Cylindrical Nanopores. *J. Phys. Chem. C* **119,** 8329–8335 (2015).

51. Daoud, M. & De Gennes, P. G. Statistics of macromolecular solutions trapped in small pores. *J. Phys. Fr.* **38,** 85–93 (1977).

52. Nikoofard, N. & Fazli, H. A flexible polymer confined inside a cone-shaped nano-channel. *Soft Matter* **11,** 4879–4887 (2015).

53. Buhler, E. & Boué, F. Chain Persistence Length and Structure in Hyaluronan Solutions: Ionic Strength Dependence for a Model Semirigid Polyelectrolyte. *Macromolecules* **37,** 1600–1610 (2004).

54. Cleland, R. L. The persistence length of hyaluronic acid: An estimate from small-angle X-ray scattering and intrinsic viscosity. *Arch. Biochem. Biophys.* **180,** 57–68 (1977).

55. Toni, T. The Machinery of Life: David S. Goodsell 2nd edn., 2009 Springer-Verlag, London. *Hum. Genomics* **4,** 369 (2010).

Discussion

Nanopores have been used as sensing device. In this chapter, two works have been done using (bio)polyelectrolytes functionalized track-etched nanopores. These works utilized two different methods of characterization. The first one took advantages of the surface charge changes due to the polyelectrolytes adsorption on ionic diode behavior. So ion current rectification has been used to detect the analyte. The second study used resistive pulse to characterize polymer translocations through nanochannels. This method measures the current blockades of each molecule which can reflect polymer conformation, polymer size and polymer interactions with the nanopore surface.

For ionic diode, the modulation of ion transport due to surface charge changes have been discussed in chapter 2. However, a biosensor based on this principle requires establishing a quantitative relationship between adsorbed polyelectrolyte and current rectification factor. The PLL has positive charges, it can be used to give track etched nanopore the ability to adsorb HEP. Moreover thanks to its weak electrolyte properties, the monolayer of PLL can be removed by increasing the pH upper than its pKa. This convenience makes it possible to reuse this sensor for more than 20 times and several weeks. The key point of this experiment is to make sure exactly the same manipulation for each time of PLL deposition. This is the most important to achieve quantitative detection because different PLL quantity adsorbed, different PLL covering length and different HEP detecting time make different results. Because of the adsorption equilibrium depends on the polyelectrolyte concentration, a quantitative relation between rectification factor and HEP concentration was established.

After achieving quantitative detection of HEP, heparinases were involved to detect OSCS. The latter has very similar structure with HEP and the tiny difference at low concentration can deceive most of classical methods like FTIR, chromatography etc. But it can be precisely distinguisched by the enzyme. Heparinases can degrade HEP while OSCS inhibates it. Hence, the presence of OSCS traces more or less inhibits the activity of heparinases. The latter effect can be presented by a higher HEP concentration in the residues after enzymatic treatment. Thus OSCS contaminants can be quantitatively detected by heparinases coupled PLL functionalized nanopore. The nanopore sensor shows higher accuracy than classical methods like chromatography, mass spectrometer and NMR with comparable cost.

Compared to fluorescent sensors with fluorescent probe and nanoparticles, nanopore based sensor largely reduces the cost and can satisfy the market needs.

In this first work, the nanopore was used to determine the follow kinetic of HA degradation. In general point of view, the enzymes have been largely used in membrane industries thanks to their irreplaceable catalyzing abilities. However enzyme interactions with substrate molecules as well as their behaviors in immobilized states remain to be studied. To know rate-off that is the time required for one reaction between enzyme and substrate at single molecule level is one challenge to learn more about enzymatic reactions. As single nanopore has been used for single molecule characterization, the resistive pulse method should also allow characterizing single enzymatic reaction. So the idea was to immobilize the enzyme inside a nanopore. The substrate behavior can be recorded in current change according to time.

Before immobilizing enzymes inside the pore, experiments were focused on the behaviors of flexible long polymers hyaluronic acids through long conical nanochannel. The successful explications of dwell time, blockade rate and free energy related to translocation by de Gennes' scaling law confirmed their theoretical predictions. Solution regime (dilute regime or semi-dilute) and pore diameters can significantly influence the HA translocations. After being clear of polymer behaviors in conical nanochannel, enzymes were immobilized inside the pore. When heparinases were immobilized at the base side, enzymatic degradations carried on like in bulk conditions. Then the products were translocated through the pore and a continuous analyze was achieved. This experiment confirmed the remaining of activity of heparinase after grafting reactions. So the immobilization of enzymes at the narrowest part of the nanochannel was then done. The polymers translocating without and with enzymes show a large difference in translocation duration. It changes from several milliseconds to second time scale. This increase can be contributed by two parts: one is due to the specific interactions between substrate molecules and enzymes; the other one can be attributed to the decrease of the channel diameter which is discussed in pore diameter effect section. To eliminate this latter contribution, the quercetin was added as inhibitors. Events of second time scale disappeared and we got only events of less than 200 ms. The prolongation of several milliseconds to 200 ms from nanochannel without enzymes to nanochannel with inhibited enzymes can be attributed to the decrease of pore diameter and the increases of

frictions between the polymers and the inhibited enzymes. Thus it can be confirmed that the long duration when polymer translocate in nanochannel with enzymes is principally due to the specific interactions between enzymes and substrates.

Combining two works, track-etched nanopore with polyelectrolytes grafted inside shows strong ability to characterize enzymatic degradations. By using ion current rectification methods, kinetics of enzymatic degradation can be measured. If the experiments are repeated by different enzyme and substrate concentrations, the kinetics constant could be at macroscopic level. At microscopic level, resistive pulse can be used to measure the duration of reaction intermediate between single substrate molecule and single enzyme. The accuracy can be attained to millisecond. Accordingly, track etched nanopore with advantages of controllable geometry and simplicity of functionalization can be a reliable platform for polymer involved reaction characterizations.

General conclusion

The goal of this thesis was to functionalize nanopores to give abilities for different applications by the immobilization of (bio)polyelectrolytes inside nanopores. The objectives were (i) the design artificial ion channels in responding to multiple stimuli (ii) the design biosensors as well as studying specific molecular interactions (ii) the design of ion selective membranes to generate osmotic energy.

For stimuli-responsive ion channels, we utilized two strategies: one used layer-by-layer self-assembly pH-sensitive polyelectrolytes (poly-L-lysine/polyacrylic acid and polyethylenimine/ polyacrylic acid) inside track etched single nanopores; the other one used chemical grafting of polymer functionalized with photo-switchable molecule (polyethylene glycol-spiropyran). Nanopores of conical shape were used as they can have ionic diode properties which can amplify the transport phenomenon. For the pH sensitive nanopore, three different channels were designed with PLL/PAA, PLL/PAA crosslinked and PEI/PAA. Charge compensations, swelling/deswelling and protonation/deprotonation were observed, these effects co-influence the ion transport properties as a function of the pH. PEG-spiropyran functionalized nanopore showed close and open states by forming self-assembled structures under UV and visible light. In UV light, charges of merocyanines can also be regulated the ionic transport by pH.

The successful functionalization of the ion channel by polyelectrolytes gives possibility to use this kind of device for osmotic energy generation. So layer-by-layer adsorption of chitosan and PAA were used to increase surface charge density inside the pore. Ion transport of single pore and bivalence metal chelation were firstly studied. Then, the osmotic energy generation was then measured under different salinity gradient. At pH 7.6 and C_{tip}/C_{base}=1000, a maximum single pore power is reached at 20 pW. The same procedure was also done on multipore membranes with pore density at 2 10^6 cm^{-2}, a power density of 0.1 W m^{-2} was obtained at the same condition. Another strategy was also achieved by synthesizing highly charged hydrogel frameworks inside the nanopores. It is confirmed that in this case, the ion selectivity is dominated by charges of hydrogels and not by the assymetry. So, cylindrical nanopore becomes the best candidate because it can be scaled up to membranes with very high pore density. The energy measurements of single nanopores,

multipore membranes and stacked membranes were achieved. With C_{tip}/C_{base}=1000 at pH 7, a power density of 0.37 W m^{-2} was obtained by stacking two pairs of membranes.

The polyelectrolytes functionalized nanopore can also be used as biosensors to detect OSCS, a contaminant found in heparin. A PLL functionalized nanopore was designed to detect quantitatively heparin by ion current rectification. The heparin detection limit is determined at 25 ng ml^{-1}. Heparinases were added to samples with heparin and different amounts of OSCS. As OSCS inhibates the degradation by heparinases, the quantitative detection of heparin in reaction residues was given by current rectification factors. The sensor has a detect accuracy of 0.01 % in weight of OSCS with a stability for more than 20 uses during three weeks. In this work, enzymatic reactions were characterized by analyzing the reaction products. Another work was to immobilize hyaluronidases inside the pore. After studying polymer translocation behaviors through conical channel, interactions between hyaluronic acid molecules and hyaluronidases were characterized. The duration of specific binding was measured at about 1 second.

These researches were achieved but lots of questions remain to be answered such as how to switch the spiropyran based ion channel in visible light in water? Can we describe the ion transport analytically of polyelectrolytes functionalized cylindrical nanopores and how are the conformations of immobilized polymers inside the confined space in different pH and ion strength etc? So the next and the on-going project will focus on ion transport properties of single nanopore with polyelectrolytes/polymers inside.

To establish analytical equations describing the ion transport in conical nanopore is still far from our ability. However, an approaching step can be done by constructing a bi-cylindrical pore using polyelectrolytes. The recently established models will be acted to describe the experimental data especially to distinguish two transport regimes: bulk and surface.

PLL single layer functionalized conical nanopore showed strong ability to detect OSCS. However, it is more complicated than it seems. Recently numerical studies by solving PNP equations show the existence of a maximum current rectification with certain PLL cover length. The ion selectivity generated by polyelectrolytes still remains to be explored in details. This will be extended to other polyeletrolyte and bilayer systems. Finally, it will permit to optimize the nanopore functionalization.

We have used PEG chains to build light responsive ion channel using their conformation changes. The details of PEG chain conformation inside nanopore in different pH, ion strength is not still very clear. We aim to study the PEG chain conformation influencing by these parameters as well as specific biomolecules by both experimental and molecular dynamic studies.

To sum up, ion and molecule transport properties through nanopore are always essential works of nanopore technology. During recent years, more and more new artificial nanopores are taken into accounts like 2D nanopores, optical nanopores and DNA origami nanopores. The understanding the fundamental behaviors and to functionalize these nanopores remain to be done. Together with other kinds of nanopores, nanopore technology will go further in single molecule detection or even beyond.

Résumé

Les canaux biologiques sont des protéines de pores situées sur la membrane cellulaire pour maintenir l'équilibre des ions et le transport des molécules. Ces canaux protéiques peuvent répondre à de multiples stimuli tels que la lumière, le pH, la force des ions et le potentiel transmembranaire pour réguler leur perméabilité et leur sélectivité. Pour imiter ces pores biologiques, des nanopores artificiels ont été fabriqués et une technologie à base de nanopores a été développée pour le séquençage de l'ADN, la détection de biomolécules et la récupération d'énergie osmotique. Les avantages des nanopores artificiels à base de matériaux solides ou polymères sont la simplicité de fabrication et la stabilité mécanique et chimique. Cependant, les faiblesses sont également évidentes: ils ont généralement moins de sélectivité et de réactivité face aux stimuli externes. Pour améliorer leurs applications, la fonctionnalisation devient essentielle. La fonctionnalisation de la surface des nanopores peut modifier leurs propriétés telles que la perméabilité, la sélectivité ou leur donner la capacité de détecter des biomolécules spécifiques, afin d'étudier le transport ionique / moléculaire fondamental dans des situations spécifiques.

Dans cette thèse, nous avons cherché à améliorer la fonctionnalisation des nanopores pour trois applications: canal ionique sensible aux stimuli, récupération de l'énergie osmotique et biosensing. Pour les canaux ioniques sensibles aux stimuli, nous avons construit deux canaux: l'un est sensible au pH et fonctionnalisé par auto-assemblage couche par couche de polyélectrolytes dans des nanopores track-etched et l'autre peut répondre à la lumière et au pH sur la base d'un greffage chimique de chaînes spiropyran-PEG. L'isomérisation induites par la lumière et la protonation / déprotonation causées par le changement de pH peuvent modifier la charge et la conformation de molécules fonctionnelles. Ainsi, ces changements peuvent moduler la perm-sélectivité des ions du canal. Pour la récupération d'énergie osmotique, nous avons conçu deux stratégies pour améliorer la sélectivité ionique de la membrane afin d'obtenir un rendement énergétique supérieur. L'une utilisait le dépôt couche par couche de polyélectrolytes sur la surface des pores pour améliorer la densité de charge, et une autre utilisait un hydrogel hautement chargé synthétisé à l'intérieur des pores. Les résultats ont montré une production d'énergie élevée pour les deux stratégies de 20 pW par pore. La fonctionnalisation en hydrogel permet d'utiliser une géométrie cylindrique adéquate pour une membrane à haute densité de pores. Pour la biodétection, nous avons développé un nanopore fonctionnalisé par PLL afin de détecter la contamination par les OSCS dans des échantillons d'héparine sur la base des principes de la diode ionique. Après avoir été traitée aux héparinases, la concentration en héparine dans les résidus peut refléter la concentration en OSCS, car celle-ci peut bloquer les héparinases. La concentration en héparine peut ensuite être caractérisée quantitativement par un nanopore fonctionnalisé par PLL basé sur le changement ICR. Cette expérience a confirmé l'aptitude d'un nanopore gravé sur piste à caractériser la cinétique de dégradations enzymatiques. Pour aller plus loin, nous avons immobilisé des hyaluronidases dans le canal afin de caractériser les réactions enzymatiques au niveau d'une molécule à l'aide d'une impulsion résistive. Les résultats ont montré que la durée du complexe entre une hyaluronidase et une molécule d'acide hyaluronique pour une réaction est d'environ 1 seconde.

Dans cette thèse, nous montrons la forte capacité des nanopore track-etched fonctionnalisés par polyélectrolytes. Ces systèmes bien conçus peuvent être facilement mis à l'échelle et ces principes bien développés peuvent être utilisés pour concevoir d'autres systèmes afin de résoudre plus problèmes de santé et d'énergie.

Abstract

Biological channels are pore proteins on the cell membrane to keep ion equilibrium and molecule transport. These protein channels can respond to multiple stimuli like light, pH, ion strength and trans-membrane potential to regulate their permeability and selectivity. To mimic these biological pores, artificial nanopores have been fabricated and nanopore technology has been developed for DNA sequencing, biomolecule detection and energy harvesting. The advantages of artificial nanopores based on solid or polymer materials are simplicity of fabrication and mechanical, chemical stability. However the shortcomings are also clear that they usually have less selectivity and responsiveness to external stimuli. To enhance their applications, the functionalization becomes vital. Functionalization of the nanopore surface can change their properties like permeability, selectivity or give them abilities to detect specific biomolecules, to study fundamental ion/molecule transport in specific situations.

In this thesis, we aimed to improve nanopore functionalization for three applications: stimuli-responsive ion channel, osmotic energy harvesting and biosensing. For stimuli-responsive ion channel, we constructed two channels: One is responsive to pH and functionalized by layer-by-layer self-assembly of polyelectrolytes in track-etched nanopores and the other one can respond to light and pH based on chemical grafting of spiropyran-PEG chains. Light induced isomerization and protonation/deprotonation caused by pH change can change the charge and conformation of functional molecules. Thus these changes can modulate ion perm-selectivity of the channel. For osmotic energy harvesting, we designed two strategies to improve ion selectivity of membrane to get higher energy output. One used layer-by-layer depositing of polyelectrolytes on pore surface to enhance charge density and another one used a high charged hydrogel synthesized inside the pore. Results showed a high energy generation for both two strategies of 20 pW per pore. The hydrogel functionalization makes it possible to use cylindrical geometry which is adequate for high pore density membrane. For biosensing, we developed a PLL functionalized nanopore to detect OSCS contamination in heparin samples based on ionic diode principles. After being treated by heparinases, the heparin concentration in residue can reflect the OSCS concentration as OSCS can block heparinases. The heparin concentration can then be characterized quantitatively by PLL functionalized nanopore based on ICR change. This experiment confirmed the ability of track-etched nanopore to characterize the kinetics of enzymatic degradations. To go further, we immobilized hyaluronidases in the channel to characterize the enzymatic reactions at single molecule level using resistive pulse. The results showed that the duration of complexion between one hyaluronidase and one hyaluronic acid molecule for one reaction is around 1 second.

In this thesis, we show the strong ability of polyelectrolytes functionalized track-etched nanopore.

These well-designed systems can be easily scaled up and these well-developed principles can be used to design other systems to solve more problems in health and energy.